In Vitro Evaluation of Anthracycline-induced Cardiotoxicity and Mitigation by Perturbation of Angiotensin Signalling

KIMBERLY LOUISE ROCKLEY

In Vitro Evaluation of Anthracycline-induced Cardiotoxicity and Mitigation by Perturbation of Angiotensin Signalling

Utilising novel methodologies to evaluate structural and functional changes in human derived cardiomyocyte models.

Kimberly L. Rockley BSc (Hons), MSc

Submitted for the degree of

Doctor of Philosophy

Division of Pharmacy

School of Medicine, Pharmacy and Health

2018

Abstract

In Vitro Evaluation of Anthracycline-induced Cardiotoxicity and Mitigation by Perturbation of Angiotensin Signalling

Key words: *Cardio-oncology, cardiotoxicity, anthracyclines, angiotensin signalling, hypertrophy, xCELLigence, doxorubicin, angiotensin receptor blockers, toxicity mitigation*.

Cardiotoxicity is a major complication of many anticancer therapies, particularly anthracyclines, which impacts the quality of life and overall survival of patients. Manifesting as both an acute toxicity and more frequently a chronic toxicity occurring months or years after conclusion of therapy, there is an urgent need for greater understanding of the molecular mechanisms responsible for these toxicities and identification of therapeutic strategies to mitigate and overcome this issue. Improved *in vitro* models for accurate prediction and modelling of these cardiac liabilities is therefore of crucial importance.

Recently, clinical studies have demonstrated that drugs which perturb angiotensin signalling may reduce the cardiotoxicity of anthracyclines. However, despite showing promise, the mechanism of toxicity is unresolved and the molecular relationship to angiotensin signalling in the heart is currently unknown. Furthermore, the majority of *in vitro* cardiotoxicity studies to date have either used inappropriate cell models or utilised end-point assays, both strategies that fail to account for the physiological parameters of cardiac cells and the progressive nature of human toxicity development.

This study has qualified the use of hiPSC-derived cardiomyocytes and the human AC10 cardiomyocyte cell line paired with impedance-based systems (xCELLigence technology) for detection of both structural and functional cardiotoxicity. A range of pharmacological and biological mediators were used to qualify these technologies, with both structural hypertrophy and physiological contractility monitorable. A major advantage of these systems over others is that longer-term real-time non-invasive experiments can be conducted, thus allowing recapitulation of the progressive nature of human toxicity development and subsequently a robust clinically relevant method for assessing drug-induced cardiotoxicity.

Using these models and technologies, this study demonstrates induction of cardiomyocyte hypertrophy by anthracyclines which is reduced by blockade of angiotensin signalling, thus implying a relationship at the cardiomyocyte level between anthracycline-induced cardiotoxicity and angiotensin signalling. Furthermore, anthracycline-induced elevated expression of the angiotensin type I receptor and several genes implicated in angiotensin II signalling in this study provides further evidence for a direct molecular relationship between anthracycline-induced cardiotoxicity and angiotensin signalling, with clear translational potential for clinical mitigation of this dose-limiting toxicity in the treatment of cancer.

Acknowledgements

Firstly, I'd like to thank my supervisor Jason for guidance, support and encouragement throughout my project, I have enjoyed working with you. I am also grateful for the opportunity to attend conferences; and for provision of merriment and scientific discussion at these events, I would also like to thank the teams at ACEA biosciences and axiogenesis.

My gratitude is also extended to Gavin for assistance with immunostaining of cells, and the MPharm project students Stephanie, Rachael and Katherine for being a joy to have around and for the generation of data that assisted with this project.

I am also grateful to the members of support staff from Queens Campus – specifically the technical staff for general help in the laboratory, George for assistance with ordering and friendly discussion, and Veronica for helping with anything and everything. I should also like to thank Durham University itself for funding of the project.

For making the day-to-day an absolute hoot and a half, and for the sustenance of morale – a big thank you to the PharmBabes of G115 and associated satellite offices. I am especially thankful for assistance with laboratory techniques, scientific discussion, copious non-scientific discussion and the trips to Morrisons. It would have been so very bleak without you.

My other thanks are handed out to friends and family – near and far – for continued encouragement throughout my studies, and for taking the time to check up on me and listening to me talk about my work, and for nodding along in agreement. This includes my purrfect companion Belle - giver of soothing purrs, receiver of belly rubs, get off my laptop, that's my pen.

Most importantly, Phil – completing this thesis is now only the second best thing to happen to me in the last 3 years. ~*Every cloud has a ~~silver~~* ***gold*** *lining*~

Finally, my parents Roger and Gloria to whom this thesis is dedicated. Thank you for all of your support and encouragement during my current work and everything leading up to this, and for always reminding me that I can do it. I would never have made it here if it wasn't for you both.

Table of Contents

Abstract ..... *i*

Acknowledgements ..... *ii*

Table of Contents ..... *iii*

List of figures ..... *ix*

List of tables ..... *xiii*

List of abbreviations ..... *xiv*

Chapter 1: Introduction *1*

1.1 Cancer **1**
1.1.1 Increasing prevalence of cancer survivors 1

1.2 Management of cancer **2**
1.2.1 DNA interacting agents 3
1.2.2 Topoisomerase interactive agents 3
1.2.3 Molecular targeted therapies 5

1.3 Cancer therapy induced cardiotoxicity **7**
1.3.1 Emergence of cardio-oncology 8

1.4 The cardiovascular system **9**
1.4.1 Cardiomyocytes: The contractile unit of the heart 10
1.4.2 Generation of contractile force: Excitation-contraction coupling 12
1.4.3 Multicellular composition of the myocardium 15
1.4.3.1 Cardiac fibroblasts 15
1.4.3.2 Cardiac microvascular endothelial cells 16
1.4.3.3 Pericytes 17
1.4.4 Myocardial cellular communications 18
1.4.4.1 Physical communications 18
1.4.4.2 Chemical communications 18
1.4.5 Intracellular signalling pathways in cardiac cells 19
1.4.5.1 Adrenergic signalling pathways in cardiomyocytes 22
1.4.5.2 Angiotensin signalling pathways in cardiomyocytes 23
1.4.5.3 Receptor cross talk within cardiac cells 24

1.5 Drug-induced cardiotoxicity **25**
1.5.1 Implications of drug-induced cardiotoxicity for drug development 25
1.5.2 Drug-induced cardiotoxicity of oncology therapeutics 26
1.5.2.1 Type I Cardiotoxicity: Structural changes 29
1.5.2.2 Type II Cardiotoxicity: Functional changes 29

1.6 Type II cardiotoxicity: Molecularly targeted therapies **30**
1.6.1 Sunitinib: Mechanism of action 31
1.6.1.1 Cardiotoxicity of sunitinib 32
1.6.2 Trastuzumab: Mechanism of action 35
1.6.2.1 Cardiotoxicity of trastuzumab 35

1.7 Type I cardiotoxicity: Anthracyclines **38**
1.7.1 Cardiotoxicity of anthracyclines 39
1.7.1.1 Doxorubicin cardiotoxicity mechanisms 40
1.7.1.1.1 Iron and free radical hypothesis 40
1.7.1.1.2 Topoisomerase-dependent cardiotoxicity hypothesis 41
1.7.1.1.3 Alterations in multidrug resistance efflux proteins 43

1.7.1.1.4 Impaired calcium handling 43
1.7.1.1.5 Impact of anthracycline metabolism and metabolites on cardiotoxicity 45
1.7.1.2 Clinical manifestation of anthracycline induced cardiotoxicity 45
1.7.1.2.1 Clinical manifestation of chronic anthracycline induced cardiotoxicity 46
1.7.1.2.2 Clinical manifestation of acute anthracycline induced cardiotoxicity 48
1.7.1.3 Risk factors for anthracycline-induced cardiotoxicity 48
1.7.1.4 Detection of anthracycline-induced cardiotoxicity 49
1.7.2 Mitigation of anthracycline-induced cardiotoxicity 50
1.7.2.1 Angiotensin blockade for cardioprotection 52

1.8 Combination therapies 57
1.8.1 Clinical effect of co-administration of type I and type II cardiotoxic therapies 57

1.9 Current *in vitro* models for identification and study of drug-induced cardiotoxicity ... 59
1.9.1 The CiPA initiative and pre-clinical evaluation of drug-induced cardiotoxicity 60
1.9.2 *In vitro* cardiomyocyte cell line models 61
1.9.2.1 Induced pluripotent stem cell derived cardiomyocytes 62
1.9.3 *In vitro* cardiotoxicity assays 64
1.9.3.1 Microelectrode arrays 64
1.9.3.2 IonOptix 65
1.9.3.3 Calcium fluctuation 65
1.9.3.4 Cellular impedance assays 66

1.10 Rationale and aims 68

Chapter 2: Materials and Methods 69

2.1 Cell lines and tissue culture 69
2.1.1 Cell lines 69
2.1.2 Cell culture and maintenance of cells 69
2.1.3 Cell counting 70
2.1.4 Cryopreservation of cells 70

2.2 Cellular viability assays 70

2.3 xCELLigence real-time cell analyser 71
2.3.1 Experimental set-up 72
2.3.2 Cell seeding 72
2.3.3 Cell maintenance and compound addition 73

2.4 xCELLigence cardio system 75
2.4.1 Experimental set-up 75
2.4.1.1 Fibronectin coating of E-plate 75
2.4.1.2 Background measurement 75
2.4.1.3 Seeding of cardiomyocytes 76
2.4.2 Maintenance of cardiomyocytes 77
2.4.3 Compound treatments 77
2.4.4 Data analysis 78

Chapter 3: Qualification of In Vitro Models for Cardiotoxicity Evaluation 79

3.1 Introduction 79
3.1.1 Limitations of hERG channel screening during drug development 81
3.1.2 Pre-clinical evaluation of cardiac effects during development of oncology drugs 81
3.1.3 Improved *in vitro* models for evaluation of drug-induced cardiac effects 82
3.1.3.1 The AC10 human ventricular cardiomyocyte cell line 83
3.1.3.2 Human induced pluripotent stem cell derived cardiomyocytes 83
3.1.4 *In vitro* technologies for determination of cardiac cell contraction 85
3.1.4.1 Cellular impedance technology 85
3.1.5 Aims and objectives 88

3.2 Materials and methods 89
3.2.1 Immunostaining 89
3.2.2 Validation of the MTT assay 91
3.2.2.1 Growth curve analysis determined by the MTT assay 91
3.2.2.2 Determination of cell number required for confluence within 24 hours 91
3.2.3 Analysis of growth kinetics of AC10 cardiomyocytes using the xCELLigence RTCA system . 92
3.2.4 Determination of cellular viability of AC10-CM following exposure to angiotensin II 92
3.2.5 Determination of cellular viability of AC10-CM following exposure to sunitinib 93
3.2.6 Determination of morphological changes induced by angiotensin II and sunitinib in AC10-CM using the xCELLigence RTCA 93
3.2.6.1 Evaluation of viability of AC10-CMs following exposure to angiotensin II and sunitinib at specific time points, determined using the MTT assay 94
3.2.7 Imaging of AC10-CMs treated with angiotensin II and sunitinib 94
3.2.8 Evaluation of drug-induced cardiotoxicity in hiPSC-CM using the xCELLigence Cardio system ...95

3.3 Results 96
3.3.1 Confirmation of the cardiac phenotype of the AC10 cardiomyocyte cell line 96
3.3.2 Optimisation of cell viability assays using AC10 cardiomyocytes 99
3.3.2.1 Measurement of growth kinetics of AC10 cardiomyocytes using the MTT assay 100
3.3.2.2 Measurement of growth kinetics of AC10 cardiomyocytes using xCELLigence real time cell analyser 103
3.3.3 Optimisation and characterisation of hiPSC-derived cardiomyocytes for the xCELLigence Cardio RTCA system 105
3.3.3.1 Establishment of contractile syncytium and measurement of cellular contraction of hiPSC-derived cardiomyocytes using the xCELLigence Cardio RTCA system 106
3.3.3.2 Confirmation of drug-induced perturbation of hiPSC-derived cardiomyocytes 108
3.3.4 Qualification of ability of cardiomyocyte cell models to detect structural changes, determined following exposure to Angiotensin II 110
3.3.4.1 Angiotensin II induces morphological changes in AC10 cardiomyocytes 111
3.3.4.2 Angiotensin II induces morphological changes and functional disturbances in hiPSC-derived cardiomyocytes 113
3.3.5 Sunitinib to qualify *in vitro* models for detection of functional cardiotoxicity 117
3.3.5.1 Effect of sunitinib on viability of AC10 cardiomyocytes 117
3.3.5.2 Qualification of ability of cardiomyocyte cell models to detect functional changes following exposure to sunitinib 119
3.3.5.3 Sunitinib induces morphological changes and functional disturbances in hiPSC-derived cardiomyocytes 122

3.4 Discussion 125
3.4.1 Suitability of the AC10 cardiomyocyte cell line 125
3.4.2 Suitability of hiPSC-derived cardiomyocytes 127
3.4.3 Qualification studies with angiotensin II 129
3.4.4 Qualification of cellular models to detect drug-induced functional changes in cardiomyocyte contractility 131
3.4.5 Conclusion 134

Chapter 4: In Vitro Evaluation of Anthracycline-induced Cardiotoxicity 135

4.1 Introduction 135
4.1.1 Cardiotoxicity of the anthracycline doxorubicin 136
4.1.1.1 Clinical manifestation of doxorubicin-induced acute cardiotoxicity 137
4.1.1.2 Clinical manifestation of doxorubicin-induced delayed and chronic cardiotoxicity.. 137
4.1.2 Cardiotoxicity of the anthracycline epirubicin 139
4.1.3 Cardiotoxicity of the anthracycline daunorubicin 140
4.1.4 Risk factors for anthracycline-induced cardiotoxicity 141
4.1.5 Aims and objectives 143

4.2 Materials and methods 144
4.2.1 Evaluation of viability of AC10-CMs following anthracycline treatment determined using the MTT assay 144
4.2.2 Investigations of morphological changes to AC10-CMs induced by anthracyclines using the xCELLigence real-time cell analyser 144
4.2.2.1 Evaluation of viability of AC10-CMs following anthracycline treatment at specific time points determined using the MTT assay 145
4.2.3 Imaging of AC10-CMs treated with doxorubicin 145
4.2.4 Evaluation of anthracycline-induced cardiotoxicity in hiPSC-CMs using the xCELLigence cardio system 146

4.3 Results 147
4.3.1 Cardiomyocyte cell types are differentially sensitive to doxorubicin 147
4.3.1.1 Doxorubicin induces morphological changes in AC10 cardiomyocytes 149
4.3.1.2 Doxorubicin induces morphological changes and functional disturbances in hiPSC-derived cardiomyocytes 152
4.3.2 Anthracyclines exhibit similar toxicity profiles in cardiomyocyte cell models 155
4.3.2.1 Anthracyclines induce morphological changes in AC10 cardiomyocytes 158
4.3.2.2 Anthracyclines induce similar morphological changes and functional disturbances in hiPSC-derived cardiomyocytes 161

4.4 Discussion 164
4.4.1 *In vitro* assessment of doxorubicin-induced cardiotoxicity 164
4.4.2 Comparative studies using the anthracyclines doxorubicin, daunorubicin and epirubicin 167
4.4.3 Translatability of *in vitro* comparative anthracycline studies 170
4.4.4 Conclusion 172

Chapter 5: In Vitro Evaluation of Angiotensin Blockade as a Strategy to Minimise Anthracycline-Induced Cardiotoxicity 173

5.1 Introduction 173
5.1.1 Clinical studies investigating cardiotherapeutic drugs to mitigate anthracycline-induced cardiotoxicity 173
5.1.1.1 Clinical studies investigating angiotensin blockade for cardioprotection against anthracycline-induced cardiotoxicity 174
5.1.2 Pre-clinical *in vivo* studies investigating angiotensin blockade for cardioprotection 176
5.1.3 Aims and objectives 178

5.2 Materials and methods 179
5.2.1 Determination of viability of proliferating AC10-CMs in response to different drug treatment protocols using the MTT assay 179
5.2.1.1 Evaluation of viability of AC10-CMs following treatment with doxorubicin and angiotensin II 179
5.2.1.2 Investigations into viability of AC10-CMs following treatment with drugs targeting the angiotensin pathway 179
5.2.1.3 Investigations into viability of AC10-CMs following combination treatment with angiotensin targeting drugs and doxorubicin 180
5.2.1.4 Investigations into viability of H460 lung cancer cells following combination treatment with telmisartan/losartan and doxorubicin 180
5.2.2 Determination of morphological changes to proliferating AC10-CMs in response to different drug treatment protocols using the xCELLigence real-time cell analyser 181
5.2.2.1 Investigations into morphology of AC10-CMs following combination treatment with doxorubicin and angiotensin II 181
5.2.2.1.1 Evaluation of viability of AC10-CMs following treatment with doxorubicin and angiotensin II at specific time points determined using the MTT assay 182
5.2.2.2 Investigations into morphology of AC10-CMs following treatment with telmisartan and losartan 182

5.2.2.3 Investigations into morphology of AC10-CMs following combination treatment with telmisartan/losartan and doxorubicin 183
5.2.3 Evaluation of contractility and morphology of hiPSC-CMs following exposure to different treatment protocols using the xCELLigence cardio system 183

5.3 Results 185
5.3.1 Angiotensin II does not alter the sensitivity of AC10 cardiomyocytes to doxorubicin 185
5.3.2 Angiotensin II does not affect the morphology of AC10 cardiomyocytes exposed to doxorubicin 187
5.3.3 Effect of a combination of angiotensin II and doxorubicin on morphology and contractility of hiPSC-derived cardiomyocytes 189
5.3.4 Cytotoxicity of angiotensin receptor blockers and angiotensin converting enzyme inhibitors against AC10 cardiomyocytes 192
5.3.5 Angiotensin receptor blockade increases the viability of AC10 cardiomyocytes treated with doxorubicin 194
5.3.6 Angiotensin receptor blockade does not decrease the therapeutic efficacy of doxorubicin in H460 lung cancer cells 194
5.3.7 Angiotensin receptor blockade reduces morphology changes induced by doxorubicin in AC10 cardiomyocytes 197
5.3.8 Angiotensin receptor blockade reduces doxorubicin-induced changes to morphology but does not affect contractility of hiPSC-derived cardiomyocytes 199

5.4 Discussion 202
5.4.1 Synergistic effects of angiotensin II and doxorubicin treatment 202
5.4.2 Synergistic effects of doxorubicin with concurrent angiotensin converting enzyme inhibitor and angiotensin receptor blocker treatment 204
5.4.3 Conclusion 209

Chapter 6: Molecular relationship between the angiotensin signalling pathway and anthracycline-induced cardiotoxicity 210

6.1 Introduction 210
6.1.1 Angiotensin signalling pathways in the cardiac system 210
6.1.2 Perturbation of the angiotensin signalling pathway as a therapeutic strategy 211
6.1.3 Inhibition of Angiotensin signalling for mitigation of anthracycline-induced cardiotoxicity 212
6.1.4 Aims and objectives 215

6.2 Materials and methods 216
6.2.1 Evaluation of protein expression by western blotting: *Cell lysate preparation of AC10 cardiomyocytes* 216
6.2.1.1 Evaluation of protein expression by western blotting: *Polyacrylamide gel electrophoresis and membrane transfer* 217
6.2.1.2 Evaluation of protein expression by western blotting: *Antibody probing and protein detection* 219
6.2.2 Analysis of anthracycline-induced changes to gene expression relating to cardiotoxicity and angiotensin signalling 220
6.2.2.1 Production of cDNA from AC10 cardiomyocytes 220
6.2.2.2 Pre-array verification of cDNA quality 222
6.2.2.3 Real-time PCR of Gene expression arrays 223

6.3 Results 224
6.3.1 Optimisation of western blotting for detection of the ATR1 224
6.3.2 Doxorubicin increases the expression of the ATR1 in AC10 cardiomyocytes 227
6.3.3 Pre-array verification of cDNA quality 230
6.3.4 Doxorubicin alters expression of genes associated with cardiotoxicity in AC10 cardiomyocytes 231
6.3.5 Doxorubicin alters expression of genes associated with GPCR signalling in AC10 cardiomyocytes 234

6.4 Discussion 238
6.4.1 Analysis of ATR1 expression in AC10 cardiomyocytes 238
6.4.2 Molecular interactions between angiotensin signalling and anthracycline-induced cardiotoxicity 240
6.4.2.1 Gene changes relating to anthracycline-induced cardiotoxicity mechanisms 240
6.4.2.2 Gene changes relating to anthracycline-induced cardiotoxicity and angiotensin signalling 241
6.4.2.3 Gene changes relating to angiotensin signalling 243
6.4.3 Conclusion 246
Chapter 7: Final discussion 247
7.1 Conclusion 258
References 259
Appendix 1: Conference Abstracts 276
Appendix 2: Axol application note 285
Appendix 3: Publications 288
Appendix 4: Solutions and gels 301
Appendix 5: Preliminary RT-PCR studies 304

List of figures

Figure 1.1 Ultrastructure of cardiomyocytes 11

Figure 1.2 Cardiac excitation-contraction coupling 14

Figure 1.3 Process of G-protein coupled receptor (GPCR) signal transduction showing ATR1 signalling as an example 21

Figure 1.4 Comparison of the characteristics of type I and type II cardiotoxicity 30

Figure 1.5 Cardiotoxicity mechanism of the multi-targeted tyrosine kinase inhibitor sunitinib .. 34

Figure 1.6 Cardiotoxicity mechanisms of the HER2 targeted therapy trastuzumab 37

Figure 1.7 Malignancies commonly treated with doxorubicin 38

Figure 1.8 Anthracycline cardiotoxicity mechanisms 44

Figure 1.9 Angiotensin II synthesis and pharmaceutical inhibition 53

Figure 2.1 Principle of impedance based cell detection 72

Figure 2.2 Cell growth monitoring using the xCELLigence impedance-based system 74

Figure 3.1 Relationship between the ventricular action potential and ionic currents 80

Figure 3.2 Effect of hERG channel inhibition on cardiac rhythm 80

Figure 3.3 The relationship between action potential (AP), $[Ca^{2+}]_i$ and cellular contraction 87

Figure 3.4 Immunostaining of AC10 cardiomyocytes for cardiac proteins 97

Figure 3.5 Immunostaining of AC10 cardiomyocytes for other proteins of interest 98

Figure 3.6 Validation of the MTT assay in AC10 cardiomyocytes 99

Figure 3.7 Growth curves of AC10 cardiomyocytes generated using MTT assay 101

Figure 3.8 Optimisation of seeding density for MTT studies in plateau growth phase 102

Figure 3.9 Growth kinetics of AC10 cardiomyocytes 104

Figure 3.10 Immunostaining of Cor4u hiPSC-derived cardiomyocytes for cardiac proteins 105

Figure 3.11 Initial growth hiPSC-derived cardiomyocytes 106

Figure 3.12 Assessment of initial contractility of hiPSC-derived cardiomyocytes 107

Figure 3.13 Effect of isoprotenerol and E-4031 on contractility of hiPSC-derived cardiomyocytes 108

Figure 3.14 Analysis of the effect of isoprotenerol and E-4031 on contractility of hiPSC-derived cardiomyocytes 109

Figure 3.15 Effect of angiotensin II on viability of AC10 cardiomyocytes 110

Figure 3.16 Angiotensin II causes hypertrophy of AC10 cardiomyocytes 112

Figure 3.17 Effect of angiotensin II on morphology of hiPSC-derived cardiomyocytes 114

Figure 3.18 Effect of 72 hours angiotensin II exposure on contractility of hiPSC-derived cardiomyocytes 115

Figure 3.19 Immediate effect of angiotensin II exposure on contractility of hiPSC-derived cardiomyocytes 116

Figure 3.20 Chemosensitivity studies with sunitinib in AC10 cardiomyocytes 118

Figure 3.21 Effect of sunitinib on morphology of AC10 cardiomyocytes in exponential growth phase..... 120

Figure 3.22 Effect of sunitinib on morphology of AC10 cardiomyocytes in plateau growth phase..... 121

Figure 3.23 Effect of sunitinib on morphology of hiPSC-derived cardiomyocytes 123

Figure 3.24 Effect of 72 hours sunitinib exposure on contractility of hiPSC-derived cardiomyocytes 124

Figure 4.1 Structures of the anthracyclines doxorubicin, epirubicin and daunorubicin 142

Figure 4.2 Effect of doxorubicin on viability of AC10 cardiomyocytes..... 148

Figure 4.3 Doxorubicin induces morphological changes in AC10 cardiomyocytes 150

Figure 4.4 Doxorubicin induces morphological changes in hiPSC-derived cardiomyocytes 153

Figure 4.5 Doxorubicin induced changes to contractility of hiPSC-derived cardiomyocytes 154

Figure 4.6 Anthracyclines exhibit similar toxicity profiles in AC10 cardiomyocytes following 24 hours exposure and a 72 hour recovery period 156

Figure 4.7 AC10 cardiomyocytes in the exponential growth phase are more sensitive than cells in plateau growth phase to anthracyclines following 96 hours exposure 157

Figure 4.8 Anthracyclines induce morphological changes of AC10 cardiomyocytes in exponential growth phase 159

Figure 4.9 Anthracyclines induce morphological changes of AC10 cardiomyocytes in plateau growth phase 160

Figure 4.10 Anthracyclines induce morphological changes in hiPSC-derived cardiomyocytes.. 162

Figure 4.11 Anthracycline induced changes to contractility of hiPSC-derived cardiomyocytes are greater following 24 hours exposure 163

Figure 5.1 Angiotensin II does not alter the sensitivity of AC10 cardiomyocytes to doxorubicin 186

Figure 5.2 Angiotensin II does not affect the morphology of AC10 cardiomyocytes exposed to doxorubicin..... 188

Figure 5.3 Effect of doxorubicin and angiotensin II on morphology of hiPSC-derived cardiomyocytes 190

Figure 5.4 Effect of a combination of doxorubicin and angiotensin II exposure on contractility of hiPSC-derived cardiomyocytes 191

Figure 5.5 Cytotoxicity of angiotensin receptor blockers and angiotensin converting enzyme inhibitors against AC10 cardiomyocytes 193

Figure 5.6 The effect of a combination of angiotensin targeting drugs and doxorubicin on viability of AC10 cardiomyocytes..... 195

Figure 5.7 Angiotensin receptor blockade does not decrease the therapeutic efficacy of doxorubicin in H460 lung cancer cells 196

Figure 5.8 Angiotensin receptor blockade reduces morphology changes induced by doxorubicin in AC10 cardiomyocytes 198

Figure 5.9 Angiotensin receptor blockade reduces doxorubicin-induced changes to morphology of hiPSC-derived cardiomyocytes 200

Figure 5.10 Angiotensin receptor blockade does not affect contractility of hiPSC-derived cardiomyocytes exposed to doxorubicin 201

Figure 5.11 Angiotensin II synthesis in the myocardium 205

Figure 6.1 Gel and PVDF membrane sandwich for protein transfer 218

Figure 6.2 The ATR1 is absent from the soluble fraction of AC10 cardiomyocyte cell lysates ... 225

Figure 6.3 The ATR1 is present in the insoluble fraction of AC10 cardiomyocyte cell lysates ... 226

Figure 6.4 Doxorubicin increases the expression of the ATR1 in AC10 cardiomyocytes 228

Figure 6.5 Doxorubicin treatment increases the expression of the ATR1 in AC10 cardiomyocytes – Densitometric analysis 229

Figure 6.6 GAPDH was detected at equal levels in cDNA generated from untreated and doxorubicin treated AC10 cardiomyocytes 230

Figure 6.7 Changes in gene expression profile of 84 genes involved in cardiotoxicity following doxorubicin exposure in AC10 cardiomyocytes 231

Figure 6.8 Doxorubicin alters expression of genes associated with cardiotoxicity in AC10 cardiomyocytes 232

Figure 6.9 Changes in gene expression profile of 84 genes involved in GPCR signalling following doxorubicin exposure in AC10 cardiomyocytes 234

Figure 6.10 Doxorubicin alters expression of genes associated with GPCR signalling 235

Figure 6.11 Molecular changes in doxorubicin treated AC10 cardiomyocytes that potentially signify a relationship between anthracycline-induced cardiotoxicity and the angiotensin signalling pathway via the ATR1 245

List of tables

Table 1.1 Possible cardiovascular damage caused by conventional chemotherapies and molecularly targeted therapies 28

Table 1.2 Summary of clinical studies investigating the use of ACEi and ARB for cardioprotection during anthracycline containing regimens 54

Table 3.1 Antibodies used for immunostaining evaluation of cardiac phenotype of AC10 cardiomyocytes 90

Table 3.2 IC_{50} values of sunitinib in AC10 cardiomyocytes 118

Table 4.1 IC_{50} values in AC10-CMs following 24 hours exposure to anthracyclines in the exponential and plateau phases of growth 156

Table 4.2 IC_{50} values in AC10-CMs following 96 hours exposure to anthracyclines in the exponential and plateau phases of growth 157

Table 5.1 IC_{50} values of AC10 cardiomyocytes and H460 lung cancer cells treated with doxorubicin alone and in combination with 1µM/5µM telmisartan and losartan for 96 hours. 196

Table 6.1 Characteristics of antibodies used in this study 219

Table 6.2 Doxorubicin alters expression of genes associated with cardiotoxicity in AC10 cardiomyocytes 233

Table 6.3 Doxorubicin alters expression of genes associated with GPCR signalling in AC10 cardiomyocytes 236

List of abbreviations

ABC	ATP-binding cassette
AC10-CM	AC10 cardiomyocyte cell line
ACE	Angiotensin converting enzyme
ACEi	Angiotensin converting enzyme inhibitor
ADRA2A	α2A-adrenergic receptor
AIC	Anthracycline-induced cardiotoxicity
AML	Acute myelogenous leukaemia
AngII	Angiotensin II
AMPK	Adenosine monophosphate activated kinase
ANOVA	Analysis of variance
ARB	Angiotensin receptor blocker
ATCC	American tissue culture collection
ATP	Adenosine triphosphate
ATR	Angiotensin receptor
ATR1	Angiotensin receptor type 1
ATR2	Angiotensin receptor type 2
BSA	Bovine serum albumin
Ca^{2+}	Calcium ions
cAMP	Cyclic adenosine monophosphate
cDNA	Complimentary DNA
cGMP	Cyclic guanosine monophosphate
CHF	Congestive heart failure
CICR	Calcium induced calcium release

CiPA	Comprehensive *in vitro* proarrhythmia assay
CML	Chronic myelogenous leukaemia
CMR	Cardiac magnetic resonance
CRH	Corticotropin-releasing hormone
CRHR1	Corticotropin-releasing hormone receptor 1
CT	Threshold cycle value
cTnT	Cardiac troponin T
Cx43	Connexin-43
DAG	Diacylglycerol
DAPI	4',6-diamidino-2-phenylindole
DAUN	Daunorubicin
DMEM	Dulbecco's Modified Eagle Medium
DMI	Doppler myocardial imaging
DMSO	Dimethyl sulfoxide
DNA	Deoxyribonucleic acid
DOX	Doxorubicin
DUS8	Dual specificity phosphatase 8
ECG	Electrocardiogram
ECHO	Echocardiogram
ECL	Enhanced chemiluminescence solution
ECM	Extracellular matrix
EDTA	Ethylenediaminetetraacetic acid
EGF	Epithelial growth factor
EGFR	Epithelial growth factor receptor
EPI	Epirubicin

E-plate	Electrode plate
ER	Oestrogen receptor
ERK	Extracellular signal-regulated protein kinase
FBS	Foetal bovine serum
Fe^{2+}	Iron ions
FEC	5-flurouracil/epirubicin/cyclophosphamide
GIST	Gastrointestinal stromal tumors
GPCR	G-protein coupled receptor
HAMP	Hepcidin antimicrobial peptide
HBSS	Hanks balanced salt solution
HER2	Human epidermal growth factor receptor 2
hERG	Human Ether-à-go-go-Related Gene
hESC-CMs	Human embryonic stem cell derived cardiomyocytes
hiPSC-CM	Human induced pluripotent stem cell derived cardiomyocytes
IC_{50}	Inhibitory concentration, 50%
IL-10	Interleukin 10
IP_3	Inositol (1,4,5)-trisphosphate
iPSC-CMs	Induced pluripotent stem cell derived cardiomyocytes
IRP	Iron regulatory protein
KO	Knock out
LDL	Low density lipoprotein
LTCC	L-type Ca^{2+} channels
LVD	Left ventricular dysfunction
LVEF	Left ventricular ejection fraction
MAb	Monoclonal antibody

MAPK	Mitogen-activated protein kinase
MDR	Multidrug resistance
MEA	Microelectrode array
Mg^{2+}	Magnesium ions
MMP	Matrix metalloproteinase
MtDNA	Mitochondrial DNA
MTT	3-(4,5-Dimethylthiazol-2-yl)-2,5-Diphenyltetrazolium Bromide
MUGA	Radionuclide ventriculography multi-gated acquisition scan
Na^{+}	Sodium ions
NCX	Sodium-calcium exchangers
NO	Nitric oxide
NRG	Neuregulin
NSAID	Non-steroidal anti-inflammatory drug
NSCLC	Non-small cell lung cancer
PBS	Phosphate buffered saline
PCR	Polymerase chain reaction
PDGFR	Platelet-derived growth factor receptor
PFA	Paraformaldehyde
PI3K	Phosphoinositide 3-kinase
PKA	Protein kinase A
PKC	Protein kinase C
PKG	Protein kinase G
PLC	Phospholipase C
PPARγ	Peroxisome proliferator activated receptor-γ
PSMA2	Proteasome subunit, alpha type, 2

PTH1R	Parathyroid hormone receptor 1
PVDF	Polyvinylidene difluoride
qRT-PCR	Real-time PCR
RAS	Renin-angiotensin system
RCT	Randomised controlled trial
RCC	Renal cell carcinoma
RIRR	ROS-induced ROS release
RNA	Ribonucleic acid
RPMI	Roswell Park Memorial Institute
ROS	Reactive oxygen species
RTCA	Real-time cell analyser
RTK	Receptor tyrosine kinase
RT-PCR	Reverse transcriptase polymerase chain reaction
RyR	Ryanodine receptor
SERCA	Sarcoplasmic reticulum Ca^{2+} ATPase
SOD2	Superoxide dismutase 2
SOX4	SRY (sex determining region Y)-box 4
SV40	Simian Virus 40
T-tubules	Transverse tubules
TAE	Tris-Acetate buffer
TBS-T	Tris-buffered saline with Tween-20
TdP	Torsades de Pointes
TKI	Tyrosine kinase inhibitor
TopImt	Mitochondrial topoisomerase I
TopIIα	Topoisomerase IIα

TopIIβ	Topoisomerase Iiβ
UCP1	Uncoupling protein 1
VCAM-1	Vascular cell adhesion molecule 1
VEGF	Vascular endothelial growth factor
VEGFR	Vascular endothelial growth factor receptor
WT	Wild type

Chapter 1: Introduction

1.1 Cancer

Cancer is a broad and complex family of diseases that can affect all tissues of the body. There are more than 100 distinct types of cancer, and subtypes of tumours can be found within specific organs. Although cancer has multiple causes and exhibits a wide range of genetic, physiological and histological features, an acceptable clinical definition states that cancer is a set of diseases characterised by upregulated cell growth leading to invasion of surrounding tissues and metastasis to different parts of the body.[1,2]

1.1.1 Increasing prevalence of cancer survivors

There are reportedly over 200 different pathological types of human cancer affecting all tissues of the body, with approximately 350,000 new cases of adult and paediatric cancers diagnosed per year in the UK. Furthermore, cancer is the second major cause of mortalities, responsible for the deaths of approximately 163,000 people in the UK per year. Consequently, it is now estimated that one person in two will be diagnosed with cancer during their lifetime and one in four will die of cancer.[3] However, as a consequence of extended life expectancy and an increase in the global population, it is predicted that over the next decade the prevalence of cancer would significantly increase, but due to better prediction and treatment the number of deaths from cancer should hopefully decrease. In this context, an upwards trend in both cancer incidence and survival has been observed in the United Kingdom in recent years, with today's cancer patients benefitting from life expectancies ten times longer than their counterparts 40 years ago.[4] In addition, future mortality rates are envisaged to decrease by 15.3% from 2014-2035,[5] thereby further increasing the size of the cancer survivor group. The improved prognosis that cancer patients now possess is prospectively due to both the general growth of the aging

population as a result of improved treatments for life shortening conditions, and more crucially, advancements in cancer screening, diagnosis and treatments.[6]

The total number of cancer survivors in the United Kingdom has been predicted to escalate by one million each decade from 2010 – 2040, assuming existing trends continue. According to these predicted trends there will be three million cancer survivors in the United Kingdom in 2020, with varied and often complex care needs bringing additional challenges to healthcare professionals.[7]

1.2 Management of cancer

Chemotherapy is the most widely used type of treatment for cancer and can be used at different stages of disease progression. Conventionally chemotherapy is directed at disrupting cell proliferation, targeting one or more of the hallmarks of cancer.[1] Currently, the majority of agents in clinical use are systemic anti-proliferative agents that target cells undergoing rapid growth by attacking DNA or the processes involved in DNA replication.[8] These established chemotherapeutic agents can be categorised according to their mode of action including DNA interacting agents, antimetabolites, antimicrotubule agents and topoisomerase inhibitors, described below.

However, although these drugs are able to kill large numbers of tumour cells their efficacy is limited by the damage they cause to proliferating normal cells such as in the cardiovascular system, gastrointestinal tract and bone marrow.[8] The therapeutic window for tumour versus normal tissue is modest with anti-proliferative compounds, toxic side effects are the norm and the development of resistance often occurs.[9]

1.2.1 DNA interacting agents

Alkylating agents such as cyclophosphamide, together with the platinum based agents such as cisplatin, act by covalently binding alkyl groups of cellular macromolecules such as DNA and protein. Such agents react covalently with DNA bases to form DNA adducts and cross links which disrupt the structure and processing of DNA leading to inhibition of replication, DNA mispairing and consequently the induction of cell death pathways.[10]

Cyclophosphamide is used to treat a variety of cancers including haematological cancers and solid tumours originating from the lung, breast, ovaries and brain. Due to the inability of these drugs to differentiate from rapidly dividing tumour cells and rapidly dividing healthy cells, many acute toxicities occur due to the drug's effects on proliferating healthy cells. Reduction in the numbers of white blood cells, platelets and red blood cells can cause an increased risk of infection, bruising and anaemia respectively. Similarly, mucosal membranes are associated with a high turnover rate and hence toxicities such as bladder irritation, mouth ulcers and vomiting are also common. The hair, skin and nails can also be affected with side effects including hair loss, dry skin, skin rashes, brittle nails, nail discolouration occurring in most patients.[11]

More serious side effects include decreases in fertility, development of secondary cancers and disturbances in heart function. Cardiac toxicity is a less common side effect, and generally occurs after a single cycle of a high dose regimen; causing a haemorrhagic necrosis that can be life threatening and, on rare occasions, fatal. In contrast to the usual progressive nature of heart failure, cardiac failure associated with cyclophosphamide can be seen as early as several days following administration, which illustrates the severity of this side effect.[11,12]

1.2.2 Topoisomerase interactive agents

Nuclear topoisomerase enzymes play a crucial role in the normal replication of DNA. In its physiological state in the chromosome, the DNA helix is supercoiled and replication requires

transient relaxation and unwinding of the parent DNA. In order to achieve this, cleavage of the DNA is required. This is mediated by the formation of a cleavable complex consisting of a covalent intermediate between topoisomerase and DNA, allowing passage of the intact strand and subsequent DNA unwinding, followed by re-ligation of the DNA strands.[13] This is crucial for protein synthesis where strands of the DNA double helix must be uncoiled for transcription to take place and subsequently recoiled.

Topoisomerase inhibitors prevent the re-ligation of the DNA strands by stabilising the complex of topoisomerase enzyme and DNA. The most common class of topoisomerase inhibitor used in the clinic are the anthracycline-class of topoisomerase II inhibitors. The DNA damage and fragments produced by these agents directly block cell replication and trigger cell death pathways.[14] Anthracyclines such as doxorubicin are among the most effective anti-cancer agents introduced in the past 50 years, and are commonly used in treatment of cancers of the breast, stomach and lung and also in haematological malignancies. Due to their inhibitory effect on DNA replication, and therefore on all rapidly proliferating cells, anthracyclines are associated with many of the acute toxicities associated with cyclophosphamide treatment described above.[15]

More serious side effects include peripheral neuropathy, development of secondary cancers and disturbances in heart function.[15] The most severe side-effect associated with anthracyclines is the development of cardiotoxicity, so much so that it is considered the prototypical anti-cancer drug to cause permanent therapy-induced cardiotoxicity. Unlike cyclophosphamide induced toxicity which can occur rapidly, anthracycline induced cardiotoxicity is cumulative and related to the maximum lifetime dose. Usually manifesting as left ventricular dysfunction, cardiotoxicity can occur acutely, or more frequently the damaging effects are dormant until many years after the completion of therapy and can culminate in heart failure.[16,17] Both the acute toxicities associated with chemotherapy, and the more severe permanent cardiac liabilities have

prompted the search for therapies that are more specific towards tumour cells whilst sparing healthy cells from toxicities.

1.2.3 Molecular targeted therapies

Over the past decade, a more advanced, although still primitive, understanding of the molecular biology of cancer has contributed to the process of discovery and development of anticancer agents from classical cytotoxic drugs to target-led, rationally designed agents. These compounds are designed to expand beyond disrupting DNA replication and exploit defined abnormalities responsible for the causation, maintenance or progression of human tumours such as genetic instability, aberrant cell cycle control, invasion, angiogenesis and the ability to metastasise.[18]

The identification of aberrant signalling pathways in cancer has led to the development of therapies that target specific oncogenic processes. The initial wave of molecular therapeutics favour the receptor tyrosine kinase (RTK)- Ras- Raf-1- extracellular signal-regulated protein kinase (ERK) signal transduction pathway.[19] This pathway was one of the earliest pathways to be understood and is frequently deregulated in human cancer. Both epithelial growth factor receptors (EGFR) and Ras genes often possess activating mutations which lead to the persistent stimulation of downstream pathways essential for cancer progression. A number of RTK inhibitors have been directed towards the EGFR and other RTKs implicated in signalling pathways important in cancers.[20] Several RTK inhibitors are now used in the clinic: Trastuzumab (Herceptin) for the treatment of HER2 positive breast cancers, Imatinib (Gleevec) for the treatment of chronic myelogenous leukaemia (CML), gliomas and gastrointestinal-stromal tumours, and Gefitinib (Iressa) for the treatment of non-small cell lung cancer (NSCLC). Other agents currently undergoing phase I/II clinical trial in NSCLC include Nazartinib (EGF816) and Avitinib (AC0010). The occurrence of developing resistance to RTK inhibitors is unfortunately commonplace, often due to the acquisition of mutations that prevent the inhibitors binding to

their target.[21] Nazartinib and Avitinib are third generation inhibitors and will hopefully remedy issues of resistance associated with the existing RTK inhibitors used to treat NSCLC.[22]

In contrast to expectations, these molecular targeted agents exhibit a range of toxicities, albeit different to the conventional DNA interacting agents. Often, the toxicities that occur are specific to the class of targeted therapy. For example, inhibitors of the EGFR such as gefitinib (Iressa) are associated with the development of skin, nail and hair reactions which occur in approximately 50% of patients. The most common of these adverse effects is an acneiform rash that usually appears on the face or upper body.[23] Within the epidermis of the skin the EGFR plays a critical role and is highly expressed in keratinocytes which form the majority of the epidermis.[24] Inhibition of EGFR signalling is thought to alter keratinocyte behaviour including proliferation, differentiation, attachment and migration. Due to the importance of EGFR signalling in the skin, the coincident inhibition of EGFR signalling in the skin may be responsible for the occurrence of dermatological toxicities in cancer patients treated with EGFR inhibitors.[25]

Specific toxicities also occur with therapies that target the vascular endothelial growth factor receptor (VEGFR), termed angiogenesis inhibitors, such as Bevacizumab (Avastin). The primary side-effect of this drug class is hypertension which occurs so frequently it is considered a biomarker of therapeutic efficacy.[26] VEGFR signalling is important in the normal vasculature and plays a role in vascular density and generation of the vasodilatory mediator nitric oxide (NO). Inhibition of this signalling by angiogenesis inhibitors used in cancer management results in vascular rarefaction and decreased NO which both contribute to hypertension by increased peripheral resistance and vasoconstriction.[27]

Although usually not life-threatening, the toxicities that arise from targeted therapies can decrease the quality of life for patients and can also require temporary treatment interruptions which could reduce therapeutic efficacy. Fortunately, the toxicities are usually reversible, and disappear upon the completion of treatment. This is especially pertinent with the occurrence

of toxicity to the cardiovascular system as the therapy-induced toxicity is less likely to adversely affect their long-term health, and is associated with a more favourable prognosis compared to cardiotoxicity induced by some chemotherapies.

1.3 Cancer therapy induced cardiotoxicity

Although increased understanding of the molecular basis of cancer over the past decade has advanced cancer chemotherapy, and many of these medicines have significantly improved cancer treatment and patient survival, it is now clear that their benefit is counterbalanced by adverse toxic effects, particularly upon the cardiovascular system.[28,29] The improved success of cancer treatment has in itself created issues regarding cardiovascular toxicity, as the prolonged patient survival allows the patient to live long enough to encounter the long-term detrimental effects of the particular therapeutic. The risk of patients developing cardiovascular related health problems post cancer treatment represents an extra hurdle for both patients and health professionals and can pose more of a threat to patients than the development of cancer recurrence.[30,31] A situation then arises in which cardiovascular toxicity can be the main determinant of quality of life and potentially be responsible for premature death, as opposed to cancer. In fact, the risk of death from cardiac related toxicities may exceed the risk of recurrence for many forms of cancer[32] and cancer survivors are estimated to be 15 times more likely to develop heart failure and 10 times more likely to develop coronary disease than their siblings.[33] Both the probability of developing cancer therapy induced cardiotoxicity and the severity of the problem depends on various patient specific factors such as age, sex and the presence of cardiovascular co-morbidities. Consequently, challenges exist with respect to identifying, managing or at least monitoring cancer-therapy related cardiovascular toxicity, to provide the most beneficial cancer treatment, and ultimately improve patient outcomes and longer-term healthcare.[34]

1.3.1 Emergence of cardio-oncology

Increases in the survival rate of patients with cardiovascular diseases have also been observed during the past three decades, which can be attributed to improved treatments and greater awareness of risk factors.[35] As a result of the increased incidence and prevalence of both cardiovascular disease and cancer, the number of patients that present with both conditions is increasing.[36] Human diversity further complicates the issue, with cancer patients coming from wide-ranging health backgrounds with varied baseline susceptibilities to cardiovascular toxicity. Common risk factors for development of cardiovascular disease include hypertension, stress, diabetes mellitus, obesity, lack of exercise and poor diet.[37] Based on these environmental and health factors, a higher likelihood for cardiovascular disease exists in the cancer population than the general population.[38]

Cardiovascular co-morbidities such as heart disease and hypertension can amplify the problem of drug-induced cardiotoxicity, as patients already have a reduced cardiac reserve, making them already one stop closer to developing complications with their heart function even before the challenge of cancer and administration of a potentially cardiotoxic therapy. For these reasons it is important that cardiovascular issues are identified and the associated risks are managed, minimised and evaluated throughout a patients' cancer treatment and beyond. This includes assessment of cardiovascular risk factors at baseline and tailoring of a suitable treatment plan that takes in to account both the existing damage and the amount of additional insults to the cardiovascular system that could be tolerated. This information would allow for a more informed decision on the type and amount of cancer therapy that could be given without causing additional cardiovascular harm, whether administration of cardioprotective drugs is necessary and how frequently monitoring of heart function and biomarkers indicative of early cardiac damage should be assessed.[39]

This forms the basis of the emerging discipline termed cardio-oncology, which aims to develop interdisciplinary expertise to effectively treat a patients cancer whilst minimising any collateral damage to the cardiovascular system.[40,41] Although cardiotoxicity is prevalent in the cancer survivor group in general, sensitivity can vary greatly between individuals, suggesting differing genetic variations or predispositions to drug-induced cardiovascular toxicity within the cancer patient population.[42] Therefore, in order to create safer yet still effective cancer treatments, a much greater appreciation of the underlying molecular mechanisms by which current therapies cause adverse effects upon the cardiovascular system and how to predict these toxicities before they arise in the clinic is required.

1.4 The cardiovascular system

The average human body contains approximately five litres of blood that is constantly travelling around the vascular system to provide an adequate supply of oxygen and nutrients to the organs, whilst simultaneously removing waste products. Also responsible for the transport of hormones and immune cells to their required sites of action; the cardiovascular system is multi-functional and essential for sustaining life. As such, it is the first functional organ to develop during embryonic development,[43] with a spontaneous heart beat arising by week four of development. Within the cardiovascular system the heart and the peripheral vasculature form a closed circulatory system where the heart is the central component. Structurally composed of four chambers, the heart is formed from specialised striated cardiac muscle surrounded by a dense coronary microvascular network that ensures the high metabolic requirements of the myocardial tissue are met.[44] A heterogeneous mixture of support cells and cardiomyocytes complete the myocardial tissue; in which the cardiomyocytes are the cell type responsible for the generation of contractile force.

1.4.1 Cardiomyocytes: The contractile unit of the heart

The heart fulfils its role of maintaining constant circulation of blood through the vascular system by its ability to continuously pump without interruption, cycling between relaxing (diastole) and contracting (systole).[44] The capability to contract in this rhythmic manner is due to the close co-ordination of cardiomyocytes which represent 30% of cells in the myocardium, the others being cardiac fibroblasts, microvascular endothelial cells and pericytes (described below). Due to the large size of cardiomyocytes, although they only constitute 30% of cell type, they are estimated to make up approximately 85% of the volume of the myocardium.[45] During embryogenesis the appropriate signals initiate the differentiation of these specialised cells from stem cells, which in their mature form contain an abundance of mitochondria and highly organised repeating arrangements of myofilaments called sarcomeres (Figure 1.1).[46] The main components of sarcomeres are thin actin filaments and thick myosin filaments, which shorten sarcomere length by sliding past each other. This forms the basis of the sliding filament theory of muscle contraction whereby the co-ordinated multi-sarcomere shortening triggers contraction of the cardiomyocyte.[47] As the myocardium exists as a syncytium, co-ordinated cardiomyocyte contractions occur which culminate in ventricular contraction and the expulsion of blood around the body.

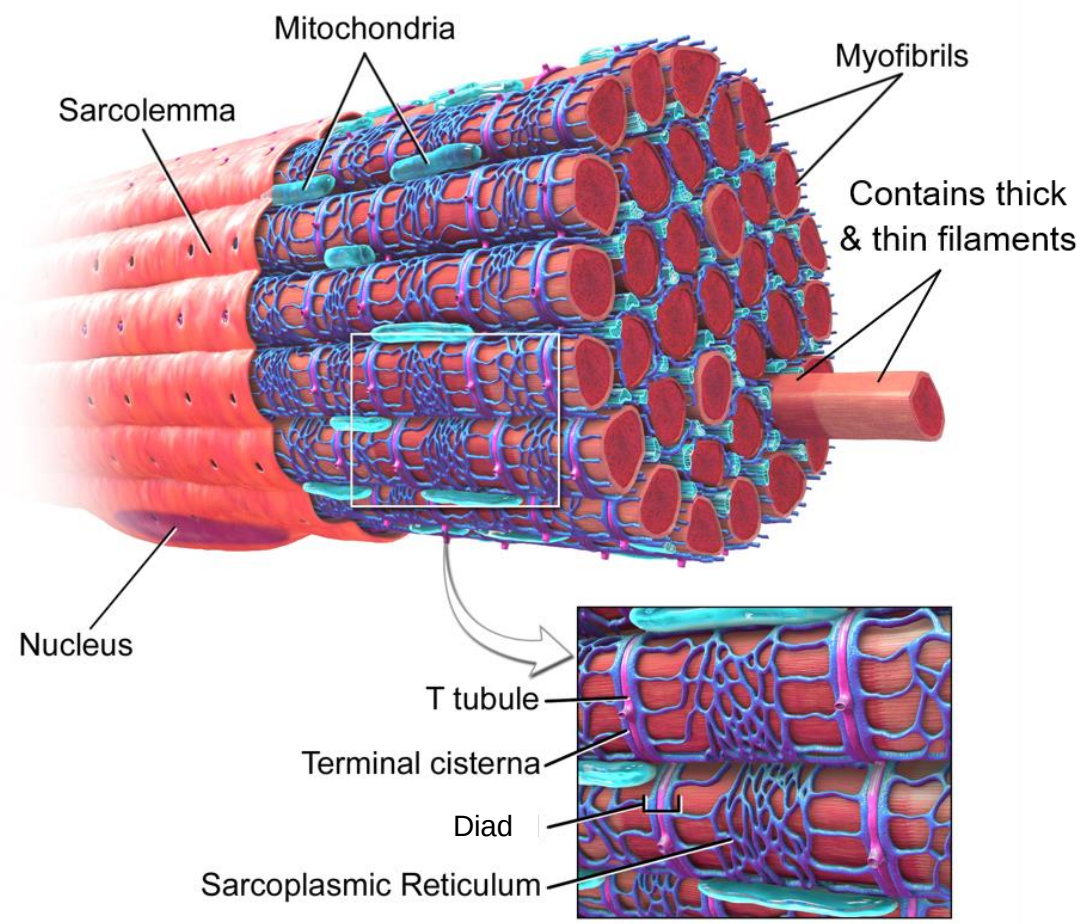

Figure 1.1 Ultrastructure of cardiomyocytes

Cardiomyocytes are specialised muscle cells composed of myofibrils that contain repeating arrangements of myofilaments called sarcomeres. T-tubules and sarcoplasmic reticulum are specialised organelles required for contraction that can form a diad structure. Adapted from reference.[48]

1.4.2 Generation of contractile force: Excitation-contraction coupling

Cardiac excitation-contraction coupling describes the series of events required to translate an electrical impulse into mechanical contraction (Figure 1.2). This process is ultimately regulated by of adenosine triphosphate (ATP) and calcium ions (Ca^{2+}), where presence of the ions elicit contraction, and subsequent dissociation causes relaxation of the myocardium.[49]

The pacemaker cells of the heart spontaneously initiate an electrical impulse in the form of an action potential which propagates through the heart causing membrane depolarisation. The action potentials utilise gap junctions to jump through cells, travel along the sarcolemma, and penetrate the cells in deep invaginations of the sarcolemma known as transverse tubules (T-tubules). The highly specialised extensive T-tubule network that cardiomyocytes possess allow the action potentials to travel into the centre of the cell and facilitate entry of Ca^{2+} through L-type Ca^{2+} channels (LTCC) which open due to membrane depolarisation. The Ca^{2+} are then sequestered by the ryanodine receptors (RyRs) of the nearby sarcoplasmic reticulum which acts as a Ca^{2+} storage unit within the cell.[50] Activation of the RyRs via extracellular Ca^{2+} binding triggers the sarcoplasmic reticulum to open, thereby releasing a much greater amount of Ca^{2+} into the cell.[51] This process known as calcium induced calcium release (CICR), results in a rapid increase in the level off free cytosolic Ca^{2+} that activates myofilaments to initiate contraction of the myocardium.[52]

Initially the myosin binding sites of the actin filaments are uncovered as the inhibitory troponin I is freed due to Ca^{2+} binding to troponin C and triggering an allosteric change. The myosin heads of the thick filaments can now form a cross-bridge to the binding sites of the thin filaments and perform power strokes with the assistance of ATP hydrolysis. This results in the thick and thin filaments sliding past each other, thereby shortening the sarcomere.[47,49]

The contraction of the myocardium described above represents the systole phase where blood is forced out of the heart. Following this the diastole phase occurs where relaxation of the

myocardium allows the heart to re-fill with blood. Here, Ca^{2+} dissociates from troponin C and is either removed from the cell via sodium-calcium exchangers (NCX) which trade one Ca^{2+} for three sodium ions (Na^{+}) or put back into storage in the sarcoplasmic reticulum by the sarcoplasmic reticulum Ca^{2+}ATPase (SERCA). The reduction of free Ca^{2+} inhibits cross-bridge formation and relaxation of the myocardium occurs.[49]

As the process of cardiac excitation-contraction coupling is a tightly regulated process involving co-ordinated movement of ions, release of calcium and cross-bridge formation, any perturbations to this process can result in disturbances to the cardiomyocyte contraction and therefore cardiac rhythm, which compromises the function of the heart at pumping blood around the body.

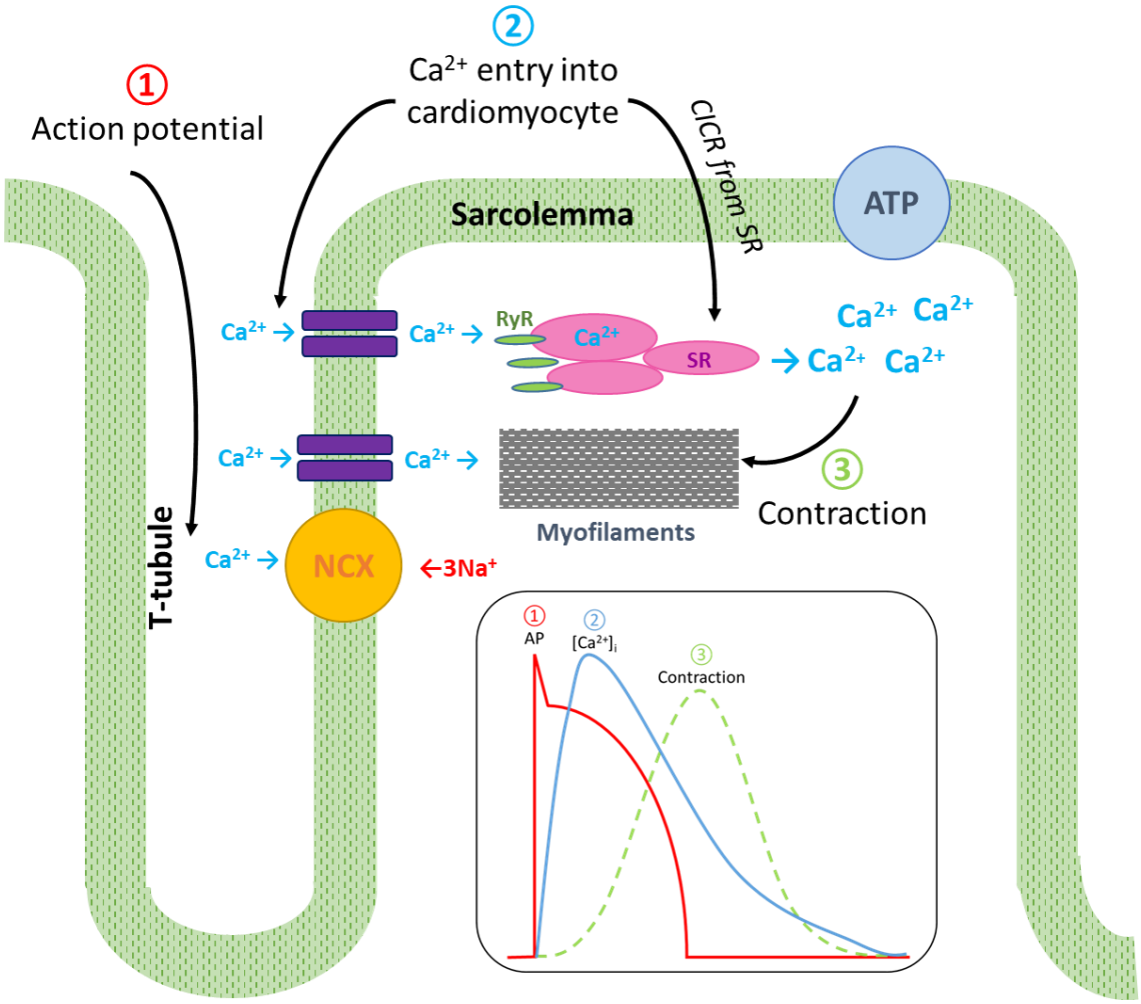

Figure 1.2 Cardiac excitation-contraction coupling

1. Action potentials (AP) travel along the sarcolemma and enter T-tubules causing membrane depolarisation **2.** This opens L-type Ca^{2+} channels (LTCC), Ca^{2+} ions enter the cardiomyocytes and bind to the ryanodine receptors (RyR) of the sarcoplasmic reticulum (SR) to cause Ca^{2+} release (Calcium induced calcium release - CICR). **3.** The Ca^{2+} binds to troponin C of the myofilaments which initiates cardiomyocyte contraction. Upon repolarisation Ca^{2+} are loaded back into the SR, transported out of the cell and Ca^{2+} dissociates from troponin C causing cardiomyocyte relaxation. The inset graph shows the relationship between AP, $[Ca^{2+}]_i$ and cellular contraction.

1.4.3 Multicellular composition of the myocardium

Although cardiomyocytes are the contractile unit of the heart and therefore represent the primary cell involved in maintaining cardiac rhythm, other cell types constitute 70% of cells in the heart numerically[45] and also play important roles in myocardial regulation and homeostasis. Cardiac function is reliant upon the dynamic interaction between the extracellular matrix (ECM) and the various cell types that compose the heart.

1.4.3.1 Cardiac fibroblasts

Cardiac fibroblasts have been previously reported to constitute the majority of the support cells of the heart, however more recent evidence suggests that they are less prominent and have an abundance of 15%.[53] These spindle shaped connective tissue cells are crucial for cardiac remodelling and maintenance of the extracellular matrix (ECM); and are responsible for the production of the majority of myocardial ECM proteins. Situated between cardiomyocytes, their close proximity teamed with the capacity to influence ECM composition provides fibroblasts with the ability to influence the phenotype of cardiomyocytes.[54] Historically fibroblasts have been considered a uniform collagen secreting cell type throughout the body, and therefore compared to cardiomyocytes cardiac fibroblasts received only minor attention.

Recent studies have challenged this dogma, and cardiac fibroblasts are now thought to play a more varied role in the heart, facilitating a plethora of events associated with the response of the myocardium to mechanical, electrical, and chemical signals. Furthermore, communications between cardiomyocytes may be supported by cardiac fibroblasts as they are reported to possess unique contractile transduction abilities, a quality absent from non-cardiac fibroblasts.[55] Although cardiomyocytes have been the classic target for drug-induced cardiotoxicity, due to the close relationship between cardiomyocytes and fibroblasts with respect to signal transduction and the response of the myocardium to various stimuli, damage to fibroblasts

could also indirectly impair cardiac contractility and function without a drug directly damaging the cardiomyocytes. Cardiac fibroblasts may also play a role in receiving and responding to distress signals from neighbouring cardiomyocytes following tissue damage. Rohde *et al.*, have shown that following tissue damage ischaemic cardiomyocytes release the Ca^{2+} binding protein S100A1 as a distress signal. This is then internalized by local cardiac fibroblasts which attempt to maintain homeostasis by assuming an immunomodulatory role and activate anti-fibrotic pathways. This interaction with local fibroblasts promotes the maintenance of tissue homeostasis and protects against fibrosis.[56] This illustrates the important interplay that exists between cardiomyocytes and cardiac fibroblasts to maintain stability within the myocardium even when challenged with environmental stress.

1.4.3.2 Cardiac microvascular endothelial cells

The cardiac microvascular endothelial cells are present both within the endocardium that forms the inner lining of the heart chambers and in intramyocardial capillaries. Their primary function is to supply cardiomyocytes with nutrients and oxygen and to ensure their high metabolic demands are met.[57] Recent evidence suggests that cardiac microvascular endothelial cells are present at a higher abundance than previously reported, and have been estimated to be the most prominent cell type in the myocardium accounting for 40% of the cells.[53] In addition, it has been estimated that there are three endothelial cells for each single cardiomyocyte in the myocardium, which ensures a minimum distance for quick cellular diffusion and exchange of oxygen and waste products.[57] Other roles of cardiac endothelial cells include aiding the adherence of immune cells, allowing inter-cellular signalling factors to be communicated and to impede thrombus formation.[58] Due to the crucial role of cardiac microvascular endothelial cells, any damage would adversely affect cardiac contractility as the supply of oxygen, nutrients and cellular signalling factors to cardiomyocytes would be compromised. The constant cycle of

cardiac excitation-contraction coupling requires uninterrupted energy, which in part relies on healthy endothelial cells allowing quick and efficient diffusion of oxygen.

1.4.3.3 Pericytes

Pericytes are contractile cells which wrap their elongated cellular processes around the microvasculature to provide structural integrity. Located adjacent to endothelial cells, they provide support to the microvasculature by means of direct physical contact and paracrine signalling. In addition to providing structural integrity, pericytes are involved in vascular homeostasis and are important regulators of vascular permeability, blood flow and coagulation.[59] The study referenced above by Pimto *et al*. revisited the cellular composition of the myocardium, however pericytes were not included in their analysis. Nees *et al*. conducted an extensive study on pericyte characterisation from various species and have suggested that they are the second most abundant cell type In the heart after endothelial cells and that each pericyte is associated with up to three endothelial cells.[60] Given the prominence of this cell type in the heart and their physiological significance with respect to regulating blood flow to the extensively vascularised myocardium, these cells are a potential target with respect to cardiotoxicity,[61] as damage to the cells could compromise the provision of an adequate blood supply to the heart.

1.4.4 Myocardial cellular communications

1.4.4.1 Physical communications

The ability of the heart to rhythmically contract in a co-ordinated manner is aided by the extensive number of cellular connections that the cells within the myocardium possess. Gap junctions represent a major type of intercellular connection that are present on both cardiomyocytes and support cells; where both homotypic (between same cell type) and heterotypic connections occur. In virtually all human cells that touch each other, gap junctions act as channels that permit direct intercellular transfer of ions and small molecules.[62]

Gap junctions are important within the heart as rapid transfer of oxygen and nutrients from the microvasculature to cardiomyocytes is essential to meet the energy requirements of this large, highly demanding organ.[57] In addition, gap junctions facilitate the conduction of electrical impulses between cardiomyocytes that precede myocardial contraction. The connexin family of gap junction proteins are critical in the rapid conduction of electrical impulses. Connexin-43 (Cx43) is the most abundant gap junction protein in cardiomyocytes and its presence is essential for normal action potential propagation.[63] As co-ordinated electrical activity is essential for synchronous contractile activity of the heart, impairments to gap junctional communication between neighbouring cardiomyocytes could result in disturbance to action potential propagation and arrhythmias. Indeed mutations of Cx43 have been associated with atrial fibrillation and more recently, sudden infant death.[64]

1.4.4.2 Chemical communications

The role of gap junctions in cardiac cells is not limited to the spread of electrical currents through the myocardium; exchange of chemical signals also occur in an autocrine and paracrine manner which is vital for tissue function. A wide array of molecules are secreted through the dense

complicated network that exists between cardiomyocytes and support cells that ultimately regulate cardiac structure, function and performance.

A key example is nitric oxide (NO) which is a small gaseous signalling molecule that passively diffuses into cells and regulates intracellular signalling.[65] A regulator of vascular and cardiac function, the physiological actions of cardiac NO include initiation of positive inotropy, (increased myocardial contractility), modulation of intra-cardiomyocyte Ca^{2+} movements, accelerated ventricular relaxation, vasodilation and regulation of cardiac metabolism.[66] The actions of NO in cardiac physiology are supported by tight regulation of the enzymes responsible for its production – NO synthases. There are three NO synthases which act in unison to increase and decrease the influence of NO as required. Loss of this balance by production of a high amount of NO could result in cellular disturbances which could lead to heart failure.[65]

1.4.5 Intracellular signalling pathways in cardiac cells

In addition to the extracellular communications and interdependencies between cell types within the heart, cardiac contractility and physiological function is further regulated by cell-surface receptors and their interaction with the local cellular environment. A plethora of specific receptors and corresponding intracellular signal transduction machinery provides the heart with a sophisticated mechanism to respond to extracellular stimuli. Signal transduction is crucial during normal physiological functioning of the heart and perturbations of this signalling can lead to pathological situations.[67] The G-protein coupled receptors (GPCR) represent the largest group of cell surface receptors that are heavily involved in signalling in the heart. Examples of GPCRs include the angiotensin receptor, α- and β- adrenergic receptor and the ET_{1B} receptors, and signalling which is orchestrated through these receptors can alter contractile strength, heart rate and vascular tone.[68] As GPCRs are expressed by both cardiomyocytes and the vasculature, aberrant signalling through these receptors can promote atherosclerosis, hypertension and

cardiac hypertrophy.[69] Figure 1.3 outlines the process of signal transduction through GPCRs, specifically relating to signalling via the angiotensin type 1 receptor (ATR1).

Phosphorylation of proteins is an important component of all signal transduction cascades, including GPCR signalling. Kinases phosphorylate protein substrates whereas phosphatases de-phosphorylate them; a fine balance exists between activity of these signalling elements as dysregulation can cause mayhem within the cells that can contribute to clinical disease. The majority of signal transduction in eukaryotic cells can be attributed to protein kinases, of which serine/threonine kinases represent a major group that add phosphate groups to either serine or threonine amino acid residues; this results in a conformational change to the protein and consequently a change in function or location.[67] For instance, protein kinase G (PKG) is a cyclic guanosine monophosphate (cGMP) dependent kinase that is central to the regulation of the pathway through which NO causes vasodilation. This involves, in part, the phosphorylation of voltage dependent calcium channels which reduces intracellular Ca^{2+} levels and therefore deteriorates the ability of the vessel wall to contract.[70] Protein phosphatases remove phosphate groups from target proteins and hence reduce the signal transduction through kinase pathways.[67]

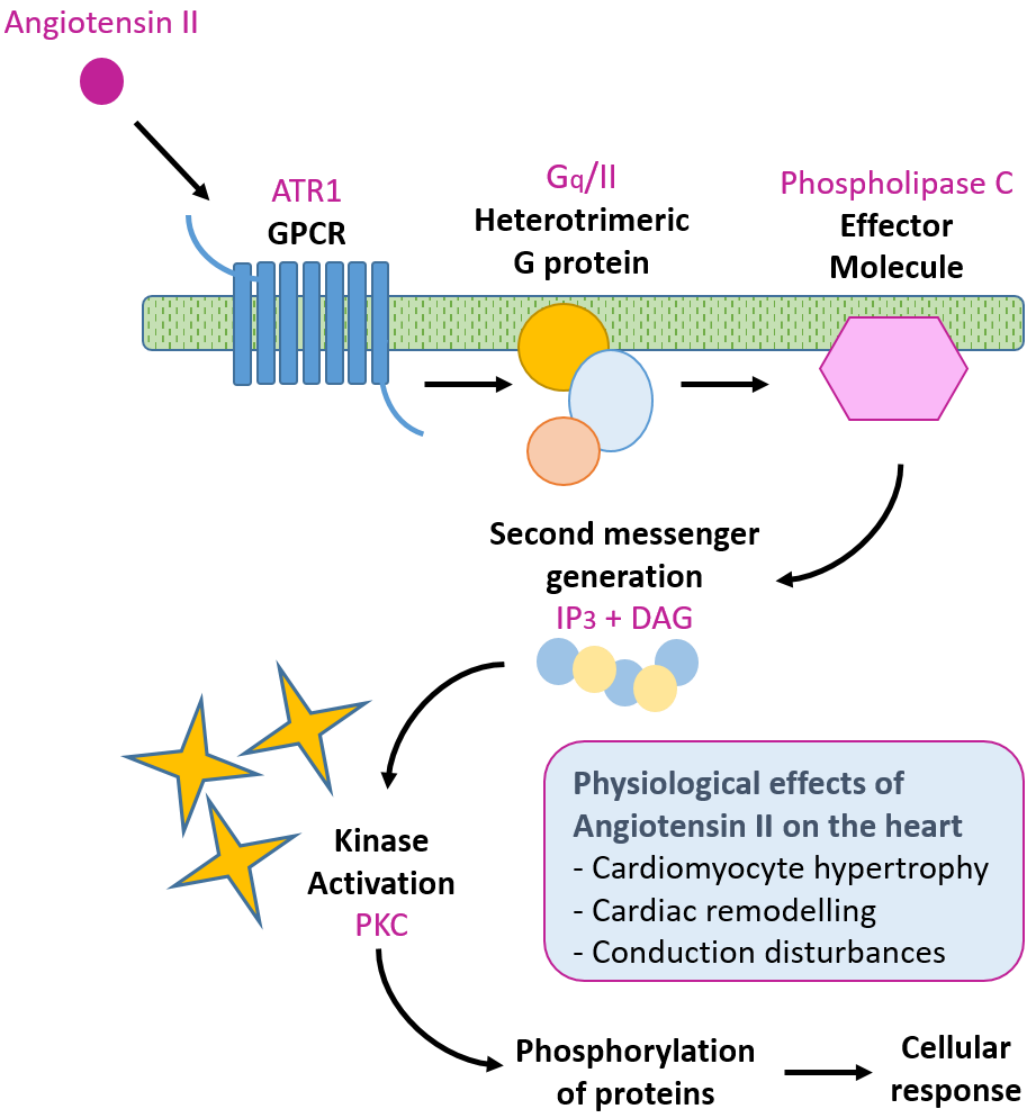

Figure 1.3 **Process of G-protein coupled receptor (GPCR) signal transduction showing ATR1 signalling as an example**

The GPCR signalling system contains a receptor, a heterotrimeric G-protein and an effector molecule. The specific type of all of these components is dependent upon cell type, receptor and agonist. In cardiovascular cells, angiotensin II binding to the ATR1 causes activation of the Gq/II heterotrimeric G-protein, which stimulates activity of the effector molecule - phospholipase C (PLC), whose enzymatic activity hydrolyses a membrane phospholipid to generate inositol (1,4,5)-trisphosphate (IP_3) and diacylglycerol (DAG). These second messengers cause an increase in the intracellular Ca^{2+} levels and activate protein kinase C (PKC). This then leads to phosphorylation of intracellular proteins and a cellular response to the stimulus. The physiological effects of angiotensin II on the heart are shown inset on the figure.

1.4.5.1 Adrenergic signalling pathways in cardiomyocytes

The adrenergic receptor signalling pathway mediates the response of cardiac cells to adrenaline, involving β-adrenergic GPCRs. There are four subtypes of β-adrenergic receptors, β_1 and β_2 are found in the heart and comprise approximately 75% and 25% of cardiac β-adrenergic receptors respectively. Each receptor type is associated with distinct signalling pathways and subsequent cellular responses. For instance, β_1- adrenergic receptor stimulation of the heart is associated with increased myocardial contractility and heart rate.[71]

Following receptor activation, adenylate cyclase (effector molecule) generates increased cyclic adenosine monophosphate (cAMP) levels (second messenger) which activates Protein kinase A (PKA). PKA then co-ordinates the response and phosphorylates various substrates including troponin I, ryanodine receptors and ion channels. This facilitates depolarisation and increases intracellular Ca^{2+} levels, thereby culminating in increased myocardial contractility and heart rate.[72] The β_2 adrenergic receptor is thought to have a similar role in increasing contractility, however utilising mitogen-activated protein kinase (MAPK) signalling and phospholipase A2 rather than adenylate cyclase and cAMP.[67]

Due to the known effects of adrenergic stimulation on the heart, disruption of this signalling is a known pharmacological target, with drugs targeting these receptors being used clinically for treatment of congestive heart failure (CHF). Reduced cardiac output in CHF, caused by a reduction in the heart's ability to pump efficiently, is followed by compensatory mechanisms leading to increased heart rate and remodelling of the heart. The purpose of the remodelling is to return cardiac output to the required level, however puts more strain on the myocardium, further deteriorates pumping efficiency and increases the risk of arrhythmias and cardiac arrest.[73]

Beta-blockers are a class of drugs that disrupt adrenergic signalling and have utility in the management of CHF. By decreasing the rate of myocardial contraction, β-blockers such as

carvedilol, decrease the work-load on the heart which curbs remodelling, improves ventricular filling and reduces further deterioration of cardiac function.[74]

1.4.5.2 Angiotensin signalling pathways in cardiomyocytes

The angiotensin receptor signalling pathway mediates the response of cardiac cells to angiotensin II, this involves angiotensin receptors (ATR), of which there are two subtypes – ATR1 and ATR2. The majority of the known physiological effects of angiotensin II are mediated by the ATR1 which are widely expressed throughout the body including the heart. Angiotensin II mediates a myriad of physiological and pathological processes in the cardiovascular system including vasoconstriction and blood pressure regulation, inflammation, atherosclerosis, hypertension, and cardiac hypertrophy/remodelling.[75] The physiological importance of angiotensin II in the cardiovascular system is paramount, as it is responsible for controlling minute to minute changes in vascular tone and blood flow, therefore ensuring adequate perfusion of the organs. Prolonged activation of ATR1 can cause the pathological effects of angiotensin II such as hypertension and cardiac hypertrophy to develop.[76] The complex activities of angiotensin II are facilitated by a number of signalling mechanisms including classical G-protein signalling (as outlined above in figure 1.3) and transactivation of other receptor types and pathways (discussed below in section 1.4.5.3).

Due to the known effects of angiotensin II on the heart and vasculature, disruption of this signalling is a known pharmacological target, with drugs targeting this pathway being used clinically for congestive heart failure (CHF). Reduced cardiac output in CHF, caused by a reduction in the heart's ability to pump efficiently, is followed by compensatory mechanisms leading to remodelling of the heart and increased heart rate. The purpose of the remodelling is to return cardiac output to the required level, however puts more strain on the myocardium,

further deteriorates pumping efficiency and increases the risk of arrhythmias and cardiac arrest.[73]

Angiotensin receptor blockers (ARB) which prohibit the binding of angiotensin II to the ATR1, thereby disrupting angiotensin signalling, have utility in the management of CHF as they can curb the remodelling of the heart and reduce blood pressure.[77] Interestingly, the ARB valsartan has been shown to simultaneously block signalling of ART1 and β2 adrenergic receptors in mice, suggesting further complex receptor interactions and perhaps more use for angiotensin signalling modulators in CHF.[78]

1.4.5.3 Receptor cross talk within cardiac cells

Increasing evidence suggests that cross talk exists between GPCRs and receptor tyrosine kinases (RTKs) which are another type of cell surface receptor. Growth factor receptors, such as those for vascular endothelial growth factor (VEGF), and epidermal growth factor (EGF) are members of the RTK family, where ligand binding promotes cell growth, proliferation and survival. Unlike GPCR's, these receptors possess intrinsic kinase activity which allows them to autophosphorylate and recruit other proteins to trigger their downstream signalling pathways. Within the cardiovascular system, RTKs are involved in signalling related to cellular differentiation, proliferation and growth.[67]

Evidence suggests that RTKs and GPCRs expressed on cells in the cardiovascular system can ''talk'' to each other as a means to co-ordinate intracellular signalling. Known as transactivation, this novel form of signal transduction allows GPCRs to hijack the signal transduction machinery of growth factor receptors for their own use. For example activation of the ATR1 GPCR by angiotensin II can directly induce cardiomyocyte growth by transactivating the EGFR which triggers specific signalling events related to the regulation of hypertrophic gene transcription. The specific signalling employed is the activation of a major protein kinase cascade called the

mitogen activated protein kinases (MAPK) cascade, which allow for crosstalk, amplification and branching of signals.[67,79]

The examples in this section aim to highlight the complex nature of the signalling that occurs within the myocardium, and represent the tip of the iceberg of what are very intricate regulatory mechanisms. The vast network is important as it allows cells to rapidly respond in unison to environmental changes and maintain homeostasis**,** even subtle changes to this network by cardiotoxic drugs could be detrimental to cardiac function.

1.5 Drug-induced cardiotoxicity

In general, cardiotoxicity is drug induced damage to the heart that occurs either by direct damage to the heart muscle or disturbances in cardiac electrophysiology or cellular pathways, resulting in either cardiac failure or cardiac arrest.[80] The disruption of the electrical machinery of the heart ultimately culminates in the inability of cardiac muscle to sustain a progressive contraction, resulting in dysrhythmia and eventually cardiac arrest.[81] Conversely, drug effects causing a perturbation in cardiomyocyte (or supporting cell) shape, orientation, or morphology causes alterations in cardiac structure and function in terms of contractility and ability to efficiently pump blood around the body. In this latter case, cardiomyocytes eventually lose sufficient ability to contract effectively, leading to reductions in left ventricular ejection fraction (LVEF) and potentially heart failure.[82]

1.5.1 Implications of drug-induced cardiotoxicity for drug development

In addition to drug-induced cardiotoxicity being a serious health problem, it is also the primary cause of drug withdrawal and attrition during drug development,[83] which has significant financial implications for the pharmaceutical industry. For instance, the non-steroidal anti-

inflammatory drug (NSAID) rofecoxib is one of the most widely used drugs ever to be withdrawn from the market, and was used worldwide by an estimated 80 million people to treat pain conditions such as arthritis and dysmenorrhea. It was withdrawn from the market in 2004 due to increased risk of heart attack and stroke; and its long term use is attributed to have caused between 88,000 and 140,000 reports of serious heart disease.[84,85] Later research suggests that the basis for rofecoxib toxicity may be related to its metabolism, specifically causing increases in the oxidative modification of cell membrane lipids and human low density lipoprotein (LDL) which is associated with the development of atherosclerosis,[86] which can lead to heart attack or stroke. In addition to being responsible for significant health problems in patients, rofecoxib caused controversy for Merck and cost billions of dollars in legal expenses.

Similarly, the first marketed non-drowsy anti-histamine, terfenadine, was also removed from the market in the 1990s. In this case, the drug induced significant effects upon cardiac electrophysiology as a consequence of blocking specific ion channels in cardiomyocytes which disrupts the electrical rhythm of the heart. Terfenadine blocks the hERG potassium ion channel; a common mechanism of cardiotoxicity for withdrawn medicines, it results in cardiac arrhythmias caused by prolongation of the QT interval. Whilst terfenadine is cardiotoxic at high doses, its major active metabolite is not. Therefore toxicity is more likely when the body's ability to remove terfenadine is reduced, possibly as a result of interaction with other medicines. The resulting increase in plasma concentration of terfenadine can result in ventricular tachycardia and the fatal condition Torsades de Pointes (TdP).[87]

1.5.2 Drug-induced cardiotoxicity of oncology therapeutics

As described previously, cardiotoxicity is becoming a major issue in cancer therapy. Although significant therapeutic *success* is now associated with the new generation of molecular targeted therapeutics, it is very important to remember that the classical antiproliferative cytotoxic

agents still underpin many treatment regimens, and are commonly delivered concurrently to these *revolutionary* therapeutics. In this context, it is well established that these classical agents have a broad range of systemic toxicities, often associated with an elevated risk for cardiotoxicity. Subsequently, this led to the viewpoint that the observed cardiovascular toxicity was purely a result of the generalised activity of the cytotoxic agent within the regimen (commonly an anthracycline), and that the toxic effects would be removed with increased targeting of cancer therapies. However, this simplistic hypothesis has now been invalidated due to our greater understanding of molecular pharmacology and improved understanding of drug-induced cardiovascular toxicity in cancer patients. Consequently, we now know that drug-induced detrimental effects upon the heart are not limited to cytotoxic therapies or a single type of therapeutic but are an inherent problem with many oncology agents.[88]

The range of possible cardiovascular damage caused by cancer therapies is broad (table 1.1), and the mechanisms by which conventional chemotherapy and molecularly targeted therapies cause cardiotoxicity appear to be distinct, and can be characterised into type I and type II cardiotoxicity depending on the effect of the drug on the heart.[29,89]

	Examples of drugs	Mechanism of action	Examples of cardiovascular damage
Conventional chemotherapy	Anthracyclines	DNA intercalation	CHF, LVD, acute myocarditis, arrhythmia
	Capecitabine	DNA antimetabolite	Ischemia, pericarditis, CHF
	Paclitaxel	Tubulin binding agent	hypotension, CHF, ventricular tachycardia
Molecularly targeted therapies	Imatinib	TKI	Arrhythmias, CHF, angioedema, LVD
	Sorafenib	TKI	Hypertension, arrhythmias
	Sunitinib	TKI	Hypertension, arrhythmias
	Trastuzumab	MAb	Arrhythmias, CHF, angioedema, LVD

Table 1.1 Possible cardiovascular damage caused by conventional chemotherapies and molecularly targeted therapies

CHF = congestive heart failure, LVD = left ventricular dysfunction, TKI = tyrosine kinase inhibitor, MAb = monoclonal antibody

1.5.2.1 Type I Cardiotoxicity: Structural changes

Conventional chemotherapies reduce the growth and proliferation of all rapidly dividing cells within the body. Due to their non-specific mechanism of action, unwanted toxicities in many different organ systems often occur.[90] Conventional chemotherapies are labelled as type I cardiotoxicants, which cause irreversible dose-dependent morphological damage to cardiomyocytes through necrosis or apoptosis. Myocardial injury may arise due to oxidative stress, structural modifications to cells or changes in calcium homeostasis. The loss of viability or decrease in functionality of cells within the myocardium can affect the pumping activity of the heart which may lead to heart failure. The anthracycline class of anticancer chemotherapy is strongly linked with the development of type I cardiotoxicity, so much so that it is considered the prototypical anti-cancer drug to cause permanent therapy-induced cardiotoxicity.[16,91] The mechanism and manifestation of anthracycline-induced cardiotoxicity is discussed in detail in section 1.7.

1.5.2.2 Type II Cardiotoxicity: Functional changes

Type II cardiotoxicity is caused by the newer generation of molecularly targeted therapies. These therapies aim to be less destructive than conventional cytotoxic chemotherapy as they specifically target cancer cells by inhibiting the action of proteins that are mutated or overexpressed in cancer, thereby limiting toxicities to healthy cells.[18] Although revolutionary in the treatment of cancer, these treatments were not as specific as originally hoped and unexpected toxicities including cardiotoxicity still occur.[92] Rather than causing permanent structural damage to cells within the myocardium, type II therapies cause cardiotoxicity by perturbation of signalling pathways that are important for normal myocardial function and survival, thereby causing acute alteration of myocardial function.[89] An important difference between the two types of cardiotoxicity is that type II is usually reversible, and cardiovascular

effects can disappear upon termination of treatment. Although this transient nature of cardiotoxicity poses less of a long-term threat than permanent damage caused by type I cardiotoxicants, the development of treatment related arrhythmias and the possibility of targeted therapies accentuating the cardiotoxic effects of type I therapies makes this type of cardiotoxicity a considerable problem.

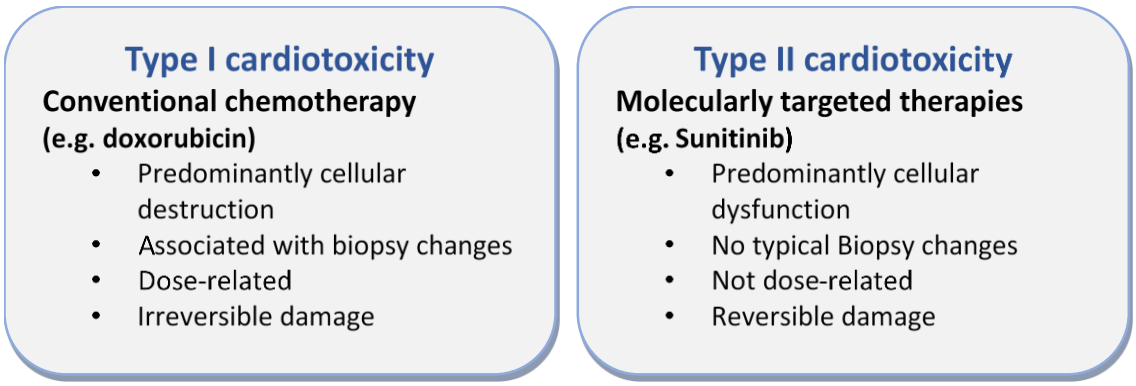

Figure 1.4 Comparison of the characteristics of type I and type II cardiotoxicity

1.6 Type II cardiotoxicity: Molecularly targeted therapies

The development of targeted therapies has dramatically shifted the approach to cancer treatment and for many patients has changed this once fatal disease into a survivable condition. Due to their specific inhibition of proteins that are mutated or overexpressed in cancer, unwanted toxicities are minimized in healthy cells. Although revolutionary in the treatment of cancer, many targeted therapies were not as specific as originally hoped and unexpected toxicities including cardiotoxicity still occur.[93]

The Bcr-Abl tyrosine kinase inhibitor imatinib was the first oncology therapeutic that showed promise for such targeted action, and has a remarkable 90% success rate in treating Philadelphia chromosome positive chronic myelogenous leukaemia (CML).[94] Approximately five years after the introduction of imatinib in 2001, reports of cardiotoxicity began to emerge starting with

Kerkela *et al*. who reported ten individuals had developed CHF whilst taking imatinib. Upon closer inspection, cardiac biopsies of two patients revealed mitochondrial abnormalities and vacuoles within the sarcoplasmic reticulum suggestive of toxic cardiomyopathy. Comparative histological findings were also detected in imatinib treated mice and imatinib induced death in isolated cardiomyocytes.[95]

Unfortunately, imatinib is not the only targeted therapy where unexpected cardiotoxicity followed the initial cancer eradication triumph. Many more targeted therapies are now available that treat a wide range of tumours, however clinicians often need to be vigilant to catch potentially harmful cardiovascular effects.

1.6.1 Sunitinib: Mechanism of action

The process of angiogenesis is required to facilitate tumour growth, making the signalling pathways involved in this process a popular target for new inhibitory drugs. The multi-targeted tyrosine kinase inhibitor sunitinib is used primarily in the treatment of advanced renal cell carcinoma (RCC) and gastrointestinal stromal tumors (GIST).[96]

In order to sustain proliferation and metastasise around the body tumours must establish their own blood supply, this is achieved by secretion of a number of pro-angiogenic factors including VEGF which cause nearby blood vessels to sprout and vascularise the tumour. This process is intrinsic to tumours becoming malignant and is hampered by sunitinib which inhibits multiple receptor kinases including the primary target vascular endothelial growth factor receptors (VEGFR) and platelet-derived growth factor receptors (PDGFR). Therefore sunitinib is both anti-angiogenic and anti-proliferative, which has a cytostatic effect as tumours are starved of oxygen and therefore unable to maintain adequate nourishment.[1,97]

1.6.1.1 Cardiotoxicity of sunitinib

As a broad spectrum multi-targeted kinase inhibitor sunitinib is designed to inhibit a selection of kinases that contribute towards the angiogenic process in tumours. However due to the decreased selectivity of the drug and similarities in the structure of all kinases, sunitinib can unintentionally inhibit other kinases, causing 'off-target' kinase inhibition.

Myocardial biopsies from patients who suffered from sunitinib induced cardiotoxicity have revealed mitochondrial swelling which suggests that cardiac production of ATP may have been compromised which could be linked to the toxicity.[98] Cardiovascular energy homeostasis is regulated mainly by protein kinases and any perturbations to the balance of energy production and use can have consequences to cardiac function as beating cardiomyocytes require constant energy supply. Adenosine monophosphate activated kinase (AMPK) plays a key role in maintaining energy homeostasis in cardiomyocytes and is an 'off-target' kinase that is inhibited by sunitinib. In times of cellular stress when energy levels are depleted, AMPK acts as a sensor and is responsible for kick-starting production of energy to sustain normal functioning of the cell.[99] Studies using rat neonatal ventricular myocytes found that gene transfer of an activated mutant of AMPK partially rescued the toxicity in the cells, suggesting that inhibition of AMPK contributes to the cardiotoxicity.[100]

As the heart is very demanding in terms of energy requirements, inhibition of AMPK by sunitinib could lead to blips in the supply of ATP which is needed to supply sarcomeres and ion channels with the energy required to play their role in contraction. This could cause electrophysiological abnormalities and ultimately lead to arrhythmias, which would be in addition to other adverse effects of sunitinib on the heart.

Although inhibition of kinases relating to angiogenesis is beneficial with respect to halting tumour progression, many of the target kinases of sunitinib play essential roles within the cardiovascular system, therefore their inhibition is related to expected cardiotoxicity.

Myocardial biopsies from patients who suffered from sunitinib induced cardiotoxicity have also revealed hypertrophy of cardiomyocytes,[98] which generally occurs as a result of an increased pressure load, such as during hypertension. Hypertension is a common cardiovascular effect of sunitinib which occurs due to inhibition of sunitinib's primary target VEGF in the cardiovascular system where it plays a crucial role in blood pressure regulation. Consequently, hypertension is considered a biomarker of therapeutic efficiency,[34] with anti-VEGF induced hypertension being initiated by effects on endothelial cells such as reduced density, increased stiffness and increased vascular resistance.[101] In terms of evidence, a study conducted by Chu *et al*. found that out of 75 patients 47% developed hypertension whilst taking sunitinib. As hypertension causes an increased workload for the heart, it is thought to be responsible for the less common but more severe cardiac toxicities of sunitinib which are reduced LVEF and heart failure which were reported to occur in 19% and 8% of patients respectively.[98]

Inhibition of PDGFR (a secondary target of sunitinib) may also contribute to the cardiotoxicity of the drug. PDGFR signaling has recently been implicated as a regulator of the compensatory cardiac response, with its expression increasing in the hearts of mice exposed to pressure overload stress. In mice lacking PDGFR, exposure to pressure overload stress caused accelerated cardiac remodeling, cardiac dysfunction and heart failure.[102] As hypertension caused by VEGF inhibition is a mechanism of pressure overload and PDGFR inhibition reduces the hearts ability to adapt to the stress, it is likely that one or both of these factors plus the energy deficiency caused by off-target AMPK inhibition contribute to clinical presentation of cardiotoxicity accompanying sunitinib treatment.

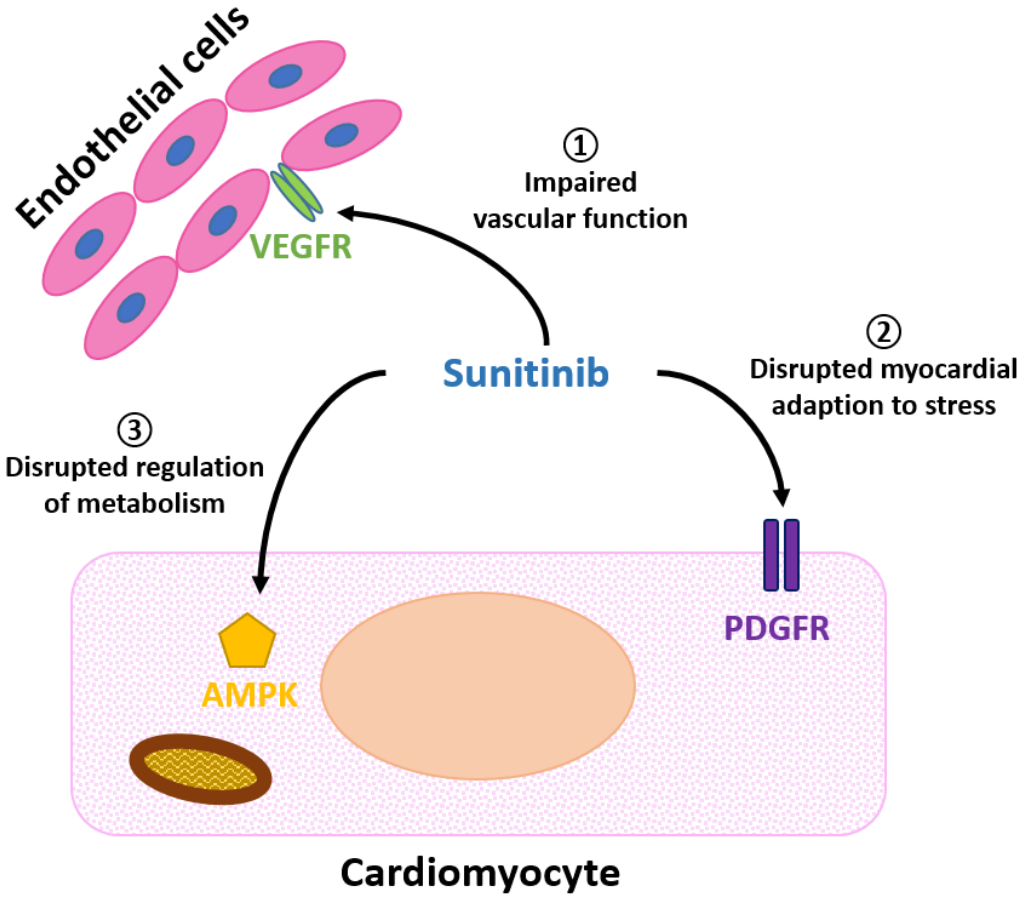

Figure 1.5 Cardiotoxicity mechanism of the multi-targeted tyrosine kinase inhibitor sunitinib

1. Sunitinib disrupts VEGF signalling in endothelial cells causing impaired vascular function, hypertension and thrombosis. **2.** Sunitinib inhibits the PDGFR which affects the myocardial stress response in cardiomyocytes. **3.** Off-target inhibition of AMPK by sunitinib disrupts the regulation of metabolism and energy homeostasis in cardiomyocytes.

1.6.2 Trastuzumab: Mechanism of action

The human epidermal growth factor receptor 2 (HER2) specific monoclonal antibody trastuzumab is a treatment for aggressive HER2-positive breast and gastric cancers.[103] The HER2 receptor belongs to the EGFR family of receptors, which dimerizes with other members of the EGFR family (EGFR3/HER3 and EGFR4/HER4) causing autophosphorylation of tyrosine residues within the cytoplasmic tail of the receptors which initiates a variety of signalling pathways involved in cellular proliferation.[104]

Over-expression of HER2 is observed in 20% of breast and gastric cancers leading to increased signaling and subsequent activation of MAPK and phosphoinositide 3-kinase (PI3K) pathways and increased cellular proliferation. Blocking these signaling pathways using trastuzumab provides a treatment alternative in patients who otherwise would have had a poor prognosis, however cardiotoxicity became evident during clinical trials for breast cancer where incidence of heart failure was 5-8.5%.[105]

1.6.2.1 Cardiotoxicity of trastuzumab

Although inhibition of the HER2 receptor is beneficial for halting caner progression in tumours overexpressing HER2, inhibiting these receptors in the heart may interfere with cardiac function as the receptors have a crucial function in this location. The proposed mechanism responsible for trastuzumab induced cardiotoxicity is thought to involve the neuregulin (NRG) signalling pathway. Neuregulins are a ligand of the EGFR receptors, and NRG-EGFR signalling is involved in cardiac development and physiology.[106] In genetically engineered mice disruption of this signalling leads to failure of cardiac development including lack of ventricular trabeculation (a process necessary for development of the ventricular wall) and improper formation of heart valves. Research in to the function of NRG-EGFR signalling in adult hearts was spurred by occurrence of trastuzumab induced cardiotoxicity, and it was found that the signalling continues

to play vital roles in the adult cardiovascular system relating to the physiological adaption to stress, cardiomyocyte maintenance and vascular homeostasis. Conditional gene knockout mice models were used to study the effects of a loss of NRG signalling in adult mice, with observations such as spontaneous dilated cardiomyopathy, increased susceptibility to stress such as pressure overload, thin myofilaments and increases in ventricular repolarisation time noted with loss of EGFR2 and EGFR4.[107,108] This suggests that the signalling pathway is related to the physiological adaptation of the heart to changes in cardiac demand, which is supported by the potential for neuregulins to be used as a treatment for heart failure.[106]

As an individual therapy trastuzumab carries a relatively low risk of cardiotoxicity, and because the perturbation of signalling in the heart causes myocardial dysfunction (not damage), this type of toxicity has a high likelihood of being reversible and a low likelihood of causing late effects on the cardiac system. However, the situation is different when used in combination with chemotherapies such as anthracyclines, where the rate of cardiac dysfunction increased from 5% to 27%[105] (discussed later in section 1.7.1).

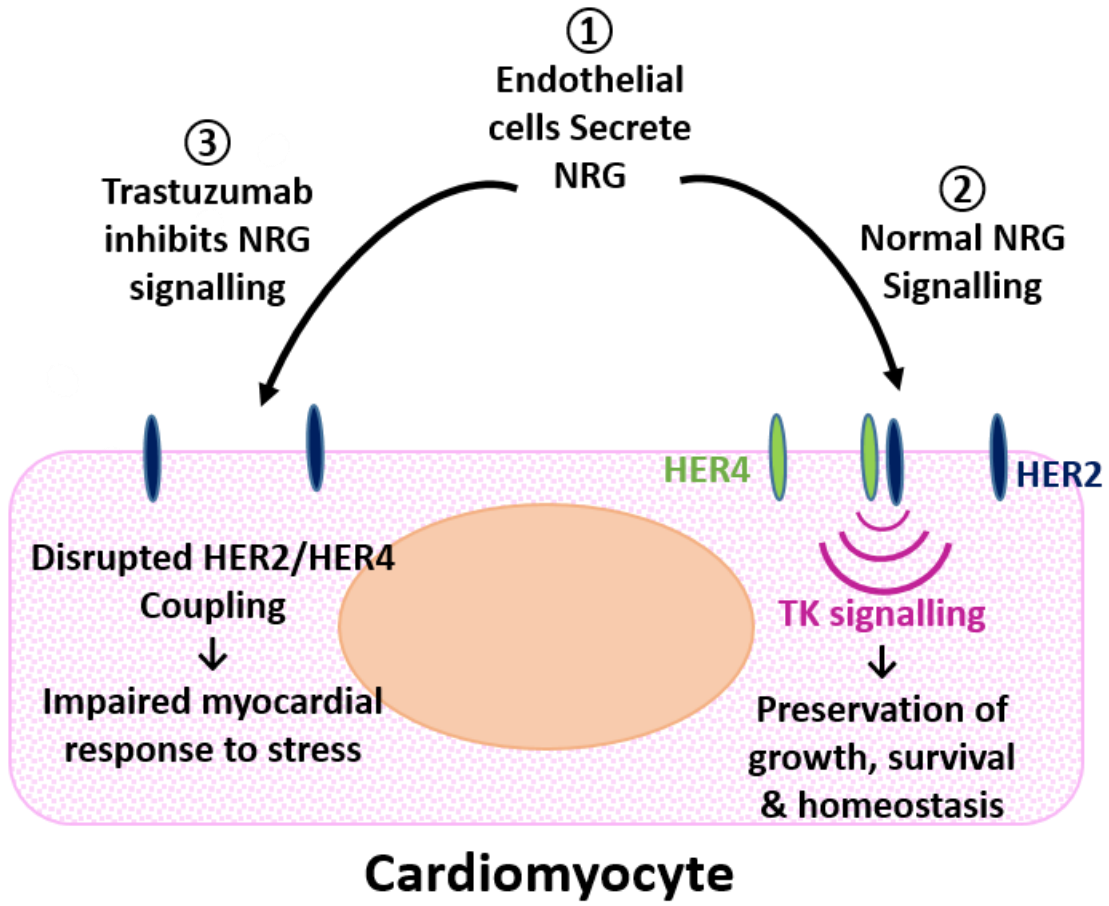

Figure 1.6 Cardiotoxicity mechanisms of the HER2 targeted therapy trastuzumab

1. Endothelial cells secrete neuregulin (NRG). **2.** NRG-HER2 tyrosine kinase (TK) signalling is required for normal cardiomyocyte growth, survival and homeostasis. **3.** Trastuzumab prevents HER2/HER4 coupling and therefore disrupts NRG-HER2 TK signalling and cardiomyocytes have impaired myocardial response to stress.

1.7 Type I cardiotoxicity: Anthracyclines

Anthracyclines (*e.g.* doxorubicin, epirubicin and daunorubicin) are probably the most common cytotoxic treatments used in the clinic, which are used to treat a wide range of paediatric and adult cancers.[15] Originally derived from the *Streptomyces peucetius* bacterium, daunorubicin was the first member of the anthracycline family to be identified – followed by doxorubicin which was found to be a more efficacious anticancer agent.[109,110] Anthracyclines exert their anti-proliferative effects on cancer cells by intercalating between DNA base pairs, generating damaging oxygen free radicals and inhibiting topoisomerase IIα (TopIIα), thereby causing DNA double strand breaks. This culminates in an array of cellular injury including damage to cellular components and disruption of DNA synthesis and replication.[15,111] Doxorubicin exhibits broad spectrum activity against many different tumour types and therefore remains one of the mainstays of oncological treatment (Figure 1.7).

However, despite this class of agent being potent and widely used cancer therapeutics, their use is undeniably associated with detrimental effects upon the cardiac system and significant concerns are now being raised regarding the aftermath of anthracycline-treatment.[16]

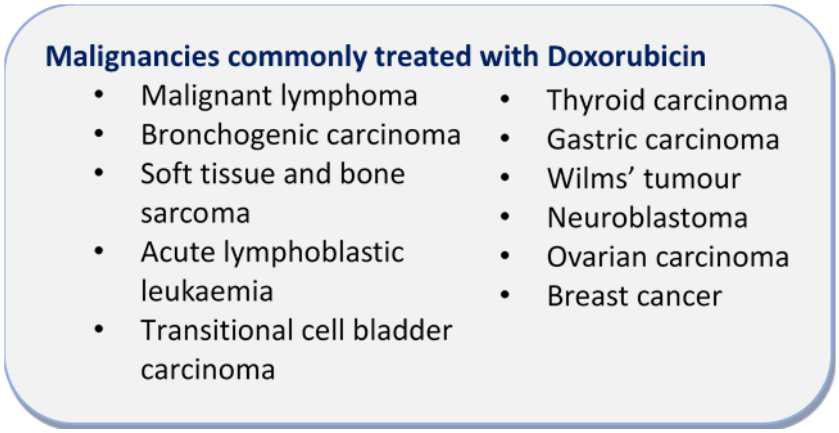

Figure 1.7 Malignancies commonly treated with doxorubicin

1.7.1 Cardiotoxicity of anthracyclines

The cardiotoxic effects of anthracyclines were first reported in 1973 by Lefrak *et al*., who observed transient electrocardiographic changes in 11% of patients treated with doxorubicin, with an additional 3% developing severe congestive heart failure (CHF).[112] The importance of cumulative dose as a determinant for development of CHF was identified shortly after by Von Hoff *et al*. who conducted a retrospective analysis of over 4000 patients treated with anthracyclines. The major risk factor for development of doxorubicin-induced cardiac dysfunction is now known to be the cumulative drug exposure, with the incidence of congestive heart failure increasing from 1.7% at a cumulative dose of 300 mg/m^2 to almost 50% at 650 mg/m^2.[113] Although the initial Von Hoff study has been critiqued due to sole utilisation of clinician identified symptoms of CHF, a sudden rise in the prevalence of CHF was observed at a cumulative dose of 550mg/m^2, which is slightly higher than the current maximum recommended cumulative lifetime dose of 450mg/m^2.[15]

A retrospective analysis of three clinical trials conducted by Swain *et al*. further investigated the importance of cumulative dose in relation to anthracycline-induced cardiotoxicity (AIC), and reported the prevalence of CHF in patients who were exposed to a range of cumulative doses of anthracycline. The incidence of CHF was found to increase with cumulative dose, with estimated incidence of 5%, 26% and 48% with 400mg/m^2, 550mg/m^2 and 700mg/m^2 cumulative dose respectively. Interestingly, the study also found an increased risk of cardiotoxicity with lower amounts of doxorubicin (<300 mg/m^2) which were previously not linked with left ventricular dysfunction.[17] Although the most significant risk factor for anthracycline-induced late onset cardiotoxicity is the cumulative dose, other contributory risk factors include the dosing rate and schedule, patient age, female gender, hypertension, and previous cardiovascular disease (Discussed in section 1.7.13).

1.7.1.1 Doxorubicin cardiotoxicity mechanisms

Although AIC has been classified as the most noted chemotherapy-induced cardiotoxicity to date,[114] it is still unclear as to how anthracyclines cause irreversible damage to cardiomyocytes. The cardiotoxicity appears to be distinguishable from the therapeutic mechanism of action of anthracyclines as cardiomyocytes in general are not proliferative, and TopIIα (a primary target of anthracyclines) is expressed at much lower levels in quiescent tissues such as the heart.[115]

Collective evidence suggests that the cardiomyopathy initiated by doxorubicin is a progressive and multi-factorial process. Microscopy has indicated that treatment with doxorubicin causes cytoplasmic vacuoles, mitochondrial membrane disruption and disorder of myofibril arrangement.[116] Possible mechanisms of doxorubicin-induced cardiomyopathy include impaired calcium handling, altered gene and protein expression, DNA breakage via inhibition of topoisomerase IIβ (TopIIβ), and the formation of oxygen free radicals that damage the mitochondria of the cells.[16,34]

1.7.1.1.1 Iron and free radical hypothesis

The iron and free radical hypothesis is the most widely accepted, whereby the formation of doxorubicin-iron complexes causes free radical formation on the inner membrane of cardiomyocytes mitochondrion. It is estimated that cardiac mitochondria occupy 40% of the volume of cardiomyocytes,[117] making these organelles powerhouses for the generation of reactive oxygen species (ROS) from doxorubicin.

Doxorubicin binds to the mitochondrial membrane protein cardiolipin which leads to mitochondrial accumulation of the drug. Here, redox cycles occur which generate a substantial amount of ROS including $\cdot O_2$- which is converted to H_2O_2. In the presence of iron (Fe^{2+}), H_2O_2 is converted into the extremely reactive $\cdot OH$.[111,118]

Perturbations to cellular iron metabolism are an important feature of this toxicity whereby doxorubicin and its metabolite doxorubicinol interfere with iron homeostasis, resulting in increased formation of doxorubicin-iron complexes and availability of Fe^{2+} to facilitate generation of ·OH.[119,120] Specifically, doxorubicin disrupts the activity of iron regulatory proteins (IRPs) which regulate the activity of intracellular iron. As a consequence of the increased intracellular iron, levels of the iron carrier protein transferrin have been found to increase following doxorubicin treatment which is thought to protect against oxidative injury and ROS formation. Due to the increased polarity of doxorubicinol it accumulates at higher levels than doxorubicin in the heart and is also more potent at dysregulating iron homeostasis which contributes to the generation of ROS.[118,120]

Cardiomyocytes are especially prone to damage by ROS as the myocardium possesses a limited capacity for detoxification. Doxorubicin further hinders this detoxification capacity as it inhibits glutathione peroxidase and catalase which are necessary for the breakdown of H_2O_2 into water and oxygen.[121] This entire process leads to a surge in oxidative stress which is extremely harmful to cardiomyocytes. The cellular damage includes oxidative modifications of cellular components, degradation of the sarcomere, mitochondrial dysfunction, DNA damage and the induction of apoptotic pathways.[91] The significance of this cardiotoxicity mechanism has been demonstrated using transgenic mice, where overexpression of the detoxification enzyme superoxide dismutase 2 (SOD2) attenuated the cardiotoxic effects of doxorubicin, whilst deletion of SOD2 potentiated them.[122]

1.7.1.1.2 Topoisomerase-dependent cardiotoxicity hypothesis

DNA topoisomerases are enzymes involved in the unwinding of DNA necessary for transcription and DNA replication to occur. Topoisomerase IIα (TopIIα) is a marker of cellular proliferation, and its overexpression in tumour cells is a major target for the anticancer activity of

doxorubicin.[115,123] Unlike TopIIα that has low expression in quiescent cells, topoisomerase IIβ (TopIIβ) is present in non-proliferating cells including cardiomyocytes. Here, a complex is formed consisting of *doxorubicin – TopIIβ – DNA* that cause double strand breaks in the DNA and ultimately cardiomyocyte death. Studies in cardiomyocyte specific TopIIβ knockout mice treated with doxorubicin showed that cardiomyocytes were protected from DNA double strand breaks and changes in transcription of genes that may be related to ROS formation and apoptosis.[124] In addition, more recent research has investigated the role of mitochondrial topoisomerase I (Top1mt) in doxorubicin induced cardiotoxicity.

The mitochondria within mammalian cells contain their own DNA genome (mtDNA), as well as specific processes for DNA replication and protein synthesis. The mtDNA encodes important proteins that are part of the mitochondrial electron transport chain responsible for oxidative phosphorylation and therefore production of ATP in the cell. Relaxation of the circular, double-stranded mtDNA relies on the presence of topoisomerase activity within the mitochondria, which enables transcription and protein synthesis to occur.[125] Therefore any perturbations to topoisomerase activity could impede energy production in cardiomyocytes which would affect the normal functioning of the myocardium. As mitochondrial dysfunctions and mtDNA lesions are a feature of human hearts exposed to doxorubicin[126] and Top1mt is involved in mtDNA homeostasis, it is possible that Top1mt is also a target for doxorubicin in the heart.

Khiati *et al*. investigated the role of Top1mt using TopImt knockout (KO) mice and found that after 8 weeks treatment with doxorubicin the Top1mt KO mice had increased mtDNA damage, mitochondrial cristae disorganisation and were unable to maintain the mitochondrial electron transport chain. These mitochondrial defects also caused an increase in damaging ROS and myofibrillar damage. These results suggest that Top1mt is critical for cardiac tolerance to doxorubicin and the adaptive response to doxorubicin cardiotoxicity.[127]

1.7.1.1.3 Alterations in multidrug resistance efflux proteins

The ATP-binding cassette (ABC) family of membrane transporters are responsible for translocation of substances across membranes. Multidrug resistance (MDR) proteins are a member of the ABC family that remove foreign potentially harmful substances from cells and are involved in regulating the efflux of anthracyclines from cardiomyocytes. Polymorphisms of the MDR1 gene have been associated with cardiotoxicity, and reduced expression of the gene was detected in cancer patients who later developed AIC.[128] As patients may be taking other medications that can block the MDR proteins, this has clinical significance as the intracellular levels of anthracyclines may be increased further, thereby increasing the risk of cardiotoxicity.

1.7.1.1.4 Impaired calcium handling

Doxorubicinol is a metabolite of doxorubicin that accumulates in cardiomyocytes, causing inhibition of Ca^{2+} uptake into the sarcoplasmic reticulum by the sarcoplasmic reticulum Ca^{2+}ATPase (SERCA).[129] As efficient calcium recycling is required for successful contraction and relaxation of cardiac muscle, this causes a considerable delay in the activation and inactivation of cardiomyocyte contractility.

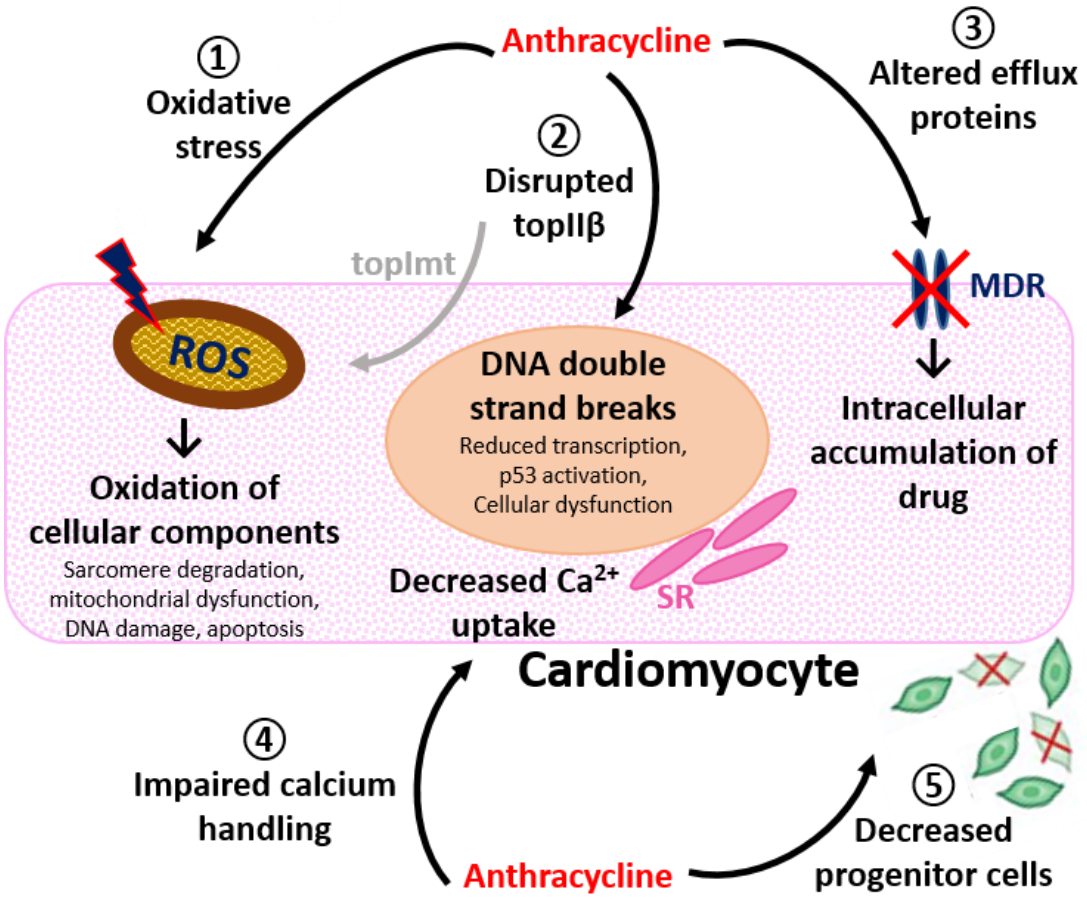

Figure 1.8 Anthracycline cardiotoxicity mechanisms

Anthracyclines damage cardiomyocytes through a variety of mechanisms: **1.** Oxidative stress induces production of damaging reactive oxygen species (ROS) in the mitochondria which are damaging to cells, **2.** Disrupted topIIβ and topImt activity causes double strand breaks in the DNA, **3.** Increased intracellular concentration of anthracyclines due to alterations in MDR efflux proteins, **4.** Decreased uptake of Ca^{2+} into the sarcoplasmic reticulum (SR) causes disturbances to myocardial contractility and **5.** Decreased mesenchymal and circulating progenitor cells reduces the regenerative capacity of the heart following damage.

1.7.1.1.5 Impact of anthracycline metabolism and metabolites on cardiotoxicity

Upon clinical administration doxorubicin is rapidly cleared from the blood and widely distributed into tissues. The drug undergoes triphasic elimination with mean half-lives of 12 minutes, 3.3 hours and about 30 hours. Doxorubicin is metabolised primarily by the liver, and the main metabolite is doxorubicinol which is an active metabolite.[15] Doxorubicinol is important with respect to cardiotoxicity as due to its polarity it more readily accumulates in cardiomyocytes where it causes dysregulation of iron homeostasis and alterations in calcium handling[119,129] (see section 1.7.1.1.1 and 1.7.1.1.4). The impact of doxorubicinol on cardiotoxicity is exemplified by studies which have shown that genetic polymorphisms in the enzymes that form doxorubicinol lead to increased levels of cardiotoxicity.[130]

Other anthracyclines follow similar metabolism and elimination patterns. For example the primary metabolites of daunorubicin and epirubicin are daunorubicinol and epirubicinol which are both pharmacologically active.[131,132] Epirubicinol is also an active metabolite however it has been reported to be formed in lower quantities than doxorubicinol in the human myocardium which may relate to the more favourable toxicity profile of epirubicin.[133] Epirubicin also has a different pharmacokinetic profile to doxorubicin characterised by a higher clearance rate and a shorter half-life, which may also contribute to the reduced toxicity of the drug clinically.[131]

1.7.1.2 Clinical manifestation of anthracycline induced cardiotoxicity

In terms of clinical presentation, AIC is classified into three types (discussed in detail below): symptomatic acute toxicity occurring soon after administration, and early- and late-onset chronic toxicity, occurring before or after one year of treatment, respectively.

1.7.1.2.1 Clinical manifestation of chronic anthracycline induced cardiotoxicity

Early- and late-onset chronic progressive cardiotoxicity are associated with electrophysiological changes and left ventricular dysfunction (LVD), and tend not to be reversible. However, if undetected or not-treated, these chronic forms of cardiotoxicity will progress and lead to a reduction in cardiac function with time.[134]

Early-onset chronic cardiotoxicity is the most prevalent manifestation of AIC. Symptoms usually present approximately one year following treatment as dilated cardiomyopathy which can lead to heart failure. Recently, Cardinale *et al*. conducted a clinical study whereby patients receiving anthracycline treatment underwent heart function monitoring at regular intervals in an attempt to elucidate the incidence and clinical features of early-onset chronic AIC. A key finding was that 9% patients developed AIC, with 98% of these cases occurring within the first year after treatment. Upon clinical recognition of significant reductions in left ventricular ejection fraction (LVEF) indicative of AIC (primary endpoint), treatment with the heart failure therapy enalapril was initiated and the potential for recovery from AIC was determined (secondary end point). The study demonstrated that initiation of heart failure therapies is beneficial for restoration of cardiac function with 71% patients demonstrating partial recovery and 11% demonstrating complete recovery.[135]

Delayed cardiotoxicity (also called late onset chronic cardiotoxicity) is particularly relevant in adult survivors of childhood cancer, whereby cardiotoxicity arises decades after exposure to doxorubicin after a long asymptomatic period.[136] Due to their younger age at the time of treatment, childhood survivors are in a developmental stage that makes them more vulnerable to adverse health effects from potentially toxic therapies, which become clinically apparent years later. Recent evidence suggests that anthracyclines decrease the number of cardiac mesenchymal and circulating progenitor cells, thereby reducing the regenerative capacity of the heart in response to damage (Figure 1.8). This may provide an explanation for the delayed

cardiotoxicity observed in children who are treated with anthracyclines.[137,138] In these survivors, cardiovascular related disease has been identified as the leading cause of morbidity and mortality after development of cancer recurrence,[31] with echocardiographic abnormalities indicative of impairments to left ventricular contractility estimated to occur in up to 65% of patients.[139]

A retrospective analysis of the childhood cancer study conducted by Mulrooney *et al*. assessed the incidence and risk of cardiovascular events in 14,358 five year survivors of childhood cancers.[30] Compared to their siblings, cancer survivors were more likely to suffer from cardiac events including CHF, pericardial disease and valvular disease. For example, at an average age of 27 years old 248 cancer survivors reported CHF and 101 had suffered a myocardial infarction; this is of particular note as such events are generally rare in young adults. The probability of developing CHF was identified to be related to cumulative dose as the risk increased from 2.4 fold higher risk at doses of up to 250mg/m^2 to 5.2 fold higher risk at doses >250mg/m^2.[30]

A similar study investigated the long-term cardiac mortality among 34,489 childhood cancer survivors diagnosed and treated across seven decades (1940-2006) in the United Kingdom. In concordance with the findings of Mulrooney *et al*.; the number of cardiac deaths was 3.4 times the expected amount and the risk of developing CHF was 5.9 times greater than expected. Interestingly, the risk of death due to heart failure was greatest amongst survivors who were diagnosed 1980-1989; with 28.9 times more excess deaths reported than those diagnosed from 1990. This decline in the risk of cardiac death that was observed post-1990 suggests that the use of alternative drugs, lower cumulative doses and more frequent monitoring for cardiac liabilities has proved beneficial as a means to reduce cardiotoxicity.[140]

1.7.1.2.2 Clinical manifestation of acute anthracycline induced cardiotoxicity

Due to the often asymptomatic nature of acute cardiotoxicity, which presents as rhythm disturbances, transient reductions in myocardial contractility, and/or hypotension, and the fact that it is reversible by discontinuation of treatment, this adverse effect is commonly not identified.

Acute toxicity as a consequence of anthracycline treatment is rare and typically occurs in the two weeks succeeding a single treatment; usually manifesting as pericarditis, transient arrhythmias or LVD.[141,142] In contrast to the chronic and delayed cardiotoxicity discussed above, the deterioration to left ventricular function is not permanent as improvements in cardiac function have been documented in some patients.[142] In addition, the mechanism of acute cardiotoxicity may differ from delayed cardiotoxicity as it is thought to involve an inflammatory response.[16]

1.7.1.3 Risk factors for anthracycline-induced cardiotoxicity

Several risk factors have been reported to increase susceptibility to developing AIC including extremes of age, concurrent treatments and pre-existing cardiac disease. A retrospective analysis of three clinical trials identified age as an important risk factor related to doxorubicin induced CHF as at a cumulative dose of 400mg/m^2 patients over 65 years old showed a greater incidence of CHF than younger patients.[143] Similarly, paediatric patients are more susceptible to delayed cardiotoxicity, and it is estimated that more than 50% childhood cancer survivors treated with doxorubicin develop some form of cardiotoxicity years after finishing cancer treatment[136]. Concurrent treatment with other cancer drugs can also exacerbate cardiotoxicity, for example the combination of anthracyclines with the monoclonal antibody trastuzumab increases cardiotoxicity risk,[105] as does concurrent radiation therapy.[144] In 1977 Minow *et al*. identified heart disease which results in an increased cardiac work-load, such as hypertension

as a risk factor for doxorubicin induced cardiotoxicity. Hypertension can cause the heart to hypertrophy; thereby reducing contractile capacity which may lower the dose of doxorubicin required to cause CHF.[145]

The lower cumulative doses required for patients with pre-existing risk factors can decrease oncological efficacy; which creates a challenge for clinicians to ensure a balance between antineoplastic effects and minimising cardiotoxicity.

1.7.1.4 Detection of anthracycline-induced cardiotoxicity

AIC is usually detected post cancer treatment when patients show signs and symptoms of heart failure. The loss of functionality becomes evident as cardiomyocyte injury or impairment has occurred to a level whereby the heart can no longer compensate for the loss of contractility and so becomes a less efficient pump.[146,136]

The lack of consensus regarding the definition of cardiotoxicity adds to the problem of detection and management of AIC. Cardiotoxicity is generally defined as "toxicity that affects the heart" although a more precise definition is lacking overall.[34] The cardiac review and evaluation committee overseeing the supervision of clinical trials for the molecular targeted chemotherapeutic trastuzumab provided perhaps the most accurate definition of drug-associated cardiotoxicity to date, whereby a patient must have one or more of the following:[147]

1) Cardiomyopathy characterised by a reduction in LVEF, either globally or specific to the septum

2) Signs or symptoms related to CHF

3) Reduced LVEF from baseline that is 5% to < 55% alongside accompanying HF signs or symptoms

4) A reduced LVEF of 10% to <55% without any additional HF signs or symptoms.

This definition relies narrowly upon changes in LVEF and development of symptomatic CHF which are indicative of systolic function; however does not encompass subclinical cardiotoxicity that occurs with AIC, where patients can develop cardiac abnormalities histologically but remain asymptomatic under general observations. Detection of damage at the earlier subclinical stage would allow for appropriate risk assessments to be made and interventions to be put in place to prevent further cell loss and resulting impairments to heart function.[148] Frequent imaging using techniques such as echocardiograms (ECHO) and radionuclide ventriculography multi-gated acquisition scan (MUGA) may assist with earlier detection of cardiotoxicity as they allow clinicians to check the structure of the heart and assess ventricular function.[146]

A new promising echocardiographic approach, Doppler myocardial imaging (DMI), has been shown to detect abnormal myocardial activity as early as one week after completion of an anthracycline therapy.[149] Analysis of biomarkers, such as cardiac troponins also represent a means to identify cardiotoxicity. The wide diagnostic window, high specificity and high sensitivity make cardiac troponins an ideal biomarker that can be assessed quickly using a simple blood test. This is highlighted by Cardinale *et al*. (2006) who identified cardiac troponin I (cTnI) as a useful biomarker in terms of identifying patients at high risk of developing AIC.[150,151]

1.7.2 Mitigation of anthracycline-induced cardiotoxicity

In recent years, there has been a shift in focus from the recognition and treatment of cardiotoxicity to prevention. Understanding the aetiology of AIC has driven the development of preventive strategies to protect the heart from permanent cardiac damage caused by anthracyclines.[28,152,153]

Dexrazoxane is the first and only drug to be licensed for anthracycline related cardioprotection. Dexrazoxane contains EDTA within its structure; EDTA is a chelating agent that can sequester metal ions such as Ca^{2+}, Mg^{2+} and Fe^{2+} which causes a decrease in their activity. When co-

administered with anthracyclines, dexrazoxane chelates iron which reduces the amount of iron that can complex with the anthracycline. This interferes with iron-mediated free radical generation that is thought to play a role in the development of AIC.[154] Although a recent meta-analysis concluded that adjuvant dexrazoxane treatment is associated with a decreased risk of heart failure,[155] use is restricted to adult patients as controversial clinical trial data has been generated including increasing the rate of secondary malignancies and acute myelogenous leukaemia (AML) in paediatric patients.[156]

Other strategies that have been explored for mitigation of AIC include the use of statins and β-blockers.[28] Statins possess both anti-inflammatory and anti-oxidative properties and are routinely used for the prevention of cardiovascular diseases. Thought to interfere with the generation of ROS and inhibition of TopIIβ associated with AIC, a small randomised controlled trial (RCT) found prophylactic atorvastatin protected patients from declines in LVEF,[157] and a larger RCT called 'Preventing anthracycline cardiovascular toxicity with statins (PREVENT)' is currently underway.[158]

β-blockers such as carvedilol are used for the treatment of CHF and angina. Carvedilol antagonises beta (β_1, β_2) and alpha (α_1) adrenergic receptors and is unique amongst β-blockers as it also possesses anti-oxidant properties.[74,159] Whereas selective β-blockers decrease the rate and force of myocardial contraction, the additional α_1 blockade properties of carvedilol are related to vasodilation, this is associated with reduced blood pressure and as a result carvedilol is more effective at treating CHF than the conventional selective β-blockers. With respect to reduction of AIC, the anti-oxidant properties of carvedilol may also be beneficial. Studies comparing the efficacy of carvedilol and atenolol at protecting cultured rat cardiomyocytes from AIC *in vitro* showed that carvedilol was able to decrease the production of damaging free radicals and prevent apoptosis of cardiomyocytes, whereas atenolol was not.[160] This suggests that carvedilol may possess the ability to protect the heart from AIC and as such it has been employed

in a number of small studies where its prophylactic effects on AIC have been investigated with encouraging results.[152] The first such study was conducted by Kalay *et al*. who concluded that carvedilol may protect both systolic and diastolic functions of the left ventricle in patients undergoing anthracycline therapy.[161]

1.7.2.1 Angiotensin blockade for cardioprotection

There is a growing body of evidence that administration of angiotensin converting enzyme inhibitors (ACEi) or angiotensin receptor blockers (ARB) can also protect the heart from the deleterious effects of anthracyclines (See table 1.2 below). ACEi are routinely used for the treatment of CHF and hypertension, and ARB are used for the treatment of hypertension and to prevent cases of stroke and myocardial infarction.[162,163] Both prevent the physiological activity of angiotensin II (angII); ACEi prevent the formation of angiotensin II whereas ARB stop angiotensin II binding to the ATR1 (figure 1.9). Angiotensin signalling has a variety of effects within the cardiovascular system including vasoconstriction and blood pressure regulation, inflammation, atherosclerosis, hypertension, and cardiac hypertrophy/remodelling.[75] (See section 1.4.5.2).

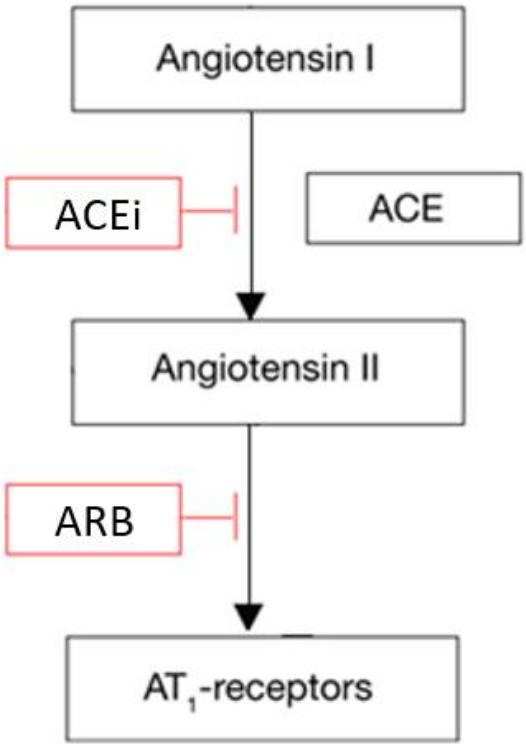

Figure 1.9 Angiotensin II synthesis and pharmaceutical inhibition

Following formation of angiotensin I by cleavage of angiotensinogen by renin, angiotensin I is cleaved by angiotensin converting enzyme (ACE) to form angII. The production of angII can be prevented using angiotensin converting enzyme inhibitors (ACEi), and the activity of angII can be inhibited using angiotensin receptor blockers (ARB) which prevent angII from binding to the ATR1.

Table 1.2 summarizes the methods and findings of a selection of clinical studies that have assessed anthracycline containing chemotherapy regimes in combination with either an ACEi or ARB alone, or with adjuvant β-blocker therapy.

Studies using Angiotensin converting inhibitors (ACEi)				
Study	**Study objective**	**Prophylaxis**	**Cardiac assessment modalities**	**Study findings**
Cardinale et al. (2006)[150]	To examine the effects of enalapril treatment in patients with high cTnI following one month of Cx C = 58, T = 56	Enalapril	Physical examination, ECG, ECHO at baseline and 1, 3, 6, and 12 months after the end of Cx. cTnI measurements performed regularly during Cx	In high-risk patients with increased cTnI levels, early treatment with enalapril prevented the development of late cardiotoxicity
Bosch et al. (2013)[164] ***OVERCOME***	To investigate the efficacy of carvedilol and enalapril at preventing LVSD in patients with haematological malignancies C = 45, T = 45	Enalapril, carvedilol	ECHO and CMR imaging studies were performed at baseline and 6 months. cTnI and biomarker analysis was also performed regularly during Cx	Enalapril and carvedilol protected patients from significant declines in LVEF that were seen in the control group at 6 months
Janbabai et al. (2017)[165]	To investigate the efficacy of enalapril in the prevention of AIC C = 35, T = 34	Enalapril	ECHO performed at baseline and 6 months. cTnI measured 1 month after the initiation of Cx	LVEF did not change in enalapril group at 6 months, but significantly decreased in control group

Table 1.2A Summary of clinical studies investigating the use of ACEi for cardioprotection during anthracycline containing regimens

Studies using Angiotensin receptor blockers (ARB)				
Study	**Study objective**	**Prophylaxis**	**Cardiac assessment modalities**	**Study findings**
Nakamae et al. (2005)[166]	To investigate whether valsartan can inhibit acute AIC in patients with non-Hodgkin's lymphoma C = 20, T = 20	Valsartan	ECHO and ECG at baseline and on days 3, 5, and 7	Valsartan prevented transient changes to the left ventricular end-diastolic diameter and QT interval that were observed in the control group
Cadeddu et al. (2010)[167]	To assess the protective effects of telmisartan on EPI induced early ventricular impairment using escalating doses C = 24, T = 25	Telmisartan	ECHO, tissue Doppler, strain rate imaging and ROS were assessed at baseline and 7 days after every new EPI dose of 100mg/m^2	As the dose of EPI increased, strain rate (indication of ventricular impairment) deteriorated in control group but normalised in the telmisartan group. Increases in ROS were not observed in the telmisartan group
Gulati et al. (2016)[168] ***PRADA***	To investigate if candesartan (Cn) or metoprolol (M) can alleviate declines in LVEF associated with anthracycline-containing regimens in breast cancer patients C = 30, (T: Cn/M = 28, Cn = 32, M = 30	Candesartan Metoprolol	CMR, blood samples, physical examinations, and ECHO performed at baseline, after first and final cycles of Cx, and for those concerned, at completion of trastuzumab or radiation therapy	Adjuvant breast cancer treatment is associated with a decline in LVEF that is alleviated by concomitant blockade with candesartan. No improvement to LVEF were observed with metoprolol

Table 1.2B Summary of clinical studies investigating the use of ARB for cardioprotection during anthracycline containing regimens

AIC = anthracycline-induced cardiotoxicity, C = number of patients on control arm of trial, CMR = cardiac magnetic resonance, cTnI = cardiac troponin, Cx = chemotherapy, ECG = electrocardiogram, ECHO = echocardiogram, EPI = epirubicin, LVEF = left ventricular ejection fraction, LVSD = left ventricular systolic dysfunction, ROS = reactive oxygen species, T = number of patients on experimental treatment arm of trial.

Limitations of the studies outlined include short follow up time of patients (ranging from 1 week – 1 year) and the low number of patients enrolled. A follow on study aimed to address the short follow up time of patients and assess if the cardioprotective effects of telmisartan observed by Cadeddu *et al*. would be maintained long-term. Their results showed that telmisartan exhibited protective effects for at least 18 months and so may be useful in preventing anthracycline-induced early onset chronic cardiotoxicity which typically presents 1-2 years following treatment.[169] The authors have indicated that this study is still ongoing and they intend to continuously monitor the patients for at least 3 years to evaluate whether the global cardiac function is similar between the two groups or whether the telmisartan group have better global cardiac function and thus a better clinical outcome.

Larger phase II and phase III clinical studies are currently underway that aim to assess the cardioprotective potential of ACEi/β-blocker combinations[170] and ACEi alone[171] in breast cancer patients receiving anthracycline treatment. These clinical trials will hopefully support the findings of the smaller studies and provide additional information regarding the optimal cardioprotective strategies and monitoring schedules for detection of sub-clinical damage.

The potential for reversal of AIC by ACEi has also been investigated in long-term cancer survivors. Enalapril therapy commenced seven years after completion of doxorubicin chemotherapy in survivors of childhood cancer reported benefits initially, however these improvements deteriorated after six years.[172] These transient benefits exemplify the permanent nature of damage caused by doxorubicin and supports the current view that concomitant angiotensin blockade alongside anthracycline treatment is the most effective way to use these agents as cardioprotectors.

The mitigation of AIC with therapeutics that limit angiotensin signalling suggests a role for the angiotensin signalling pathway in mediating this toxicity; therefore it is imperative to understand

downstream signalling events of the ATR1 and how these signalling events may interplay with mechanisms of AIC. This is discussed in chapter 6 of this thesis.

1.8 Combination therapies

Using a combination of therapies represents a potent method of cancer treatment as cancer cells are attacked using a variety of mechanisms. For example the regimen 'R-CHOP' consists of the targeted therapy rituximab, the conventional chemotherapies cyclophosphamide, doxorubicin hydrochloride, vincristine (Oncovin) and the steroid prednisolone. Rituximab is a monoclonal antibody used to treat leukaemia and lymphomas and specifically targets the CD20 cell surface receptor that is present on both healthy and cancerous B cells, leading to apoptosis of the cells. Cyclophosphamide, doxorubicin and vincristine are conventional chemotherapies that attack proliferating cells by interacting with DNA, inhibiting enzymes required for DNA replication and preventing microtubule assembly respectively.[173] All of these therapies individually are associated with different cardiotoxicities such as acute arrhythmias and progressive development of heart failure. Although beneficial for reducing tumour burden, combination therapies may have a synergistic effect which increases the severity and likelihood of developing therapy induced cardiotoxicity.[153]

1.8.1 Clinical effect of co-administration of type I and type II cardiotoxic therapies

In clinical trials of trastuzumab the incidence of heart failure was 5-8.5%, a figure which increased dramatically to 27% with concurrent anthracycline therapy.[105] Following analysis of the pivotal clinical trials in this therapeutic area, previous anthracycline exposure and concurrent anthracycline use were listed as risk factors related to trastuzumab cardiotoxicity.[174]

As discussed previously, anthracyclines such as doxorubicin cause direct damage to cardiomyocytes which leads to impairment of cardiomyocyte function (See section 1.7.1). Anthracyclines are an example of a type I cardiotoxicant, whereby the agent causes permanent dose-related structural damage to cardiomyocytes which can impact the pumping ability of the ventricles therefore causing left ventricular dysfunction. In contrast trastuzumab is a type II cardiotoxicant, which causes cellular dysfunction (not damage) of cardiomyocytes which is not dose-dependent and usually reversible upon termination of treatment. An important distinction between the cardiotoxicity of the two drugs is that anthracyclines are associated with chronic and delayed forms, where patients are asymptomatic for years before disturbance to ventricular function becomes apparent, whereas trastuzumab is generally not associated with causing long-term cardiac sequelae.[16,89,105]

A cumulative lifetime dose of doxorubicin has been established at 450mg/m^2 in attempt to reduce the risk of cardiotoxicity in patients.[15] However before alterations to cardiac function become clinically apparent, sub-clinical cardiomyocyte injury occurs that creates a population of vulnerable cardiomyocytes that are reliant on repair mechanisms to minimise the damage and resume normal function.[29] The mechanism of trastuzumab cardiotoxicity has been postulated to involve inhibition of neuregulin signalling which has vital roles in the adult cardiovascular system relating to the physiological adaption to stress and cardiomyocyte maintenance (See section 1.6.2.1). Conditional gene knockout mice models were used to study the effects of a loss of neuregulin signalling in adult mice, with observations such as spontaneous dilated cardiomyopathy, increased susceptibility to stress such as pressure overload, thin myofilaments and increases in ventricular repolarisation time noted.[108] This suggests that the signalling pathway is related to the physiological adaptation of the heart to changes in cardiac demand, which is a change that occurs with anthracycline therapy. Therefore trastuzumab's interference with this critical survival signalling pathway in cardiomyocytes which reduces the repair capacity of vulnerable cardiomyocytes may increase severity of anthracycline toxicity as

the cells are less able to repair the sub-clinical damage caused by the type I cardiotoxicant.[175] Consistent with this proposed mechanism of toxicity, disrupted HER2 signalling in mice exacerbates anthracycline cardiotoxicity and myocardial HER2 is up-regulated following anthracycline exposure in humans.[176]

1.9 Current *in vitro* models for identification and study of drug-induced cardiotoxicity

Cardiotoxicity is assessed during all stages of the drug development process, starting in the early pre-clinical stages of drug discovery. As defined in the ICH S7 guidelines, pre-clinical assessment of drug-induced cardiac liabilities is a regulatory requirement.[177] Historically, cardiac liabilities were initially determined via assessment of drug effects upon the hERG potassium channel, a known toxicity target with relationships to clinical effects. This assay utilised an *in vitro* cell system whereby a non-cardiac cell line was engineered to artificially express a functional hERG channel.[177] The *in vitro* evaluation against hERG was then followed by assessment of the drug *in vivo* against a larger mammalian species, primarily dog. However, although successfully identifying several drugs with cardiac liabilities, the complexity of the cardiac system and involvement of several ion channels in cardiomyocyte contractility was such that many drugs progressed into animal studies, and occasionally clinical trials, unnecessarily.[178,179] Consequently, there is an urgent need for development of *in vitro* assays to robustly detect such effects reliably. This has now led to the development of the CiPA initiative (comprehensive *in vitro* proarrhythmia assay).[180]

1.9.1 The CiPA initiative and pre-clinical evaluation of drug-induced cardiotoxicity

The ICH S7B guidelines have proven successful in preventing the introduction of drugs that are potentially torsadogenic to the market, however the focus on the ability of drugs to block the hERG potassium channel and cause QT prolongation as the sole determinants of cardiotoxicity risk needs revising.[181] The cardiac action potential is governed by activity of many ion channels, and cardiotoxicity itself can be caused by other factors (e.g. structural damage); as such potential cardiotoxicants could slip under the radar with the current screen if they cause structural damage, whereas others may appear hazardous with respect to hERG block but pose little actual risk for TdP in the clinic.

The Comprehensive *in Vitro* Proarrhythmia Assay (CiPA) initiative aims to develop a new paradigm for assessing proarrhythmic risk, utilising new technologies and an expanded understanding of cardiotoxicity beyond hERG block.[181] Development and validation of a set of predominantly pre-clinical assays is currently underway that is envisaged to enable a more precise prediction of clinical proarrhythmia risk using the three pillars of CiPA.

These are:

i) Assessment of drug effects on the critical human ventricular ion channel currents

ii) *in silico* integration of the ion channel effects to determine the net effects on the cardiac action potential

iii) A check for discrepancies in fully integrated biological systems (*in vitro* cardiomyocyte models).

The third pillar of CiPA involves evaluating the acute effects of drugs on the electrical activity of induced pluripotent stem cell derived cardiomyocytes (iPSC-CMs) using high throughput approaches such as microelectrode arrays and impedance technology that enable more

comprehensive and robust assessments earlier in the drug discovery process. These cell types and approaches are discussed in detail in the following sections.

1.9.2 *In vitro* cardiomyocyte cell line models

A variety of models are available including primary cells, cell lines and induced pluripotent stem cell derived cardiomyocytes (iPSC-CMs).[182] Perhaps the most frequently used model, the immortalised rat cardiomyoblast H9c2 cell line was derived in 1976 and has since been widely used to assess cardiac biology and electrophysiology. Although morphologically distinct from cardiomyocytes and without contractile ability, they do express relevant contractile proteins, ion channels and fuse to form multinucleated myotubes.[183] The cells have been successfully utilised as an *in vitro* model to measure the cardiac hypertrophic effect of several agents such as doxorubicin and sunitinib.[184,185] This is because the H9c2 cells showed almost identical hypertrophic responses to those observed in primary cardiomyocytes.[186]

Another cell model is the HL-1 murine atrial cardiomyocyte cell line model. This cell line expresses relevant ion channels and forms organised sarcomeric structures and therefore spontaneously contracts *in vitro*, whilst maintaining proliferative capacity.[187] Their energy metabolism differs from cardiomyocytes and due to the differences between the mouse and human cardiac action potential limited toxicity screening has been conducted.

Although growing in culture, the major issue with these cell lines is their rodent derivation, degree of maturity, originating cell type, and their subsequent inability to fully represent or recapitulate a human cardiac cell model. In this context, a series of cell lines (AC1, AC10, AC12, AC16) were created via fusion of immortalised SV40 protein transformed human fibroblasts with primary human ventricular cardiomyocytes.[188] Based on their human origin and immortality these cells were postulated as being useful as an *in vitro* screening model. However current data remains limited, the cells are reportedly in a pre-contractile state, but with expression of many

cardiac specific transcription factors, contractile proteins and functional gap junctions.[188] As a series of immortalised cell lines, AC cells may be applicable for use in high-throughput screening assays for detection of structural toxicity, and complement data obtained for the more physiologically relevant induced pluripotent stem cell derived cardiomyocytes (iPSC-CMs).

1.9.2.1 Induced pluripotent stem cell derived cardiomyocytes

The discovery that somatic cells can be reprogrammed into pluripotent stem cells,[189] and the subsequent development of the processes required to differentiate these cells into functional human cardiomyocytes[190] instigated the growing preference of human iPSC-CMs for pre-clinical cardiotoxicity assessment of new drugs. Although iPSC-CMs possess many favourable features such as the ability to spontaneously contract, responsiveness to cardioactive drugs and expression of important cardiac ion channels and receptors;[191] It is has been frequently noted that these cells resemble embryonic cardiomyocytes and are described as having an immature phenotype. Robertson *et al*. reviewed this subject in depth and discussed the differences between embryonic and adult cardiomyocytes.[192]

With reference to size, embryonic cardiomyocytes are approximately 30µm in length making them approximately 80% smaller than adult cardiomyocytes that are large, cylindrical and approximately 150µm long. Differences in organelle size and number have also been noted, for example adult cardiomyocytes are usually bi- or multinucleated, whereas embryonic cardiomyocytes are mononucleated. In adult cardiomyocytes the contractile apparatus and mitochondria constitute around two thirds of the cytoplasmic space, this is reduced in embryonic cells where much smaller sarcomeres and fewer mitochondria are seen. With respect to contractile function, contractile strength is reduced due to the lack on an extensive T-tubule network in embryonic cells.[192] This results in slower excitation-contraction coupling and calcium entry primarily through the sarcolemma rather than released from the sarcoplasmic reticulum

through CICR. Long term experiments appear to improve the phenotype to having a higher level of maturity, including increased use of the sarcoplasmic reticulum, increased multinucleation and improved myofibrillar arrangement.[193]

Despite the immature phenotype of human iPSC-CMs, they are still considered more clinically and physiologically relevant than other *in vitro* models such as the rat H9c2 cell line. In addition, these cells represent a source of human adult cardiomyocytes that can be cultured easily for long periods of time and are readily available for routine drug testing - A feature absent from other human derived *in vitro* models.[194] Therefore these cells have become fundamental to many *in vitro* cardiotoxicity assays, and have shown considerable promise to accurately detect cardiac liabilities in drugs with known cardiac effects on a number of platforms. Another potentially exciting advancement, is the development of patient-specific iPSC-CMs which can be used to study drug effects in the context of a particular risk factor or disease.[195]

Although commonly used as a confluent spontaneously beating monolayer, the use of iPSC-CMs is now expanding to 3D models. Various types of 3D cell culture techniques have been developed, some use scaffolds, whilst others rely upon the innate interactions of cells. All of these models were developed with the aim of more accurately recapitulating *in vivo* cellular morphology and physiology than that of the more commonly used 2D cell models.[196] Although 3D cell culture techniques have existed for some time, it is only since the recent development iPSC-CMs that efforts have been directed towards utilizing these techniques to potentially increase model maturity for cytotoxicity screening. Many 3D models incorporate different cell types, often cardiomyocytes, fibroblasts and endothelial cells which usually approximate the ratios found in the human heart (See section 1.4.3)[197] Such models have been used to measure cardiac hypertrophy and structural cardiotoxicity; where increases in the size of spheroids and perturbations to mitochondrial function (measured as ATP level) in response to cardiotoxicants

are visible using microscopy. Therefore 3D spheroid models have applications in improving pre-clinical cardiotoxicity screening.[198]

1.9.3 *In vitro* cardiotoxicity assays

The requirement of *in vitro* cardiac cell assays and the identification of new cardiac cell lines and advent of iPSC-CMs has led to a surge in the development of new high-throughput assays that allow the structural and functional activity of cardiomyocytes to be assessed. The driving principle of these assays is the measurement of electrophysiological changes that precede contraction or quantification of the contraction itself. Traditionally, monitoring electrophysiological fluctuations of excitable cells was carried out using patch clamping.[199] Although this technique allows for the activity of single ion channels to be assessed, it is labour intensive, limited to isolated cardiomyocytes, and evaluates cell effects at a snapshot in time, making this technique unsuitable for high-throughput screening.

1.9.3.1 Microelectrode arrays

Microelectrode arrays (MEAs) are plate based assays whereby electrically active cells such as iPSC-CMs are seeded into the wells of specialised plates that have a series of electrodes on the bottom of the wells. Once the cells form a cohesive monolayer and begin to spontaneously contract, their electrophysiological profile is captured by the electrodes in real-time allowing parameters such as beat rate, field potential duration, amplitude and conduction velocity to be assessed.[200] In contrast to the traditional patch-clamp approach, MEAs measure the total extracellular change of ions and therefore assess changes in all major ion channels implicated in the action potential. A recent blinded study by Blinova *et al*. assessed the ability of iPSC-CMs to detect drug-induced arrhythmias using an MEA platform. The results were promising, drugs that

block key potassium and calcium channels were positively identified, there was however more variable success at detecting sodium channel blockers.[201]

1.9.3.2 IonOptix

Cardiac tissue is characterised by the appearance of bands within the individual cardiomyocytes known as sarcomeres. These are the basic unit of muscle and contain the contractile proteins and molecular machinery responsible for cardiac contractility (See section 1.4.1). The rate and size of sarcomere shortening and lengthening provide important information relating to cellular contractility and changes in inotropy and chronotropy induced by drugs. Changes in cardiomyocyte contractility can be monitored using the IonOptix cell geometry system which monitors sarcomere movements in real-time using video-based detection.[202] A perfused cardiomyocyte monolayer is observed using a microscope which collects optical intensity data representing the light and dark bands present within the sarcomere. Contraction of the cells results in the movement of these bands which translates into transients of peaks and troughs which are then analysed to provide quantification of contractility. This technique was recently used by Pointon *et al*. who evaluated the ability of iPSC-CMs to detect changes in contractility by 11 reference compounds (8 negative inotropes, 2 positive inotropes and 1 inactive compound). All of the negative isotopes and the inactive compound were positively detected, however although the positive inotropes were detected by the system, they exhibited a negative rather than positive inotrope response.[203]

1.9.3.3 Calcium fluctuation

As Ca^{2+} is intrinsically involved in cardiomyocyte contraction, measurement of intracellular Ca^{2+} transients can also be used as a surrogate measure of contraction. Calcium specific fluorescent dyes are added to monolayers of cells in a plate based format, and as the iPSC-CMs

spontaneously beat and their intracellular Ca^{2+} levels fluctuate, the peaks and troughs in fluorescence intensity are recorded.[204] This technique allows changes in contraction force and frequency to be quantified, however it should be noted that compounds which affect the contractile machinery, such as the myosin II inhibitor blebbistatin will not be detected and the toxicity of the dyes limits how long drug effects can be monitored.

1.9.3.4 Cellular impedance assays

Cellular impedance technology allows for real-time, label free monitoring of cardiomyocyte viability and beating over sustained periods. Minute cardiomyocyte movements that occur during contraction cause transient changes in impedance; these small morphological changes to cardiomyocytes are detected by electrodes which creates a surrogate pattern based on the contractility of the cells. In addition to changes in contractility, this technology can detect changes in cellular viability and morphology as impedance readings also provide a measure of overall cell health and therefore may be useful in detecting structural changes. These features allow for sensitive and robust monitoring of the effects of compounds on cardiomyocyte function and health in a high-throughput approach that is reflective of clinical exposures.[205,206]

As cardiomyocyte contraction is downstream of the cardiac action potential and calcium flux in cardiac excitation-contraction coupling (See section 1.4.2 and figure 1.2), the surrogate measurement of contractility generated by cellular impedance technology has the potential to detect drug induced disturbances to the action potential, calcium flux and mechanical contraction. For example, the reduced contraction strength caused by the myosin II inhibitor blebbistatin can be demonstrated using impedance technology, however effects of the drug are absent using both MEAs and calcium fluctuation assays which measure endpoints higher in the cascade.[207]

As a result, cellular impedance technology has the potential to detect both functional and structural drug-induced cardiotoxicity, which could lead to earlier cardiovascular hazard identification in the drug development process. A recent study by Doherty *et al*. assessed if a multi-parameter *in vitro* screen could detect cardiotoxicity across multiple drug classes with known clinical cardiac risks. A range of studies were carried out, however the most sensitive test was the impedance based xCELLigence cardio system which detected 16/18 known cardiotoxicants as cardiotoxic.[208] Similarly *Gou et al.* compared the utility of MEA and the impedance based xCELLigence cardio system to detect functional changes in iPSC-CMs following treatment with 28 different compounds with known cardiac effects and attained comparable results from both sytems,[207] therefore highlighting illustrating the utility of impedance-based technology at accurately detecting cardiac liabilities in iPSC-CMs.

1.10 Rationale and aims

The cardioprotective potential of therapies that act on the angiotensin signalling pathway has been demonstrated in recent clinical studies, which strongly suggests that a relationship exists between anthracycline-induced cardiotoxicity and angiotensin signalling. Although a number of *in vivo* studies have added further support for the cardioprotective nature of these drugs, there is a lack of *in vitro* studies, and the molecular mechanisms underpinning the cardioprotective mechanisms are currently unclear.

The aim of this study was to investigate the structural and functional cardiotoxicities caused by anthracyclines using *in vitro* models paired with novel impedance-based technologies, and to ascertain if toxicity mitigation was detectable in these models upon concomitant administration of angiotensin receptor blockers.

This thesis is divided into four sections:

i) Development and qualification of *in vitro* cardiac cell models (AC10 cardiomyocyte cell line (AC10-CMs) and hiPSC-CMs) for the *in vitro* assessment of drug-induced cardiotoxicity, using impedance-based methodologies. Changes in cellular viability, morphology and functionality will be assessed using impedance-based detection (xCELLigence technology) in response to drugs and cardiac regulatory factors.

ii) Assessment of the mechanistic basis for cardiotoxicity induced by anthracyclines

iii) Assessment of the potential for the adverse toxicological effects of anthracyclines to be mitigated by perturbation of the angiotensin signalling pathway.

iv) Identification of the mechanistic basis for the effects of anthracyclines upon the cardiac system and the impact of angiotensin signalling in mediating this toxicity

Specific aims are detailed in each section.

Chapter 2: Materials and Methods

All reagents were obtained from Sigma-Aldrich Company Ltd (UK) unless otherwise stated. Plastic tissue culture materials were supplied by Sarstedt (UK).

2.1 Cell lines and tissue culture

2.1.1 Cell lines

The proliferating human cardiomyocyte cell line AC10 was originally derived by fusion of adult ventricular heart cells with SV40 transformed fibroblasts as described by Davidson *et al*.;[188] these cells were kindly donated by Dr Barbara Savoldo from Texas Children's Hospital, Texas, USA. The H460 cell line is an immortalised human cancer cell line from non-small cell lung cancer (NSCLC) origin that was originally obtained from American tissue culture collection (ATCC).

2.1.2 Cell culture and maintenance of cells

Cell lines were grown as monolayers *in vitro* and incubated at 37°C in a constant humidified atmosphere of 5% carbon dioxide. The AC10 cell line was maintained in Dulbecco's modified eagle medium (DMEM) -F12 medium (Life technologies) supplemented with 12.5% foetal bovine serum (FBS), 1% L-glutamine and 1% penicillin/streptomycin. The H460 cell line was maintained in Roswell Park Memorial Institute (RPMI) 1640 medium supplemented with 10% FBS and 1% L-glutamine. Cells were passaged when flasks were ~75-80% confluent by washing the monolayer with hanks balanced salt solution (HBSS) and addition of 0.25% trypsin-EDTA, a pellet was then obtained by centrifugation at 1000g for 5 minutes and the cells were re-suspended in fresh medium and passaged into a new flask or cell pellets were stored at -20°C for molecular analysis.

2.1.3 Cell counting

Cell number was determined using a haemocytometer where 10µl of cell suspension was pipetted under a coverslip and the number of cells counted in five 1mm^2 sections. Due to the dimensions of the haemocytometer the average value of cells *(N)* in the five sections equates to *N* x10^4 cells/ml.

2.1.4 Cryopreservation of cells

Cells that were not passaged were frozen for future use. Confluent AC10 cells were trypsinised and centrifuged at 1000g for 5 minutes, the supernatant was then removed and the cells were re-suspended in 1ml of fresh medium. Cells were transferred to a 1.5ml cryovial and 10% dimethyl sulfoxide (DMSO) was added before the tubes were placed in a cryogenic freezing container in a -80°C freezer. The following day cells were transferred to a liquid nitrogen storage dewar for long term storage.

2.2 Cellular viability assays

The MTT (3-(4,5-Dimethylthiazol-2-yl)-2,5-Diphenyltetrazolium Bromide) assay is a colourimetric assay that relies upon mitochondrial conversion of a soluble tetrazolium dye to insoluble purple formazan crystals, whereby the amount of purple crystals created reflects the number of viable cells.[209]

Following determination of the optimum cell seeding density (AC10 exponential = 2x10^3 cells/well; AC10 plateau = 3.5 - 4x10^4 cells/well; H460 exponential = 5x10^2/well) cells were seeded in flat-bottomed 96 well plates which were left in the incubator to adhere overnight, one lane of the plate contained medium only to act as a cell blank control. The cells were then treated with drug solutions and a vehicle control as required throughout the experiment, with

the DMSO vehicle concentration being no higher than 0.1% per well. Following the total incubation period for the experiment the medium was removed and replaced with medium containing a 1:10 dilution of MTT (5mg/ml), and incubated for an additional 4 hours to allow the formation of formazan crystals. Following removal of the MTT solution the crystals were dissolved in DMSO and the absorbance of each well was read at 550nm using a UV-Vis spectrophotometer plate reader. A vehicle control lane of 0.1% DMSO was used to ensure that any observed effect was due only to the drugs added and not an effect of the vehicle. Analysis of absorbance readings was conducted using Microsoft excel; the average absorbance for each treatment group was determined from which the average of the blank lane was deducted, and average absorbance's relating to treatment with a compound expressed as a percentage of the vehicle control (0.1% DMSO).

All experiments were performed in triplicate, IC_{50} values were determined by implementing curve fitting by non-linear regression on GraphPad Prism (Version 7.04, GraphPad Software, Inc.). Statistical analysis on IC_{50} values was conducted where necessary using a One way analysis of variance (ANOVA) test, and a post-hoc Dunnett's test when required on GraphPad Prism (Version 7.04, GraphPad Software, Inc.).

2.3 xCELLigence real-time cell analyser

The xCELLigence DP16 real-time cell analyser (RTCA) is an *in vitro* impedance-based cell analysis system that allows changes in cell survival, morphology and drug response to be evaluated on adherent cell lines in real time using 16 well electrode plates (E-plates).[210] In wells containing only medium the electric current can flow freely, thus completing the circuit between the electrodes. However as cells adhere and begin to proliferate on the electrode the current flow between the electrodes is impeded – This provides very accurate information relating to changes in cell number, morphology and attachment (Figure 2.1).

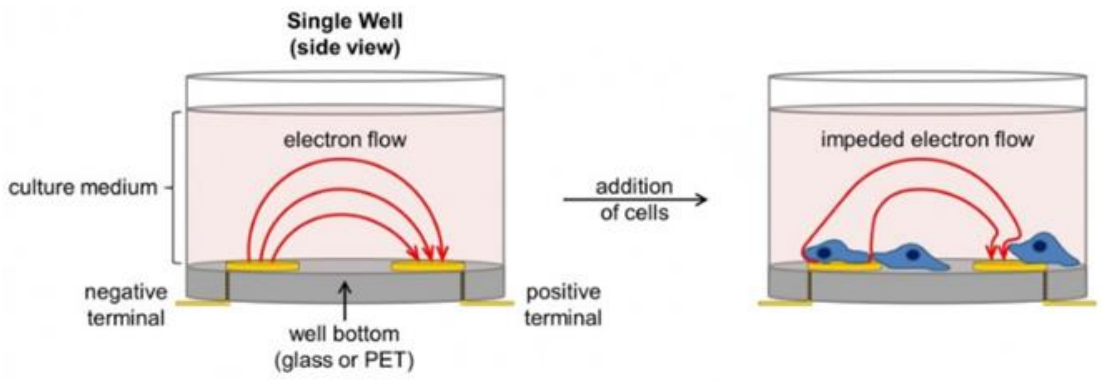

Figure 2.1 Principle of impedance based cell detection

In wells containing only medium the electric current can flow freely, thus completing the circuit between the electrodes (left). However when cells are added and adhere to the bottom of the wells the current flow between the electrodes is impeded (right). Once cells begin to proliferate on the electrode the current flow between the electrodes is impeded further, therefore impedance increases. Image courtesy of ACEA biosciences.

2.3.1 Experimental set-up

The RTCA software was started and experiments were set up as per manufacturer's guidance notes (ACEA Biosciences, San Diego). The layout of the plate was outlined with information including cell type, cell number and compounds to be added to each well. The length of the experiment and number and frequency of impedance readings to be taken (sweeps) was also input into the experimental schedule page.

2.3.2 Cell seeding

Prior to cell seeding 100µl of DMEM-F12 medium was added to all wells of a 16 well E-plate which was then put to one side to allow the medium and E-plate to achieve equilibrium. A suspension of AC10 cells was then created and the number of cells contained in the solution was determined using a haemocytometer. The cell concentration was then adjusted to contain

$5x10^4$cells/ml for experiments examining cells in the exponential growth phase or to $10x10^4$cells/ml for experiments requiring cells to be in the plateau phase of growth.

The 16 well E-plate was transferred in to the cradle of the RTCA instrument and the background impedance reading was taken. After completion of the background measurement 100µl of cell suspension was to the wells, with one pair of wells left with medium only. The E-plate was then left for 30 mins at room temperature to allow the cells to settle in an evenly distributed manner at the bottom of the wells. Following this the E-plate was transferred back into the cradle and impedance measurements were recorded every 30 mins.

2.3.3 Cell maintenance and compound addition

Following attachment of the cells compounds were added as required. For experiments examining the effects of compounds to cells in exponential growth phase compounds were added at 24 hours and after. For experiments examining the effects of compounds to cells in plateau growth phase compounds were added once the growth and therefore impedance readings (designated as cell index) became stable (Usually around 72 hours). When the effects of a single compound were to be assessed, double strength compounds were prepared and added by removing 100µl of medium from the wells and replacing with 100µl of the double strength compound. On all subsequent additions of that compound 100µl of drug solution was removed from the wells and replaced with 100µl of single strength compound.

All experiments were performed in triplicate unless stated otherwise. Statistical analysis on normalised cell index values was conducted where necessary using a one way analysis of variance (ANOVA) test, and a post-hoc Dunnett's test when required on GraphPad Prism (Version 7.04, GraphPad Software, Inc.).

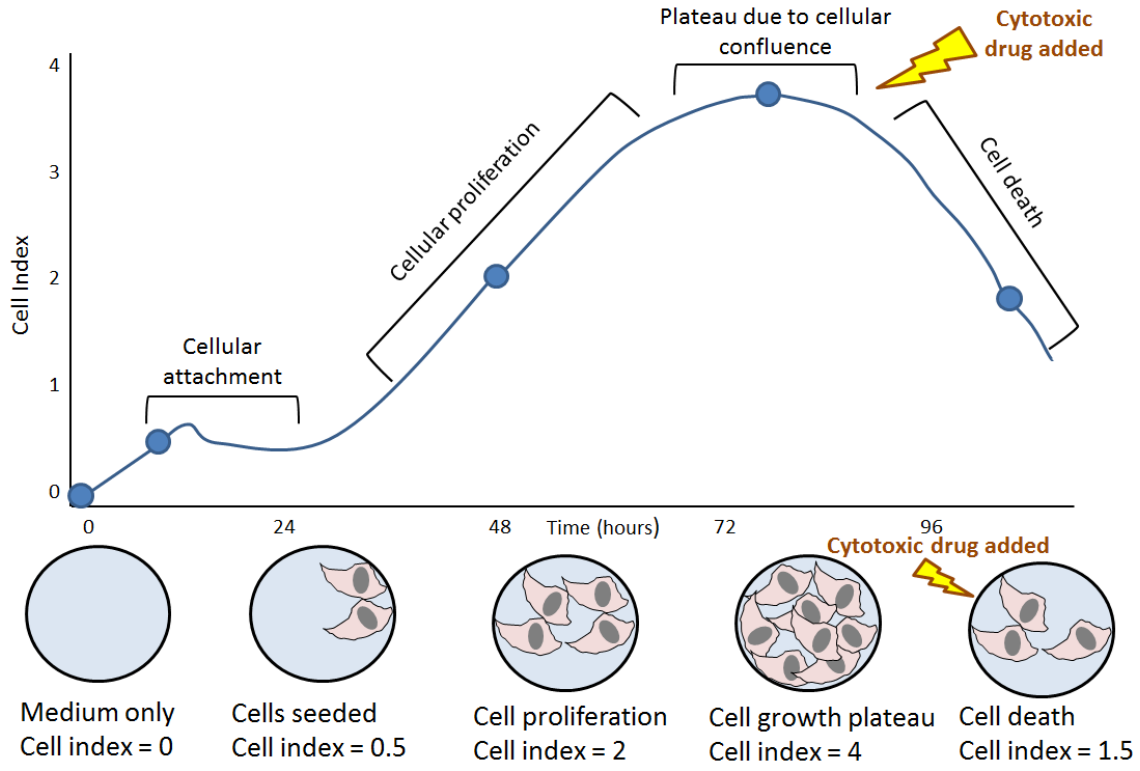

Figure 2.2 Cell growth monitoring using the xCELLigence impedance-based system

Schematic showing the output on the xCELLigence impedance-based system when monitoring cellular growth and response to cytotoxic drugs, whereby cell index (measurement of impedance) is related to the phase of cellular growth and the cell density in the wells.

2.4 xCELLigence cardio system

The xCELLigence RTCA Cardio is an *in vitro* impedance-based cell analysis system that allows changes in cell survival, morphology, drug response and contractility to be evaluated in human iPSC-derived cardiomyocytes (hiPSC-CMs).[205,211] Experiments were conducted as per standardised protocol produced by Axiogenesis, who supplied the hiPSC-CMs used throughout these studies.[212]

2.4.1 Experimental set-up

The RTCA Cardio software was started and experiments were set up as per manufacturer's guidance notes (ACEA biosciences, San Diego). The layout of the 96 well Cardio E-plate was outlined with information including cell type, cell number and compounds to be added to each well. The length of the experiment and number and frequency of impedance readings to be taken (sweeps) was also input into the experimental schedule page.

2.4.1.1 Fibronectin coating of E-plate

Prior to cell seeding the E-plate was coated with fibronectin to facilitate cellular adhesion. A 10µg/ml fibronectin coating solution was prepared by diluting 60µl fibronectin stock solution (1mg/ml) in 6ml PBS with Ca^{2+} and Mg^{2+}, 50µl of which was added to each well of the E-plate and incubated overnight at 4˚C.

2.4.1.2 Background measurement

The following day the fibronectin coating solution was carefully aspirated from the E-plate and 180 µl pre-warmed Cor.4U culture medium (axiogenesis) was added to each well using a multi-

channel pipette. The E-plate was then transferred into the cradle of the RTCA Cardio instrument and incubated for 5 minutes before the background reading was taken.

2.4.1.3 Seeding of cardiomyocytes

A vial containing 4 x 10^6 Cor.4U hiPSC-CMs (axiogenesis) was removed from liquid nitrogen and transferred on ice to a 37˚C water bath and thawed for approximately 2 minutes. The cell suspension was then carefully pipetted into 3ml of pre-warmed Cor.4U medium, and the cryovial washed with a further 1ml of medium, resulting in a total cell suspension volume of 5ml.

The number of live cardiomyocytes was ascertained by performing a cell count with trypan blue. A 1:1 mixture of trypan blue and cell suspension was created and 10µl was applied to a haemocytometer and the number of viable (clear) and dead (blue) cells was determined.

The number of cells in the suspension was then calculated taking into account the chamber factor (1x10^4), dilution factor (2) and total volume (5). The cell suspension was adjusted to contain 3 x10^6 viable cells in 18ml of Cor.4U medium.

The E-plate was disengaged from the RTCA cardio instrument and put inside the cell culture cabinet. The medium in the wells of E-plate was carefully aspirated and 180µl of the cell suspension was added to each well from a sterile reagent reservoir using a multi-channel pipette. This equates to a plating density of 3 x10^4 cardiomyocytes per well. The E-plate was then left for 30 mins at room temperature to allow the cells to settle in an evenly distributed manner at the bottom of the wells. Following this the E-plate was transferred back into the cradle and the recording of impedance measurements was initiated.

2.4.2 Maintenance of cardiomyocytes

The following day the culture medium was exchanged twice – Once in the morning approximately 18 hours after seeding and then again in the evening approximately 26 hours after seeding. For each medium change a 100% medium replacement was performed in four steps – Whereby 90µl of medium was removed from all wells and the same amount of fresh medium was added from a sterile reagent reservoir. For a complete medium change 36ml of pre-warmed of Cor.4U culture medium was required to repeat the process four times. Subsequently a 100% medium change was performed once daily until the addition of compounds.

2.4.3 Compound treatments

Compounds were added to the cardiomyocytes once the cell growth had plateaued and stable baseline beating was observed. The following criteria were checked before commencing with compound addition: An absolute cell index >3, beat rate of 40-100bpm and beat amplitude of >0.02.

Approximately 2 hours prior to compound addition a 100% medium change was performed as described above. The compounds to be added were prepared at double the concentration required in Cor.4U growth medium, and at least 110µl of compound was added to each well of a 96 well plate in the defined plate layout. The 96 well plate containing the compounds was put in to the cell culture incubator for 30 minutes to equilibrate, and immediately prior to addition of the compounds an 11 minute baseline beating measurement was performed. The E-plate was then disengaged and taken to the cell culture cabinet together with the compound plate; compounds were added by removal of 90µl medium from the top each well followed by addition of 90µl of the appropriate double concentrated compound. Once all compounds were added

the E-plate was transferred back into the cardio instrument and the measurements were resumed.

On subsequent days compounds were added again by removing 90µl compound solution from the top of the well followed by addition of 90µl of the appropriate single concentrated compound, or compounds were washed out using the four step medium change method.

2.4.4 Data analysis

Parameters relating to contractility of hiPSC-CMs such as beat frequency and beat amplitude were analysed using the data analysis function of the RTCA Cardio software V1.0.

Statistical analysis on normalised cell index, normalised beat rate and normalised beat amplitude were conducted using a one way analysis of variance (ANOVA) test, and a post-hoc Dunnett's test when required. Where only two data groups were compared a paired T-test was used. Statistical analysis was performed using GraphPad Prism (Version 7.04, GraphPad Software, Inc.).

Chapter 3: Qualification of *In Vitro* Models for Cardiotoxicity Evaluation

3.1 Introduction

Cardiotoxicity is a leading cause of drug attrition and withdrawal, and is categorised as the second leading toxicity responsible for 16% of withdrawals according to the WITHDRAWN database.[213] The current method of pre-clinical testing for cardiac liabilities outlined by the ICH-S7B guidelines focusses narrowly on the ability of compounds to block the human ether-à-go-go related gene (hERG) potassium channel *in vitro*, followed by evaluation of the ability to prolong ventricular repolarisation and therefore prolong the QT-interval *in vivo*.[177]

Contractility of cardiomyocytes involves coordinated regulation and activity of a multitude of ion channels, transferring potassium, calcium and sodium ions into and out of the cell, resulting in an action potential and cardiomyocyte contraction (Figure 3.1). One of these channels, the rapid delayed rectifier potassium current (IKr) or hERG1 channel, is essential for ventricular repolarisation and therefore essential to maintain normal cardiac rhythmicity. Prevention of the flow of potassium ions through this channel can result in arrhythmogenicity and possible development of fatal disorders such as long QT syndrome and Torsades de pointes (TdP) [214,215] (Figure 3.2). These conditions can both occur due to drug inhibition of the hERG channel, with several drugs such as terfenadine and cisapride now withdrawn from the market due to prolongation of the QT interval via hERG channel inhibition.[80]

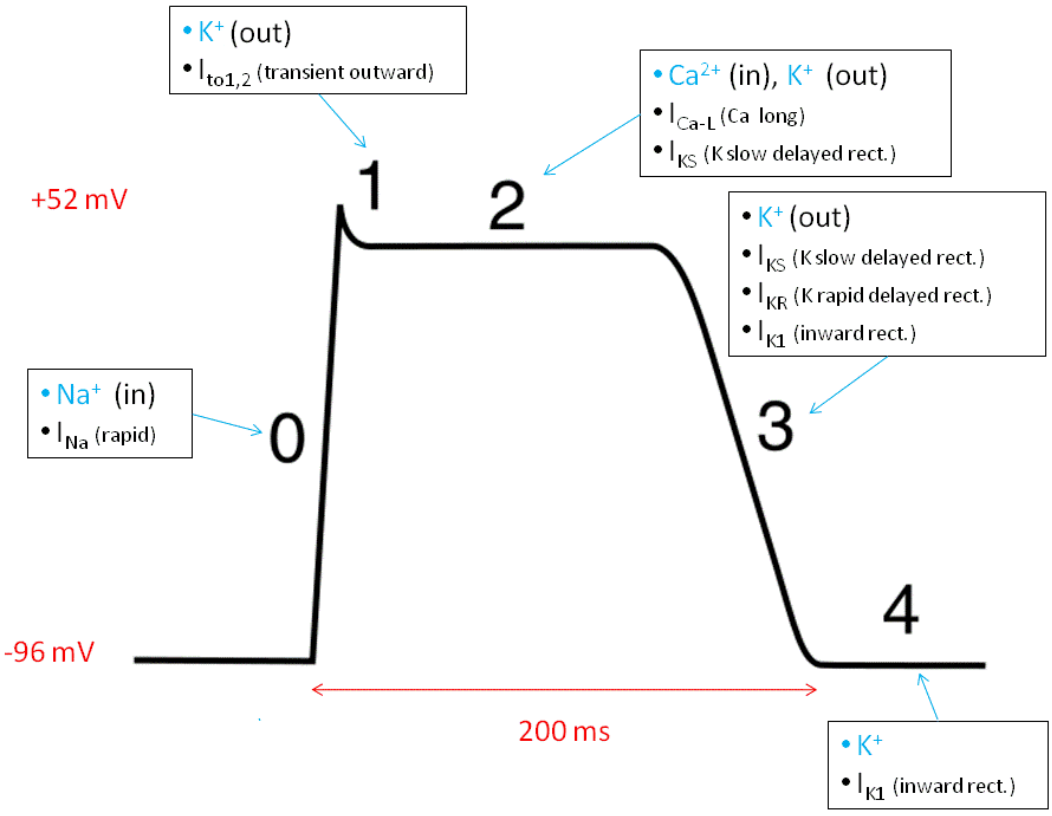

Figure 3.1 Relationship between the ventricular action potential and ionic currents

Schematic representation of the ventricular action potential with phases 0-4 indicated and the ionic currents responsible for the action potential phases. Adapted from reference.[216]

Figure 3.2 Effect of hERG channel inhibition on cardiac rhythm

Schematic representation of a normal ECG trace and an ECG trace with a prolonged QT interval, with waves, segments, and intervals labelled (Left). Schematised ECG strip showing a normal rhythm and a Torsades de Pointes rhythm (Right). Adapted from reference.[217]

3.1.1 Limitations of hERG channel screening during drug development

Although inhibition of the hERG channel is responsible for approximately half of drug withdrawals related to appearance of cardiac adverse effects,[80] drugs can disturb cardiac function in a host of other ways including structural damage to the myocardium, perturbation of signalling pathways relating to cardiac homeostasis, function and survival, and modulation of other ion channels important for generating the cardiac action potential that precedes cardiomyocyte contraction.[80]

Such cardiotoxicities are overlooked as the hERG channel screen is too simplistic, as it evaluates a single channel in isolation, and therefore not representative of the complex nature of cardiomyocyte electrophysiology and function. Although many of these disturbances, if not detected via hERG screening, could be identified using subsequent telemetric analysis *in vivo* if they culminate in a change to cardiac rhythm. However, *in vivo* models are costly, and are somewhat of an unethical substitute for a poor *in vitro* assay,[218] which do not always translate to humans due to differences in electrophysiology.[219] As such, there is an urgent need for better pre-clinical models that are able to accurately capture information on a compound's ability to cause both functional and structural cardiotoxicity, which would ideally start during the *in vitro* phase of safety testing.[181]

3.1.2 Pre-clinical evaluation of cardiac effects during development of oncology drugs

In contrast to development of 'conventional' drugs, a degree of toxicity risk is generally accepted during the development of oncology drugs. By definition these agents do not have a safety margin and therefore must be screened using a paradigm focused on mechanism of action and monitorability, as defined in the ICHS9 guidelines.[220] Such a strategy aims to identify

cardiovascular side effects during discovery and identify and mitigate the occurrence of undesirable cardiovascular toxicities in oncology drug development.

Furthermore, in addition to measurement of drug-induced proarrhythmia induced during and directly after initiation of oncology treatment, these drugs are now known to also cause latter chronic forms of toxicity including pathological cardiac changes.[29,221] Moreover, since chronic progressive cardiomyopathies are now a major concern for clinical use of cancer drugs, there is a need to build upon our improved understanding of mechanisms of drug-induced cardiotoxicity to explore and predict long-term effects of many anticancer therapeutics.[83]

In light of the inherent cardiac risks of treatment with cancer therapeutics and the increasingly sensitive patient population, as with other drug classes, improved screening paradigms are also required for the development of oncology drugs.

3.1.3 Improved *in vitro* models for evaluation of drug-induced cardiac effects

Historically, there has been a lack of *in vitro* cardiac models that were both clinically and physiologically relevant i.e. human derived cells that exhibit a cardiac phenotype and possess contractile ability. Such models are essential for detection of drug effects upon cardiac cells, including both structural and functional changes. Several studies have addressed the use of primary human cardiomyocytes for this purpose, and methodologies have been developed for their maintenance in culture which allow spontaneous beating in a synchronised manner for brief periods. However, barriers to supply and the existence of a narrow window by which to monitor cardiomyocyte contraction limits their applicability for routine screening.[194] Consequently, new cellular models are required with the ability to monitor drug effects in a cardiac and physiological relevant manner, and with capability for longer-term assessment.

3.1.3.1 The AC10 human ventricular cardiomyocyte cell line

AC10 cardiomyocytes (AC10-CMs) are a recently developed cell line derived by fusing human ventricular cardiomyocytes with fibroblasts transformed with SV40 virus and devoid of mitochondrial DNA.[188] Although other cell lines with capability for long-term *in vitro* culture exist, such as the HL-1 mouse atrial cardiomyocyte cell line,[187] and the H9c2 rat cardiomyoblast cell line,[183] these cells being non-human have limited use in examining effects of ventricular cardiomyopathies in humans. Conversely, the AC10-CM cell line, despite being in a pre-contractile state, express many cardiac specific transcription factors, contractile proteins and possess functional gap junctions.[188] As an immortalised cell line, AC10-CMs may be applicable for use in high-throughput screening assays for detection of structural toxicity, however current data remains limited. The cells have been used for toxicity studies focussed on the effects of methylmercury on mitochondrial bioenergetics and cell viability[222] and also to investigate pathways relating to cellular hypertrophy of cardiomyocytes.[223] The major limitation in the use of this cell line is its lack of contractility, meaning that it may have applicability for structural but not functional contractile studies.

3.1.3.2 Human induced pluripotent stem cell derived cardiomyocytes

The recent development of hiPSC-derived cardiomyocytes (hiPSC-CMs) provides a resolution to assessment of drug-induced functional changes in cardiomyocytes, as they are functionally active and spontaneously contract *in vitro*, and importantly are easily obtainable as they are created from human pluripotent stem cells.[191,190] These cells address the concerns related to the simplistic nature of the hERG channel screen, as they are more representative of the complex nature of cardiomyocyte electrophysiology and cardiac cell function and therefore have the potential to detect both structural and functional cardiotoxicity.

Although hiPSC-CMs possess many favourable features, It is has been frequently noted that many current available models resemble embryonic cardiomyocytes and are described as having an immature phenotype. Robertson *et al*. reviewed this subject in depth and discussed the differences between embryonic and adult cardiomyocytes[192] which are outlined in section 1.8.2.1. Despite the immature phenotype of hiPSC-CMs, they are still considered more clinically relevant than other *in vitro* cardiac cell models, such as the rodent cell lines H9c2 and HL-1, and the non-contractile human AC10 or AC16 cell lines, which have been utilised in preliminary cardiac studies *in vitro*.[182]

The hiPSC-CM model represents a physiologically relevant source of human adult cardiomyocytes that can be cultured easily for long periods of time and are readily available for routine drug testing - A feature absent from other human derived *in vitro* models.[194] Therefore hiPSC-CMs and their inherent contractile activity have become applicable to many *in vitro* cardiotoxicity assays, and have shown considerable promise to accurately detect cardiac liabilities in drugs with known cardiac effects on a number of platforms.[201,203] The success of this cell model will have significant potential for a further exciting advancement, the development of patient-specific hiPSC-CMs which can be used to study personalised and precision medicines in the context of a particular risk factor or disease.[195]

The increased use of hiPSC-CMs within cardiac safety assessment studies has caused a surge in the development of new high-throughput assays that allow the functional activity of cardiomyocytes to be assessed, such as video microscopy, microelectrode arrays and impedance-based assays. These assays measure the electrophysiological changes that precede contraction or quantify the contraction itself. Impedance-based cellular analysis is an innovative method of assessing the contractility of hiPSC-CMs and has emerged as an exceptional platform for monitoring cardiomyocyte beating and viability.

3.1.4 *In vitro* technologies for determination of cardiac cell contraction

Traditionally, monitoring electrophysiological fluctuations of excitable cells was carried out using patch clamping. Although this technique allows for the activity of single ion channels to be assessed, it is labour intensive, limited to isolated cardiomyocytes, and evaluates cell effects at a snapshot in time, making this technique unsuitable for high-throughput screening.[199] Microelectrode arrays (MEAs) are plate based assays whereby hiPSC-CMs are seeded into the wells of specialised plates that have a series of electrodes on the bottom of the wells. Once the cells form a cohesive monolayer and begin to spontaneously contract, their electrophysiological profile is captured by the electrodes in real-time allowing parameters such as beat rate, field potential duration, amplitude and conduction velocity to be assessed.[200] In contrast to the traditional patch-clamp approach, MEAs measure the total extracellular change of ions and therefore assess changes in all major ion channels implicated in the action potential. Cellular impedance-based assays measure the contraction of hiPSC-CMs, and therefore also assess changes in the activity of all ion channels in addition to the monitoring of other factors that may affect contractility.[206]

3.1.4.1 Cellular impedance technology

Cellular impedance technology allows for real-time, label free monitoring of cardiomyocyte viability and beating over sustained periods (As described previously in section 1.8.3.4). Minute cardiomyocyte movements that occur during contraction cause transient changes in impedance; these small morphological changes to cardiomyocytes are detected by electrodes which creates a surrogate pattern based on the contractility of the cells. These features allow for sensitive and robust monitoring of the effects of compounds on cardiomyocyte function and health in a high-throughput approach that is reflective of clinical exposures.[205]

As cardiomyocyte contraction is downstream of the cardiac action potential and calcium flux in cardiac excitation-contraction coupling, the surrogate measurement of contractility generated by cellular impedance technology has the potential to detect drug induced disturbances to the action potential, calcium flux and mechanical contraction (Figure 3.3). Whereas patch clamping and MEA technologies would be applicable to detection of electrophysiological cellular changes, these technologies are unable to detect alterations in intracellular signalling leading to modulation in cardiomyocyte contractility. For example, the reduced contraction strength caused by the myosin II inhibitor blebbistatin can be demonstrated using impedance technology, however effects of the drug are absent using both microelectrode arrays (MEAs) and calcium fluctuation assays which measure endpoints higher in the cascade.[207] As a result, impedance technology has the potential to detect both functional and structural drug-induced cardiotoxicity, which could lead to both earlier cardiovascular hazard identification in the drug development process and robust assessment of mechanisms of drug interactions.

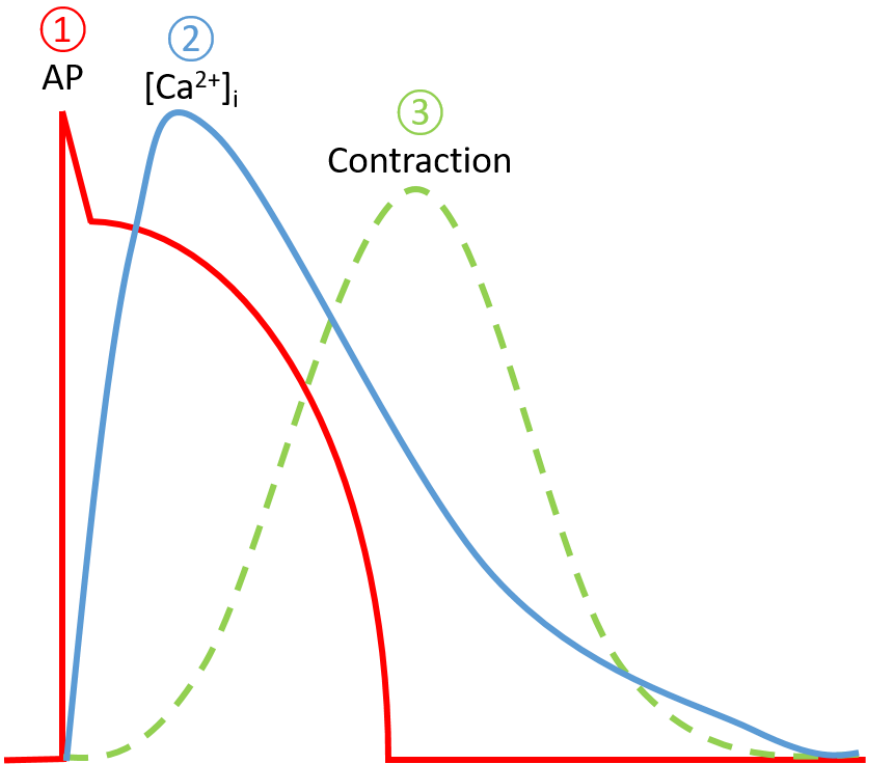

Figure 3.3 **The relationship between action potential (AP), $[Ca^{2+}]_i$ and cellular contraction**

A recent study by Doherty *et al*. assessed if a multi-parameter *in vitro* screen could detect cardiotoxicity across multiple drug classes with known clinical cardiac risks. A range of studies were carried out, however the most sensitive test was the impedance based xCELLigence cardio system which detected 16/18 known cardiotoxicants as cardiotoxic.[208] The results from this study support the development of the new cardio safety paradigm Comprehensive *in vitro* Proarrhythmia Assay (CiPA) which is currently being developed (see section 1.9.1). The overall goal of CiPA is to develop a new screening strategy that places greater emphasis on the accurate prediction of cardiotoxicity using various *in vitro* high-throughput hiPSC-CM assays combined with patch clamp assays and *in silico* simulations. If successfully implemented CiPA could avoid the unwarranted attrition of useful drugs, accelerate the development of safe drugs and reduce development costs.[180,181]

3.1.5 Aims and objectives

The aim of this chapter is to characterise the suitability of the AC10 cardiomyocyte cell line (AC10-CMs) and hiPSC-derived cardiomyocytes (hiPSC-CMs) for detection of structural and functional cardiotoxicity, in order to qualify their use for *in vitro* screening paradigms.

Specifically:

i) Characterisation of the cardiac phenotype of AC10-CMs. The expression of cardiac specific proteins and markers of cellular proliferation will be determined followed by examination of their growth kinetics and optimisation of cytotoxicity protocols.

ii) Optimisation of AC10-CMs for detection of structural cardiotoxicants. In AC10-CMs, viability and morphology of cells exposed to the hypertrophic mediator angiotensin II and the structural and functional cardiotoxicant sunitinib will be determined using the xCELLigence RTCA and the MTT assay.

iii) Optimisation of the hiPSC-CM model for detection of structural and functional cardiotoxicants *in vitro*. The initial growth and contractility of these cells will be monitored on the impedance based xCELLigence cardio instrument, followed by assessment of their responsiveness to drugs with known cardiac effect once stable beating is detected. The established methodology will then be qualified using the hypertrophic mediator angiotensin II and the structural and functional cardiotoxicant sunitinib, with survival, contractility and cellular morphology monitored using the xCELLigence cardio system.

Similar to the optimisation and qualification of hiPSC-CMs described within this chapter, an additional study was conducted using Axol hiPSC-CMs which was later published in Nature Methods Application Notes in November 2016 (Appendix 2).

3.2 Materials and methods

3.2.1 Immunostaining

AC10 cardiomyocytes (AC10-CMs) were immunostained to verify the expression of a variety of cardiac specific proteins including contractile proteins and transcription factors. The immunostaining protocol detailed below was developed by Dr Gavin Richardson (Newcastle University) who kindly provided reagents, antibodies and assistance with this technique.

A suspension of AC10-CMs was created and cell number determined using a haemocytometer. The cell number was adjusted and cells were seeded in chamber cell culture slides (NUNC, USA) at a density of $1x10^5$ cells per chamber. The cells were left overnight to adhere to the slide surface.

Cells were washed with PBS and then incubated with 1ml 4% paraformaldehyde (PFA) at room temperature for 20 minutes. Following this the cells were washed once with PBS and incubated in PBS at 4°C until commencing staining. Slides were then incubated in 0.4% triton-X-100 for 20 minutes and then blocked with 20% FBS for 30 minutes. Following addition of primary antibody (1:200 dilution in PBS) or no antibody control (PBS alone) the slides were incubated overnight at 4°C. Slides were washed (3 x 5 minutes) in PBS and then incubated at room temperature for one hour with the relevant secondary antibody (1:500 dilution in PBS, see table 3.1 below for antibody details) and the nuclear stain 4',6-diamidino-2-phenylindole (DAPI; 1:500 dilution in PBS). For no secondary antibody control chambers, PBS and DAPI were used. Slides were then washed in PBS (3x 5 minutes), and antifade solution and the coverslips added. Slides were subsequently visualised on a Nikon Eclipse Ti confocal fluorescence microscope and images captured using NIS elements software V4.2.

Primary antibody	*Antibody type*	*Secondary antibody**	*Fluorescent tag*	*Colour emitted*
Troponin I	Goat polyclonal	Anti-goat	Alexa 594	red
Troponin C	Goat polyclonal	Anti-goat	Alexa 488	green
Tropomyosin	Rabbit polyclonal	Anti-Rabbit	Alexa 488	green
Alpha actinin	Rabbit polyclonal	Anti-Rabbit	Alexa 488	green
NKX2.5	Rabbit polyclonal	Anti-Rabbit	Alexa 488	green
BMP-2	Goat polyclonal	Anti-goat	Alexa 488	green
PCM1	Rabbit polyclonal	Anti-Rabbit	Alexa 488	green
Ki-67	Murine monoclonal	Anti-mouse	Alexa 594	red
Vimentin	Chicken monoclonal	Anti-chicken	Alexa 594	red
α-smooth muscle actin	Rabbit polyclonal	Anti-Rabbit	Alexa 488	green
**All secondary antibodies sourced from Invitrogen*				

Table 3.1 Antibodies used for immunostaining evaluation of cardiac phenotype of AC10 cardiomyocytes

3.2.2 Validation of the MTT assay

Cell suspensions of AC10-CMs were created containing $4x10^4$ and $3x10^4$ cells/ml. These were serial diluted in 2-fold increments to obtain a range of 9 concentrations ($4x10^4$, $3x10^4$, $2x10^4$, $1.5x10^4$, $1x10^4$, $7.5x10^3$, $5x10^3$, $3.55x10^3$ and $2.5x10^3$ cells/ml) which were added to 8 wells of a 96-well plate in 100µl volumes equating to plating densities of 4,000, 3,000, 2,000, 1,500, 1,000, 750, 500, 375 and 250 cells/well. The following day 1:10 MTT was added and absorbance readings were obtained and analysed as described in section 2.2.

3.2.2.1 Growth curve analysis determined by the MTT assay

Cell suspensions of AC10-CMs were created containing $1x10^4$, $2x10^4$, $1x10^5$ and $2x10^5$ cells/ml; each density was seeded in to 6 wells of five 96-well plates at 100µl volume equating to plating densities of 1,000, 2,000, 10,000 and 20,000 cells/well. MTT solution was added to one plate every day for the next 5 days and absorbance readings obtained and analysed as described in section 2.2. From the growth curve analysis a plating density of 2,000 cells/well was chosen for experiments using AC10-CMs in the exponential growth phase.

3.2.2.2 Determination of cell number required for confluence within 24 hours

A suspension of AC10-CMs was created containing $6x10^5$ cells/ml, this was diluted accordingly to obtain suspensions at an additional 10 densities, reducing by 50,000 cells each time. Seeded at 100µl per well in 8 wells of a 96-well plate, this equated to plating densities of 60,000, 55,000, 50,000, 45,000, 40,000, 35,000, 30,000, 25,000, 20,000, 15,000 and 10,000 cells/well. The following day the wells were observed under a microscope to check for gaps in the monolayers and attainment of confluence, MTT solution was then added and absorbance readings were obtained and analysed as described in section 2.2. Based on the results a plating density of 35-40,000 cells/well was chosen for experiments using AC10-CMs in the plateau growth phase.

3.2.3 Analysis of growth kinetics of AC10 cardiomyocytes using the xCELLigence RTCA system

The growth kinetics of AC10-CMs were analysed using the xCELLigence real-time cell analyser (RTCA) to identify the optimum seeding density of AC10-CMs for future experiments. The protocol was carried out as described in section 2.3 except a serial dilution of cells was created starting with $2x10^5$ cells/ml which was then serial diluted in 2 fold dilution increments five times to obtain a total range of six cell concentrations ($2x10^5$, $1x10^5$, $5x10^4$, $2.5x10^4$, $1.25x10^4$ and $6.25x10^3$ /ml), 100µl of each was added in duplicate to a 16 well E-plate. Following cell seeding a 1:2 medium change was performed every 48 hours until termination of the experiment by removing 100µl of medium from the wells and adding 100µl of fresh medium. A seeding density of 5000 cells/well ($5x10^4$cells/ml) was chosen as the optimum seeding density for cells in the exponential phase of growth. For experiments requiring cells to be in the plateau phase of growth, cells were plated at of 10,000 cells/well ($10x10^5$cells/ml) and left for approximately 72 hours for the cells to reach confluence.

3.2.4 Determination of cellular viability of AC10-CM following exposure to angiotensin II

AC10-CMs were seeded into 96-well plates as previously described in section 2.2 for exponential phase studies. Concentrations of angiotensin II were prepared ranging from 600-200pM which were applied to AC10-CMs the following day. The experiment was terminated following 96 hours exposure to angiotensin II by addition of MTT solution, absorbance readings were obtained and analysed as described in section 2.2.

3.2.5 Determination of cellular viability of AC10-CM following exposure to sunitinib

AC10-CMs were seeded into 96-well plates as previously described in section 2.2 for exponential and plateau phase studies. After 24 hrs, sunitinib was added to cells by performing a 1:2 serial dilution across the wells, resulting in final concentrations ranging from 20µM to 0.078µM. The experiment was terminated after 96 hours exposure to sunitinib by addition of MTT solution, absorbance readings were obtained and analysed as described in section 2.2 and IC_{50} values were determined by implementing curve fitting by non-linear regression on GraphPad Prism (Version 7.04, GraphPad Software, Inc.).

3.2.6 Determination of morphological changes induced by angiotensin II and sunitinib in AC10-CM using the xCELLigence RTCA

Experiments were set up as described in section 2.3. For studies in exponential growth phase, Angiotensin II or sunitinib addition commenced at 24 hours and continued at 24 hour intervals until the experiment was complete (96 hours exposure for angiotensin II and 72 hours exposure for sunitinib). For studies in plateau growth phase, sunitinib addition commenced once the cell index demonstrated confluence (approximately 72 hours) and continued at 24 hour intervals until a total of 72 hours exposure. All experiments were performed in triplicate and statistical analysis on normalised cell index values was conducted using a One way analysis of variance (ANOVA) test, and a post-hoc Dunnett's test when required using GraphPad Prism (Version 7.04, GraphPad Software, Inc.).

3.2.6.1 Evaluation of viability of AC10-CMs following exposure to angiotensin II and sunitinib at specific time points, determined using the MTT assay

Cellular viability was also determined following exposure to angiotensin II and sunitinib at specific time points to complement data obtained using the xCELLigence RTCA. For these studies, cells were plated for exponential phase studies as previously described and 200pM and 300pM angiotensin II was added to cells every 24 hours for 4 consecutive days. Experiments were terminated at 96 hour exposure, and absorbance readings were obtained and analysed as described in section 2.2.

For determination of cell viability of sunitinib exposed AC10-CMs, cells were plated for exponential phase and plateau phase studies as previously described and 50nM, 250nM and 500nM sunitinib was added to cells the following day. Experiments were terminated following 24 hour exposure to sunitinib, and absorbance readings were obtained and analysed as described in section 2.2.

3.2.7 Imaging of AC10-CMs treated with angiotensin II and sunitinib

For studies involving angiotensin II, AC10-CMs were seeded into T25 flasks at a density of 2.5 x 10^4 cells. After 24hrs, 300pM angiotensin II was added every 24 hours for 4 consecutive days. At 96 hours exposure the cells were fixed using 4% PFA as previously described (see section 3.2.1).

For studies involving sunitinib AC10-CMs were plated at a density of $5x10^4$ cells/well in 6 well plates. The following day 500nM sunitinib was added to 2 wells and following 24 hours exposure cells were fixed using 4% PFA (detailed in section 3.2.1). All experiments included a time matched vehicle control. Cellular images were collected using a Leica DIC DMI6000B inverted microscope and analysed using the Leica application suite. All studies were repeated in triplicate.

3.2.8 Evaluation of drug-induced cardiotoxicity in hiPSC-CM using the xCELLigence Cardio system

The xCELLigence cardio system was used to analyse the initial growth and contractility of Cor.4U hiPSC-derived cardiomyocytes (hiPSC-CMs). Briefly, this involved set up of the experiment on the RTCA cardio software as per manufacturer's guidelines, fibronectin coating of the e-plate and seeding of hiPSC-CMs at a density of 30,000 cells/well. The day after cell seeding a full medium exchange was performed twice and then once daily thereafter. Full experimental details are described in section 2.4. Once stable beating was detected investigation of the effects of the β-adrenergic agonist isoproterenol and the hERG potassium channel blocker E-4031 on contractility was determined. Changes in morphology and contractility were also evaluated following addition of sunitinib and angiotensin II, which were added at 24 hour intervals over 72 hours. For the first addition of a compound, half the media (90µl) was removed from each well and replaced with media containing twice the required drug concentration. For all subsequent compound additions, half the drug solution (90µl) was removed from each well and replaced with media containing required drug concentration. The protocol followed for use of the xCELLigence cardio system can be found in section 2.4.

Statistical analysis on normalised cell index, normalised beat rate and normalised beat amplitude were conducted using a one way analysis of variance (ANOVA) test, and a post-hoc Dunnett's test when required. Where only two data groups were compared a paired T-test was used. Statistical analysis was performed using GraphPad Prism (Version 7.04, GraphPad Software, Inc.).

3.3 Results

The purpose of this phase of the project was to determine the suitability of the AC10 cardiomyocyte cell line (AC10-CMs) and human hiPSC-derived cardiomyocytes (hiPSC-CMs) for detection of structural and functional cardiotoxicity. Following characterisation of growth kinetics in both cell types, cytotoxicity protocols were optimised for AC10-CMs and the response of hiPSC-CMs to drugs with known cardiac effects was determined. The established methodology was then qualified using the hypertrophic mediator angiotensin II and the structural and functional cardiotoxicant sunitinib.

3.3.1 Confirmation of the cardiac phenotype of the AC10 cardiomyocyte cell line

The AC10-CMs are a proliferative cell line created by fusion of healthy human ventricular cardiomyocytes with SV40 transformed fibroblasts devoid of mitochondrial DNA.[188] Immunocytochemical analyses were used to determine the expression of cardiac proteins (Figure 3.4), markers of cellular proliferation, mesenchymal specific proteins and vascular proteins (Figure 3.5).

Expression of the contractile proteins troponin I, troponin C, tropomyosin and α-actinin were detected in addition to the cardiac specific transcription factor NKX2.5 and bone morphogenetic protein 2 (BMP-2) which is involved in cardiac cell differentiation (Figure 3.4). The cellular proliferation markers pericentriolar material 1 (PCM1) and Ki-67 were also present, as was the mesenchymal protein vimentin. Negative expression was obtained for alpha smooth muscle actin, which is the predominate form of actin found in vascular muscle cells. (Figure 3.5).

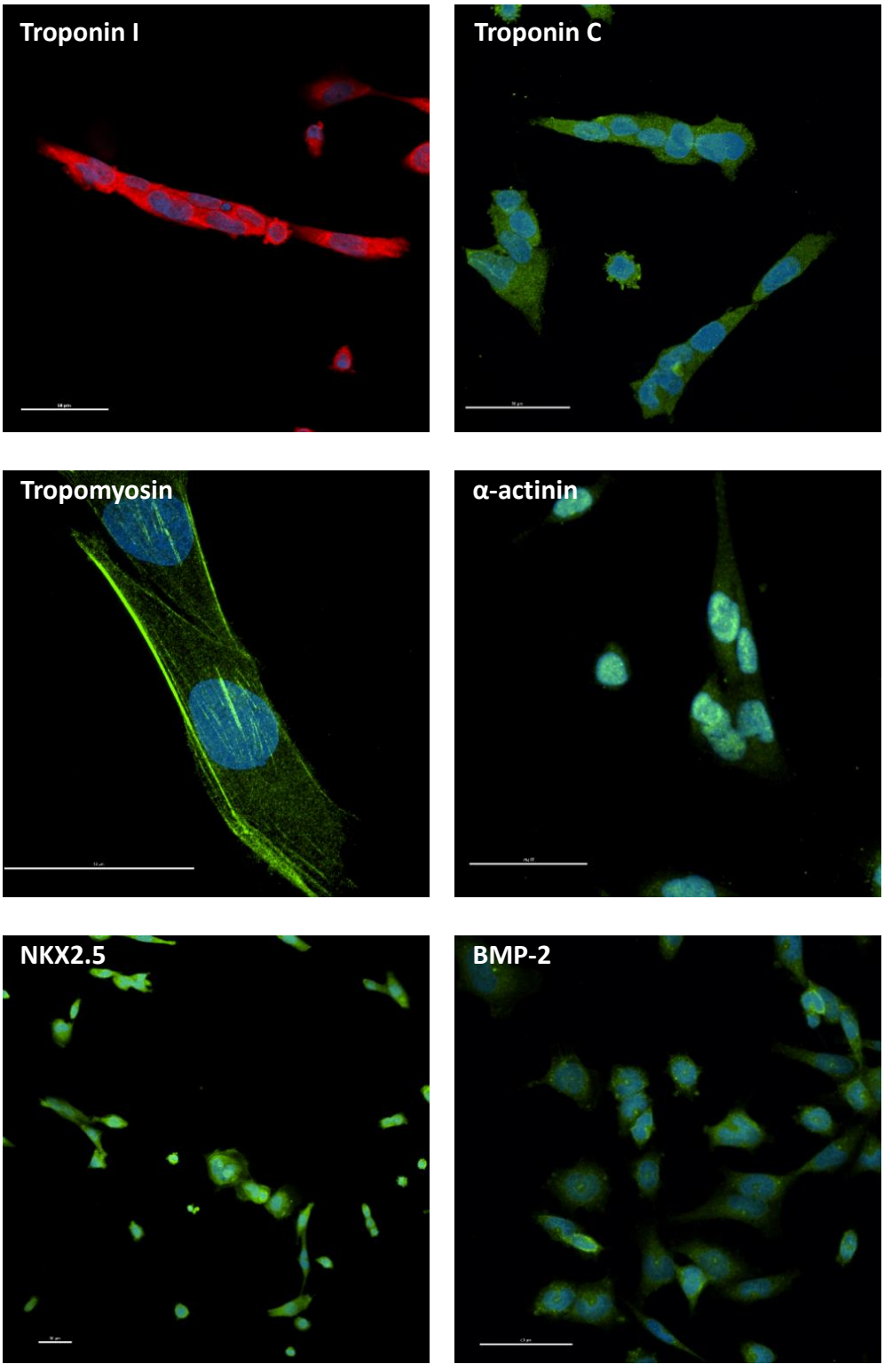

Figure 3.4 Immunostaining of AC10 cardiomyocytes for cardiac proteins

Positive staining for troponin I, troponin C, tropomyosin, α-actinin, NKX2.5 and BMP-2. Proteins of interest are stained red or green, nuclei are stained blue with DAPI. Images shown are at either high (x40) or low (x10) magnification with 50μM scale bar shown on images.

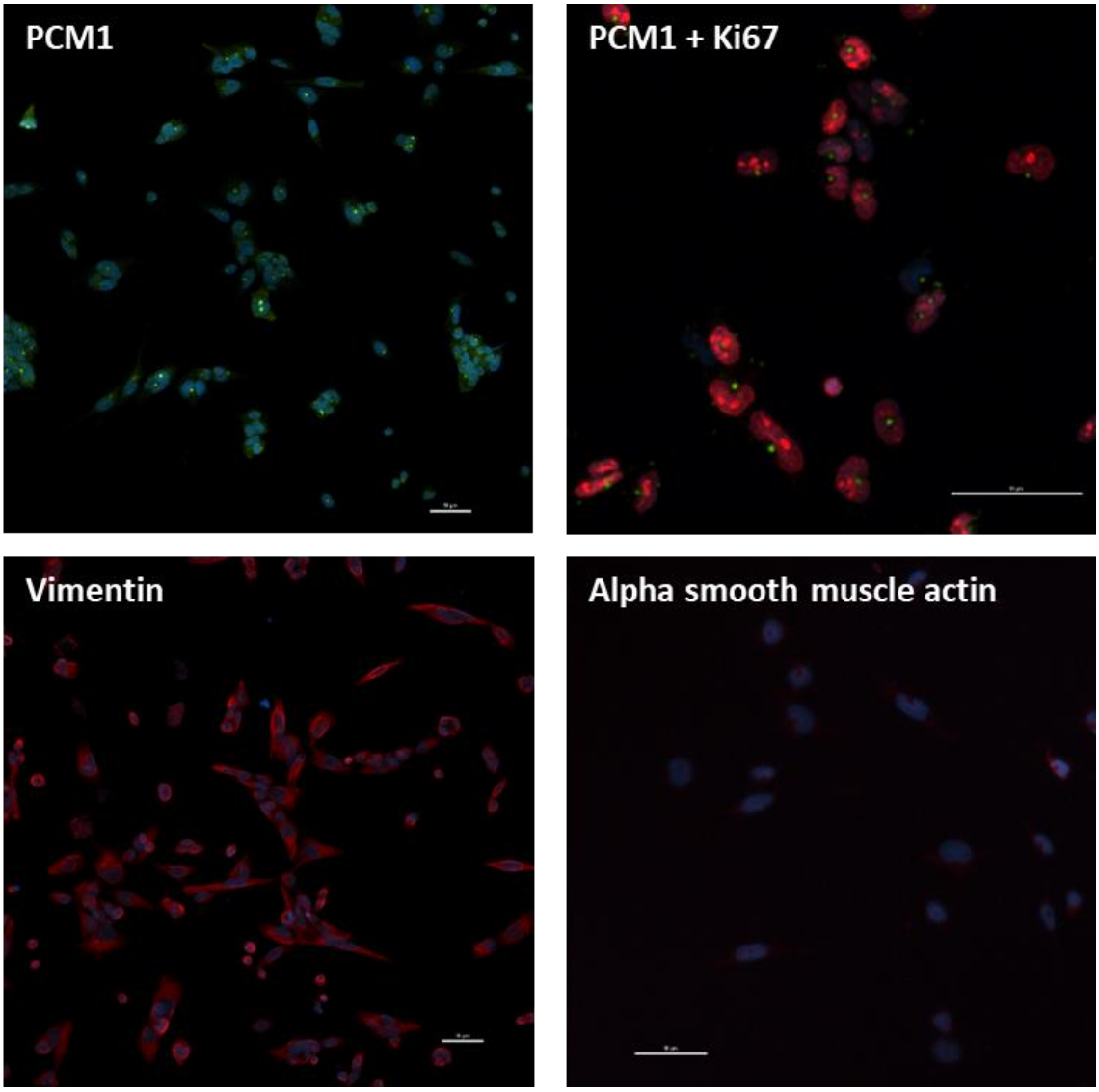

Figure 3.5 Immunostaining of AC10 cardiomyocytes for other proteins of interest

Positive staining for the proliferative markers PCM1 and Ki-67 and the mesenchymal marker vimentin. Negative staining was obtained for alpha smooth muscle actin. Proteins of interest are stained red or green, nuclei are stained blue with DAPI. Images shown are at either high (x40) or low (x10) magnification with 50µM scale bar shown on images.

3.3.2 Optimisation of cell viability assays using AC10 cardiomyocytes

The MTT assay as a methodology for quantifying cell number was validated by investigating the relationship between cell number, determined manually, and MTT conversion via quantification of absorbance at 550nm. Figure 3.6 shows a linear relationship between cell number of AC10-CMs and absorbance, exemplified by the R^2 value of 0.9944.

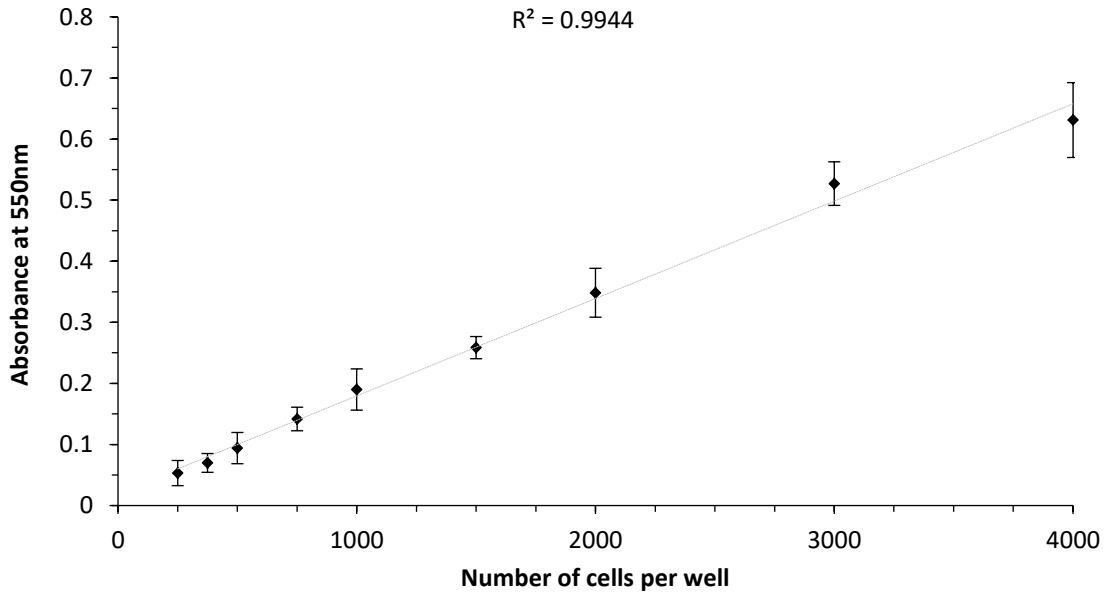

Figure 3.6 Validation of the MTT assay in AC10 cardiomyocytes

Cell number vs absorbance at 550nm of various densities of AC10-CMs 24 hours after cell seeding. Data points show average values ± SD, $R^2 = 0.9944$.

3.3.2.1 Measurement of growth kinetics of AC10 cardiomyocytes using the MTT assay

Cells were seeded at various densities (1000, 2000, 10,000 and 20,000 cells/well) and the absorbance quantified for the MTT assay on five consecutive days (Figure 3.7). Cells seeded at 1,000 cells/well shows little proliferation over 5 days, whereas seeding densities of 10,000 and 20,000 cells/well showed immediate exponential growth and lack of a lag phase of cell growth, with cells approaching confluence after 72 hours. Cells seeded at an initial density of 2,000 cells/well showed a relatively short lag phase, with exponential growth beginning after 1 day and lasting the duration of the experiment. Subsequently, a seeding density of 2000 cells/well was chosen for MTT studies of cells in the exponential growth phase.

In order to identify the optimal seeding density to obtain plateau cellular growth within 24 hours, AC10-CMs were seeded at densities between 10,000 and 60,000 cells/well. Analysis of absorbance using MTT assay revealed the absorbance to be relatively stable at cell densities above 30,000 cells (figure 3.8), therefore a density of 35-40,000 cells was chosen as the seeding density for MTT studies in the plateau growth phase.

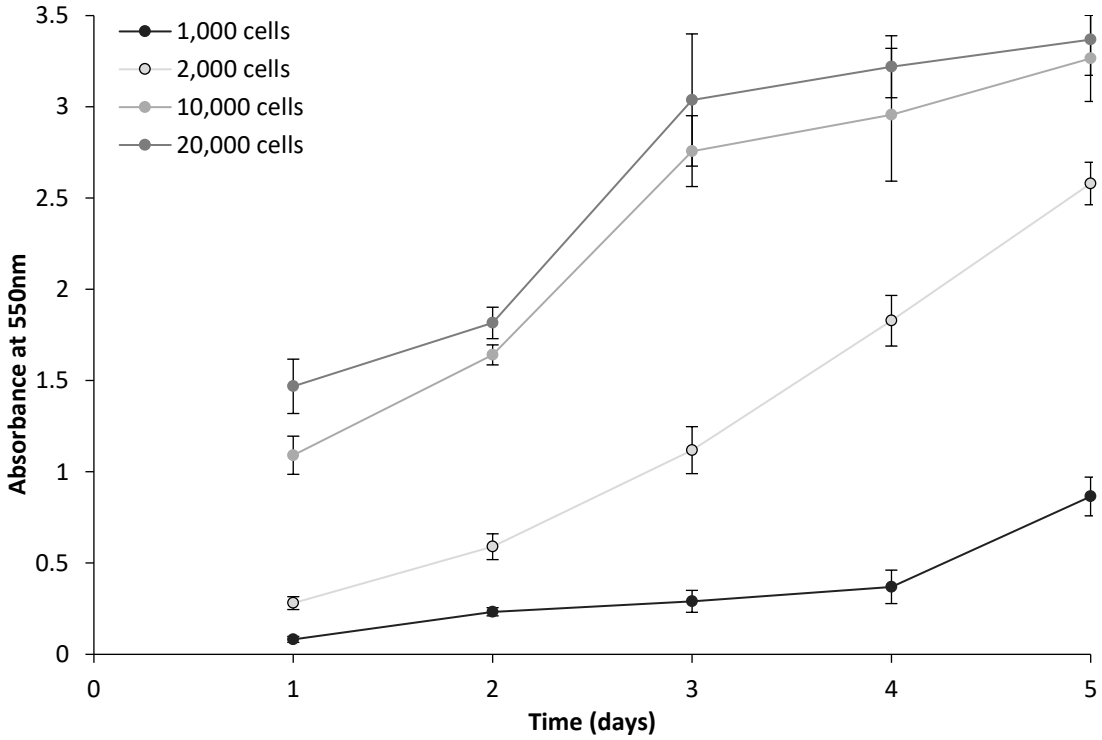

Figure 3.7 Growth curves of AC10 cardiomyocytes generated using MTT assay

Absorbance at 550nm of AC10-CMs seeded at 1,000, 2,000, 10,000 and 20,000 cells/well over a time course of 5 days. Data points show average values ± SD.

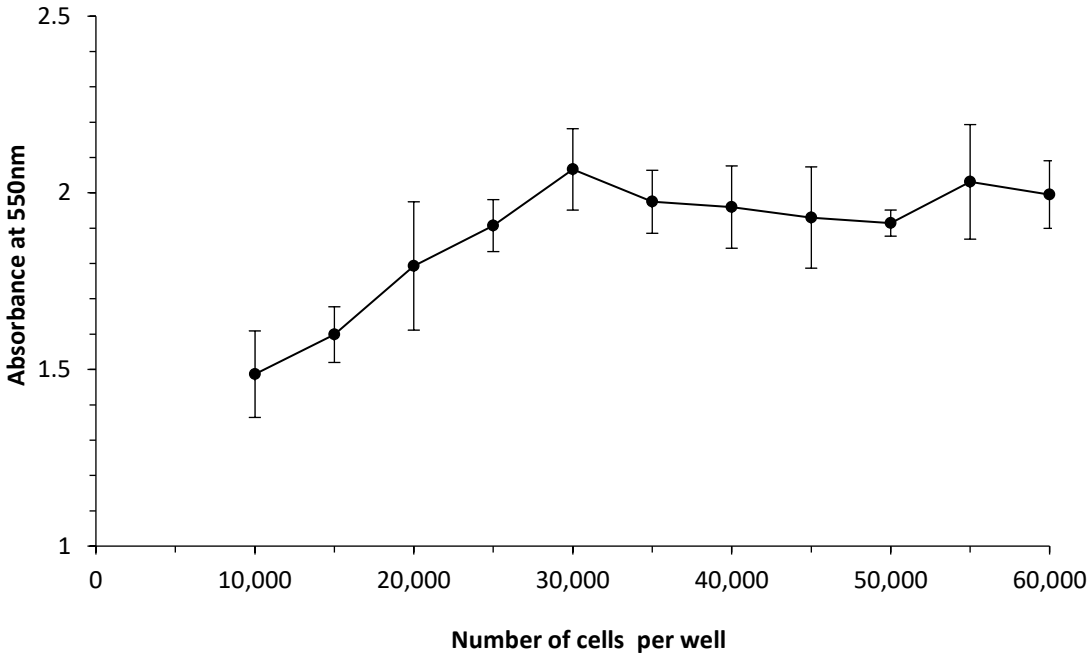

Figure 3.8 Optimisation of seeding density for MTT studies in plateau growth phase

Cell number vs absorbance at 550nm for various densities of AC10-CMs 24 hours after cell seeding. Data points show average values ± SD.

3.3.2.2 Measurement of growth kinetics of AC10 cardiomyocytes using xCELLigence real time cell analyser

The xCELLigence RTCA was used to assess the proliferation of AC10-CMs in real-time. The growth of cells plated at high density (20,000, 10,000 and 5,000 cells/well) and low density (2,500, 1,250 and 625 cells/well) are shown in Figures 3.9A and 3.9B, respectively. Cells plated at higher densities reached the plateau phase of growth sooner than cells plated at lower density and showed a much shorter lag phase. The longer lag phase observed with cells plated at low density resulted in a delay in exponential growth that was not seen in cells plated at higher densities. Based on these findings a seeding density of 5,000 cells was chosen for exponential growth phase studies, as this cell number exhibited a short lag phase and long exponential phase (until 100 hours), maintaining cells in exponential growth for the duration of experiments. When cells were required to be confluent (plateau growth phase), cells were plated at a density of 10,000 cells and left to proliferate for approximately 72 hours before beginning experimental protocols.

3.9A

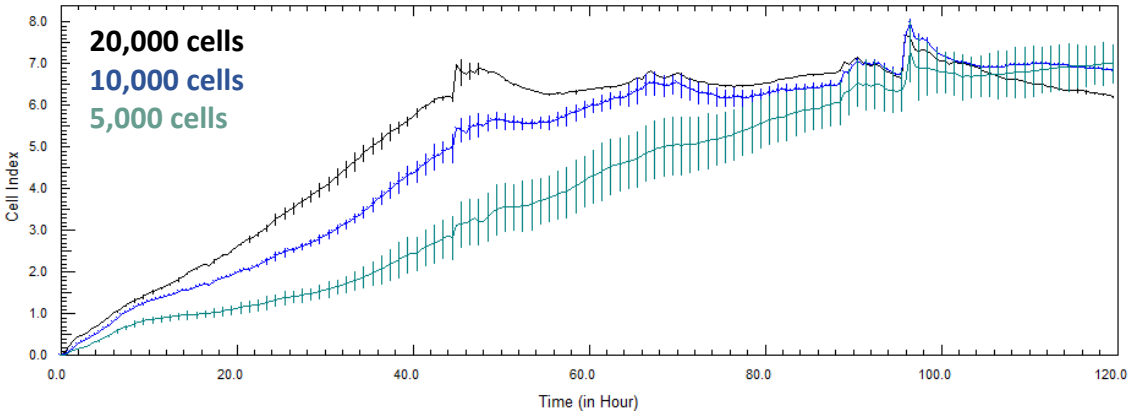

3.9B

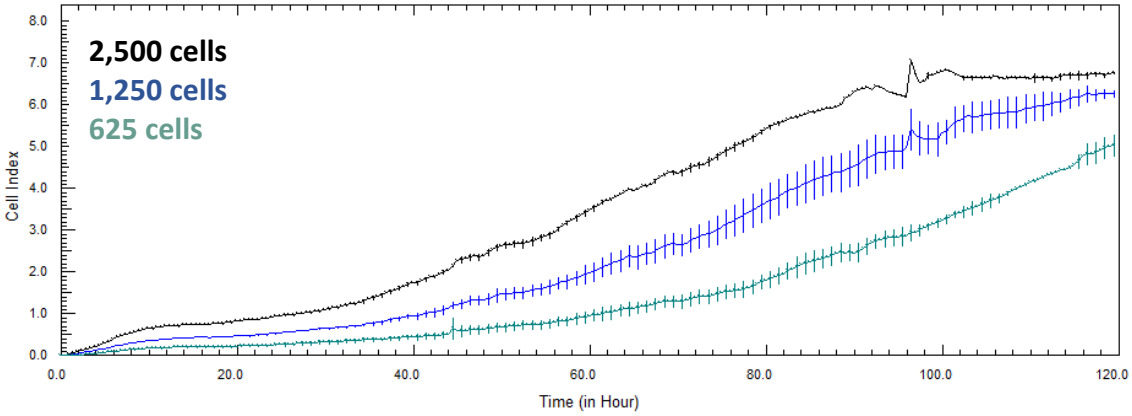

Figure 3.9 Growth kinetics of AC10 cardiomyocytes

xCELLigence traces showing time (hours) vs cell index for **A.** AC10-CMs plated at high density (20,000, 10,000 and 5,000 cells/well) and **B.** AC10-CMs plated at low density (2,500, 1,250 and 625 cells/well) Data is representative of n=2, data points show average values ± SD.

3.3.3 Optimisation and characterisation of hiPSC-derived cardiomyocytes for the xCELLigence Cardio RTCA system

The hiPSC-derived cardiomyocytes (hiPSC-CMs) used in this study were the Cor.4U cells (Axiogenesis, Germany). These cardiomyocytes have been well characterised and express critical contractile proteins, possess functional ion channels, form functional syncytia and contract *in vitro*. The cardiac phenotype of these cells is shown by positive expression of the sarcomeric protein α-actinin (Figure 3.10).

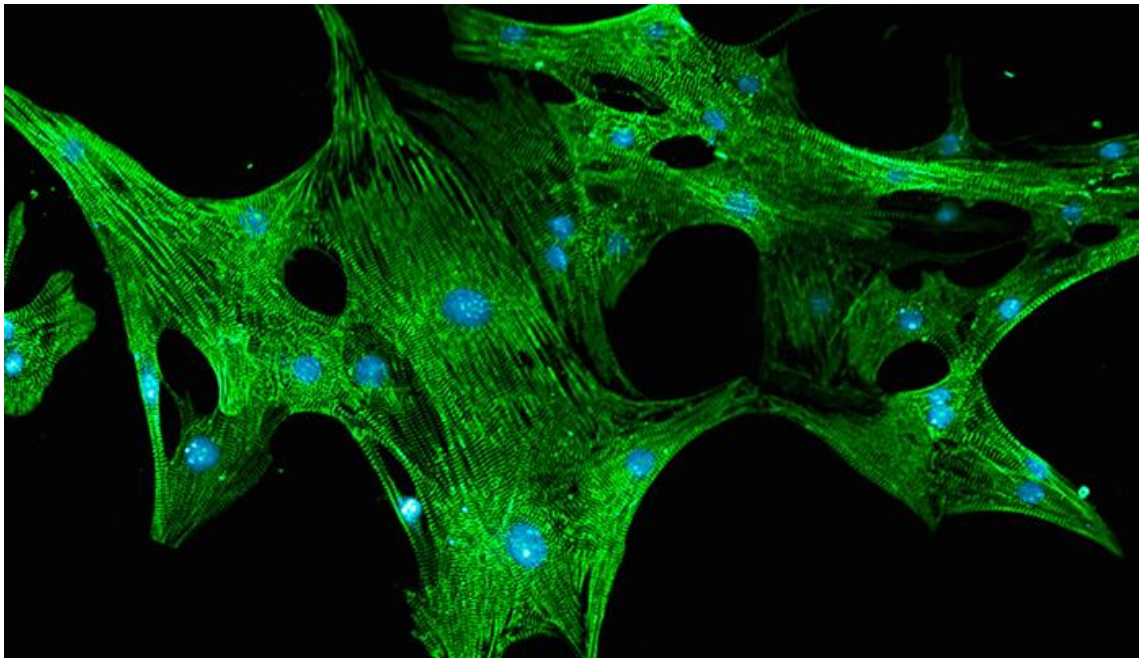

Figure 3.10 Immunostaining of Cor4u hiPSC-derived cardiomyocytes for cardiac proteins

Positive staining for α-actinin (green) with nuclei stained blue with DAPI. Image courtesy of Axiogenesis, Germany.

3.3.3.1 Establishment of contractile syncytium and measurement of cellular contraction of hiPSC-derived cardiomyocytes using the xCELLigence Cardio RTCA system

Cor.4U hiPSC-CM cells were seeded at 30,000 cells/well, as per standardised protocol produced by Axiogenesis.[212] Figure 3.11 shows the growth of the cells gradually increases over time, with cells fully confluent at approximately 75 hours. The arrows on the figure indicate the points of medium exchange.

Throughout the initial growth period the contractility of the cells was monitored at regular intervals. Figure 3.12 shows example traces taken from a representative well at 12, 24, 36, 48, and 72 hours. Primitive beating is seen at 36 hours, with stable beating observed in the hiPSC-CMs at 72 hours

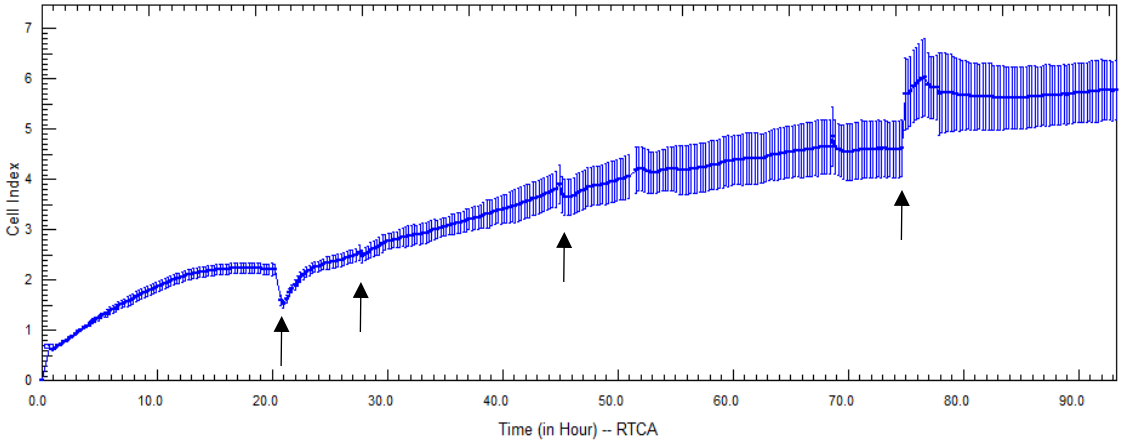

Figure 3.11 Initial growth hiPSC-derived cardiomyocytes

xCELLigence cardio trace showing time vs. cell index for Cor.4U hiPSC-CMs plated at 30,000 cells/well. Arrows indicate points of medium exchange, data points show average values of 4 representative wells ± SD.

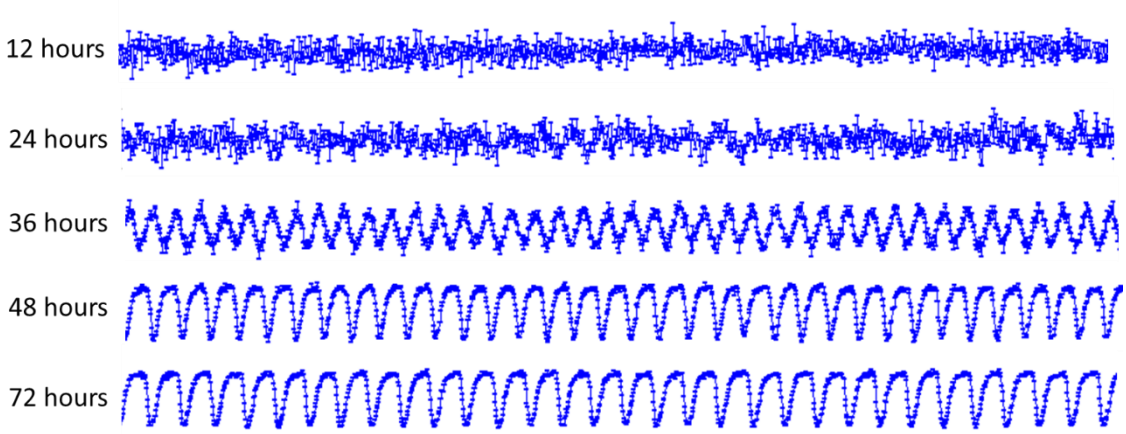

Figure 3.12 Assessment of initial contractility of hiPSC-derived cardiomyocytes

xCELLigence cardio traces showing contractility of Cor.4U hiPSC-CMs over a time course of 12, 24, 36, 48 and 72 hours. Data was obtained from one representative well.

3.3.3.2 Confirmation of drug-induced perturbation of hiPSC-derived cardiomyocytes

hiPSC-CMs as a contractile confluent monolayer were exposed to the β-adrenergic agonist isoproterenol and the hERG potassium channel blocker E-4031. Traces showing stable baseline beating and beating 2 hours after compound addition are shown in figures 3.13A and 3.13B respectively. No visible changes were observed between the two control traces, however addition of isoproterenol caused the beat rate to increase and E-4031 caused both beat amplitude and beat rate to decrease. These effects are summarised in figures 3.14A and 3.14B.

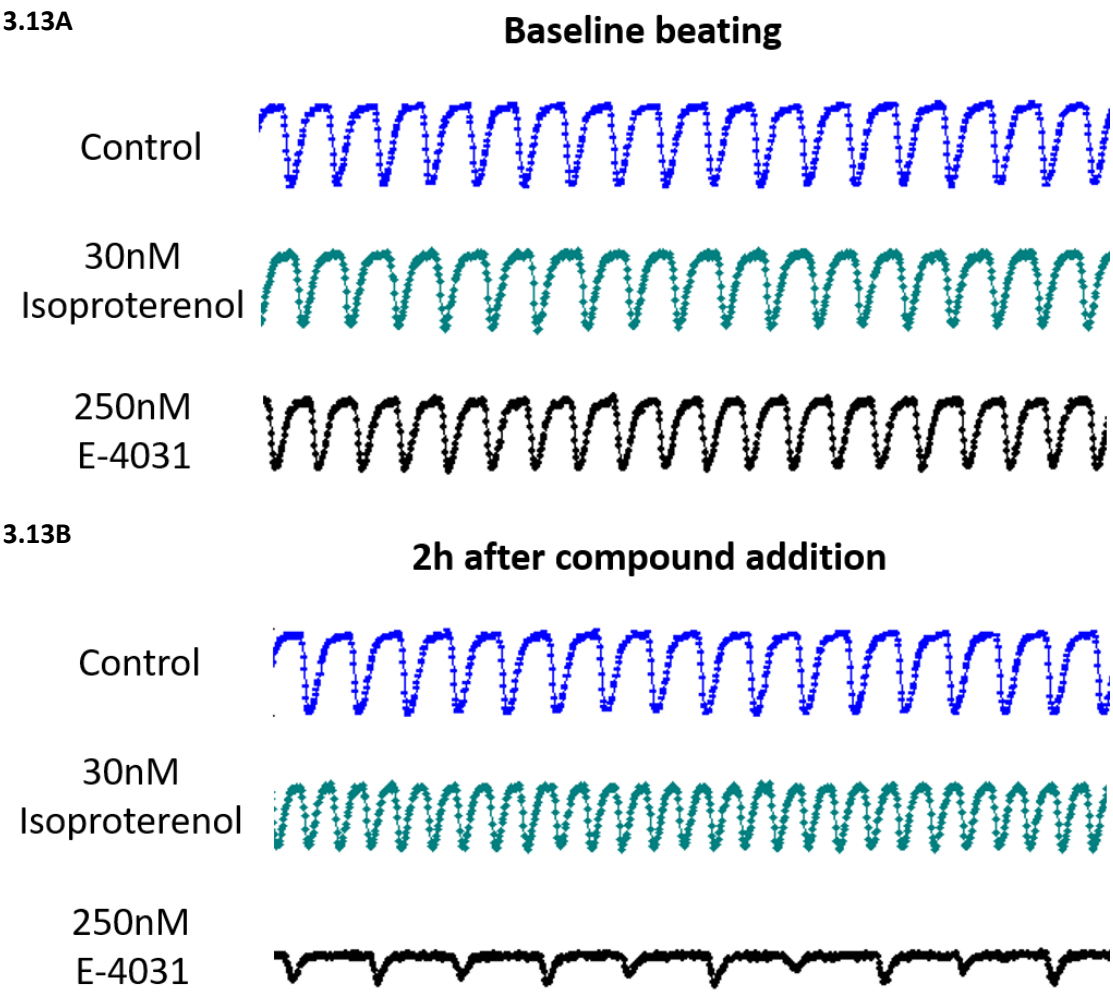

Figure 3.13 Effect of isoproterenol and E-4031 on contractility of hiPSC-derived cardiomyocytes

A. Traces of stable baseline beating before compound addition, **B**. Traces of beating 2 hours after compound addition

3.14A Beating rate before compound addition **Beating rate after compound addition**

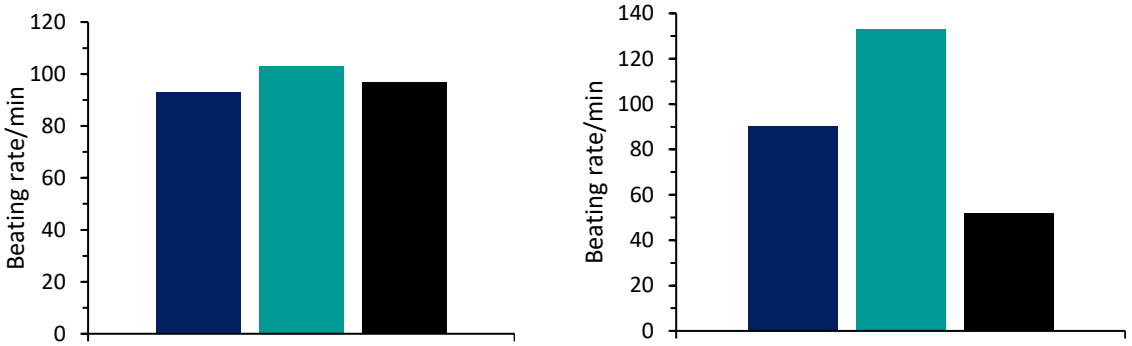

3.14B Beat amplitude before compound addition **Beat amplitude after compound addition**

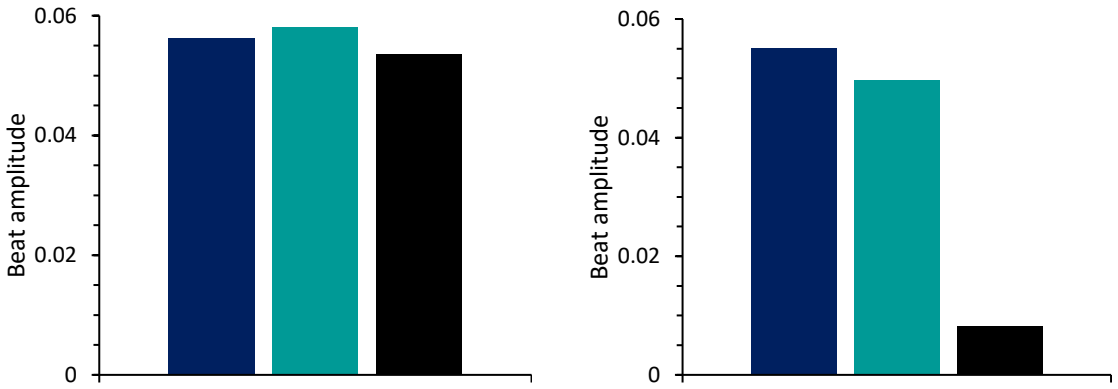

Figure 3.14 Analysis of the effect of isoproterenol and E-4031 on contractility of hiPSC-derived cardiomyocytes

A. Bar graph showing beating rate/minute before compound addition and 2 hours after compound addition. **B.** Bar graph showing beat amplitude before compound addition and 2 hours after compound addition. Data obtained from one representative well for each treatment group, ■ control, ■ isoproterenol, ■ E-4031.

3.3.4 Qualification of ability of cardiomyocyte cell models to detect structural changes, determined following exposure to Angiotensin II

Angiotensin II has pleiotropic roles within the cardiovascular system and causes vasoconstriction, increases in heart rate and cardiac remodelling.[76] As a well known mediator of cardiac hypertrophy, it was used to qualify the *in vitro* models used in this study for detection of structural cardiotoxicity.

Prior to investigating morphological effects, the effect of angiotensin II on viability of ACI0-CMs was ascertained using the MTT assay. Figure 3.15 shows that exposure to clinically relevant concentrations of angiotensin II for 96 hours caused no significant change to cellular viability of AC10-CMs. For future experiments concentrations of 200pM and 300pM angiotensin II were used.

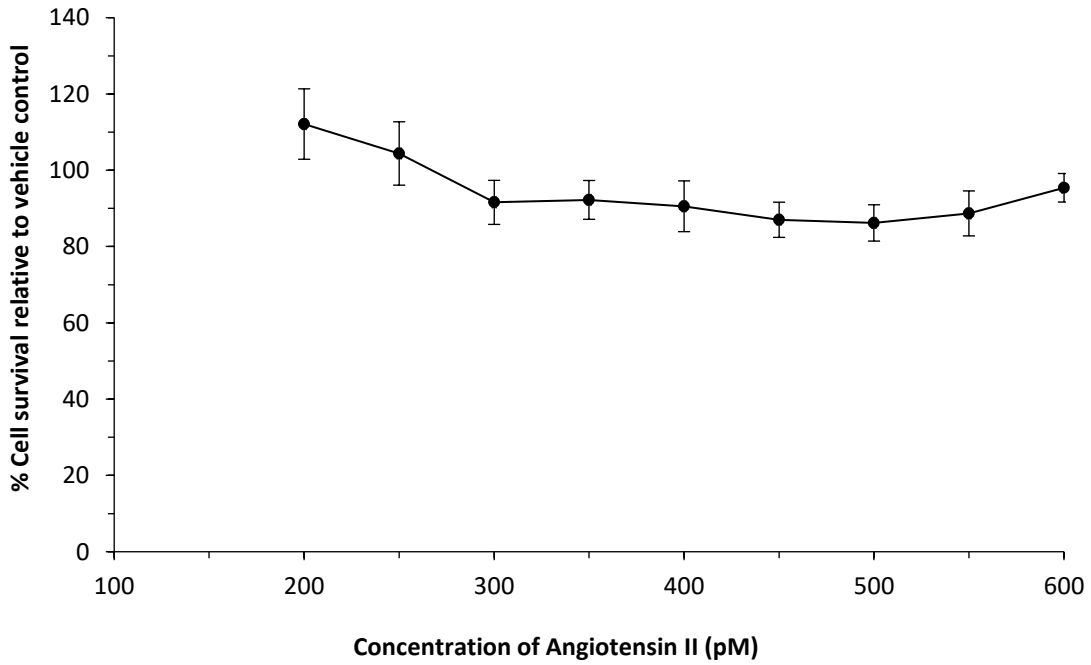

Figure 3.15 Effect of angiotensin II on viability of AC10 cardiomyocytes

Dose response curve showing the effect of 600pM – 200pM angiotensin II on cell viability following 96 hour exposure, expressed as % cell survival relative to vehicle control. Data is representative of n=3 ± SE.

3.3.4.1 Angiotensin II induces morphological changes in AC10 cardiomyocytes

The xCELLigence RTCA was used to assess the effect of angiotensin II on the morphology of AC10-CMs. As shown in figure 3.16A, when normalised to the point of first angiotensin II addition, cell index gradually increased higher than the level of control in cells exposed to angiotensin II, with the greatest difference in cell index following 96 hours exposure (figure 3.16B). To ascertain if this increase in cell index was due to increased cellular proliferation or a change to cellular morphology, an MTT assay was carried out – AC10-CMs exposed to angiotensin II in an identical manner showed no difference in viability (figure 3.16C), indicating that the increase in cell index observed using xCELLigence was likely due to a change in morphology (figure 3.16D).

3.16A

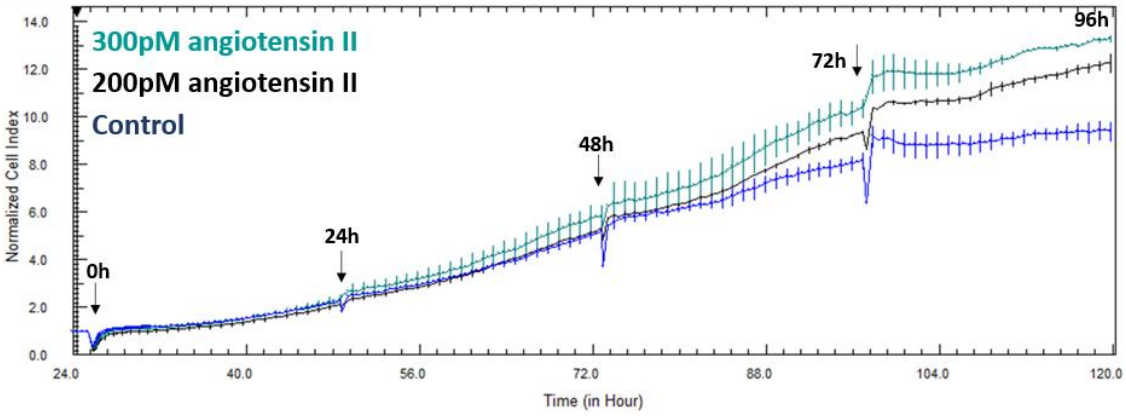

3.16B

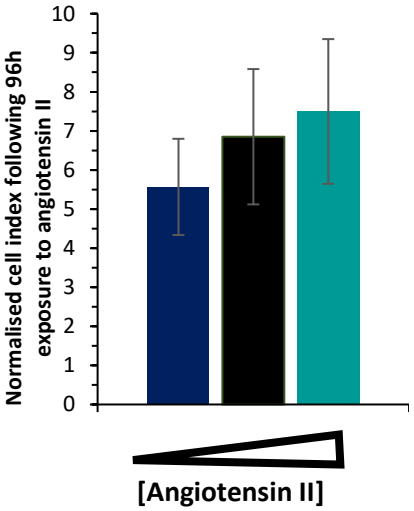

3.16C

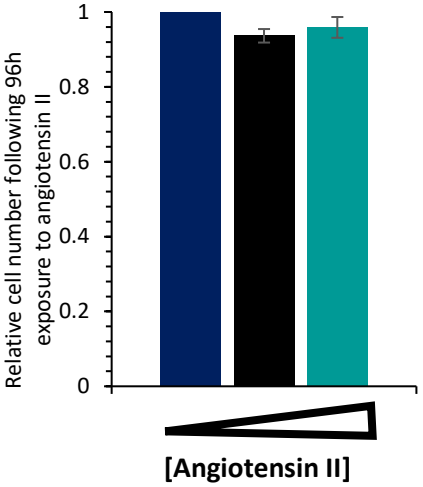

3.9D

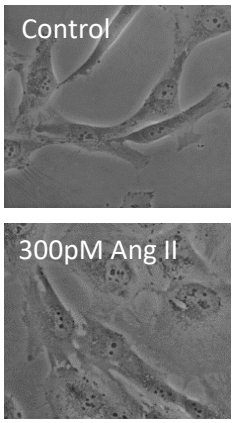

Figure 3.16 Angiotensin II causes hypertrophy of AC10 cardiomyocytes

A. xCELLigence trace showing time (hours) vs normalised cell index of AC10-CMs exposed to angiotensin II with points of angiotensin II (arrows) and exposure time indicated, data representative of n=3, data points shown are average ± SD. **B.** Normalised cell index following 96h exposure to angiotensin II, data is n=3 ± SE. **C**. Relative cell number following 96h exposure to angiotensin II measured by MTT assay, data is n=3 ± SE and **D.** Images of untreated and angiotensin II treated AC10-CMs showing a change in morphology. Images were taken at 40x magnification following 96h exposure angiotensin II.

■ control, ■ 200pM Angiotensin II, ■ 300pM Angiotensin II.

3.3.4.2 Angiotensin II induces morphological changes and functional disturbances in hiPSC-derived cardiomyocytes

Stably beating Cor.4U cells were exposed to angiotensin II every 24 hours for a total of 72 hours, and the effects on cell behaviour were monitored in real-time. As shown in figure 3.17A, when normalised to the point of first angiotensin II addition, cell index increased higher than the level of control in cells exposed to 200pM angiotensin II, with the greatest difference in cell index approximately 72 hours after angiotensin II was initially added (figure 3.17B), indicating that angiotensin II induced a morphology change to the cells.

Assessment of the effect of angiotensin II on contractility of hiPSC-CMs was carried out after 72 hours exposure to angiotensin II, as the cells showed the greatest degree of hypertrophy at this time-point. The representative traces of contractility shown for control and angiotensin II treated cells in figure 3.18A show no visible changes in contractility with angiotensin II addition. Detailed analysis of beat rate and amplitude is shown in figures 3.18B and 3.18C respectively.

Assessment of the effect of angiotensin II on contractility of hiPSC-CMs was also carried out immediately after the first addition of angiotensin II. The representative traces of contractility shown for control and angiotensin II treated cells in figure 3.19A show visible changes to increases to beat rate and decreases to beat amplitude immediately after angiotensin II addition. Detailed analysis of beat rate and amplitude is shown in figures 3.19B and 3.19C respectively.

3.17A

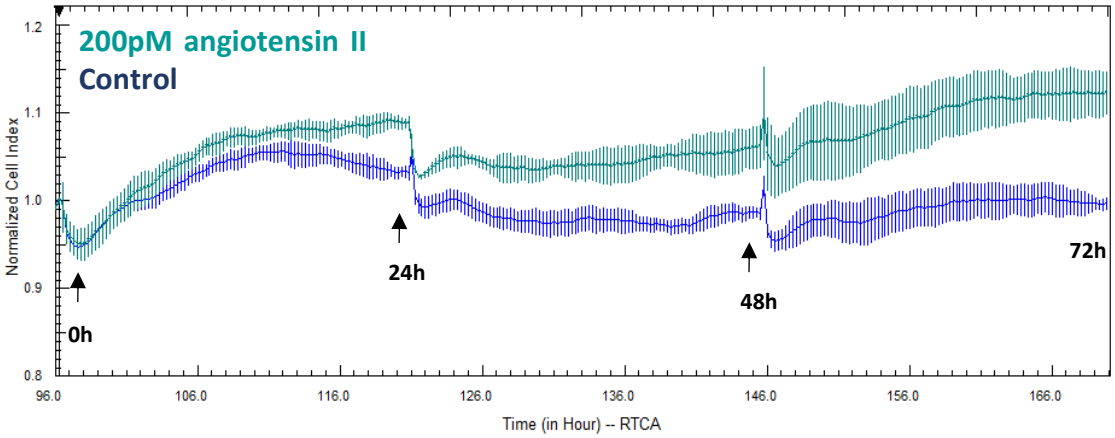

3.17B

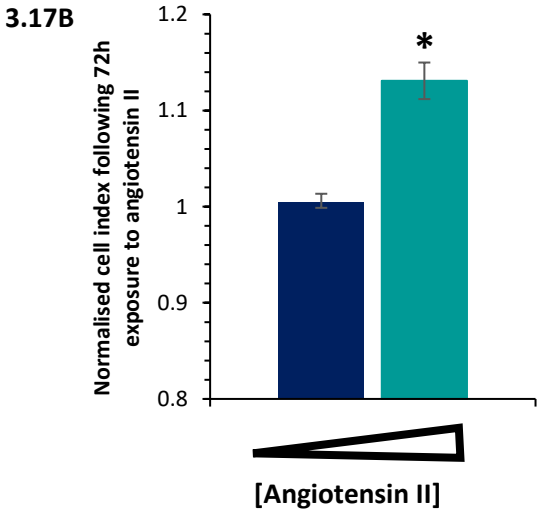

Figure 3.17 Effect of angiotensin II on morphology of hiPSC-derived cardiomyocytes

A. xCELLigence trace showing time (hours) vs normalised cell index of hiPSC-CMs exposed to angiotensin II with points of angiotensin II addition (arrows) and exposure time indicated, data representative of n=2, data points shown are average ± SD. **B.** Normalised cell index at 170 hours following 72 hours exposure to angiotensin II**.** Data points show average of 3 wells ± SE. ∗ p< 0.05, ■ control, ■ 200pM Angiotensin II.

3.18A

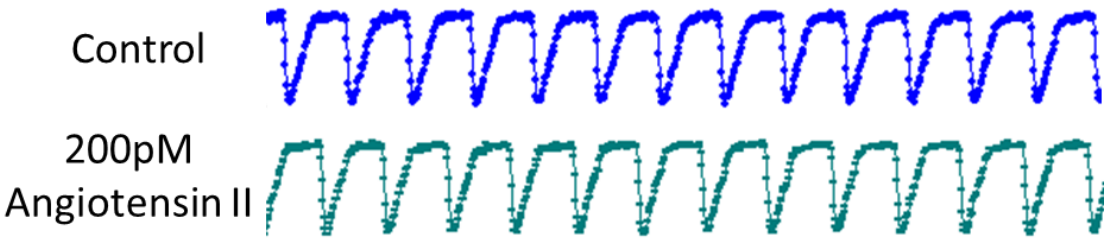

3.18B BEATING RATE

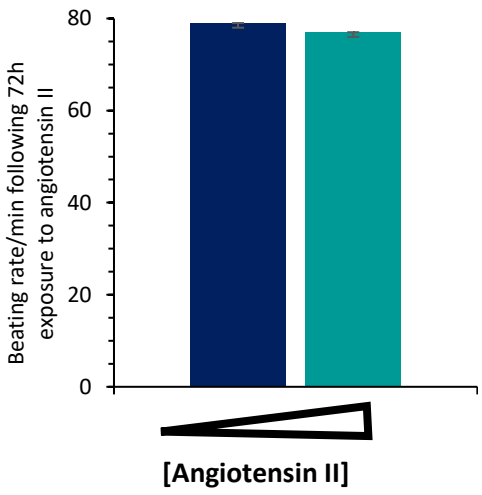

3.18C BEAT AMPLITUDE

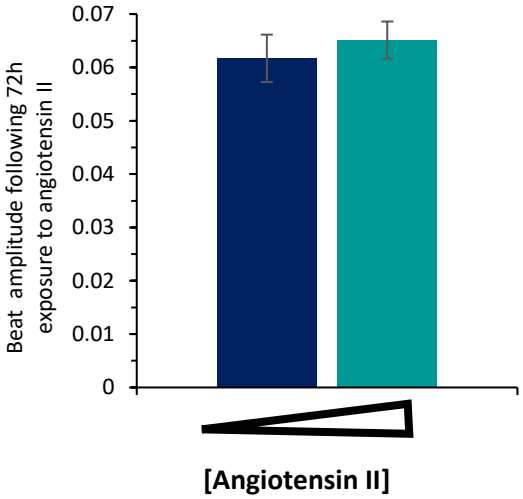

Figure 3.18 Effect of 72 hours angiotensin II exposure on contractility of hiPSC-derived cardiomyocytes

A. Representative traces showing contractility of control cells and cells following exposure to 200pM angiotensin II for 72 hours, **B.** Beating rate/min following 72 hours exposure to angiotensin II, data points show average of 3 wells ± SE and **C.** Beating amplitude following 72 hours exposure angiotensin II. Data points show average of 3 wells ± SE.

■ control, ■ 200pM Angiotensin II.

3.19A

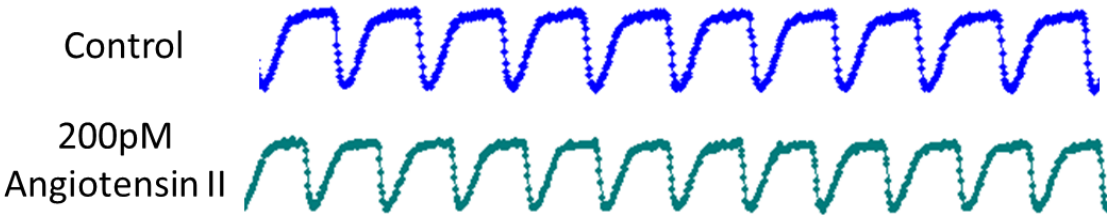

3.19B BEATING RATE

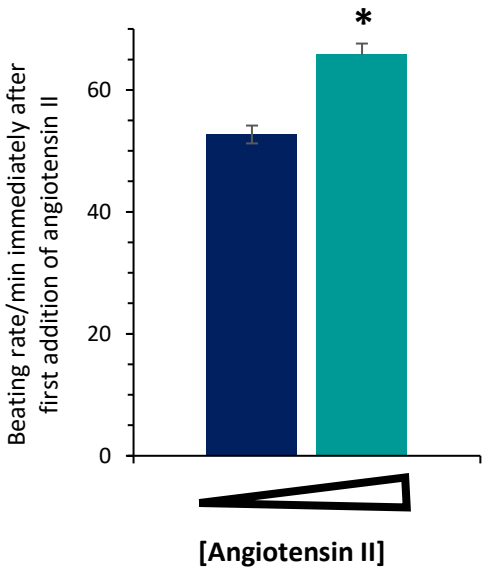

3.19C BEAT AMPLITUDE

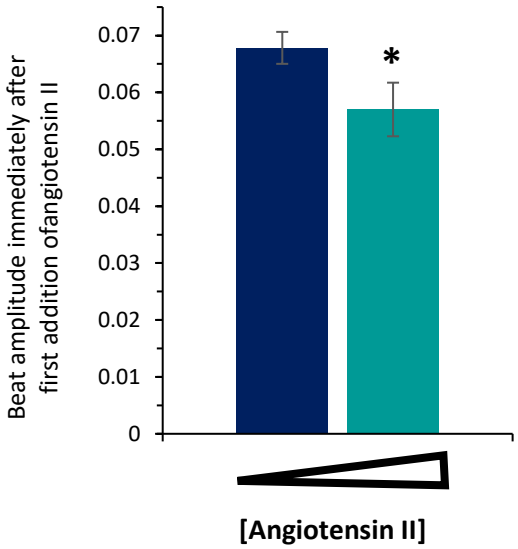

Figure 3.19 Immediate effect of angiotensin II exposure on contractility of hiPSC-derived cardiomyocytes

A. Representative traces showing contractility of control cells and cells immediately after angiotensin II addition, **B.** Beating rate/min immediately after angiotensin II addition, data points show average of 3 wells ± SE and **C.** Beating amplitude immediately after angiotensin II addition. Data points show average of 3 wells ± SE, ∗ $p < 0.05$.

■ control, ■ 200pM Angiotensin II.

3.3.5 Sunitinib to qualify *in vitro* models for detection of functional cardiotoxicity

Sunitinib is a cancer therapy that targets multiple tyrosine kinases including the vascular endothelial growth factor receptor (VEGF-R) which is its primary target. As such, it is mainly indicated for the treatment of highly vascularised malignancies such as renal cancer; although successful at inhibiting angiogenesis and halting tumour growth its use is associated with numerous cardiotoxicities including development of arrhythmias, hypertension and impairments to ventricular function.[96] As a well-known functional cardiotoxicant and mediator of cardiac hypertrophy, it will be used to qualify the *in vitro* models used in this study for detection of functional and structural cardiotoxicity.

3.3.5.1 Effect of sunitinib on viability of AC10 cardiomyocytes

Prior to investigating morphological effects, the toxicity profile of sunitinib in ACl0-CMs was determined in both the exponential and plateau growth phases. Figure 3.20 shows the sensitivity of AC10-CMs exposed to a range of sunitinib concentrations (20µM - 0.078µM) continuously for 96 hours, with the C_{Max} indicated by the dashed line. At concentrations below the C_{Max} little cell death occurred in both growth phases, however above the C_{Max} varying degrees of response to the sunitinib were seen, with cells in exponential growth showing increased sensitivity. The IC_{50} values obtained for both growth phases are shown in table 3.2, the value calculated for exponential growth phase was 10.7 ± 1.5µM, this value at least doubled for cells in the plateau phase to greater than 20µM.

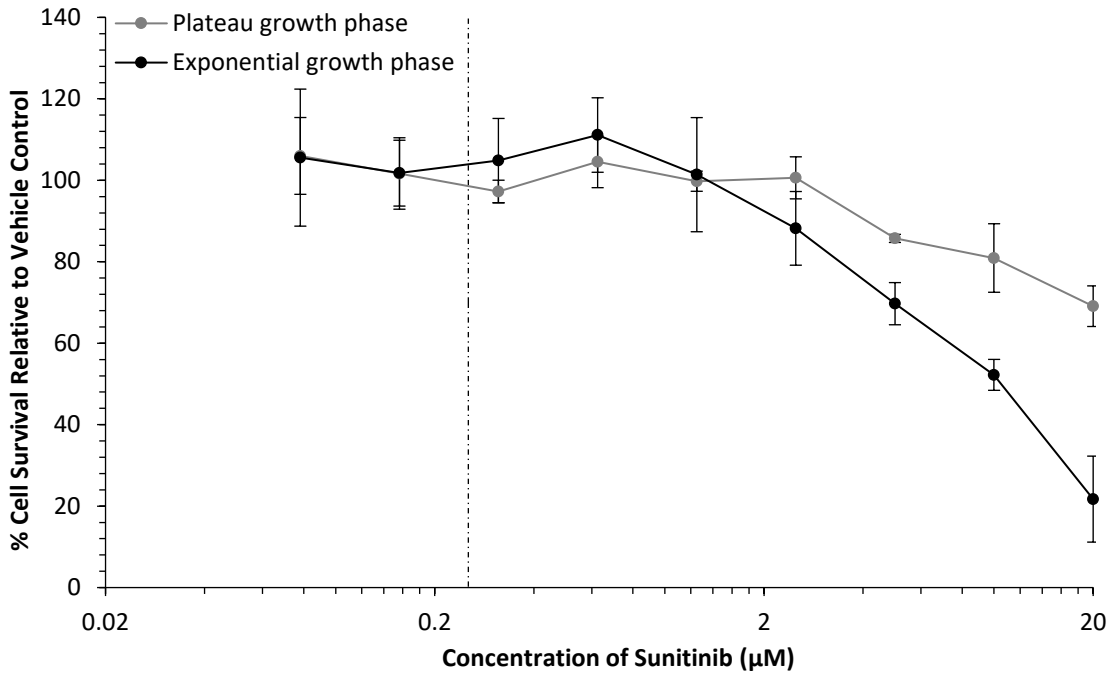

Figure 3.20 Chemosensitivity studies with sunitinib in AC10 cardiomyocytes

Dose response curves showing the effect of sunitinib on cell viability expressed as % cell survival relative to vehicle control for cells in exponential and plateau growth phases. The dashed line represents the C_{Max} of sunitinib (253nM)[224], data is representative of n=3 ± SE.

IC_{50} of sunitinib ± SE (µM)	
Plateau growth phase	> 20
Exponential growth phase	10.7 ± 1.5

Table 3.2 IC_{50} values of sunitinib in AC10 cardiomyocytes

3.3.5.2 Qualification of ability of cardiomyocyte cell models to detect functional changes following exposure to sunitinib

Cells in exponential and plateau growth phase were exposed to varying concentrations of sunitinib, and the effects on cell behaviour were monitored in real-time. As shown in figure 3.21A and summarised in figure 3.21B following 24 hours sunitinib exposure, when normalised to the point of first sunitinib addition, cells in exponential growth phase exposed to 500nM and 250nM sunitinib exhibited an immediate increase in cell index that was maintained throughout the experiment, whereas the cell index of cells exposed to 50nM was unaffected. To ascertain if this increase in cell index was due to increased cellular proliferation or a change to cellular morphology an MTT assay was carried out – AC10-CMs exposed to sunitinib for 24 hours showed no major differences in viability (figure 3.21C), indicating that the increase in cell index observed using xCELLigence was due to a change in morphology (figure 3.21D). A parallel study conducted in cells in the plateau phase of growth showed similar findings, the results of which are shown in figure 3.22A-C. An additional finding in the plateau growth phase studies was that the cells exposed to 50nM sunitinib also showed immediate increases in cell index that were maintained throughout the experiment (figure 3.22A), with dose-dependent increases in cell index observed after 24 hours exposure (figure 3.22B).

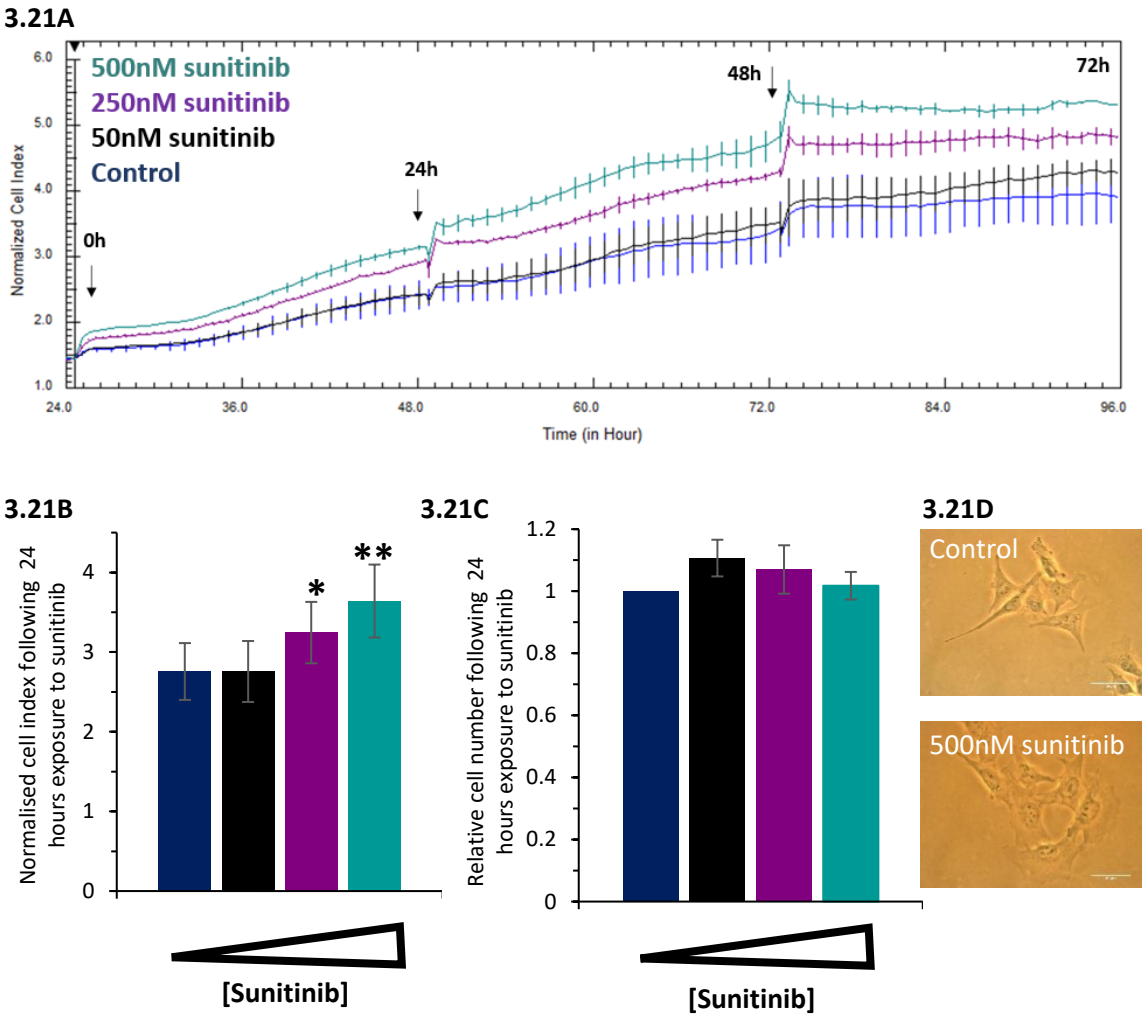

Figure 3.21 Effect of sunitinib on morphology of AC10 cardiomyocytes in exponential growth phase

A. xCELLigence trace showing time (hours) vs normalised cell index of AC10-CMs in exponential growth phase exposed to sunitinib with points of sunitinib addition (arrows) and exposure time indicated, data representative of n=3, data points shown are average ± SD. **B.** Normalised cell index following 24 hours exposure to sunitinib**,** data is n=3 ± SE. **C**. Relative cell number following 24 hours exposure to sunitinib measured by MTT assay, data is n=3 ± SE and **D.** Images of untreated and sunitinib treated AC10 cardiomyocytes showing a change in morphology. Images were taken at 40x magnification following 24 hours exposure to sunitinib. ∗ p< 0.05, ∗∗ p< 0.001 (treatment groups compared to control). ■ control, ■ 50nM sunitinib, ■ 250nM sunitinib, ■ 500nM sunitinib.

3.22A

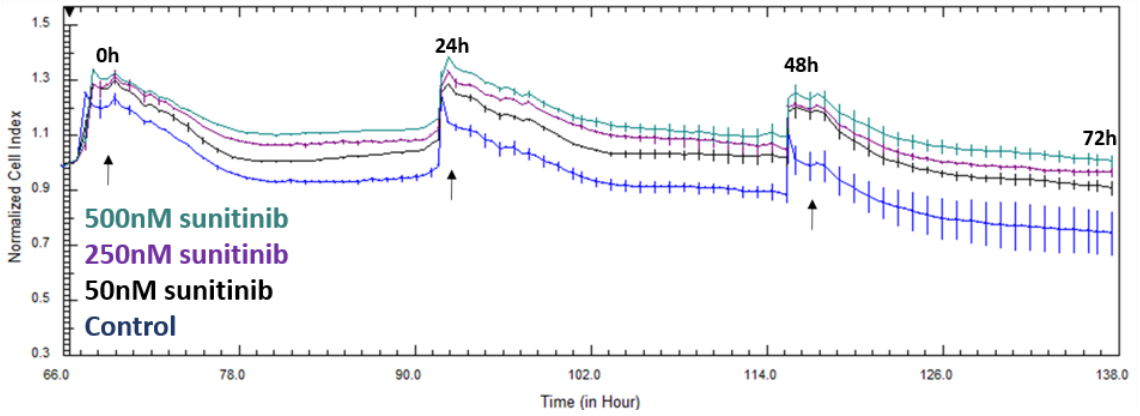

3.22B

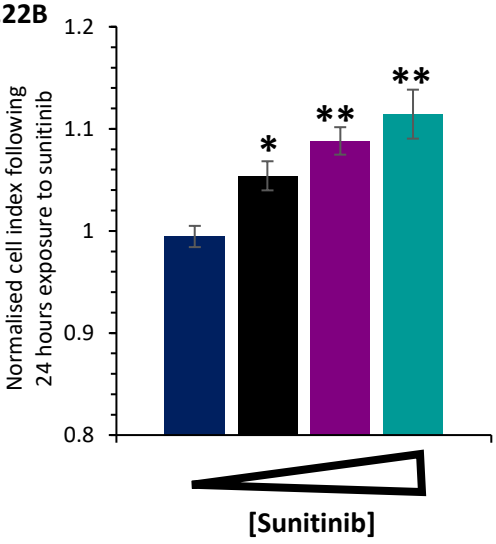

3.22C

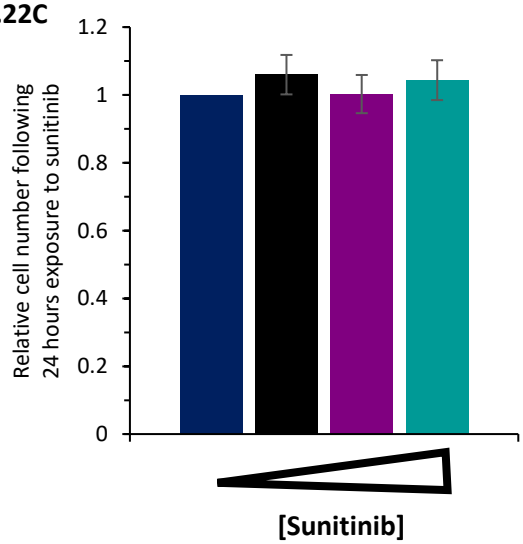

Figure 3.22 Effect of sunitinib on morphology of AC10 cardiomyocytes in plateau growth phase

A. xCELLigence trace showing time (hours) vs normalised cell index of AC10-CMs in plateau growth phase exposed to sunitinib with points of sunitinib addition (allows) and exposure time indicated, data representative of n=3, data points shown are average ± SD. **B.** Normalised cell index following 24 hours exposure to sunitinib**,** data is n=3 ± SE. and **C**. Relative cell number following 24 hours exposure to sunitinib measured by MTT assay, data is n=3 ± SE. ∗ p< 0.05, ∗∗ p< 0.005 (treatment groups compared to control), ■ control, ■ 50nM sunitinib, ■ 250nM sunitinib, ■ 500nM sunitinib.

3.3.5.3 Sunitinib induces morphological changes and functional disturbances in hiPSC-derived cardiomyocytes

The xCELLigence cardio system was used to assess the effect of sunitinib on the morphology and contractility of hiPSC-CMs. As shown in figure 3.23A, when normalised to the point of first sunitinib addition, cell index immediately increased higher than the level of control in cells exposed to 50nM, 250nM and 500nM sunitinib in a dose-dependent manner, with the greatest difference in cell index approximately 72 hours after sunitinib was initially added (figure 3.23B), indicating that sunitinib induced a morphology change to the cells.

Assessment of the effect of sunitinib on contractility of hiPSC-CMs was carried out after 72 hours exposure to sunitinib as the cells showed the greatest degree of hypertrophy at this time-point. The representative traces of contractility shown for control and sunitinib treated cells in figure 3.24A show visible changes in contractility, with beat number decreasing with increasing concentrations of sunitinib and increased amplitude with 500nM sunitinib. Detailed analysis of beat rate and amplitude is shown in figures 3.24B and 3.24C respectively.

3.23A

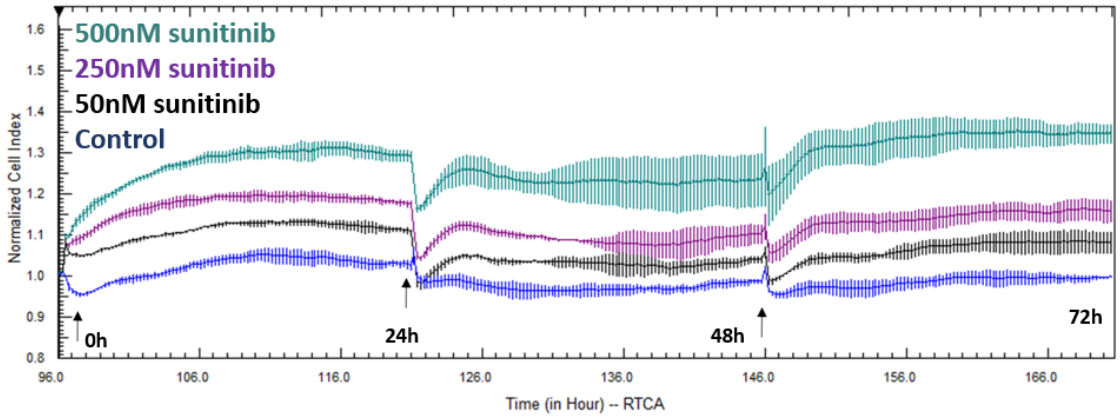

3.23B

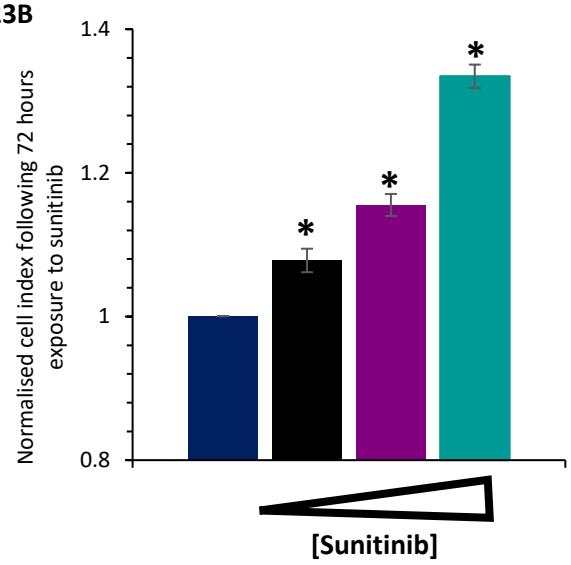

Figure 3.23 Effect of sunitinib on morphology of hiPSC-derived cardiomyocytes

A. xCELLigence trace showing time (hours) vs normalised cell index of hiPSC-CMs exposed to sunitinib with points of addition (arrows) and exposure time indicated, data points shown are average ± SD. **B.** Normalised cell index following 72 hours exposure to sunitinib**,** data points show average of 3 wells ± SE. ∗ p< 0.0001 (treatment groups compared to control).

■ control, ■ 50nM sunitinib, ■ 250nM sunitinib, ■ 500nM sunitinib.

3.24A

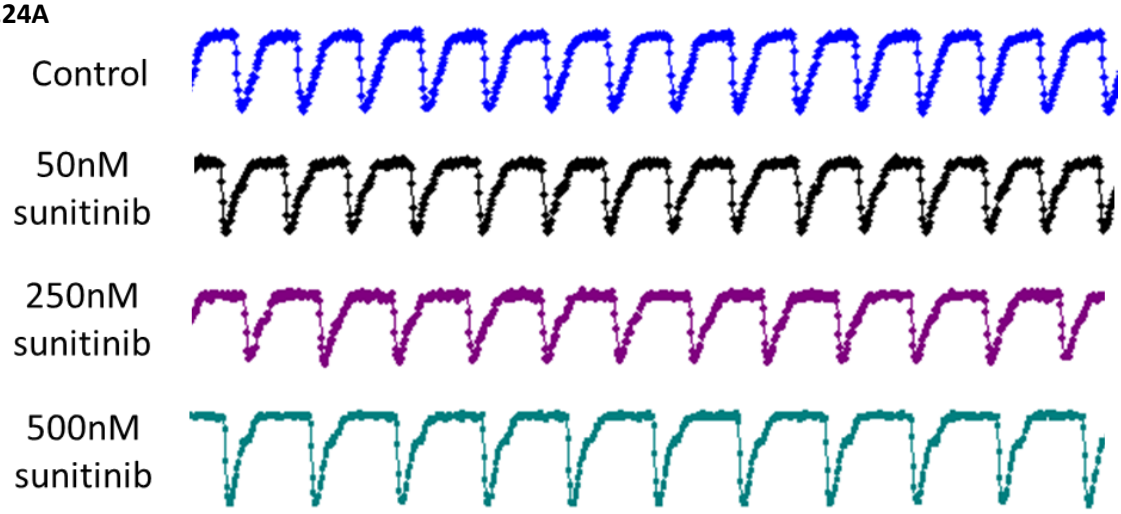

3.24B BEATING RATE

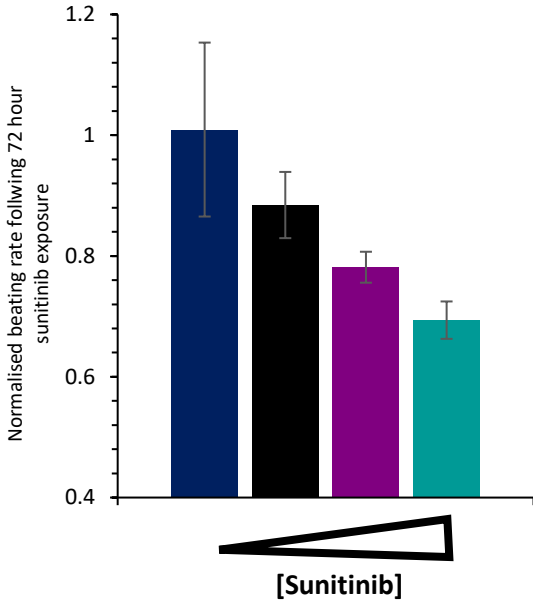

3.24C BEAT AMPLITUDE

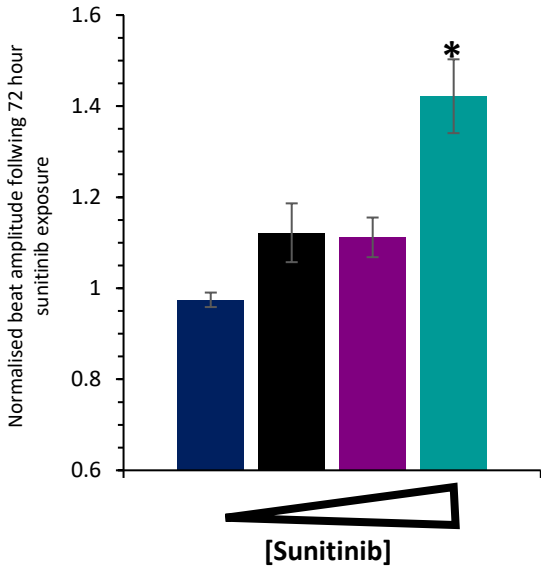

Figure 3.24 Effect of 72 hours sunitinib exposure on contractility of hiPSC-derived cardiomyocytes

A. Representative traces showing contractility of control cells and cells exposed to sunitinib for 72 hours, **B.** Normalised beating rate/minute following 72 hours exposure to sunitinib, data points show average of 3 wells ± SE and **C.** Normalised beat amplitude following 72 hours exposure to sunitinib, data points show average of 3 wells ± SE. ∗ p< 0.001 (treatment groups compared to control). ■ control, ■ 50nM sunitinib, ■ 250nM sunitinib, ■ 500nM sunitinib.

3.4 Discussion

Cardiotoxicity is a leading cause of drug withdrawal, and its occurrence related to the use of cancer therapies is a considerable problem;[179,225] suggesting that the current *in vitro* methods for identification of cardiotoxicity are inadequate. The purpose of this phase of the project was to determine the suitability of the AC10 cardiomyocyte cell line (AC10-CMs) and hiPSC-derived cardiomyocytes (hiPSC-CMs) for detection of structural and functional cardiotoxicity.

3.4.1 Suitability of the AC10 cardiomyocyte cell line

AC10 cardiomyocytes (AC10-CMs) are a recently developed cell line created by Davison *et al*., whereby human ventricular cardiomyocytes were fused with fibroblasts transformed with SV40 virus and devoid of mitochondrial DNA. The cells were well characterised by Davison *et al*. and although they are in a pre-contractile state, they express many contractile proteins.[188] In agreement with Davison *et al*., positive expression of troponin I and α-actinin was detected in AC10-CMs in this current study in addition to the contractile proteins troponin C and tropomyosin. The pattern of immunostaining observed is distinct from what would be expected in mature cardiomyocytes, there is minimal indication of filamentous protein structure and no evidence of sarcomeres. Due to the lack of organised contractile machinery and functional ionic currents, the AC10-CMs are unable to spontaneously contract and are described as being in a pre-contractile state.

The cardiac specific transcription factors GATA4, MYCD and NFATc4 that are involved in cardiac development and function were identified using real-time polymerase chain reaction (qRT-PCR) by Davison *et al*., in this study the transcription factor NKX2.5 was also found to be expressed in AC10-CMs by immunostaining. NKX2.5 is involved in cardiogenesis in early cardiac development and has been shown to interact with GATA4, the presence of cardiac specific transcription factors in the cells are useful markers of cardiac myogenesis and provide further evidence that

AC10-CMs are committed to a cardiac-like phenotype.

In contrast to Davison *et al*. who found bone morphogenetic protein 2 (BMP-2) only upon silencing of the SV40 gene, BMP-2 was detected in AC10-CMs in this study without SV40 silencing. Due to the involvement of BMP-2 in cardiomyocyte differentiation, its presence suggests that the AC10-CMs may be further into the process of cardiomyocyte differentiation and exist at an intermediate stage of development.

In accordance with their proliferative potential, the cellular proliferation markers pericentriolar material 1 (PCM1) and Ki-67 were also present, as was the mesenchymal protein vimentin. Vimentin is found in mesenchymal cells such as fibroblasts and would not be found in primary cardiomyocytes, indeed the study by Davison *et al*. reported that vimentin was not present in the AC10-CMs. However as the cells are a fusion cell line of cardiomyocytes and fibroblasts, this may explain why positive expression of vimentin was found in this study. As discussed in section 1.4.3 although cardiomyocytes form the bulk of the myocardium, they are outnumbered by support cells of the myocardium which make up 70% of the cells in the heart; 15% of which are fibroblasts.[53] Fibroblasts are responsible for a plethora of events in the myocardium including cardiac remodelling and maintenance of the ECM,[54] therefore the presence of vimentin within the AC10-CMs may favour studies investigating morphological changes induced by cardiotoxicants. An additional positive feature of these cells is their ability to form functional gap junctions, although not investigated within this study, Davison *et al*. reported the presence of functional gap junctions exemplified by expression of Cx-40, Cx-43 and dye coupling studies.[188]

Despite the cells inability to spontaneously contract, their expression of contractile proteins, cardiac specific transcription factors and the presence of functional gap junctions demonstrate that the AC10-CMs are committed to the cardiac lineage and therefore suitable for studies into structural cardiotoxicity and viability following exposure to cardiotoxicants.

As cardiomyocytes in the heart are terminally differentiated and possess limited capacity for regeneration, studies throughout this research were conducted, where necessary, in both the exponential and plateau phases of growth in an attempt to recapitulate the adult human heart and investigate if different responses are obtained in each growth phase. For MTT studies this equated to seeding densities of 2,000 cells/well for exponential growth phase studies and 35-40,000cells/well for studies in the plateau growth phase. Analysis of the proliferation of AC10-CMs using the xCELLigence RTCA showed that the cells were able to adhere to the plates and their proliferation rate was monitored in real time. The growth kinetics analysis allowed identification of 5,000 cells/well and 10,000/cells as appropriate seeding densities for conducting studies in the exponential and plateau phases of growth respectively, where exponential studies would begin 24 hours after seeding and plateau studies would commence once the cells reach the plateau phase of growth (at approximately 72 hours).

As the xCELLigence RTCA uses impedance to monitor the behaviour of cells, it is a suitable platform for evaluation of structural cardiotoxicity and viability following exposure to cardiotoxicants, as decreases to cell index may represent cytotoxicity or reduction in cell size, whereas increases to cell index may represent increased proliferation or increases in cell size. The use of complimentary MTT studies and imaging would provide a comprehensive assessment of cellular status at a specific time-point and therefore allow for identification of structural cardiotoxicity.

3.4.2 Suitability of hiPSC-derived cardiomyocytes

The growth and contractility of Cor.4U hiPSC-CMs (axiogenesis) was monitored using the impedance based xCELLigence cardio system, once cells were fully confluent and stable beating was observed hiPSC-CMs were exposed to the β-adrenergic agonist isoproterenol and the hERG potassium channel blocker E-4031.

Isoproterenol exhibits both positive inotropy and chronotropy, meaning that clinically it causes an increase in both the force and rate of contraction. Analysis of contractility 2 hours after the addition isoproterenol showed an increased rate of contraction, however the amplitude of the beats (an indication of the strength of contraction) was slightly less, meaning that positive inotropy was not observed. Similar results were reported by Pointon *et al*. who found that the positive inotropes digoxin and isoproterenol altered contraction strength measured by IonOptix, however the direction was reversed with negative inotropy rather than positive inotropy being detected.[203]

These discrepancies may be due to the immature phenotype of hiPSC-CMs. As discussed in section 1.9.2.1 there are many differences between adult and embryonic cardiomyocytes, including smaller sarcomeres, reduced numbers of mitochondria, lack of an extensive T-tubule network and reduced SERCA and RyR expression. Consequently, the dynamics of calcium handling are different in embryonic cardiomyocytes, which results in calcium entry primarily through the sarcolemma rather than released from the sarcoplasmic reticulum and slower cardiac excitation-contraction coupling.[192] The reduced contractile capacity of hiPSC-CMs compared to adult cardiomyocytes may render them unable to increase their contractile strength in response to positive inotropes such as isoproterenol.

Efforts to develop maturity in these cells, perhaps by co-culture with support cells, may help to detect positive inotropy in hiPSC-CMs. Work in this area has been conducted by ACEA biosciences who demonstrated that electrical pacing of hiPSC-CMs for three weeks prior to exposure to positive inotropes reverses the negative-force frequency relationship of hiPSC-CMs and increases in beat amplitude are observed. Although further characterisation of the paced cells is required, improved sarcomeric structure and better localisation of RyRs may be responsible for the observed improvements to contractility.[226]

E-4031 blocks the rapid delayed rectifier outward potassium current (I_{KR}) and thereby delays ventricular repolarisation, which increases the duration of the myocardial contraction. Analysis of contractility 2 hours after the addition of E-4031 showed the expected result of decreases to both beat number and amplitude. As therapeutic inhibition of the hERG channel is associated with arrhythmogenesis and fatal disorders such as Torsades de pointes (TdP),[214,215] accurate detection of the contractile deficits caused by these inhibitors pre-clinically is of great importance, and demonstrates the utility of these cells in future screening for cardiac liabilities.

This study has demonstrated that hiPSC-CMs monitored on the xCELLigence cardio system are able to spontaneously contract after approximately 72 hours, and irrespective of their immature phenotype are responsive to positive chronotropy (isoproterenol) and negative chronotropy and inotropy (E-4031), and is therefore a suitable platform for the assessment of changes in cardiomyocyte contractility. Changes in viability and morphology will also be possible using hiPSC-CMs grown on the xCELLigence cardio system. Similar to the xCELLigence RTCA, increases in cell index may represent increases to cell size, and decreases to the cell index may be due to cytotoxicity or decreases in cell size.

3.4.3 Qualification studies with angiotensin II

As a well-known mediator of cardiac hypertrophy angiotensin II was used to qualify the *in vitro* models developed for detection of structural cardiotoxicity. A hypertrophic response was detected in AC10-CMs using the xCELLigence RTCA following repeated addition of clinically relevant doses of angiotensin II, which was confirmed using cellular viability studies and imaging. A similar response was observed in hiPSC-CMs using the xCELLigence cardio system, with immediate increases in cell index occurring following addition of 200pM angiotensin II. Many groups have reported cardiomyocyte hypertrophy upon angiotensin II addition *in vivo* and *in vitro* and have attempted to identify other contributory factors to angiotensin II induced

hypertrophy. Studies using isolated neonatal rat cardiomyocytes have detected angiotensin II induced hypertrophy and assessed the impact of TAK-1 and Smad2/3,[227] whilst studies using isolated adult rat cardiomyocytes compared the hypertrophic response of cardiomyocytes from normal and post-infarcted rats when cultured in angiotensin II.[228] The potential of fibroblasts to augment angiotensin II induced hypertrophy was also investigated by Gray *et al*., who isolated neonatal rat cardiomyocytes and fibroblasts and conducted co-culture experiments. The results showed that co-culture of cardiomyocytes with fibroblasts enhanced cardiomyocyte hypertrophy due to paracrine signalling,[229] thus illustrating the crucial role of support cells such as fibroblasts within the myocardium.

This study is the first to show that angiotensin II induced hypertrophy can be detected using impedance based systems *in vitro* using the human derived models AC10-CMs and hiPSC-CMs. This has significant implications in terms of 3R's benefits, as it demonstrates that the human derived *in vitro* models used are able to respond as expected to the hypertrophic mediator and therefore may replace or reduce the use of primary cardiomyocytes from animal sources for these purposes which require difficult culture techniques and animal sacrifice.[218]

The use of these *in vitro* models for detection of hypertrophy also extends towards improved pre-clinical testing of pharmaceuticals as a means for early identification of structural cardiotoxicity. As previously mentioned, the current method of pre-clinical testing for cardiac liabilities focusses narrowly on the ability of compounds to block the hERG potassium channel *in vitro*, followed by evaluation of the ability to prolong ventricular repolarisation and therefore prolong the QT-interval *in vivo.*[177] This screening strategy overlooks the development of structural changes, which are associated with a number of cancer therapeutics with the potential to cause cardiovascular liabilities.[144] Structural changes can have a huge impact on the pumping ability of the heart, therefore early identification of the problem is of crucial importance.

The initiation of hypertrophy in response to angiotensin II suggests both the presence of the ATR1 on AC10-CMs and hiPSC-CMs and functional signalling cascades that upon receptor activation cause cellular hypertrophy. Angiotensin signalling via the ATR1 receptor has been outlined in section 1.4.5.2 and figure 1.3.

In hiPSC-CMs, further analysis to contractility found that hypertrophy induced by 72 hours exposure to angiotensin II did not affect contractility of the cells in terms of amplitude and beat number, however immediately after angiotensin II addition increases in beat number and decreases to beat amplitude were detected. Positive chronotropy and negative inotropy has been previously detected in isolated rat cardiomyocyte cultures, in addition to increases in calcium flux into the cells following a few minutes exposure to angiotensin II.[230] The lack of contractile changes reported in this study following long-term exposure may be due to the short half-life of angiotensin II, in circulation the half-life of angiotensin II can be as short as 30 seconds which can increase to 30 minutes in tissues.[231] It is difficult to determine in the presented studies how long angiotensin II remained active *in vitro,* but it is likely that effects on contractility will only occur up 30 minutes following addition so only acute responses can be observed. It is worth noting that although changes to contractility were detected immediately after angiotensin II addition, hiPSC-CMs are particularly sensitive to changes in temperature, so following return of the cells to the incubator transient reductions in beat number are seen on the whole. For this reason changes in contractility are usually assessed 2 hours after drug addition at the earliest.

3.4.4 Qualification of cellular models to detect drug-induced functional changes in cardiomyocyte contractility

Sunitinib is an angiogenesis inhibitor used in the treatment of highly vascularised malignancies such as renal cancer. Although successful at halting tumour growth its clinical use is associated with numerous cardiotoxicities including development of arrhythmias, hypertension and

impairments to ventricular function.[96] As a well-known functional cardiotoxicant and mediator of cardiac hypertrophy, it was used to qualify the *in vitro* models used in this study for detection of functional and structural cardiotoxicity.

The toxicity profile of sunitinib was determined in both the exponential and plateau phases of growth in AC10-CMs following 96 hours exposure to varying concentrations of sunitinib. Cells in both growth phases showed no toxicity at the C_{Max} of sunitinib, (250nM). Interestingly, at concentrations higher than the C_{Max} cells in exponential growth exhibited increased sensitivity to sunitinib with an IC_{50} of 10.7 ± 1.5µM, this value at least doubled for cells in the plateau phase to greater than 20µM. This could be due to the mechanism of action of sunitinib. As a tyrosine kinase inhibitor, sunitinib has the ability to suppress the growth of rapidly proliferating cells such as cancer cells by inhibiting growth factor signalling. This results in decreases to cell growth, proliferation and angiogenesis in tumours and may explain the increased sensitivity of AC10-CMs in the exponential growth phase, as it is possible that these cells express higher levels of sunitinib's targets than the non-proliferating cells in plateau phase.

Analysis of morphological changes to AC10-CMs using the impedance based xCELLigence RTCA showed induction of dose-dependent hypertrophy in both the exponential and plateau phases of growth following repeated addition of sunitinib. Clinically relevant concentrations of sunitinib (500nM = 2x C_{Max}, 250nM = C_{Max} and 50nM = 0.2 C_{Max}) were used, with all except 50nM causing hypertrophy in the exponential growth phase and all three concentrations causing hypertrophy in the plateau phase of growth. Occurrence of hypertrophy was verified using cellular viability studies and imaging following 24 hours exposure to sunitinib. A similar pattern of hypertrophy was observed in hiPSC-CMs with all three concentrations of sunitinib causing an immediate increase in cell index that was sustained throughout repeated addition of sunitinib.

Other groups have also reported hypertrophy as a result of sunitinib treatment *in vivo* and *in vitro*. For example, Chu *et al*. found evidence of hypertrophy in myocardial biopsies taken from

the myocardium of patients who had developed chronic heart failure post-sunitinib treatment.[98] In hiPSC-CMs, addition of 3µM sunitinib for 48 hours caused an enlarged, hypertrophic like cell shape.[232] Investigations in the rat H9c2 cell line, concluded that application of 1, 2.5 and 5µM sunitinib induced cellular hypertrophy.[184] The mechanism of sunitinib induced hypertrophy to cardiomyocytes is currently unclear but it is thought to be at least partially due to inhibition of PDGFR by sunitinib (see section 1.6.1.1). Evidence from the H9c2 cell line also implicates involvement of the aryl hydrocarbon receptor, as antagonism of this receptor was found to reduce sunitinib induced hypertrophy.[184]

This study is the first to demonstrate sunitinib induced hypertrophy using impedance based systems *in vitro* with the human derived models AC10-CMs and hiPSC-CMs. In contrast to previous studies, where hypertrophy was detected at higher sunitinib concentrations, this study identified sunitinib hypertrophy at lower clinically relevant doses over prolonged periods that are more reflective of clinical exposures. This illustrates the utility of the xCELLigence systems to detect morphology changes to AC10-CMs and hiPSC-CMs in a manner that is translational to the clinical setting.

Analysis of contractility in the hiPSC-CMs revealed that sunitinib caused dose-dependent decreases in beat number and increased beat amplitude with sunitinib following 72 hour exposure. Other groups have reported changes to contractility following sunitinib exposure using the xCELLigence cardio system. For example, Doherty *et al*. also found dose-dependent reductions in beat rate following 2 hours and 24 hours exposure to 625nM, 2.5µM and 10µM sunitinib. Although beat amplitude was not measured by Doherty *et al*., the effects of sunitinib on ionic currents was assessed by patch clamping, where sunitinib was found to inhibit the hERG channel with an IC_{50} of 500nM, and inhibit specific sodium (Nav1.5) and calcium (Cav1.2) currents at higher concentrations.[232] It is possible that the increase in beat amplitude observed

in this current study with sunitinib is due to inhibition of one or a mixture of these ion channels.

3.4.5 Conclusion

The aim of this phase of the study was to determine the suitability of the AC10 cardiomyocyte cell line (AC10-CMs) and hiPSC-derived cardiomyocytes (hiPSC-CMs) for detection of structural and functional cardiotoxicity. The Induction of hypertrophy that was observed in AC10-CMs and hiPSC-CMs following exposure to angiotensin II and sunitinib qualifies the use of these cell models for detection of structural cardiotoxicity and supports the use of these cells on an impedance-based platform in screening assays for detection of structural toxicity. The contractility assessments of hiPSC-CMs exposed to isoproterenol, E-4031, angiotensin II and sunitinib support the use of the impedance-based xCELLigence cardio system to detect changes in cardiomyocyte contractility by assessment of transient changes to impedance.

Chapter 4: *In Vitro* Evaluation of Anthracycline-induced Cardiotoxicity

4.1 Introduction

An integral component of multiple chemotherapy regimes since their introduction in the 1960's; their widespread use makes anthracyclines (e.g. doxorubicin, daunorubicin and epirubicin) one of the most successful drug categories. Anthracyclines are potent cytotoxic drugs whose broad spectrum activity makes them suitable for use as single agents or alongside other drugs where they are used in a curative, adjuvant or palliative manner.[15] Their anti-proliferative effects are exerted on cancer cells by intercalating between DNA base pairs, generating damaging oxygen free radicals and inhibiting the DNA replicative enzyme topoisomerase IIα. (TopIIα) thereby causing DNA double strand breaks. This culminates in an array of cellular injury including damage to cellular components and disruption of DNA synthesis and replication.[111] Despite the oncological success of anthracyclines in treating a wide range of adult and paediatric malignancies, their use is hampered by the occurrence of acute, chronic and delayed cardiotoxicity which considerably limits their clinical usefulness.[16]

Strategies employed in an effort to reduce the cardiotoxicity of anthracyclines include development of less toxic analogues, modification to dosing schedules, creation of new delivery and nano-formulations, enzymatic pro-drug conjugates to restrict anthracycline location to the tumour site, concurrent administration of cardioprotective therapies and improved imaging modalities and approaches to assess cardiac function.[28,151,233] These modifications and strategies all fall under the umbrella of cardio-oncology, a new multi-disciplinary approach that aims to effectively treat a patients' cancer whilst minimising the collateral damage to the cardiovascular system.[41,153,234]

4.1.1 Cardiotoxicity of the anthracycline doxorubicin

Doxorubicin is the most well studied of the anthracyclines, exhibiting broad spectrum activity against many different tumour types, and thus is considered the standard anthracycline to which all of the other family members may be compared (Figure 4.1).[15] The cardiotoxic effects of anthracyclines were first reported by Lefrak *et al*. in 1973, who observed heart failure in patients following doxorubicin treatment.[112] Although doxorubicin-induced cardiotoxicity has been classified as the most noted chemotherapy-induced cardiotoxicity to date,[114] it is still unclear as to how anthracyclines such as doxorubicin cause irreversible damage to cardiomyocytes.

Collective evidence suggests that the adverse cardiac effects initiated by doxorubicin is progressive and multi-factorial. From a tissue and cellular level, doxorubicin is reported to cause significant cytotoxicity of post-mitotic differentiated cardiomyocytes (and supporting cells, such as fibroblasts) and subsequent loss of cellular mass.[144] Tissue changes to the myocardium include widespread areas of myocardial interstitial fibrosis, fibroblast proliferation, increased macrophage infiltration and scattered vacuolated cardiomyocytes with a loss of regular shape.[235] At the subcellular level doxorubicin causes cytoplasmic vacuoles, mitochondrial membrane disruption and disorder of myofibril arrangement.[116] From a molecular perspective, mechanisms of doxorubicin-induced cardiomyopathy include impaired calcium handling, altered gene and protein expression of key pathways involved in cardiomyocyte survival and function, DNA breakage via inhibition of cellular topoisomerase IIβ (TopIIβ), intracellular collation of iron, inhibition of mitochondrial topoisomerase I (TopImt) and consequent function, and the formation of oxygen free radicals that damage the mitochondria of the cells.[16,34,118,124,127] These mechanisms of doxorubicin-induced cardiotoxicity are discussed in detail in section 1.7.1.1.

4.1.1.1 Clinical manifestation of doxorubicin-induced acute cardiotoxicity

Acute cardiotoxicity can occur within weeks of treatment, although this is fairly rare and usually self-limiting and reversible.[16] The incidence of acute cardiotoxicity has been estimated at approximately 11% and presents as drug-induced pericarditis and perturbations in cardiac contractility causing cardiac dysrhythmias.[142,235] Doxorubicin-induced electrophysiological disturbances are centred around non-specific ST-T changes and decreased amplitude of the QRS complex. A case study by Steinberg *et al*. evaluated the cardiac function of 29 patients post-doxorubicin treatment and concluded that arrhythmias in the first hour after doxorubicin treatment are very uncommon, however occur more commonly over the next 23 hours, usually in the form of ventricular premature beats and non-sustained ventricular tachycardia.[141] In addition, the mechanism of acute cardiotoxicity is thought to involve an inflammatory response, shown by Pecoraro *et al*. who observed increased levels of pro-inflammatory cytokines with a concomitant reduction of the anti-inflammatory cytokine IL-10 in a 24 hour mouse study of acute doxorubicin cardiotoxicity.[236]

Despite in many cases these early toxicities not posing an immediate threat or necessitation of treatment interruption, they may 'prime' the heart to subsequent remodelling and occurrence of the move severe forms of delayed toxicity. Acute cardiotoxicity as a consequence of doxorubicin treatment is discussed in section 1.7.1.2.2.

4.1.1.2 Clinical manifestation of doxorubicin-induced delayed and chronic cardiotoxicity

The cardiotoxicity demonstrated by anthracyclines, including doxorubicin, is largely irreversible and related to the total cumulative dose that patients have been exposed to. The importance of cumulative dose as a determinant for development of heart failure was identified by Von Hoff *et al*. who conducted a retrospective analysis of over 4000 patients treated with anthracyclines.

Although this study has been critiqued due to sole utilisation of clinician identified symptoms of heart failure, a sudden rise in the prevalence of heart failure occurred at a cumulative dose of 550mg/m^2,[113] which is slightly higher than the current maximum recommended cumulative lifetime dose of 450mg/m^2.[15] A retrospective analysis of three clinical trials conducted by Swain *et al*. further investigated the importance of cumulative dose in relation to anthracycline-induced cardiotoxicity (AIC), and reported the prevalence of heart failure in patients who were exposed to a range of cumulative doses of anthracycline. The incidence of heart failure was found to increase with cumulative dose, with estimated incidence of 5%, 26% and 48% with 400mg/m^2, 550mg/m^2 and 700mg/m^2 cumulative dose, respectively. Interestingly, this study also found an increased risk of cardiotoxicity with lower amounts of doxorubicin (<300 mg/m^2) which were previously not linked with left ventricular dysfunction.[17]

The notable short and long term effects of doxorubicin on the cardiac system are development of left ventricular dysfunction (LVD) which can lead to heart failure (HF). This progressive form of drug-induced cardiotoxicity usually occurs following completion of treatment, either within one year of treatment (chronic cardiotoxicity) or decades after chemotherapy has been completed (delayed cardiotoxicity).[134] Chronic cardiotoxicity is the most prevalent and clinically relevant manifestation of anthracycline-induced cardiotoxicity. Symptoms usually present approximately one year following treatment as dilated cardiomyopathy a prerequisite for heart failure.[135]

Delayed cardiotoxicity is particularly relevant in adult survivors of childhood cancer, whereby cardiotoxicity arises decades after exposure to doxorubicin after a long asymptomatic period.[136] Due to their younger age at the time of treatment, childhood survivors are in a developmental stage that makes them more vulnerable to adverse health effects from potentially toxic therapies, which become clinically apparent years later. In these survivors, cardiovascular related disease has been identified as the leading cause of morbidity and mortality after development of cancer recurrence.[31]

4.1.2 Cardiotoxicity of the anthracycline epirubicin

Epirubicin is a derivative of doxorubicin (Figure 4.1), used in the treatment of many tumour types including haematological malignancies and cancers of the breast, lung, ovary and bladder.[131] Its use has been evaluated mainly in breast cancer patients where it is preferred over doxorubicin due to its more favourable toxicity profile. These 'safer drug' benefits of epirubicin compared to doxorubicin include reduced neutropenia and nausea, making this drug more tolerable for patients which may allow for greater dose escalation and combination with other potentially cardiotoxic therapies.[237] However, although disease free and overall survival was improved for patients who received 5-flurouracil/epirubicin/cyclophosphamide (FEC) compared to those who received methotrexate instead of epirubicin, the rate of heart failure increased from 0.3% to 1.4% in epirubicin treated patients.[238] A retrospective analysis conducted by Ryberg *et al*. in 1998 evaluated the influence of cumulative dose, dose intensity and schedule on the development of heart failure in 469 breast cancer patients treated with epirubicin.[239] The study found, similar to doxorubicin, that the risk of developing heart failure is linked to cumulative lifetime exposure, with 7.2% patients developing heart failure after a median follow-up of 75 months, with toxicity risks increasing alongside higher cumulative doses. The risk was 4% at 900mg/m^2, increasing to 15% at 1000mg/m^2,[239] therefore the maximum recommended cumulative dose for epirubicin is clinically recognised at 900mg/m^2,[131] which could be considered analogous to receiving 450 - 550mg/m^2 doxorubicin.[237] Many randomised controlled trials (RCTs) have been conducted comparing epirubicin and doxorubicin at equimolar doses, where epirubicin was found to possess similar oncological efficacy to doxorubicin but was less cardiotoxic.[237]

4.1.3 Cardiotoxicity of the anthracycline daunorubicin

Daunorubicin was the first anthracycline to be identified (Figure 4.1), and was isolated from the *Streptomyces peucetius* bacteria in the 1950's.[109] Daunorubicin is used much less frequently than other anthracyclines, mainly in the treatment of acute leukaemia in children and leukaemia in adults, often as part of a combination regimen. Much like the other anthracycline agents, cardiotoxicity is a major limitation of daunorubicin use and clinically the maximum cumulative dose is 550mg/m^2 in adults or 300mg/m^2 in children.[132] The first clinical trial to assess the cardiotoxic potential of daunorubicin was conducted by Halazun *et al*. in 1974 who compared schedules consisting of methotrexate, vincristine, mercaptopurine, prednisolone +/- daunorubicin in children with acute lymphocytic leukaemia. The study found that heart failure occurred suddenly in patients treated with daunorubicin, where the incidence was 9.9%. A wide range of doses were used throughout the study (360 – 1260mg/m^2), all of which caused cardiotoxicity – however in general incidence increased with increasing doses of daunorubicin.[240] Studies comparing daunorubicin to doxorubicin are not as plentiful as daunorubicin is used far less frequently than other anthracyclines, however analogous to epirubicin, daunorubicin is believed to be less cardiotoxic than doxorubicin. A study conducted using data pooled from various studies analysed 15,815 survivors of childhood cancer and found that heart failure was less prevalent in daunorubicin treated patients than those treated with doxorubicin.[241] This has potential implications because if the two anthracyclines are equally efficient at killing cancer cells in a patient population, then daunorubicin may represent a better option in terms of preservation of cardiac function in paediatric cancer cases.

4.1.4 Risk factors for anthracycline-induced cardiotoxicity

Whilst the notion of total lifetime cumulative dose exists to protect patients from developing anthracycline induced cardiotoxicity, it has become evident that some patients develop cardiotoxicity following exposure to lower cumulative doses, whereas others are able to withstand much higher amounts of drug without developing cardiac abnormalities. Several risk factors have been reported to increase susceptibility to developing AIC including extremes of age, concurrent treatment with the molecular-targeted agent trastuzumab or radiation therapy and pre-existing cardiac disease.[16,105,144,145] Risk factors for AIC are discussed in section 1.7.1.3.

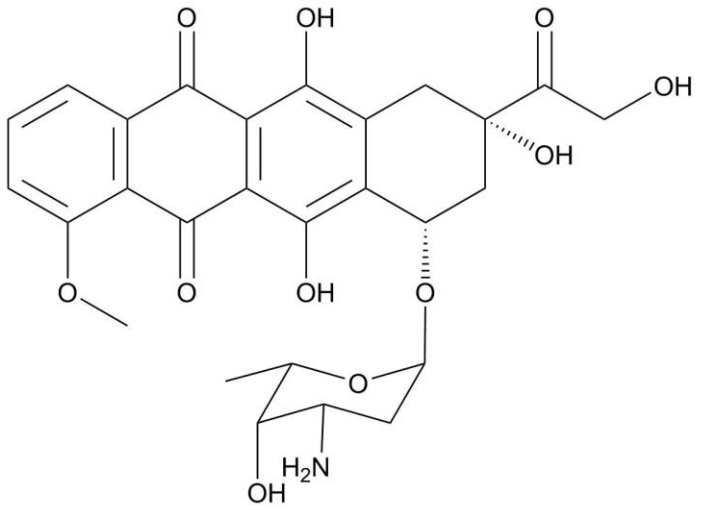

Doxorubicin

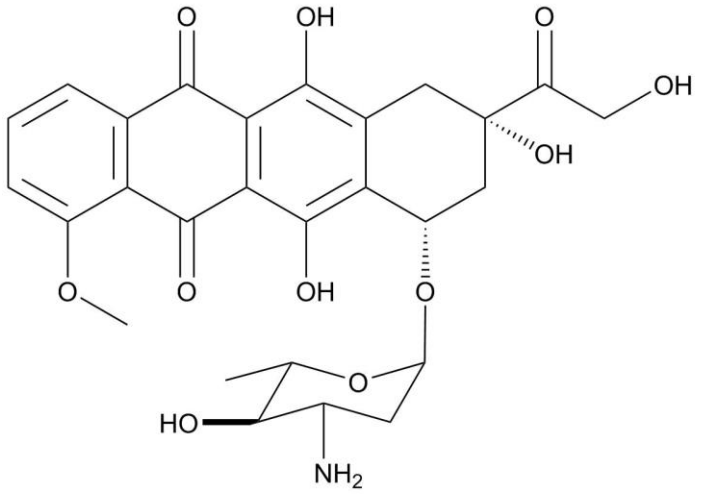

Epirubicin

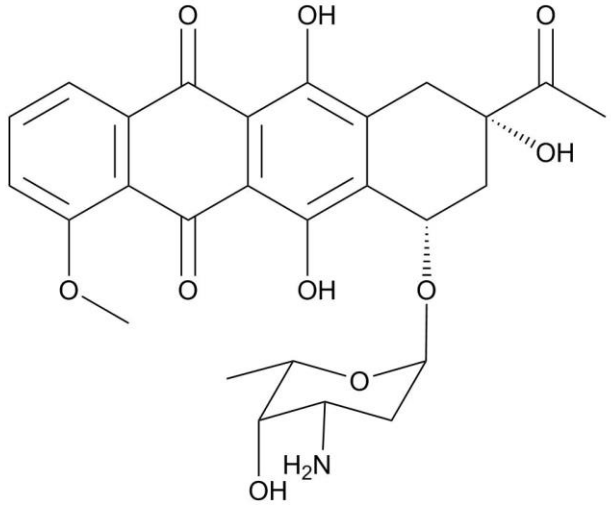

Daunorubicin

Figure 4.1 **Structures of the anthracyclines doxorubicin, epirubicin and daunorubicin**

4.1.5 Aims and objectives

The occurrence of cardiac liabilities following anthracycline treatment is well established clinically, particularly doxorubicin induced cardiotoxicity. The aim of this phase of the study is to use the *in vitro* models and methods that were qualified in chapter 3 to determine if the structural and functional acute cardiotoxicity induced by anthracyclines in the clinic can be detected using these *in vitro* cardiomyocyte models.

Specifically:

i) Determination of the sensitivity of AC10 cardiomyocytes (AC10-CMs) to doxorubicin, with clinically relevant doses of the drug used to assess structural changes to cells using the xCELLigence RTCA system. Parallel studies will be conducted using human induced pluripotent stem cell derived cardiomyocytes (hiPSC-CMs) where functionality and morphology following exposure to doxorubicin will be monitored using the xCELLigence cardio system.

ii) Studies will be conducted in AC10-CMs to investigate the differential effects of an anthracycline panel comprised of doxorubicin, daunorubicin and epirubicin. Investigations will be conducted in both the exponential and plateau phases of growth for 24 hours and 96 hours exposure times to assess the sensitivity of the cells to the anthracycline panel and elucidate the effects of proliferative capacity and exposure time on cell sensitivity to the drugs.

iii) Structural changes following addition of clinically relevant doses of the anthracycline panel will be assessed using the xCELLigence RTCA on AC10-CMs in both the exponential and plateau phases of growth. Parallel studies will be conducted using hiPSC-CMs where functionality and morphology following exposure to the anthracycline panel will be monitored using the xCELLigence cardio system.

4.2 Materials and methods

4.2.1 Evaluation of viability of AC10-CMs following anthracycline treatment determined using the MTT assay

AC10-CMs were seeded into 96-well plates as previously described in section 2.2 for exponential and plateau phase studies. After 24 hours the anthracyclines doxorubicin, daunorubicin and epirubicin were added to cells in separate plates, with a 1:5 serial dilution performed across the wells, resulting in final concentrations ranging from 5µM to 128pM, 2µM to 25nM or 1µM to 2nM, respectively. Following 24 hours exposure, drugs were removed and media replaced with fresh medium. For 96 hour exposure studies, cells were exposed to the drugs for the duration of the experiment. After 96 hours post drug addition, cell viability was assessed using the MTT assay (see section 2.2). All studies were repeated a minimum of three times and IC_{50} values determined by implementing curve fitting by non-linear regression on GraphPad Prism (Version 7.04, GraphPad Software, Inc.).

4.2.2 Investigations of morphological changes to AC10-CMs induced by anthracyclines using the xCELLigence real-time cell analyser

Experiments were set up as described in section 2.3. For continuous exposure studies in exponential growth phase, doxorubicin was added at 24 hours and cells were exposed to 50nM, 100nM, 250nM and 500nM doxorubicin for 96 hours. For studies analysing 24 hours exposure in exponential growth phase, anthracyclines (doxorubicin, daunorubicin and epirubicin; 50nM and 500nM) were added at 24 hours and replaced with fresh medium following 24 hours exposure. For studies in plateau growth phase, anthracyclines (doxorubicin, daunorubicin and epirubicin; 50nM and 500nM) were added once the cell index demonstrated confluence (approximately 72 hours) and replaced with fresh medium following 24 hours exposure. All experiments were performed in triplicate and statistical analysis on normalised cell index values

was conducted using a one way analysis of variance (ANOVA) test, and a post-hoc Dunnett's test when required using GraphPad Prism (Version 7.04, GraphPad Software, Inc.).

4.2.2.1 Evaluation of viability of AC10-CMs following anthracycline treatment at specific time points determined using the MTT assay

In parallel, cellular viability was determined to complement data obtained using the xCELLigence real-time cell analyser (RTCA). AC10-CMs were seeded into 96-well plates as previously described in section 2.2 for exponential and plateau phase studies. For continuous exposure in exponential growth phase, doxorubicin (50nM, 100nM, 250nM and 500nM) was added 24 hours after cell seeding and experiments terminated following 48 hours exposure. For studies analysing 24 hours exposure in both exponential and plateau growth phase, anthracyclines (doxorubicin, daunorubicin and epirubicin; 50nM and 500nM) were added 24 hours after cell seeding and experiments terminated after 24 hours exposure. Absorbance readings were obtained and analysed as described in section 2.2. All experiments were performed in triplicate.

4.2.3 Imaging of AC10-CMs treated with doxorubicin

AC10-CMs were plated at a density of $5x10^4$ cells/well in 6 well plates. The following day 50nM doxorubicin was added to 2 wells and following 48 hours exposure the cells were fixed using 4% PFA (see section 3.2.1). All experiments included a time matched vehicle control. Cellular images were collected using a Leica DIC DMI6000B inverted microscope and analysed using the Leica application suite. All studies were repeated in triplicate.

4.2.4 Evaluation of anthracycline-induced cardiotoxicity in hiPSC-CMs using the xCELLigence cardio system

hiPSC-CMs were plated into a cardio E-plate at a density of 30,000cells/well, in wells pre-coated with fibronectin (Cell plating and maintenance described in section 2.4). Once stable beating was detected, half the media (90µl) was removed from each well and replaced with media containing twice the required drug concentration. Doxorubicin was added to a final concentration of 50nM, 100nM and 250nM, whereas epirubicin and daunorubicin were added at 50nM only. Changes to the cell index and contractility following drug addition were analysed at various points throughout 24 hours exposure to the drugs, as per standard xCELLigence assay. Following 24 hours exposure to anthracyclines the drugs were washed out using the four step medium change method (see section 2.4.2) and cells were re-challenged with the same anthracycline 96 hours later.

Statistical analysis on normalised cell index, normalised beat rate and normalised beat amplitude were conducted using a one way analysis of variance (ANOVA) test, and a post-hoc Dunnett's test when required. Statistical analysis was performed using GraphPad Prism (Version 7.04, GraphPad Software, Inc.).

4.3 Results

The purpose of this phase of the study was to apply the methodologies previously established to investigate the structural and functional cardiotoxicity related to anthracyclines. Initially the sensitivity of AC10 cardiomyocytes (AC10-CMs) to doxorubicin was evaluated, followed by investigations into morphological changes to these cells and changes to the morphology and contractility of hiPSC-derived cardiomyocytes (hiPSC-CMs) after exposure to doxorubicin. Comparative studies using the anthracyclines doxorubicin, daunorubicin and epirubicin were then convened using the same methodology to investigate if the observed responses were specific to doxorubicin or are a ubiquitous effect related to the anthracycline class.

4.3.1 Cardiomyocyte cell types are differentially sensitive to doxorubicin

Prior to investigating morphological effects, the effect of doxorubicin on viability of AC10-CMs in the exponential growth phase was ascertained using the MTT assay. Figure 4.2 shows that exposure to concentrations of doxorubicin ranging from 5µM to 12.8pM for 96 hours caused a dose-dependent decrease in the cellular viability of AC10-CMs, with an IC_{50} of 14.66 ± 3.31nM. The C_{Max} of doxorubicin is 1.1µM (indicated on the graph), for future experiments investigating the morphological changes to cells, concentrations of 0.5, 0.25, 0.1 and 0.05 C_{Max} were used, which equates to concentrations of 500nM, 250nM, 100nM and 50nM doxorubicin.

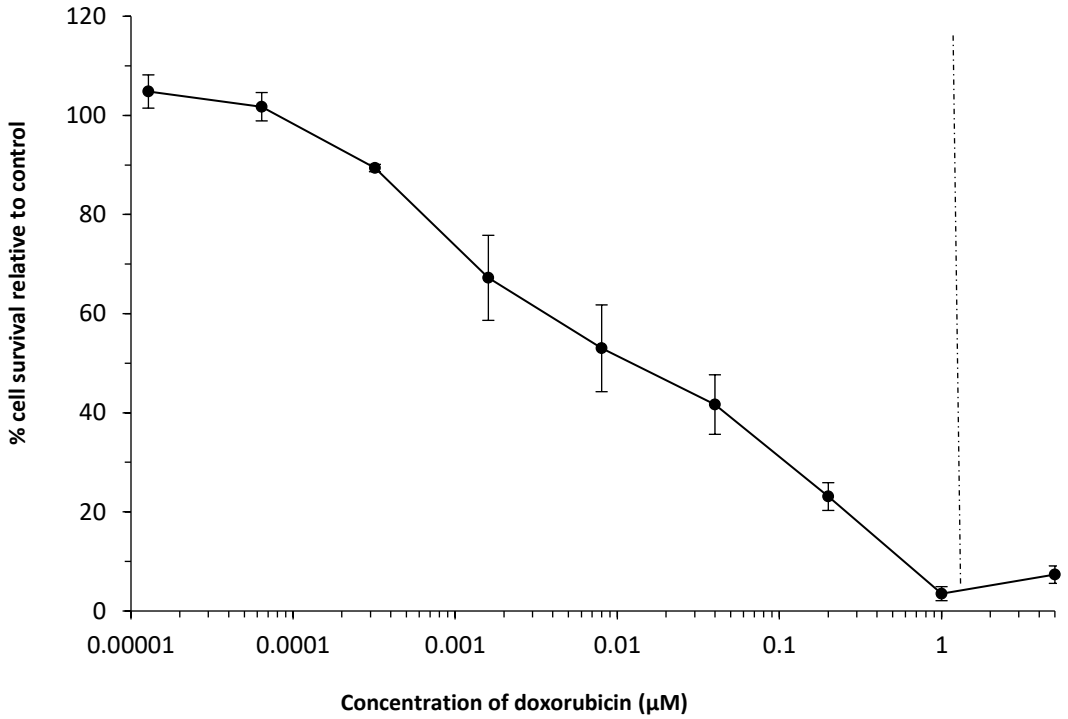

Figure 4.2 Effect of doxorubicin on viability of AC10 cardiomyocytes

Dose response curve showing the effect of doxorubicin on cell viability following 96 hours exposure expressed as % cell survival relative to vehicle control for cells in exponential growth phase. The dashed line represents the C_{Max} of doxorubicin (1.1µM), data is representative of n=3 ± SE.

4.3.1.1 Doxorubicin induces morphological changes in AC10 cardiomyocytes

The xCELLigence RTCA was used to assess the effect of doxorubicin on the morphology of AC10-CMs. As shown in figure 4.3A and 4.3B, when normalised to the point of doxorubicin addition, cell index initially increased higher than the level of control in cells exposed to doxorubicin. The cell index of cells treated with 250nM and 500nM doxorubicin then declined (figure 4.3B), whereas the cell index of cells treated with 50nM and 100nM doxorubicin continued to increase, with the highest cell index observed at 48 hours exposure to 50nM doxorubicin (figure 4.3A). This data is summarised in figure 4.3C. To ascertain if the increases in cell index was due to increased cellular proliferation or a change to cellular morphology an MTT assay was carried out. With respect to AC10-CMs treated with 50nM and 100nM doxorubicin, if cell index were based purely on cell number then treatment with 50nM doxorubicin would increase cell number, and treatment with 100nM doxorubicin would not impact cell number significantly. However, AC10-CMs exposed to 50nM and 100nM doxorubicin in an identical manner showed dose-dependent decreases in cell viability (figure 4.3D), indicating that the increase in cell index observed using xCELLigence was due to a change in morphology (figure 4.3E).

4.3A

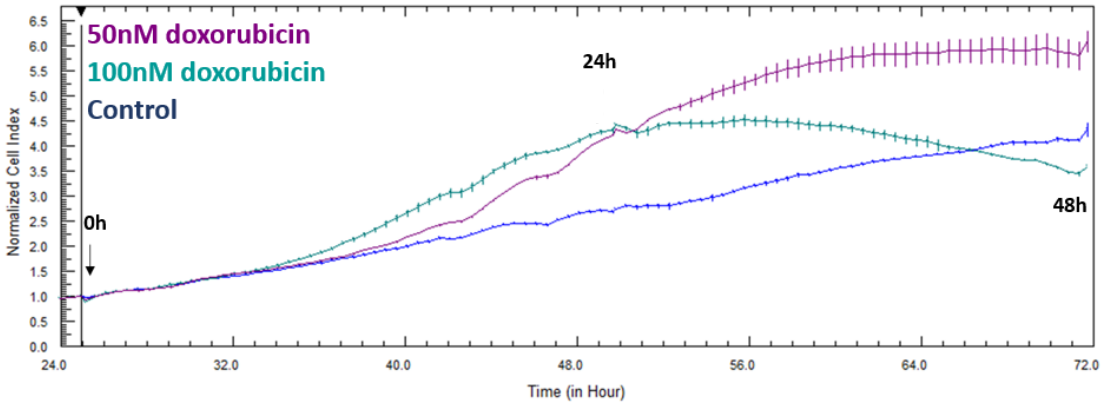

4.3B

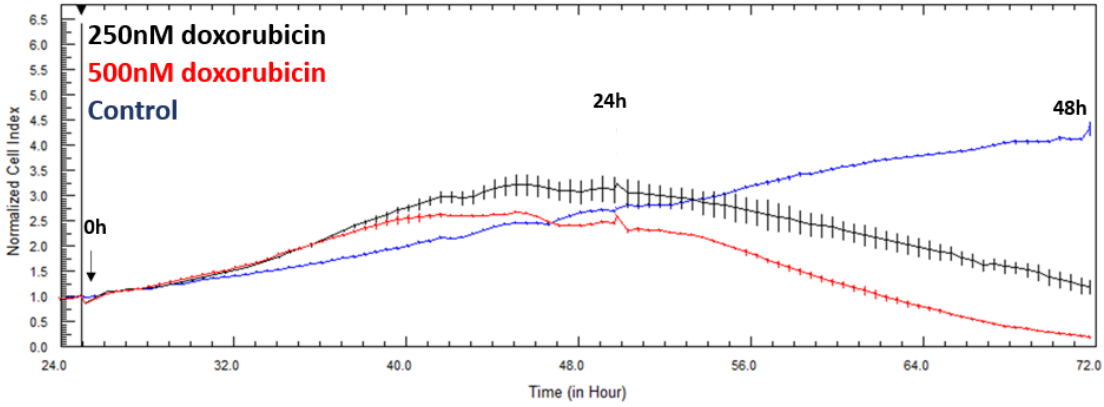

Figure 4.3 Doxorubicin induces morphological changes in AC10 cardiomyocytes (1)

A/B. xCELLigence traces showing time (hours) vs normalised cell index of AC10-CMs in exponential growth phase exposed to doxorubicin with point of doxorubicin addition (arrow) and exposure time indicated, data representative of n=3, data points shown are average ± SD

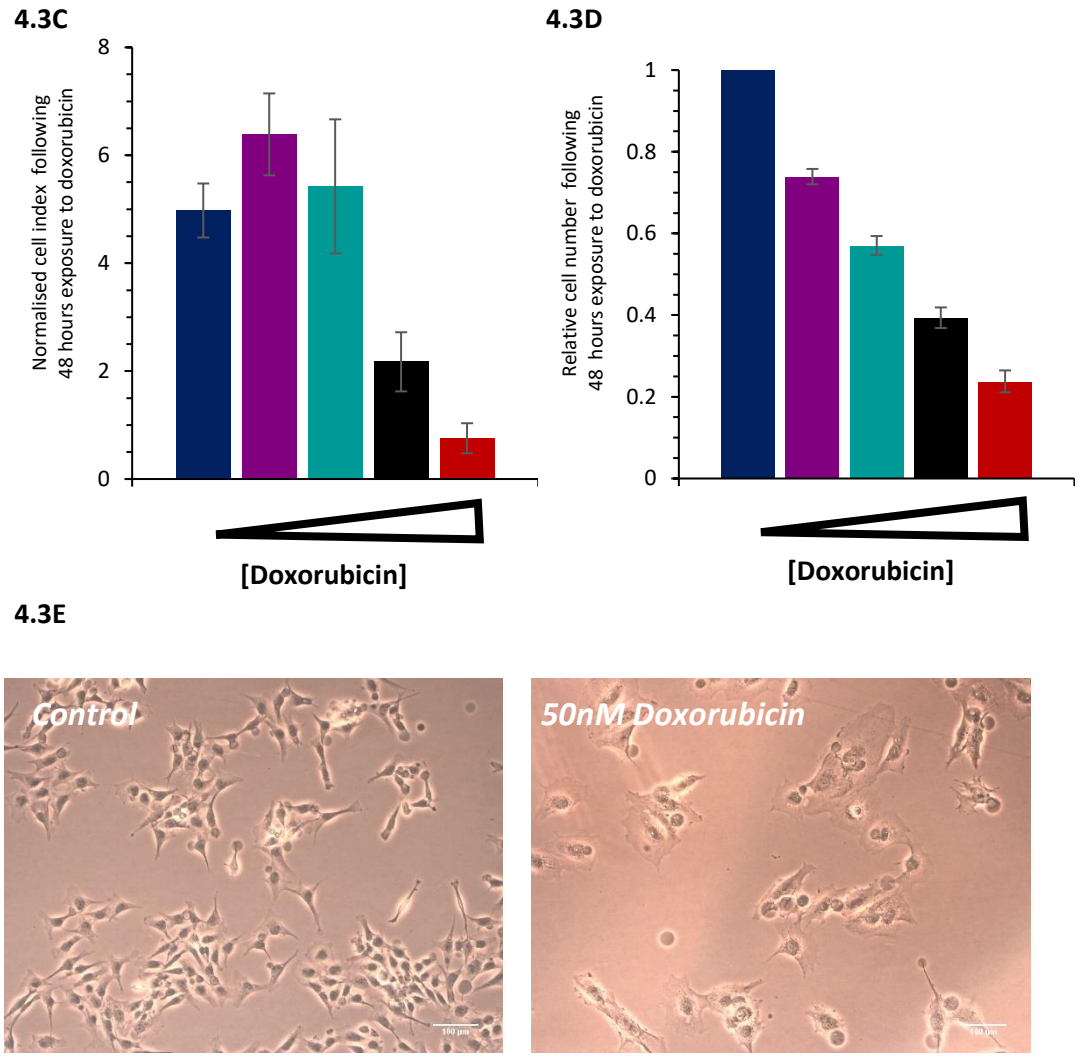

Figure 4.2 Doxorubicin induces morphological changes in AC10 cardiomyocytes (2)

C. Normalised cell index following 48 hours exposure to doxorubicin**,** data is n=3 ± SE. **D**. Relative cell number following 48 hours exposure to doxorubicin measured by MTT assay, data is n=3 ± SE and **E.** Images of untreated and doxorubicin treated AC10 cardiomyocytes showing a change in morphology. Images were taken at 10x magnification following 48 hours exposure to doxorubicin. ■ control, ■ 50nM doxorubicin, ■ 100nM doxorubicin, ■ 250nM doxorubicin, ■ 500nM doxorubicin.

4.3.1.2 Doxorubicin induces morphological changes and functional disturbances in hiPSC-derived cardiomyocytes

Stably beating Cor.4U cells were exposed to doxorubicin for 24 hours and the effects on cell morphology and contractility were monitored in real-time. As shown in figure 4.4A, when normalised to the point of doxorubicin addition, cell index immediately increased higher than the level of control in cells exposed to 50nM, 100nM and 250nM doxorubicin, with the greatest difference in cell index approximately 6 hours after doxorubicin was initially added (figure 4.4B), indicating that doxorubicin induced a morphology change to the cells.

Assessment of the effect of doxorubicin on contractility of hiPSC-CMs was carried out after 6 and 24 hours exposure, as these time points represent the greatest degree of hypertrophy and maximum exposure to the drug respectively. The representative traces of contractility shown for control and doxorubicin treated cells in figure 4.5A show no visible changes in contractility following 6 hours exposure, however visible changes to both beat rate and amplitude are evident following 24 hours exposure. Detailed analysis of beat rate and amplitude is shown in figures 4.5B and 4.5C respectively.

4.4A

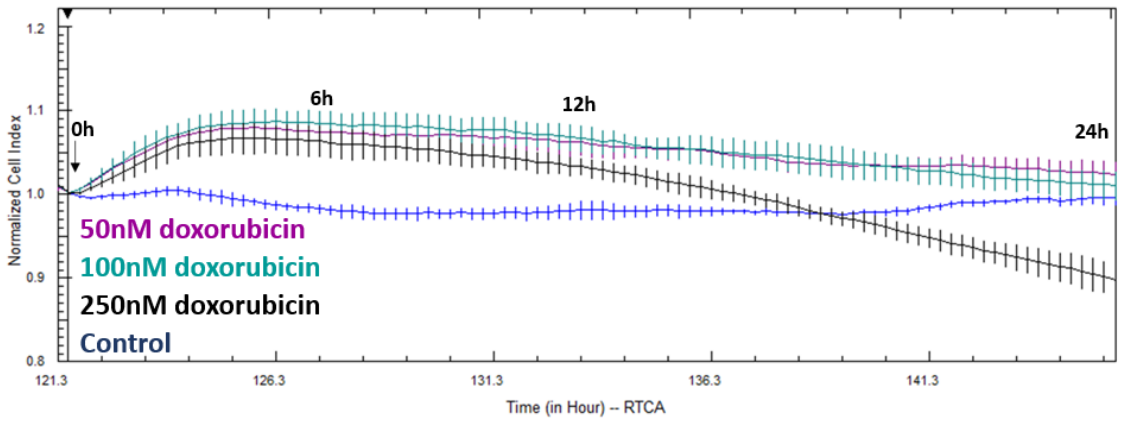

4.4B

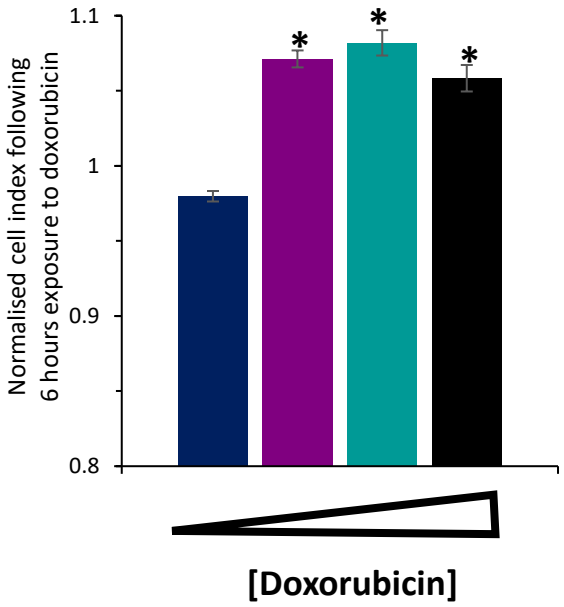

Figure 4.4 Doxorubicin induces morphological changes in hiPSC-derived cardiomyocytes

A. xCELLigence trace showing time (hours) vs normalised cell index of hiPSC-CMs exposed to doxorubicin with point of doxorubicin addition (arrow) and exposure time indicated, data representative of n=2, data points shown are average ± SD. **B.** Normalised cell index following 6 hours exposure to doxorubicin**,** data points show average of 4 wells ± SE. ∗ p< 0.0001 (treatment groups compared to control). ■ control, ■ 50nM doxorubicin, ■ 100nM doxorubicin, ■ 250nM doxorubicin.

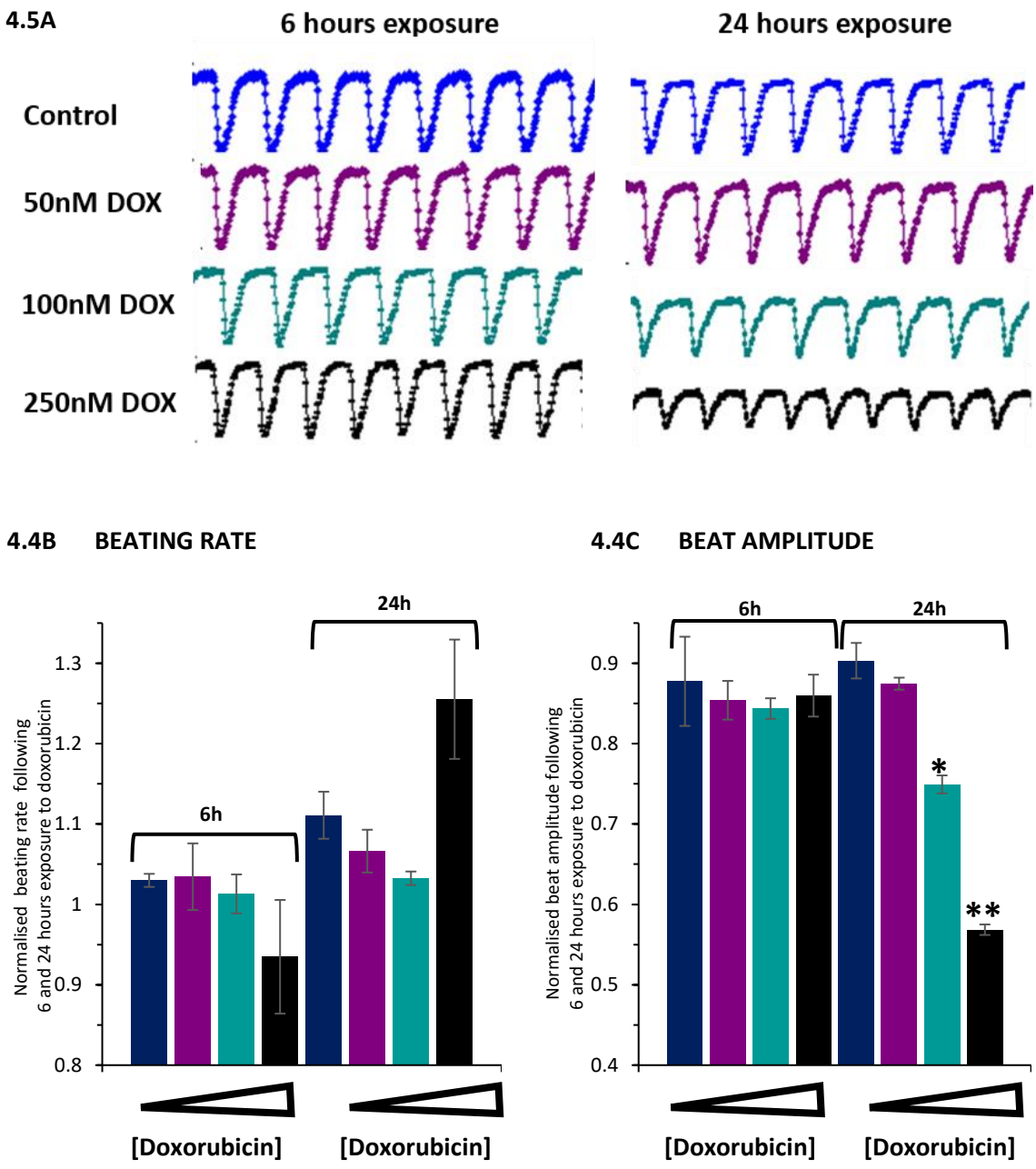

Figure 4.5 Doxorubicin induced changes to contractility of hiPSC-derived cardiomyocytes are greater following 24 hours exposure

A. Representative traces showing contractility of control cells and cells exposed to doxorubicin (DOX) for 6 and 24 hours. **B.** Normalised beating rate following 6 and 24 hours exposure to doxorubicin, data points show average of 3 wells ± SE. **C.** Normalised beat amplitude following 6 and 24 hours exposure to doxorubicin, data points show average of 3 wells ± SE. * p< 0.001, ** p< 0.0001 (treatment groups compared to control). ■ control, ■ 50nM doxorubicin, ■ 100nM doxorubicin, ■ 250nM doxorubicin.

4.3.2 Anthracyclines exhibit similar toxicity profiles in cardiomyocyte cell models

Prior to investigating morphological changes, the effect of doxorubicin, daunorubicin and epirubicin on viability of ACl0-CMs was investigated in the exponential and plateau phases of growth for both 96 hours continuous exposure and 24 hours exposure plus a 72 hours recovery period. Figure 4.6 shows the viability of AC10-CMs following 24 hours exposure (plus recovery period) to the anthracyclines in both the exponential and plateau phases of growth. In general, similar chemosensitivity profiles were obtained in both growth phases, with cells in the exponential growth phase being slightly more sensitive to all of the anthracyclines, as evidenced by the IC_{50} values (table 4.1). In contrast, following 96 hour exposure to anthracyclines, AC10-CMs in the exponential phase of growth were more sensitive compared to cells exposed to 24 hours anthracyclines only (Figure 4.7). The increased exposure time did not affect the sensitivity of cells in the plateau growth phase, with similar IC_{50} values obtained for 24 and 96 hours exposure times (table 4.1 and 4.2). For future experiments investigating the morphological changes to cells, exposure times of 24 hours were chosen as the current studies suggest that the majority of anthracycline induced damage occurs within this timeframe.

As the data presented in table 4.1 includes a 72 hour recovery period following 24 hours anthracycline exposure the IC_{50} values presented are not true IC_{50} values.

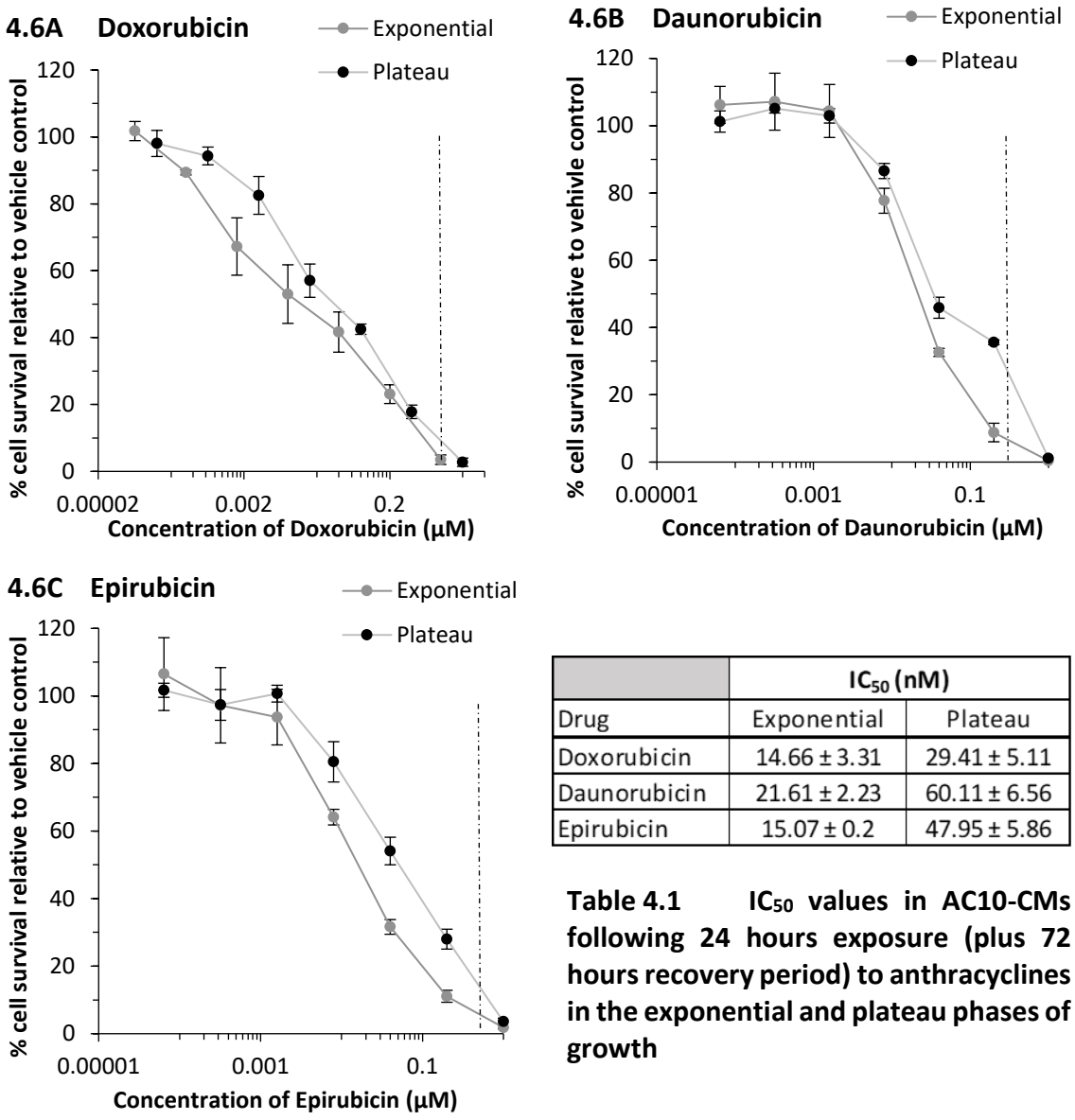

	IC_{50} (nM)	
Drug	Exponential	Plateau
Doxorubicin	14.66 ± 3.31	29.41 ± 5.11
Daunorubicin	21.61 ± 2.23	60.11 ± 6.56
Epirubicin	15.07 ± 0.2	47.95 ± 5.86

Table 4.1 IC_{50} values in AC10-CMs following 24 hours exposure (plus 72 hours recovery period) to anthracyclines in the exponential and plateau phases of growth

Figure 4.6 Anthracyclines exhibit similar toxicity profiles in AC10 cardiomyocytes following 24 hours exposure and a 72 hour recovery period

Dose response curves showing cell viability expressed as % cell survival relative to vehicle control for cells in exponential and plateau growth phases exposed for 24 hours to **A**. Doxorubicin, **B**. Daunorubicin and **C.** Epirubicin. The dashed line represents the C_{Max} of the drug (daunorubicin = 430nM,[242] doxorubicin = 1.1µM,[243] epirubicin = 766nM[244]). Data is n=3 ± SE, IC_{50} values shown inset in table 4.1.

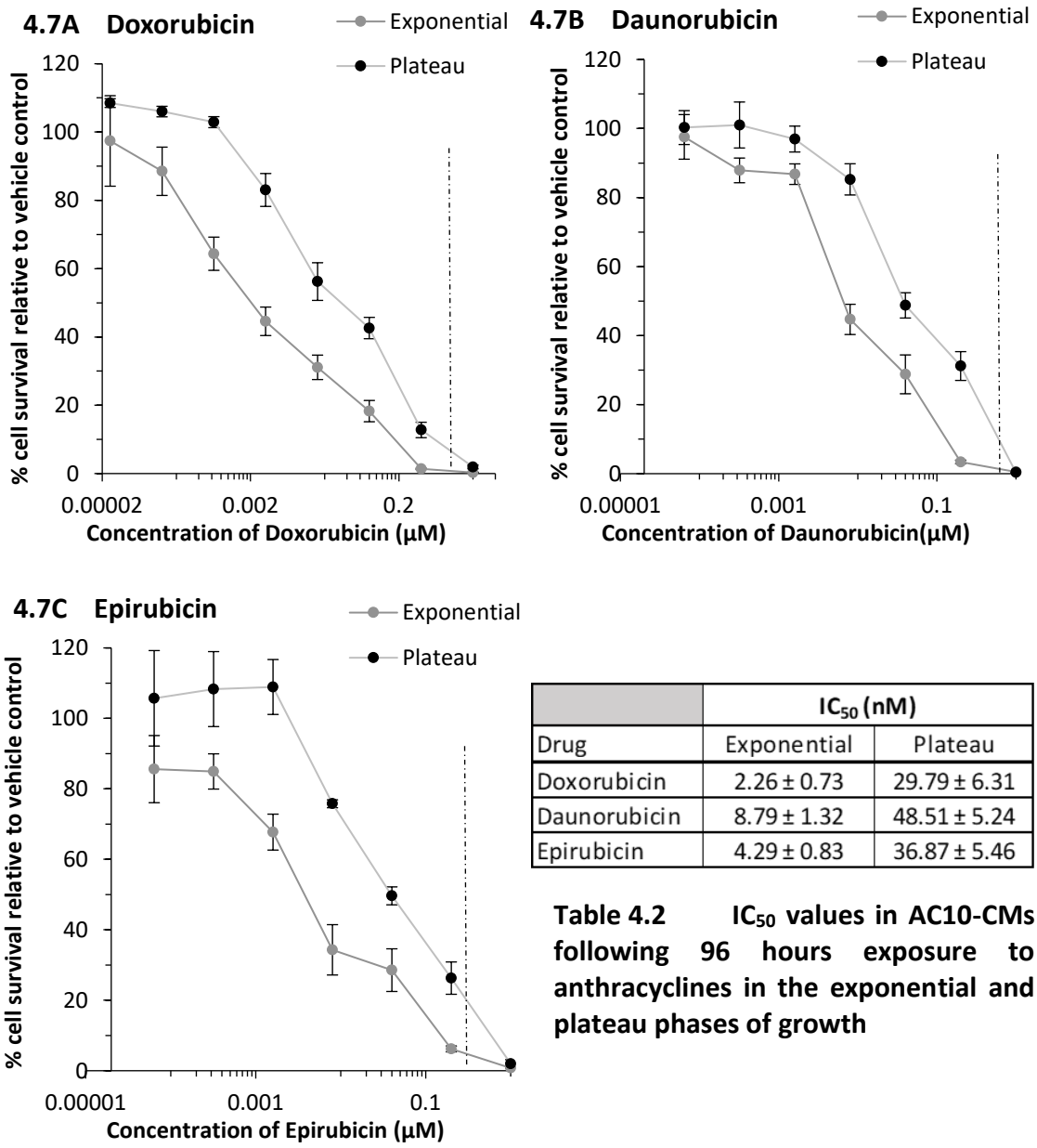

	IC_{50} (nM)	
Drug	Exponential	Plateau
Doxorubicin	2.26 ± 0.73	29.79 ± 6.31
Daunorubicin	8.79 ± 1.32	48.51 ± 5.24
Epirubicin	4.29 ± 0.83	36.87 ± 5.46

Table 4.2 IC_{50} values in AC10-CMs following 96 hours exposure to anthracyclines in the exponential and plateau phases of growth

Figure 4.7 AC10 cardiomyocytes in the exponential growth phase are more sensitive than those in plateau growth phase to anthracyclines following 96 hours exposure

Dose response curves showing cell viability expressed as % cell survival relative to vehicle control for cells in exponential and plateau growth phases exposed for 96 hours to **A**. Doxorubicin, **B**. Daunorubicin and **C.** Epirubicin. The dashed line represents the C_{Max} of the drug (daunorubicin = 430nM,[242] doxorubicin = 1.1µM,[243] epirubicin = 766nM[244]). Data is n=3 ± SE, IC_{50} values shown inset in table 4.2.

4.3.2.1 Anthracyclines induce morphological changes in AC10 cardiomyocytes

Cells in exponential and plateau growth phase were exposed to 50nM (~0.05 C_{Max}) and 500nM (~0.5 C_{Max}) anthracyclines for 24 hours, and the effects on cell behaviour were monitored in real-time. As shown in figure 4.8A/B following 24 hours anthracycline exposure, when normalised to the point of anthracycline addition, cells in exponential growth phase exposed to 50nM and 500nM anthracyclines exhibited an immediate increase in cell index. The cell index continued to increase following 24 hours exposure to 50nM anthracyclines whereas with exposure to 500nM anthracyclines the cell index began to decrease at approximately 18 hours exposure. The normalised cell index following 24 hours exposure to anthracyclines is summarised in figure 4.8C. To ascertain if the increases in cell index were due to increased cellular proliferation or a change to cellular morphology an MTT assay was carried out - AC10-CMs exposed to 50nM and 500nM anthracyclines for 24 hours showed dose-dependent decreases in viability (figure 4.8D), indicating that the increases in cell index observed using xCELLigence was due to a change in morphology. A parallel study conducted in cells in the plateau phase of growth showed similar findings, however in this growth phase 500nM anthracyclines resulted in a higher cell index than 50nM anthracyclines following 24 hours exposure. The cell index began to decrease after 24 hours exposure to 500nM anthracyclines, whereas with 50nM anthracyclines the cell index remained steady after this time point (Figure 4.9A/B). The results of this study are shown in figure 4.9A-D.

4.8A

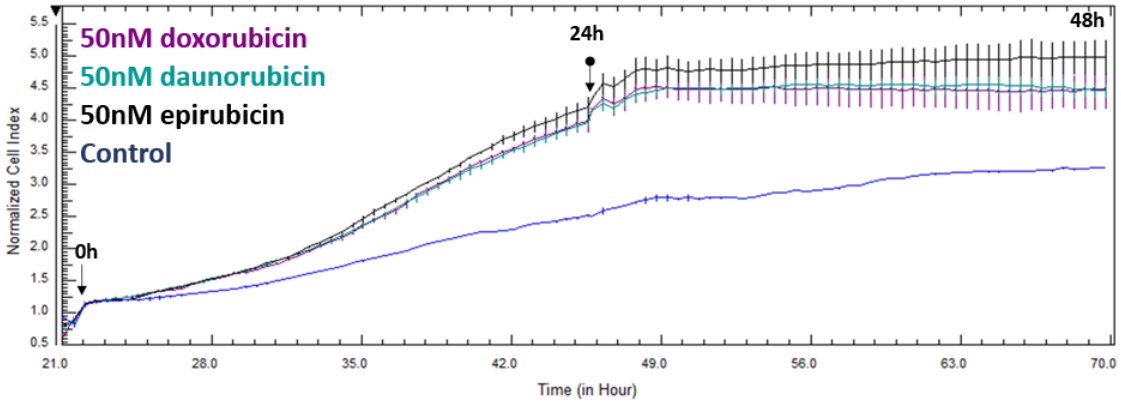

4.8B

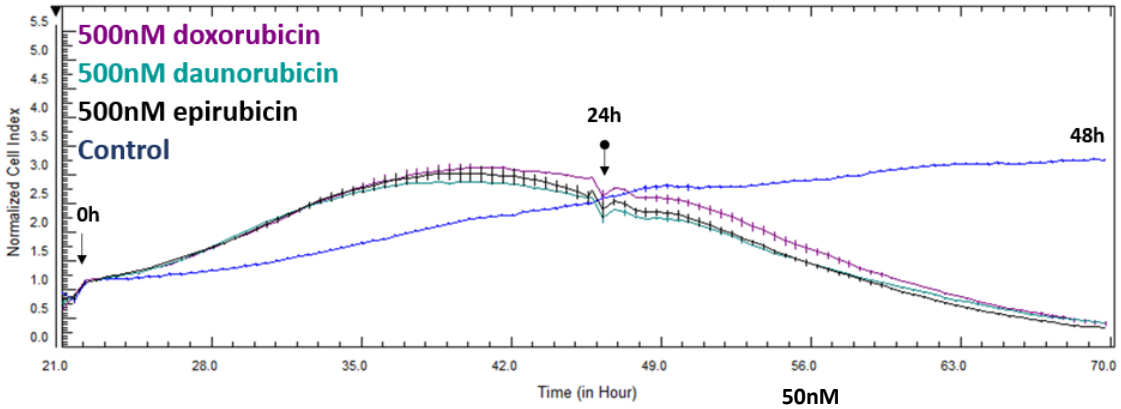

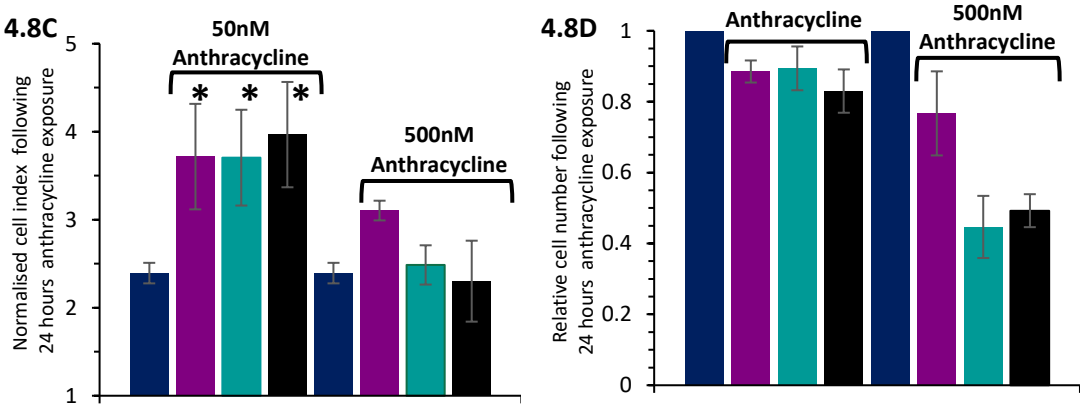

Figure 4.8 **Anthracyclines induce morphological changes of AC10 cardiomyocytes in exponential growth phase**

A/B. xCELLigence traces showing time (hours) vs normalised cell index of AC10-CMs in exponential growth phase exposed to **A.** 50nM and **B.** 500nM anthracyclines with point of anthracycline addition (arrow), anthracycline removal (round-headed arrow) and exposure time indicated, data representative of n=3, data points shown are average ± SD. **C.** Normalised cell index following 24 hours anthracycline exposure**,** data is n=3 ± SE and **D**. Relative cell number following 24 hours anthracycline exposure measured by MTT assay, data is n=3 ± SE. ∗ p< 0.05 (treatment groups compared to control). ■ control, ■ 50nM doxorubicin, ■ 50nM daunorubicin, ■ 50nM epirubicin.

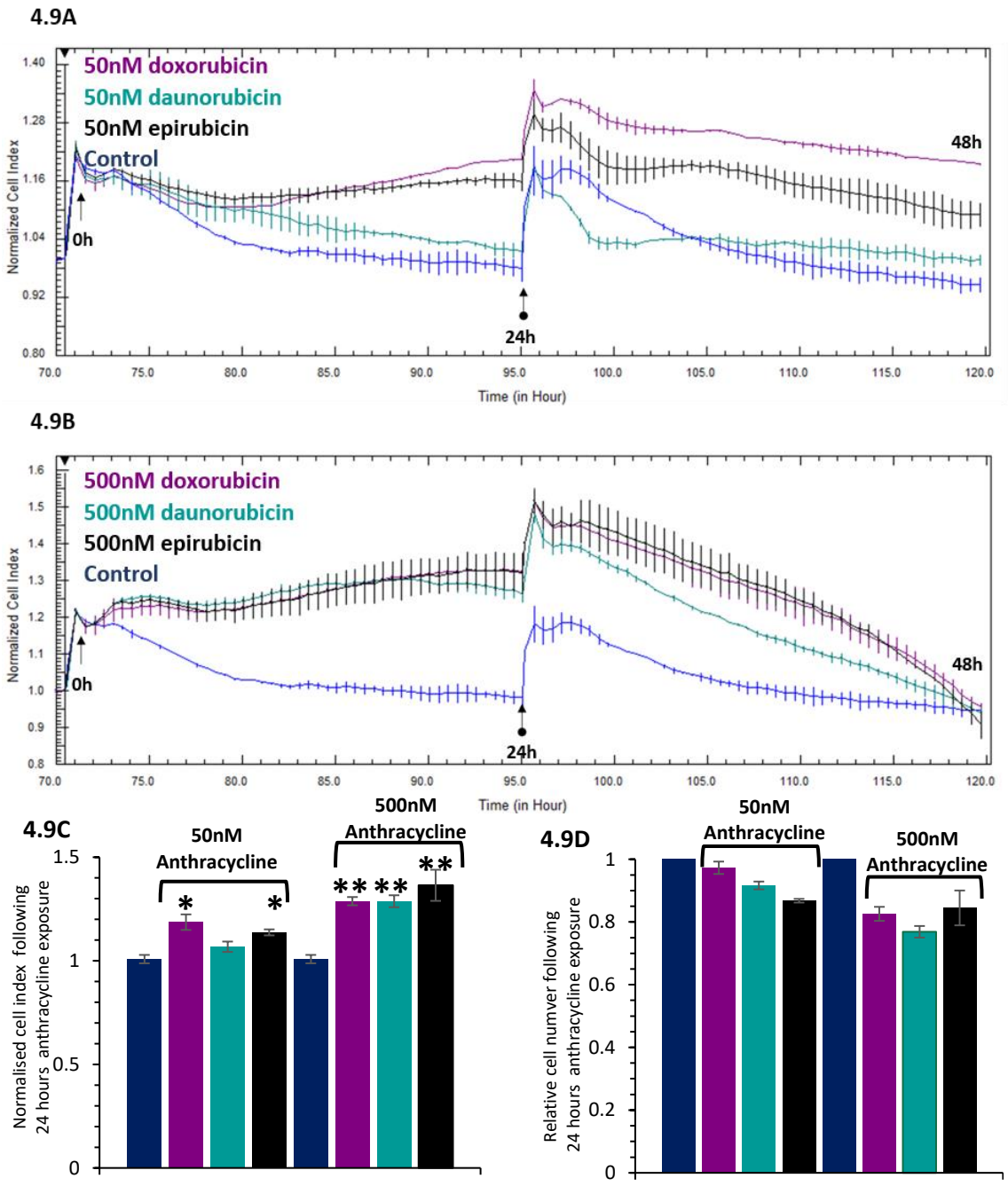

Figure 4.9 Anthracyclines induce morphological changes of AC10 cardiomyocytes in plateau growth phase

A/B. xCELLigence traces showing time (hours) vs normalised cell index of AC10-CMs in plateau growth phase exposed to **A.** 50nM and **B.** 500nM anthracyclines with point of anthracycline addition (arrow), anthracycline removal (round-headed arrow) and exposure time indicated, data representative of n=3, data points shown are average ± SD. **C.** Normalised cell index following 24 hours anthracycline exposure**,** data is n=3 ± SE and **D**. Relative cell number following 24 hours anthracycline exposure measured by MTT assay, data is n=3 ± SE. ∗ p< 0.05, ∗ p< 0.01 (treatment groups compared to control). ■ control, ■ 50nM doxorubicin, ■ 50nM daunorubicin, ■ 50nM epirubicin.

4.3.2.2 Anthracyclines induce similar morphological changes and functional disturbances in hiPSC-derived cardiomyocytes

Stably beating Cor.4U cells were exposed to 50nM anthracyclines for 24 hours and the effects on cell morphology and contractility were monitored in real-time. As shown in figure 4.10A, when normalised to the point of anthracycline addition, cell index immediately increased higher than the level of control in cells exposed to all of the anthracyclines, with the greatest difference in cell index approximately 6 hours after the anthracyclines were added (figure 4.10B), indicating that all of the anthracyclines induced a morphology change to the cells.

Assessment of the effect of the anthracyclines on contractility of hiPSC-CMs was carried out after 6 and 24 hours exposure to anthracyclines, as these time points represent the greatest degree of hypertrophy and maximum exposure to the drug respectively. The representative traces of contractility shown for control and anthracycline treated cells in figure 4.11A show no visible changes in contractility following 6 hours exposure, however visible changes to both beat rate and amplitude are evident following 24 hours exposure. Detailed analysis of beat rate and amplitude is shown in figures 4.11B and 4.11C respectively.

4.10A

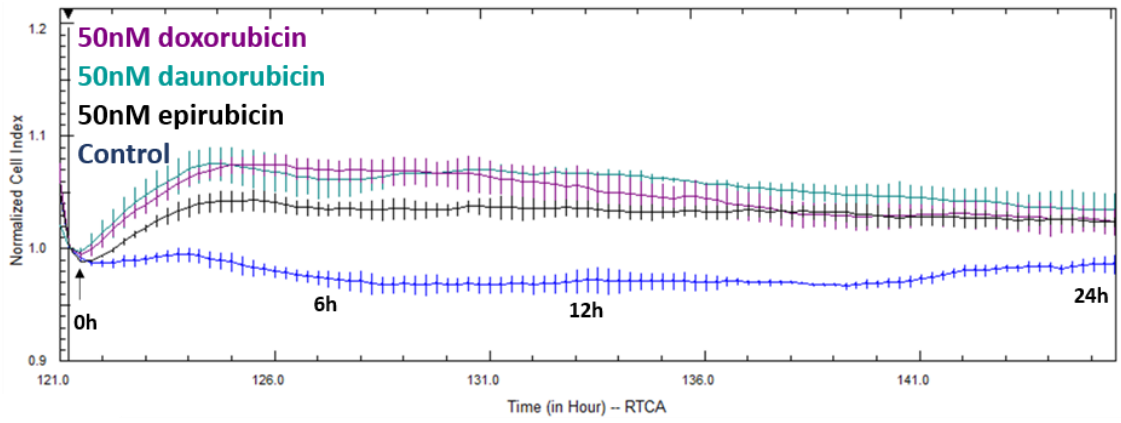

4.10B

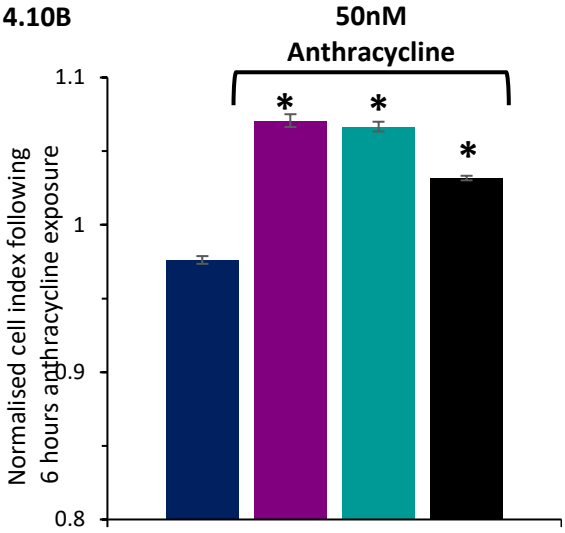

Figure 4.10 Anthracyclines induce morphological changes in hiPSC-derived cardiomyocytes

A. xCELLigence trace showing time (hours) vs normalised cell index of hiPSC-CMs exposed to anthracyclines with point of addition (arrow) and exposure time indicated, data points shown are average ± SD. **B.** Normalised cell index following 6 hours exposure to anthracyclines**,** data points show average of 4 wells ± SE. ∗ p< 0.0001 (treatment groups compared to control). ■ control, ■ 50nM doxorubicin, ■ 50nM daunorubicin, ■ 50nM epirubicin.

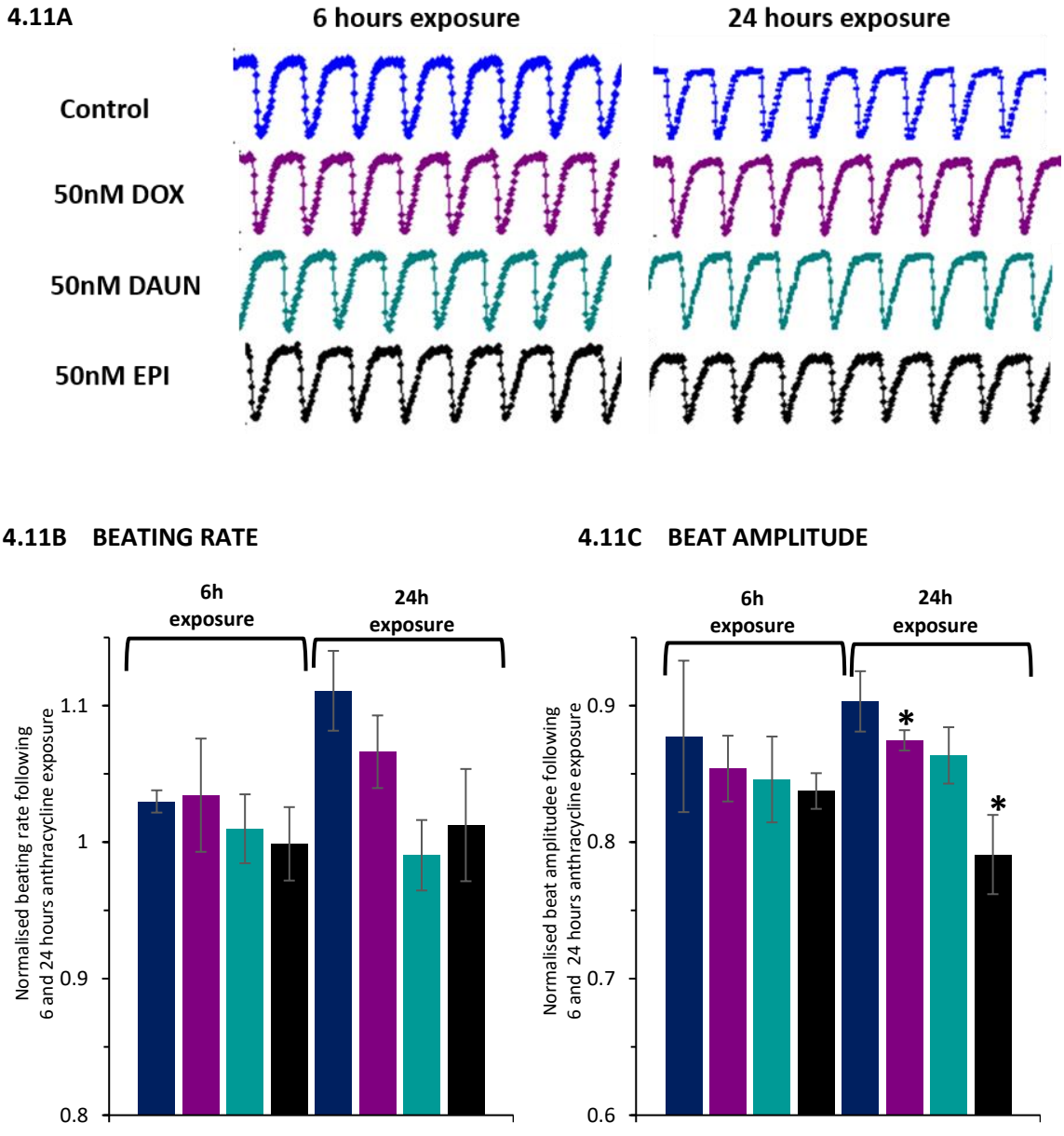

Figure 4.11 Anthracycline induced changes to contractility of hiPSC-derived cardiomyocytes are greater following 24 hours exposure

A. Representative traces showing contractility of control cells and cells exposed to anthracyclines (DOX = doxorubicin, DAUN = daunorubicin and EPI = epirubicin) for 6 and 24 hours. **B.** Normalised beating rate following 6 and 24 hours exposure to anthracyclines, data points show average of 3 wells ± SE and **C.** Normalised beat amplitude following 6 and 24 hours exposure to anthracyclines, data points show average of 3 wells ± SE. ∗ $p < 0.05$ (treatment groups compared to control). ■ control, ■ 50nM doxorubicin, ■ 50nM daunorubicin, ■ 50nM epirubicin.

4.4 Discussion

The occurrence of cardiac liabilities following anthracycline treatment is well established clinically, particularly doxorubicin induced cardiotoxicity. The challenge addressed in this phase of the study was to utilise the previously characterised *in vitro* models to determine if the structural and functional cardiotoxicity induced by anthracyclines in the clinic can be detected using *in vitro* cardiomyocyte models.

4.4.1 *In vitro* assessment of doxorubicin-induced cardiotoxicity

Doxorubicin is the most frequently used anthracycline and is notoriously associated with cardiotoxicity;[16] hence is considered the archetypal anthracycline for comparison of other anthracyclines. Following 96 hours exposure, the IC_{50} value of doxorubicin in AC10 cardiomyocytes (AC10-CMs) in the exponential growth phase was 14.66 ± 3.31nM. This is considerably less than the C_{Max} of doxorubicin in humans (1.1µM), however is clinically relevant as following administration doxorubicin is quickly cleared from the blood, metabolised by the liver and distributed into tissues, therefore the concentration of active drug that contacts the myocardium will be lower than the C_{Max}.[15] In a study using five cancer cell lines originating from different tissues, the IC_{50} values of doxorubicin ranged from 20 – 420nM,[245] and in the rat H9c2 cardiomyoblast cell line, Chularojmontri *et al*. reported an IC_{50} value of 142nM following 48 hours exposure of the cells to doxorubicin.[246]

Exposure to four clinically relevant concentrations (50nM, 100nM, 250nM and 500nM) of doxorubicin initiated a hypertrophic response in AC10-CMs, which was confirmed using cellular viability studies and imaging. At 48 hours exposure a dose-dependent response was observed in cell index, with 50nM doxorubicin showing the highest cell index and 500nM showing the lowest cell index, this paired with the viability studies conducted at this time point illustrate that the cell index values depict a balance between cell death and hypertrophy. Studies in hiPSC-CMs

using the xCELLigence cardio system showed a similar response to doxorubicin, with immediate increases in cell index occurring following addition of 50nM, 100nM and 250nM doxorubicin, indicating that doxorubicin had also induced hypertrophy in this cell type.

Many groups have reported cardiomyocyte hypertrophy upon doxorubicin addition *in vivo* and *in vitro.* Myocardial biopsies performed in human hearts after doxorubicin treatment revealed an increase in both the size of the cells and the sarcoplasmic reticulum and T-tubules following 24 hours exposure.[247] Studies using the rat H9c2 myoblast cell line also reported doxorubicin induced hypertrophy[248] and morphological alterations, including alterations to fibrous structural proteins, mitochondrial damage and membrane blebbing with associated with changes to cellular shape.[185] The results in this study progress these preliminary findings and have now confirmed this morphological and phenotypic change, in a clinically applicable manner and using novel methodologies permissive of real-time and physiologically relevant analyses.

Despite the activity of hiPSC-CMs being investigated following doxorubicin treatment previously, the main focus was primarily on identifying changes to beat parameters using higher doses of doxorubicin, thus lacking clinical significance. For example, a recent study by Koci *et al*. used a range of doxorubicin concentrations from 0.3µM - 100µM and monitored contractility over 72 hours. Changes in contractility were seen with all concentrations of doxorubicin used by 72 hours, however cell death occurred quickly with all concentrations so hypertrophy would be difficult to ascertain.[249] The use of high doses of doxorubicin caused a rapid loss of cardiomyocytes in the study by Koci *et al*., demonstrated by sharp declines in cell index. The majority of the concentrations of doxorubicin used in the aforementioned study are much higher than the level exposed to the body and lack relevance as the acute cardiotoxicity response to doxorubicin is associated with inflammation rather than a loss of tissue mass. In contrast, the current study used much lower clinically relevant concentrations and found initiation of morphological changes and altered contractility with all doses of doxorubicin applied within 24

hours. At the point when cells showed the greatest degree of hypertrophy (6 hours exposure) following exposure to doxorubicin at 50nM and 100nM no changes in contractility were observed, however in cells treated with 250nM doxorubicin (close to the lowest dose used by Koci *et al*.) a reduction in beat frequency was observed. This illustrates that it is possible to detect changes in the contractility of hiPSC-CMs with low clinically relevant doses of doxorubicin following a much shorter exposure time of 6 hours.

In the same cells following 24 hours exposure to doxorubicin, hiPSC-CMs treated with all doses used in this study exhibited alterations to their contractility. Treatment with 50nM doxorubicin caused decreases in beat frequency and amplitude which were further decreased in cells challenged with 100nM doxorubicin. Interestingly, treatment with 250nM doxorubicin caused a large decrease in beat amplitude paired with a large increase in beat frequency relative to control. As the highest dose used in the study, 250nM doxorubicin was toxic to cells as shown by the decrease in cell index and hence decrease in beat amplitude following 24 hours exposure. The beat frequency of the cells would also be anticipated to decrease (as was the case with the lower doses used), however it increased. This may be due to the toxicity of the drug causing cell death resulting in gaps in the syncytium. A fully formed syncytium is essential for efficient monitoring of contractility using xCELLigence technology, and any disturbances could cause the system to detect 'flutters' of the disrupted syncytium rather than organised cellular contraction.

Nevertheless, the results of the current work have shown that it is possible to detect both hypertrophy and contractile disturbances in human derived cell types using *in vitro* impedance based systems, with cellular changes occurring in response to clinically relevant concentrations of doxorubicin in as little as 6 hours. These changes potentially relate to the acute cardiotoxicity of doxorubicin, which in humans manifests as transient arrhythmias and inflammation[141,142] which may be involved in increasing susceptibility to the more severe chronic form of doxorubicin-induced cardiotoxicity.

4.4.2 Comparative studies using the anthracyclines doxorubicin, daunorubicin and epirubicin

The studies indicative of induction of doxorubicin-induced hypertrophy in AC10-CMs and hiPSC-CMs, led to comparative studies using the anthracyclines doxorubicin, daunorubicin and epirubicin to investigate if this response is specific to doxorubicin or is a ubiquitous effect related to the anthracycline class.

Viability studies conducted using AC10-CMs in the exponential and plateau phases of growth for both 24 and 96 hours continuous exposure showed comparable levels of toxicity. In general, similar chemosensitivity profiles were obtained in both growth phases, with cells in the exponential growth phase being slightly more sensitive to all of the anthracyclines, and increased sensitivity following 96 hours exposure compared to 24 hours exposure only - as evidenced by the IC_{50} values. Owing to the mechanism of action of anthracyclines in cancer cells, which cause disruption of DNA synthesis and replication in proliferating cells, increased toxicity would be expected in cells in the exponential growth phase as the anthracyclines would be able to interfere more readily with DNA replication and topoisomerase II than in cells in the plateau growth phase, as these cells would be in a more quiescent state and therefore have reduced levels of proliferation. Increased duration of exposure would also be expected to increase toxicity as the drugs have more time to induce cellular damage, as was the case with the current study.

As the effects on viability were detectable within 24 hours exposure to anthracyclines, subsequent studies investigating the morphological changes to cells were focused on this timeframe, which also reflects the plasma half-life of the anthracyclines. Taking doxorubicin as an example, the drug undergoes rapid metabolism by the liver and undergoes triphasic elimination with a terminal half-life of approximately 30 hours.[15] This means that its takes approximately 30 hours for 50% of doxorubicin to be eliminated from the body, and a total of 6

half-lives (approximately one week) for one intravenous administration of doxorubicin to be completely eliminated from the body. In this study AC10-CMs were exposed to high (500nM) and low (50nM) clinically relevant concentrations of anthracyclines for 24 hours, as this represents the different stages following clinical administration of anthracyclines, specifically soon after administration and a few days into the elimination process.

Exposure of AC10-CMs to all of the anthracyclines used showed hypertrophy in both the exponential and plateau growth phase which was confirmed using cellular viability studies. These results demonstrate the interplay that exists between cell death and hypertrophy in response to anthracyclines in the exponential growth phase and the influence of proliferative capacity in the plateau growth phase. In the plateau phase of growth addition of 500nM anthracyclines resulted in a higher cell index than 50nM anthracyclines following 24 hours exposure, whereas in exponential growth phase the cells exposed to 500nM anthracyclines had already began to die by this time point, thus demonstrating that cells in the plateau growth phase are less sensitive to anthracycline toxicity in terms of occurrence of cellular death due to their quiescent state, but perhaps are more affected by the damaging effects of the drugs in terms of changes to cellular structure. This illustrates that this growth phase may more accurately model the cardiomyocytes of the human heart.

A similar response was observed in hiPSC-CMs using the xCELLigence cardio system, with immediate and sustained increases in cell index occurring following addition of 50nM of all anthracyclines used, indicating that the anthracyclines also induced hypertrophy in this cell type. As previously discussed, cardiomyocyte hypertrophy in response to doxorubicin has been described using different *in vitro* cardiomyocyte models, however studies using other anthracyclines are scarcer. Until now, the only studies into this area have used animal derived cell lines such as the H9c2 rat cardiomyoblast cell line, where its use identified morphological changes following treatment with daunorubicin.[250] Although effects on morphology were not

assessed, an interesting study by Toldo *et al*. compared the effects of doxorubicin and epirubicin in the HL-1 mouse atrial cell line with respect to reactive oxygen species (ROS) generation, DNA damage and apoptosis. The study found that both anthracyclines exhibited similar toxicity profiles, however reduced toxicity was observed with a liposomal formulation of doxorubicin.[251] The results in this study build on these findings and have now confirmed that morphological changes occur in both doxorubicin and epirubicin treated human derived cardiomyocyte cells at comparable levels using novel methodologies permissive of real-time and physiologically relevant analyses.

As previously discussed, the majority of studies undertaken to date using hiPSC-CMs have utilised higher doses of anthracyclines and focussed on changes to beat parameters. For example, Doherty *et al*. reported that 5µM daunorubicin caused 20% decreases to beat rate and amplitude of hiPSC-CMs which were preceded by increases to ROS, suggesting that the generation of ROS contributes to the early cardiotoxicity of daunorubicin.[208] Studies in isolated rat cardiomyocytes conducted by Chan *et al.* compared contractility following 20 minutes exposure to 10µM doxorubicin and epirubicin and found that all indices of contractility were decreased in equal amounts, and that the antioxidant enzymes superoxide dismutase and catalase afforded protection against these changes to contractility.[252] The exposure time of 20 minutes used in the aforementioned study does not accurately reflect clinical exposure times, therefore the current study has used an increased exposure time of 24 hours and much lower doses to provide a more clinically relevant analysis of the effects of anthracyclines on contractility.

Upon addition of 50nM of the anthracyclines to hiPSC-CMs minimal changes to contractility were seen following 6 hours exposure (when the cells showed the greatest degree of hypertrophy). However following 24 hours exposure, hiPSC-CMs treated with all anthracyclines used in this study exhibited alterations to their contractility. Treatment with 50nM doxorubicin

caused decreases in beat frequency and amplitude which were decreased slightly more in cells challenged with epirubicin and daunorubicin.

4.4.3 Translatability of *in vitro* comparative anthracycline studies

The studies by Toldo *et al*. and Chan *et al*. both compared doxorubicin and epirubicin using *in vitro* cardiomyocyte models and reported no differences between the two anthracyclines with their ability to structurally damage cells and induce contractility changes.[251,252] The work presented herein has confirmed anthracycline induced hypertrophy in AC10-CMs and hiPSC-CMs, both human relevant models, at clinically relevant concentrations and in an *in vitro* model system. However, there was a lack of substantial differences between the degree of hypertrophy observed with any of the anthracyclines, as was also the case with the IC_{50} values that were determined using chemosensitivity studies.

These results are not in line with the current clinical view that epirubicin is less cardiotoxic then doxorubicin.[237] Randomised controlled clinical trials conducted in breast cancer patients comparing epirubicin and doxorubicin at equimolar doses found epirubicin possesses similar oncological efficacy to doxorubicin but is significantly less cardiotoxic as fewer patients developed heart failure on the epirubicin arm of the trials compared to the doxorubicin treated patients. Therefore epirubicin is preferred over doxorubicin as it is currently perceived to possess a more favourable toxicity profile including reduced risk of cardiotoxicity and neutropenia and a lower incidence of nausea and vomiting. The effects of anthracyclines on cardiac function in humans is dependent on many factors in addition to induction of damage to cardiomyocytes, which may explain why little differences have been observed between anthracyclines using *in vitro* cardiomyocyte models. For example, epirubicin has a different pharmacokinetic profile to doxorubicin characterised by altered drug metabolism, a higher clearance rate and a shorter half-life, all of which may contribute to the reduced toxicity of the

drug clinically.[131,237] An *in vitro* study by Ramanathan *et al*. investigated the interaction of doxorubicin and epirubicin with blood components and assessed their binding to erythrocytes, haemoglobin and plasma proteins and found that epirubicin was more able to bind to haemoglobin and therefore sits inside erythrocytes, whereas doxorubicin was less able to bind to haemoglobin and remained on the surface of the erythrocytes. These differences may influence the disposition of the drugs in the bloodstream and affect their cardiotoxic profiles in patients.[253]

Finally, whilst cardiomyocytes are the classic target for anthracycline-induced cardiotoxicity, damage can also occur to the support cells of the myocardium, which is not assessed using *in vitro* cardiomyocyte models such as those utilised in this study. Fibroblasts, constitute 15% of the myocardium, and are crucial for cardiac remodelling and maintenance of the ECM.[53] Kania *et al*. exposed human fibroblast cell lines to the anthracyclines aclarubicin, daunorubicin and idarubicin and reported morphological changes, increases to intracellular calcium levels and activation of caspase-3 which is related to apoptosis.[254] Studies in cardiomyocytes, endothelial cells and fibroblasts isolated from neonatal rat hearts found that fibroblasts and endothelial cells were more sensitive to doxorubicin-induced cardiotoxicity than cardiomyocytes, thus illustrating that adverse effects following anthracycline exposure also in occur in support cells such as fibroblasts and endothelial cells.[255] Due to the crucial role of cardiac endothelial cells, any drug-induced damage would adversely affect cardiac function as the supply of oxygen, nutrients and cellular signalling factors to cardiomyocytes would be compromised. Likewise, fibroblasts have the ability to influence the phenotype of cardiomyocytes, receive and respond to distress signals from neighbouring cardiomyocytes following tissue damage, and therefore potentially play a role in the development of anthracycline induced cardiotoxicity.

4.4.4 Conclusion

In summary, the Induction of hypertrophy that was observed in AC10-CMs and hiPSC-CMs following exposure to anthracyclines demonstrates the detection of structural cardiotoxicity and provides additional data to support the use of these cells on an impedance-based platform in screening assays for detection of structural toxicity. The contractility assessments of hiPSC-CMs suggest that the hypertrophy induced by low-dose (50nM) anthracyclines does not affect the contractility of the cells following 6 hours exposure, however changes became evident following 24 hours exposure, which were more pronounced with higher doses of doxorubicin. These changes potentially relate to the acute cardiotoxicity of doxorubicin, which in humans manifests as transient arrhythmias and inflammation which may be involved in increasing susceptibility to the more severe chronic form of doxorubicin-induced cardiotoxicity. The lack of distinguishability between the severity of toxicity induced by the anthracyclines does not correspond with the toxicity profile displayed in the clinic, however there are many factors that influence the development of anthracycline-induced cardiotoxicity in patients that are not accounted for using *in vitro* cardiomyocyte models.

Chapter 5: *In Vitro* Evaluation of Angiotensin Blockade as a Strategy to Minimise Anthracycline-Induced Cardiotoxicity

5.1 Introduction

Anthracycline-induced cardiotoxicity (AIC) has been classified as the most noted chemotherapy-induced cardiotoxicity to date, and many strategies have been explored for reducing the associated cardiotoxicity such as modification of dosing schedules, the use of liposomal formulations and concurrent administration of cardioprotective therapies.[16,28] The formation of damaging free radicals and oxidative stress are implicated as central mechanisms underlying the cardiotoxic nature of doxorubicin.[91,118] In this context, many experimental drug treatments have been evaluated to ameliorate the toxicity focussed on the use of anti-oxidants and iron chelators such as dexrazoxane.[154,155] Unfortunately due to controversial clinical trial data, the use of dexrazoxane has been contraindicated in paediatric patients,[156] and barriers to the use of anti-oxidants include difficulty achieving constant plasma concentrations coupled with poor uptake by the myocardium in humans.[256]

5.1.1 Clinical studies investigating cardiotherapeutic drugs to mitigate anthracycline-induced cardiotoxicity

The use of clinically-utilised therapeutics focused on the cardiac system have also been evaluated in terms of AIC, such as statins and β-blockers.[152]

Statins, which are used clinically to inhibit cholesterol synthesis and treat ischaemic heart disease possess both anti-inflammatory and anti-oxidative properties. Thought to interfere with

the generation of ROS and inhibition of Topoisomerase IIβ (TopIIβ) associated with AIC, a small randomised controlled trial (RCT) found prophylactic atorvastatin protected patients from declines in LVEF,[157] and a larger RCT called 'Preventing anthracycline cardiovascular toxicity with statins (PREVENT)' is currently underway.[158]

With regards to β-blockers, their negative chronotropic and inotropic properties induce declines in the myocardial consumption of oxygen and nutrients, thus reducing the workload of the heart in patients with cardiovascular diseases. Carvedilol is unique amongst β-blockers as it possess additional vasodilatory and anti-oxidant properties.[74,159] With respect to reduction of AIC, the anti-oxidant properties of carvedilol may be beneficial. Studies comparing the efficacy of carvedilol and atenolol at protecting cultured rat cardiomyocytes from AIC *in vitro* showed that carvedilol was able to decrease the production of damaging free radicals and prevent apoptosis of cardiomyocytes, whereas atenolol was not.[160] This suggests that carvedilol may possess the ability to protect the heart from AIC and as such it has been employed in a number of small studies where its prophylactic effects on AIC have been investigated with encouraging results.[152] The first such study was conducted by Kalay *et al*. who concluded that carvedilol may protect both systolic and diastolic functions of the left ventricle in patients undergoing anthracycline therapy.[161]

5.1.1.1 Clinical studies investigating angiotensin blockade for cardioprotection against anthracycline-induced cardiotoxicity

There is a growing body of evidence that administration of angiotensin converting enzyme inhibitors (ACEi) or angiotensin receptor blockers (ARB) can protect the heart from the damaging effects of anthracyclines.[28,152] ACEi and ARB are routinely used in the management of congestive heart failure (CHF) and hypertension.[162,163] Both prevent the physiological activity of angiotensin II; ACEi prevent the formation of angiotensin II and therefore decrease circulating levels, whereas ARB stop angiotensin II binding to the angiotensin type I receptor (ATR1). Angiotensin

II is the principal effector of the renin–angiotensin system (RAS), which plays a crucial role in the pathogenesis of several cardiovascular events including vasoconstriction, cardiac hypertrophy and cardiac remodelling.[75,76] The mechanism and clinical use of these agents is addressed in section 1.4.5.2.

As previously described, AIC manifests primarily as heart failure and cardiac remodelling (section 1.7.1.2.1), factors which also show a physiological relationship to activity of the angiotensin signalling pathway. Consequently, it was hypothesised that perturbation of this pathway may be a viable strategy for treatment of AIC. Several studies have now been conducted to evaluate this potential therapeutic intervention. Prophylactic use of the ACEi enalapril has been shown in several studies to produce positive results against mitigation of AIC, mainly in the area of preventing declines in left ventricular function.[150,164,165] Similarly, studies investigating the use of ARB such as valsartan, telmisartan and candesartan have also yielded similar positive results, including alleviations to decline of left ventricular function, prevention of acute transient rhythm abnormalities and decreases in the levels of damaging ROS.[166–168] The outcomes of these studies are summarised in section 1.7.2.1 (table 1.2).

Although findings of these studies was primarily positive overall, they are not without limitations which include short follow up time of patients (ranging from 1 week – 1 year) and the low number of patients enrolled. Larger phase II and phase III clinical studies are currently underway that aim to assess the cardioprotective potential of ACEi/β-blocker combinations (SAFE clinical trial)[170] and ACEi alone (PROACT Trial – Newcastle University)[171] in breast cancer patients receiving anthracycline treatment. These clinical trials will hopefully support the findings of the smaller studies and provide additional information regarding the optimal cardioprotective strategies and monitoring schedules for detection of sub-clinical damage.

In addition to prophylactic or preventative use of ACEi and ARB against AIC, the potential for reversal of established AIC using ACEi has also been investigated in long-term survivors of

childhood cancer, where only transient benefits were reported.[172] This exemplifies the permanent nature of damage caused by anthracyclines and supports the current view that concomitant angiotensin blockade alongside anthracycline treatment is the most effective way to use these agents as cardioprotectors.

5.1.2 Pre-clinical *in vivo* studies investigating angiotensin blockade for cardioprotection

Further to the encouraging results clinically with ACEi and ARB against AIC, a considerable number of studies have also been investigated with these agents against AIC *in vivo* have also been undertaken, to ascertain optimal therapeutic strategies and provide mechanistic information. In mice, the ARB candesartan showed a cardioprotective effect against daunorubicin, reversing deteriorations to left ventricular function and myocardial pathological changes.[257] A study investigating telmisartan against doxorubicin-induced cardiotoxicity in rats showed histological disruption of cardiac tissues in the doxorubicin treated group which was reduced with telmisartan treatment.[258] Furthermore, telmisartan treatment decreased lipid peroxidation in cardiac tissue and elicited a significant decrease in the activities of the antioxidant enzyme catalase in comparison with the doxorubicin treated group.[258] However, some of these effects are likely to be a consequence of telmisartan also being a partial peroxisome proliferator activated receptor-γ (PPARγ) agonist, as such telmisartan possesses additional anti-inflammatory and antioxidant properties.[259] More recently, a study involving the novel ARB fimasartan also reported similar positive cardioprotection against AIC, and additionally made a distinction between high and low dose fimasartan which improved survival rates accordingly with 100% and 75% survival rates respectively, compared to 50% survival in rats treated with doxorubicin only.[260] Echocardiography showed preserved left ventricular

function in the high fimasartan group and that cardiac remodelling was attenuated in both the low and high fimasartan groups compared to the doxorubicin only treated rats.[260]

Similar to studies with ARB, treatment using ACEi have also generated positive results in pre-clinical studies. For example, treatment with the ACEi captopril and enalapril before doxorubicin administration was found to decrease the level of lipid peroxidation compared to the doxorubicin only treatment group, and also prevented decreases in superoxide dismutase 2 (SOD2) that occurred in the doxorubicin only treated rats.[261] A more recent study evaluated the mitochondrial function of rats treated with enalapril and doxorubicin, in addition to changes in cardiac contractility and generation of ROS. In this study, rats pre-treated with enalapril were protected from losses in left ventricular contractility and increases in ROS formation compared to rats treated with doxorubicin only, and were also protected from decreases in mitochondrial function associated with doxorubicin treatment.[262]

A comparison between the ability of the ACEi captopril and the ARB telmisartan to improve cardiac outcomes in doxorubicin treated rats showed co-administration of telmisartan and captopril equally ameliorated the cardiotoxic effects of doxorubicin on all parameters measured, suggesting that both drug types provide equivalent protection against doxorubicin induced cardiotoxicity, thus implying that angiotensin II signalling plays a role in the development of doxorubicin induced cardiotoxicity.[263]

5.1.3 Aims and objectives

Despite mitigation of anthracycline-induced cardiotoxicity being demonstrated by ACEi and ARB both pre-clinically *in vivo* and clinically, the direct effects upon, and involvement of the cardiac system, as well as the molecular mechanism involved have yet to be resolved. The aim of this stage of the project is to address these issues and determine if the previously discussed structural and functional cardiotoxicity induced by anthracyclines can be mitigated by the addition of ACEi and ARB using *in vitro* cardiomyocyte models.

Specifically:

i) The mitigation of AIC with therapeutics that limit angiotensin signalling suggests a role for the angiotensin signalling pathway in mediating this toxicity; therefore initially the sensitivity of AC10 cardiomyocytes (AC10-CMs) to doxorubicin alone and in the presence of angiotensin II will be evaluated, followed by investigations into morphological changes to these cells and changes to the morphology and contractility of hiPSC-derived cardiomyocytes (hiPSC-CMs) following simultaneous treatment with doxorubicin and angiotensin II.

ii) This will then be expanded to investigate the differential effects on viability of AC10-CMs following treatment with doxorubicin alone and in combination with angiotensin targeting drugs. Morphological changes to AC10-CMs and changes to the morphology and contractility of hiPSC-CMs following simultaneous treatment with doxorubicin and ACEi/ARB will then be assessed to determine the impact of ACEi and ARB on mitigating the structural and functional changes associated with doxorubicin treatment.

iii) Where applicable, the differential effects on viability of H460 lung cancer cells will be determined following treatment with doxorubicin alone and in combination with ARB and/or ACEi.

5.2 Materials and methods

5.2.1 Determination of viability of proliferating AC10-CMs in response to different drug treatment protocols using the MTT assay

The MTT assay (previously detailed in section 2.2) was used to determine the cytotoxic sensitivity of AC10-CMs to a combination of doxorubicin and angiotensin II, and also to investigate the effects on viability of the test drugs (enalapril, enalaprilat, telmisartan and losartan) alone and in combination with doxorubicin in AC10-CMs. Similar experiments involving doxorubicin and telmisartan/losartan were also conducted in H460 lung cancer cells.

5.2.1.1 Evaluation of viability of AC10-CMs following treatment with doxorubicin and angiotensin II

Briefly, AC10-CMs were seeded into 96-well plates as previously described in section 2.2. Cells were dosed over three days as follows: Day 1 - Angiotensin II (150pM – 500pM) was added to cells; day 2 – Angiotensin II was added in addition to 50nM doxorubicin, alongside a doxorubicin only treatment group (absence of angiotensin II); day 3 – doxorubicin was removed and angiotensin II was added as per day 1 (doxorubicin only treated cells received medium only). Experiments were terminated following 96 hours from the point of first angiotensin II addition and the MTT assay conducted as described in section 2.2. All experiments were performed in triplicate.

5.2.1.2 Investigations into viability of AC10-CMs following treatment with drugs targeting the angiotensin pathway

AC10-CMs were seeded into 96-well plates as previously described in section 2.2. The following day cells were exposed to the ACEi enalapril and enalaprilat or the ARBs telmisartan and losartan, with a 1:2 serial dilution in drug concentration performed across the plate, resulting in

final concentrations ranging from 10µM to 78nM. Drug exposures were repeated on a daily basis and cell viability ascertained at 96 hours by MTT assay, as described in section 2.2. All experiments were performed in triplicate.

5.2.1.3 Investigations into viability of AC10-CMs following combination treatment with angiotensin targeting drugs and doxorubicin

AC10-CMs were seeded into 96-well plates as previously described in section 2.2. The following day cells were exposed to enalapril (1µM/10µM), enalaprilat (1µM/10µM), telmisartan (1µM/5µM) and losartan (1µM/5µM) - One plate per drug, half plate for each concentration, one plate containing medium only. Following 24 hours exposure, a 1:5 serial dilution of doxorubicin was applied to all plates resulting in final concentrations of 5µM – 0.32nM. The cells un-exposed to test drugs were exposed to doxorubicin only, whereas the test drugs were added to the previously pre-treated cells. Following 24 hours exposure to doxorubicin, drug dilutions were removed and replaced with either medium (doxorubicin only treated cells), or appropriate test drugs. Cell viability was determined at 96 hours exposure from the first test drug addition as described in section 2.2. All experiments were performed in triplicate and IC_{50} values were determined by implementing curve fitting by non-linear regression on GraphPad Prism (Version 7.04, GraphPad Software, Inc.). Statistical analysis of IC_{50} values was conducted using a one way analysis of variance (ANOVA) test, and a post-hoc Dunnett's test when required using GraphPad Prism (Version 7.04, GraphPad Software, Inc.).

5.2.1.4 Investigations into viability of H460 lung cancer cells following combination treatment with telmisartan/losartan and doxorubicin

H460 lung cancer cells were seeded into 96-well plates as previously described in section 2.2. The following day cells were exposed to telmisartan (1µM/5µM) and losartan (1µM/5µM) - One plate per drug, half plate for each concentration, and one plate containing medium only.

Following 24 hours exposure, a 1:5 serial dilution of doxorubicin was applied to all plates resulting in final concentrations of 5µM – 0.32nM. The cells un-exposed to test drugs were exposed to doxorubicin only, whereas the test drugs were added to the previously pre-treated cells. Following 24 hours exposure to doxorubicin, drug dilutions were removed and replaced with either medium (doxorubicin only treated cells) or appropriate test drugs. Cell viability was determined at 96 hours exposure from the first test drug addition as described in section 2.2. All experiments were performed in triplicate, and IC_{50} values were determined by implementing curve fitting by non-linear regression on GraphPad Prism (Version 7.04, GraphPad Software, Inc.). Statistical analysis of IC_{50} values was conducted using a one way analysis of variance (ANOVA) test, and a post-hoc Dunnett's test when required using GraphPad Prism (Version 7.04, GraphPad Software, Inc.).

5.2.2 Determination of morphological changes to proliferating AC10-CMs in response to different drug treatment protocols using the xCELLigence real-time cell analyser

The xCELLigence real-time cell analyser (RTCA) was used to investigate the effects a combination of doxorubicin and angiotensin II on the morphology of AC10-CMs, and also to assess the effects of telmisartan and losartan alone and in combination with doxorubicin on the morphology of AC10-CMs. The protocol followed for use of the xCELLigence RTCA is detailed in section 2.3.

5.2.2.1 Investigations into morphology of AC10-CMs following combination treatment with doxorubicin and angiotensin II

Experiments were set up as described in section 2.3. Cells were dosed over three days as follows: Day 1 – 200pM angiotensin II/50nM doxorubicin and 50nM doxorubicin alone was added to cells; day 2 and day 3 –200pM angiotensin II was added to the cells previously treated with

doxorubicin/angiotensin II and medium added to the cells treated with doxorubicin only. All experiments were performed in triplicate and statistical analysis on normalised cell index values was performed between treatment groups using a paired T-test on GraphPad Prism (Version 7.04, GraphPad Software, Inc.).

5.2.2.1.1 Evaluation of viability of AC10-CMs following treatment with doxorubicin and angiotensin II at specific time points determined using the MTT assay

Separate experiments were performed to complement data obtained from the xCELLigence RTCA at both 24 hours and 48 hours exposure times. Cells were plated for exponential studies and dosed as follows: For 24 hours exposure – 200pM angiotensin/50nM doxorubicin and 50nM doxorubicin alone was added to cells and viability determined following 24 hours exposure; for 48 hours exposure – angiotensin II and doxorubicin were added as above, following 24 hours exposure 200pM angiotensin II was added to the doxorubicin/angiotensin II treated cells and medium was added to the cells exposed to doxorubicin only. Following 48 hours exposure, cell viability was determined as described in section 2.2. All experiments were performed in triplicate.

5.2.2.2 Investigations into morphology of AC10-CMs following treatment with telmisartan and losartan

Experiments were set up as described in section 2.3. Cells were exposed to telmisartan (1µM/5µM) and losartan (1µM/5µM) the following day which was repeatedly added every 24 hours until termination of the experiment. All experiments were performed in triplicate.

5.2.2.3 Investigations into morphology of AC10-CMs following combination treatment with telmisartan/losartan and doxorubicin

Experiments were set up as described in section 2.3. Cells were dosed over three days as follows: Day 1 – Cells were exposed to telmisartan (1µM/5µM) or losartan (1µM/5µM); day 2 – 50nM doxorubicin was added to the pre-treated cells and to previously untreated cells, telmisartan (1µM/5µM) or losartan (1µM/5µM) was added to the previously pre-treated cells; day 3 – Telmisartan (1µM/5µM) or losartan (1µM/5µM) was added to the previously pre-treated cells and medium added to the cells treated with doxorubicin only. All experiments were performed in triplicate and statistical analysis on normalised cell index values was performed using a one way analysis of variance (ANOVA) test, and a post-hoc Dunnett's test when required using GraphPad Prism (Version 7.04, GraphPad Software, Inc.).

5.2.3 Evaluation of contractility and morphology of hiPSC-CMs following exposure to different treatment protocols using the xCELLigence cardio system

The xCELLigence cardio system was used to analyse changes in morphology and contractility of hiPSC-derived cardiomyocytes (hiPSC-CMs) following addition of a combination of 50nM doxorubicin and 200pM angiotensin II, and to assess the effects of telmisartan and losartan alone and in combination with 50nM doxorubicin on the morphology and contractility of hiPSC-CMs. hiPSC-CM cells were plated into a cardio e-plate at a density of 30,000cells/well, in wells pre-coated with fibronectin (described in section 2.4). Once stable beating was detected, half the media (90µl) was removed from each well and replaced with media containing twice the required drug concentration. Final concentrations are as follows: doxorubicin - 50nM; telmisartan - 1µM; losartan - 1µM and angiotensin II – 200pM. The treatment protocol included 24 hours pre-treatment with losartan, telmisartan and angiotensin II, followed by 24 hours exposure to the same pre-treatment compound plus 50nM doxorubicin. Changes to the cell

index and contractility following drug addition were analysed at various points throughout 24 hours exposure to the doxorubicin. Following the treatment protocols drugs were washed out using the four step medium change method (see section 2.4.2) and cells were re-challenged with the same treatment protocol 96 hours later. The protocol followed for use of the xCELLigence RTCA can be found in section 2.4.

Statistical analysis on normalised cell index, normalised beat rate and normalised beat amplitude were conducted between treatment groups using a paired T-test. When more than two groups were compared a one way analysis of variance (ANOVA) test was performed, followed by a post-hoc Dunnett's test when required. Statistical analysis was performed using GraphPad Prism (Version 7.04, GraphPad Software, Inc.).

5.3 Results

The objective of this stage of the project was to utilise the previously reported *in vitro* cardiomyocyte models to determine if the structural and functional cardiotoxicity induced by anthracyclines can be mitigated by the addition of angiotensin converting enzyme inhibitors (ACEi) and angiotensin receptor blockers (ARB), and evaluate the direct involvement of cardiomyocytes, and subsequently elucidate the direct relationship between the angiotensin signalling pathway and mitigation of anthracycline-induced cardiotoxicity (AIC).

5.3.1 Angiotensin II does not alter the sensitivity of AC10 cardiomyocytes to doxorubicin

Initially the sensitivity of AC10 cardiomyocytes (AC10-CMs) to doxorubicin alone and in the presence of angiotensin II was evaluated using MTT assay. This study has shown previously that angiotensin II had no effect on the viability of AC10-CMs at clinically relevant concentrations (Section 3.3.4); here a range of concentrations of angiotensin II were added to a subclinical dose (50nM) of doxorubicin to assess if angiotensin II alters the sensitivity of the cells to doxorubicin. Figure 5.1 shows that simultaneous exposure of 150pM – 500pM angiotensin II with 50nM doxorubicin did not affect the sensitivity of cells as compared to cells treated with doxorubicin only.

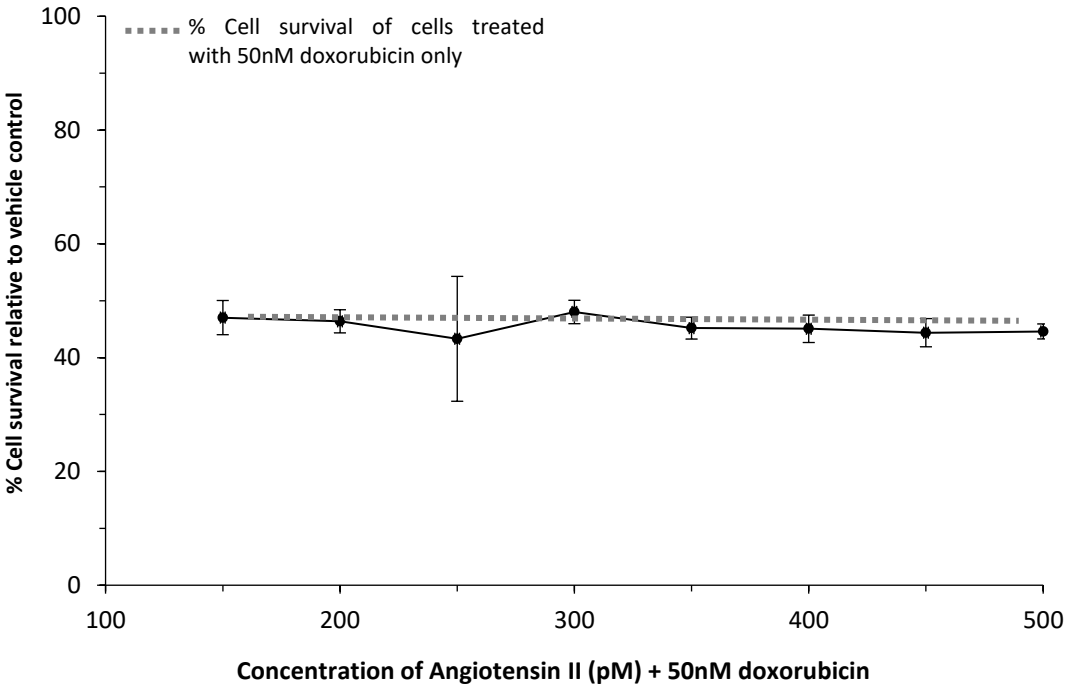

Figure 5.1 Angiotensin II does not alter the sensitivity of AC10 cardiomyocytes to doxorubicin

Dose response curve showing the effect of a combination of 150pM – 500pM angiotensin II and 50nM doxorubicin on cell viability following 96 hour exposure, expressed as % cell survival relative to vehicle control. The dashed line represents the % cell survival of AC10-CMs treated with 50nM doxorubicin only, data is representative of n=3 ± SE.

5.3.2 Angiotensin II does not affect the morphology of AC10 cardiomyocytes exposed to doxorubicin

Previous studies have confirmed the ability of the AC10 *in vitro* model to detect angiotensin II induced hypertrophy (section 3.3.4.1) and the induction of cellular hypertrophy as a response to doxorubicin exposure (section 4.3.1.1). The effect of combination of angiotensin II and doxorubicin upon cellular morphology and behaviour were thereby monitored in real-time using the xCELLigence RTCA. Cells in exponential growth phase were exposed to angiotensin II for a total of 72 hours, within which cells were exposed to doxorubicin for 24 hours. Figure 5.2A shows that when normalised to the point of doxorubicin addition, cell index increased higher than the level of control in cells in both treatment groups, with very little difference observed in the cell index of both treatment groups throughout the experiment (Figure 5.2B). To ascertain if the changes to cell index were accompanied by changes to cell number, MTT assays were simultaneously performed – AC10-CMs exposed to doxorubicin only and doxorubicin plus angiotensin II in an identical manner, showed no difference in viability following 24 hours and 48 hours exposure (figure 5.2C), indicating that the addition of angiotensin II to doxorubicin treated cells did not induce further morphological changes or effects upon cellular viability.

Although not shown below in figure 5.2, previous studies have confirmed the ability of the AC10 *in vitro* model to detect Angiotensin II induced hypertrophy (section 3.3.4.1).

5.2A

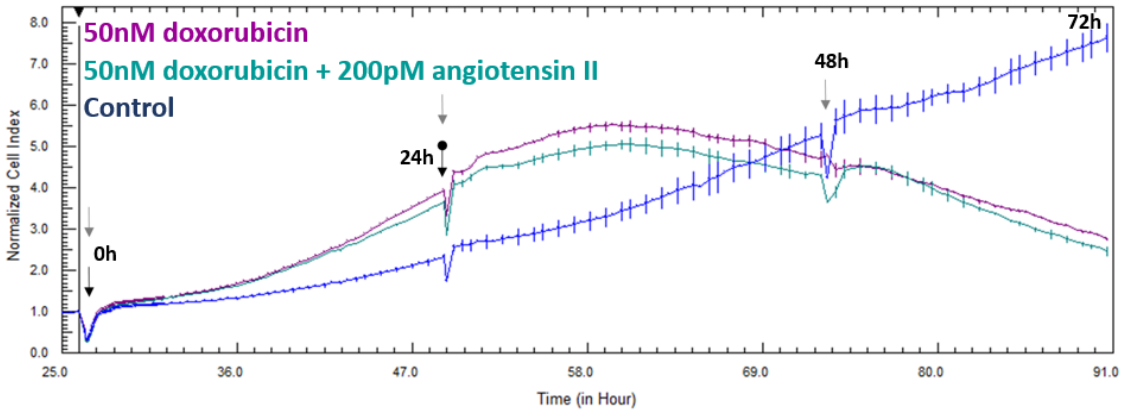

5.2B

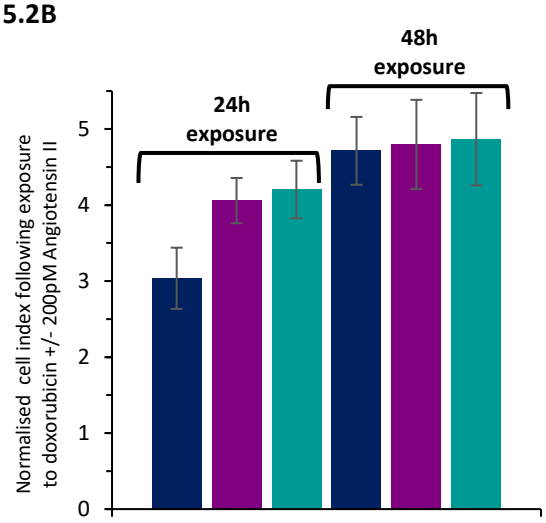

5.2C

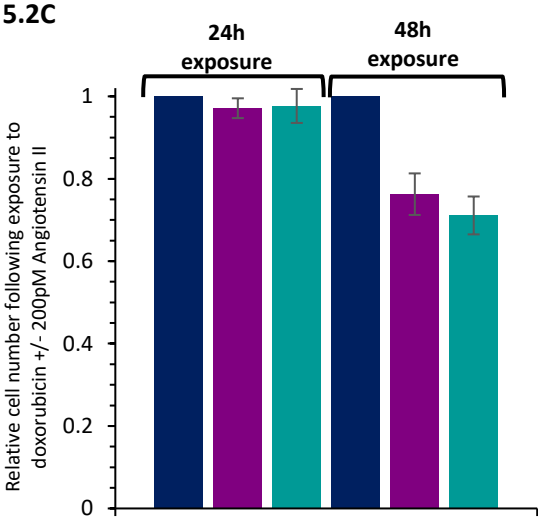

Figure 5.2 Angiotensin II does not affect the morphology of AC10 cardiomyocytes exposed to doxorubicin

A. xCELLigence trace showing time (hours) vs normalised cell index of AC10-CMs exposed to doxorubicin and angiotensin II with points of angiotensin II addition (grey arrows), doxorubicin addition (black arrow), doxorubicin removal (round headed arrow) and exposure time indicated, data representative of n=3, data points shown are average ± SD. **B.** Normalised cell index following 24h and 48h exposure, data is n=3 ± SE. **C**. Relative cell number following 24h and 48h exposure measured by MTT assay, data is n=3 ± SE. ■ control, ■ 50nM doxorubicin, ■ 50nM doxorubicin + angiotensin II.

5.3.3 Effect of a combination of angiotensin II and doxorubicin on morphology and contractility of hiPSC-derived cardiomyocytes

The previous studies had shown angiotensin II and doxorubicin both individually induced morphological and contractile changes of hiPSC-CMs (section 3.3.4.2 and 4.3.1.2). The xCELLigence cardio system was therefore used to assess whether combination of these two agents would result in further effects upon morphology and contractility of hiPSC-CMs.

Stably beating Cor.4U cells were exposed to angiotensin II and doxorubicin for 24 hours and the effects on cell behaviour were monitored in real-time. As shown in figure 5.3A, when normalised to the point of doxorubicin addition, cell index increased higher than the level of control in cells exposed to 50nM doxorubicin alone and in combination with 200pM angiotensin II, with cells treated with doxorubicin only showing a greater increase in cell index. The greatest difference in cell index was approximately 6 hours after angiotensin II and doxorubicin were added (figure 5.3B), indicating induction of morphology changes to the cells, however the cells were not imaged as E-plates have a metal base which does not allow for visualisation of the monolayer.

Assessment of the effect of angiotensin II and doxorubicin on contractility of hiPSC-CMs was evaluated after 6 hours and 24 hours exposure to these agents, as these time-points represent the highest degree of hypertrophy observed and maximum exposure time. The representative traces of contractility shown for control and cells treated with doxorubicin +/- angiotensin II in figure 5.4A show no visible changes in contractility between the two treatment groups following 6 hours exposure, however following 24 hours exposure, decreases in beat amplitude can be seen with angiotensin II addition. Detailed analysis of beat rate and amplitude is shown in figures 5.4B and 5.4C respectively.

5.3A

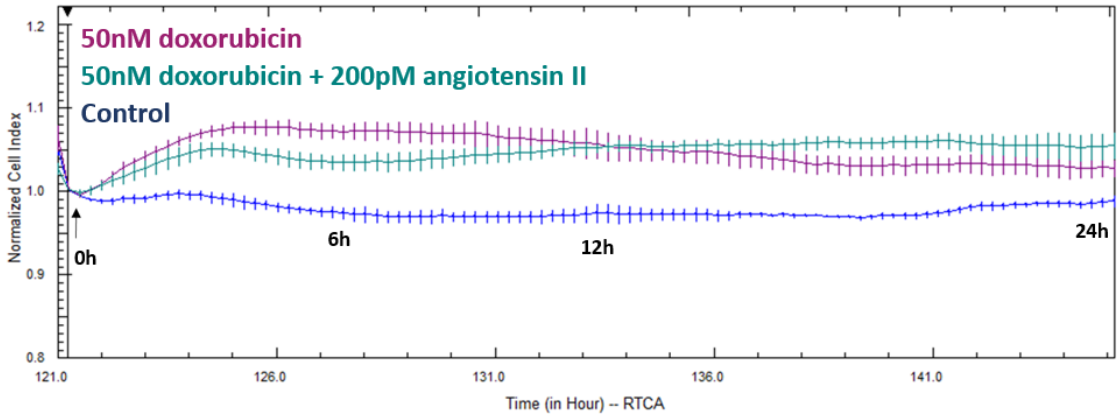

5.3B

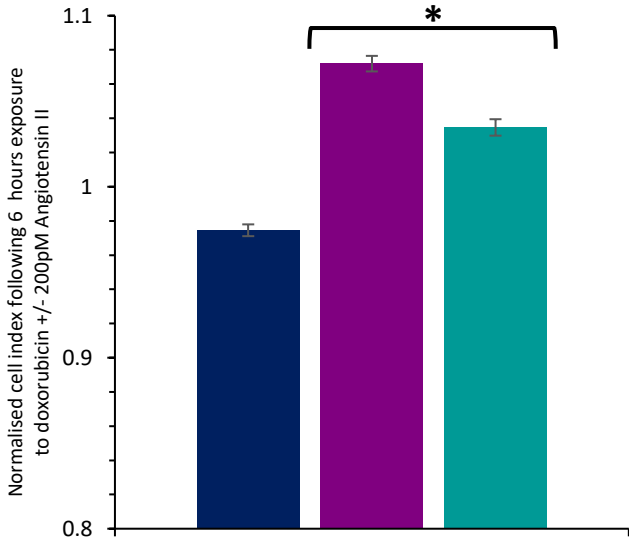

Figure 5.3 Effect of doxorubicin and angiotensin II on morphology of hiPSC-derived cardiomyocytes

A. xCELLigence trace showing time (hours) vs normalised cell index of hiPSC-CMs exposed to doxorubicin +/- angiotensin II with point of addition (arrow) and exposure time indicated, data points shown are average ± SD. **B.** Normalised cell index following 6 hours exposure to doxorubicin +/- angiotensin II**,** data points show average of 3 wells ± SE. ∗ p< 0.05 (comparison between treatment groups). ■ control, ■ 50nM doxorubicin, ■ 50nM doxorubicin + angiotensin II.

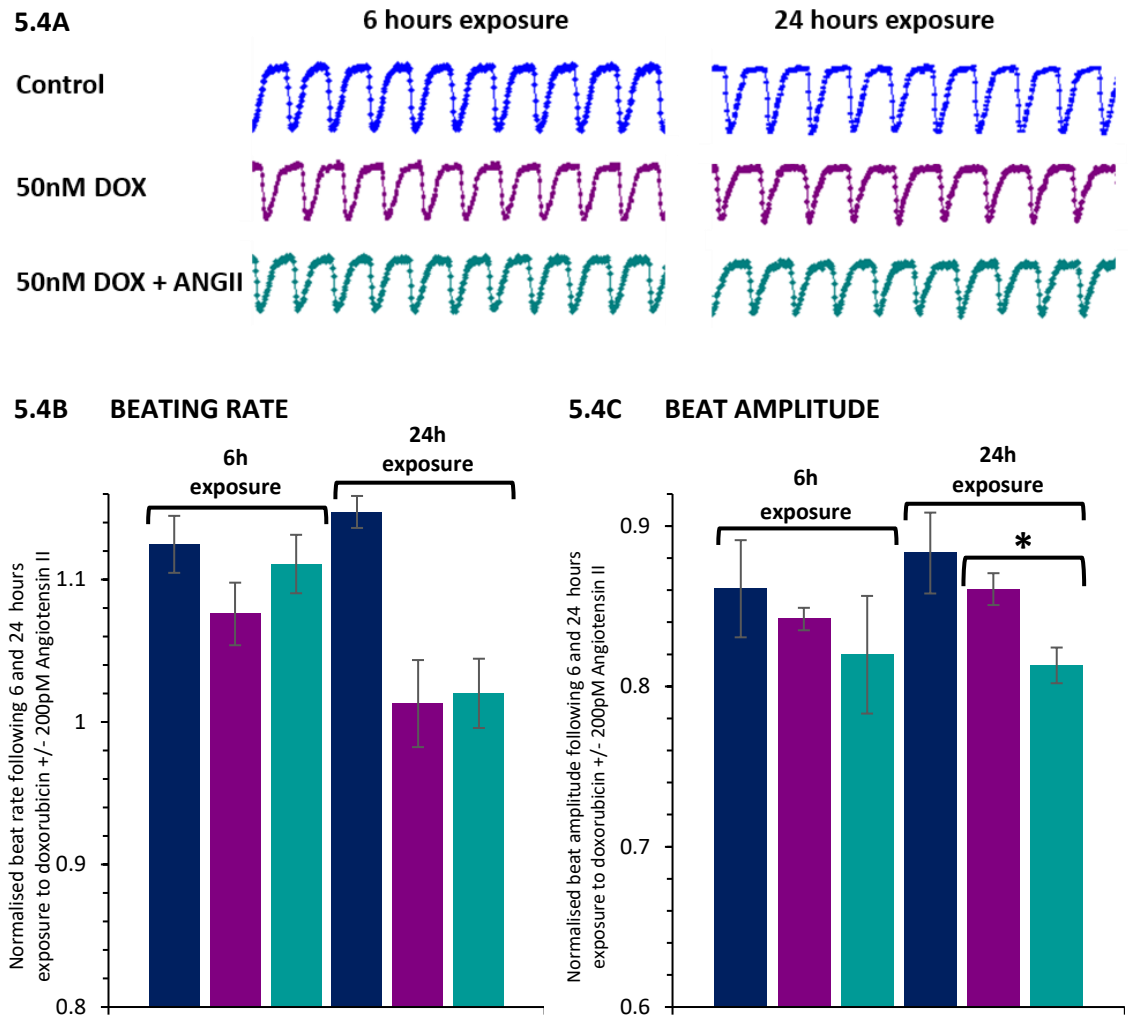

Figure 5.4 Effect of a combination of doxorubicin and angiotensin II exposure on contractility of hiPSC-derived cardiomyocytes

A. Representative traces showing contractility of control cells and cells exposed to doxorubicin (DOX) +/- 200pM angiotensin II (ANGII) for 6 and 24 hours, **B.** Normalised beating rate following 6 and 24 hours exposure to doxorubicin +/- 200pM angiotensin II, data points show average of 3 wells ± SE and **C.** Normalised beat amplitude following 6 and 24 hours exposure to doxorubicin +/- 200pM angiotensin II, data points show average of 3 wells ± SE. ∗ p< 0.001 (comparison between treatment groups). ■ control, ■ 50nM doxorubicin, ■ 50nM doxorubicin + angiotensin II.

5.3.4 Cytotoxicity of angiotensin receptor blockers and angiotensin converting enzyme inhibitors against AC10 cardiomyocytes

The sensitivity of AC10-CMs in the exponential growth phase to both ARB (telmisartan and losartan) and the ACEi enalapril and its active form enalaprilat were evaluated using MTT assay. Figure 5.5 shows that exposure to concentrations of the test drugs ranging from 10µM to 78nM for 96 hours did not significantly affect viability of AC10-CMs, with the exception of the highest dose used of the ARB telmisartan and losartan. The C_{Max} values of the test drugs are approximately 265nM, 86nM, 330nM and 685nM for enalapril, enalaprilat, telmisartan and losartan respectively[264] (indicated on the figure). For future experiments investigating the effects of the test drugs on viability of AC10-CMs exposed to doxorubicin, concentrations of 1µM/10µM were used for enalapril and enalaprilat and concentrations of 1µM/5µM were used for telmisartan and losartan as these concentrations are greater than the C_{Max} and therefore should allow complete blockade of the targets whilst not causing toxicity to the cells.

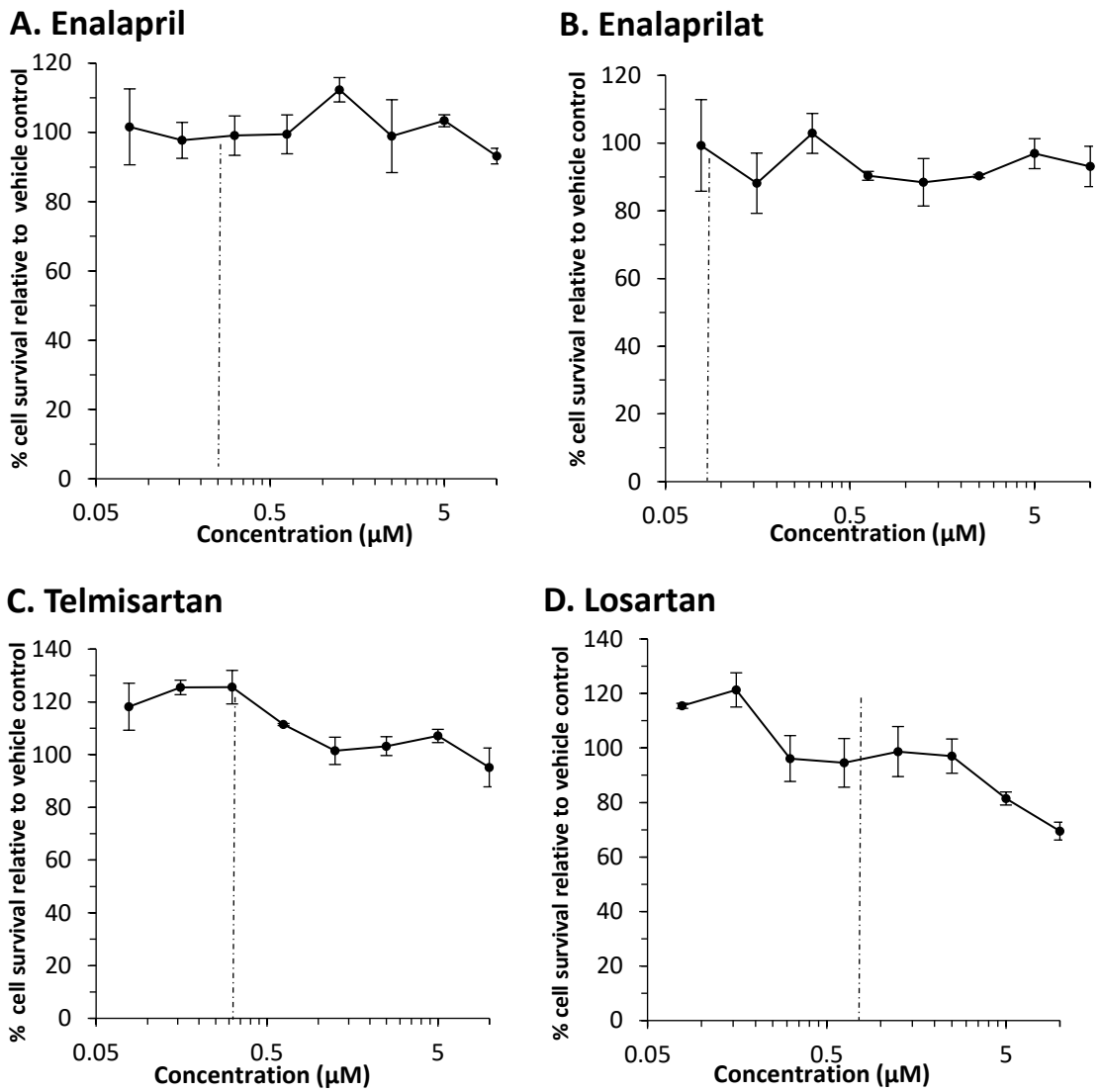

Figure 5.5 Cytotoxicity of angiotensin receptor blockers and angiotensin converting enzyme inhibitors against AC10 cardiomyocytes

Dose response curves showing the effects on cell viability following 96 hour exposure to 10µM – 78nM of **A.** Enalapril, **B.** Enalaprilat, **C.** Telmisartan and **D.** Losartan. Results are expressed as % cell survival relative to vehicle control. The dashed line represents the C_{Max} of the drugs, data is representative of n=3 ± SE.

5.3.5 Angiotensin receptor blockade increases the viability of AC10 cardiomyocytes treated with doxorubicin

The MTT assay was used to investigate the effect of the angiotensin targeting drugs on viability of AC10-CMs in the exponential growth phase treated with a serial dilution of doxorubicin for 96 hours. Figure 5.6 shows that exposure to both enalapril and enalaprilat at 1µM and 10µM did not affect the sensitivity of the cells to doxorubicin (5.6A and B), whereas exposure to the ARBs telmisartan and losartan at 1µM and 5µM did affect the sensitivity of the cells to doxorubicin, as the dose response curves for these treatment groups were shifted to the right of the doxorubicin only curve. This is shown by the higher IC_{50} values compared to doxorubicin only treated cells in table 5.1

5.3.6 Angiotensin receptor blockade does not decrease the therapeutic efficacy of doxorubicin in H460 lung cancer cells

As the ARBs telmisartan and losartan were found to increase the viability of AC10-CMs treated with doxorubicin, a parallel experiment was conducted to assess the effect of these drug combinations on H460 non-small cell lung cancer cells to ensure that concomitant ARB treatment would not reduce the therapeutic efficiency of doxorubicin. Figure 5.7 shows that exposure to both telmisartan and losartan at 1µM and 5µM did not decrease the therapeutic efficacy of doxorubicin in H460 cells, and treatment with 1µM and 5µM telmisartan increased the sensitivity of the cells to doxorubicin. The IC_{50} values for all treatment groups are shown in table 5.1.

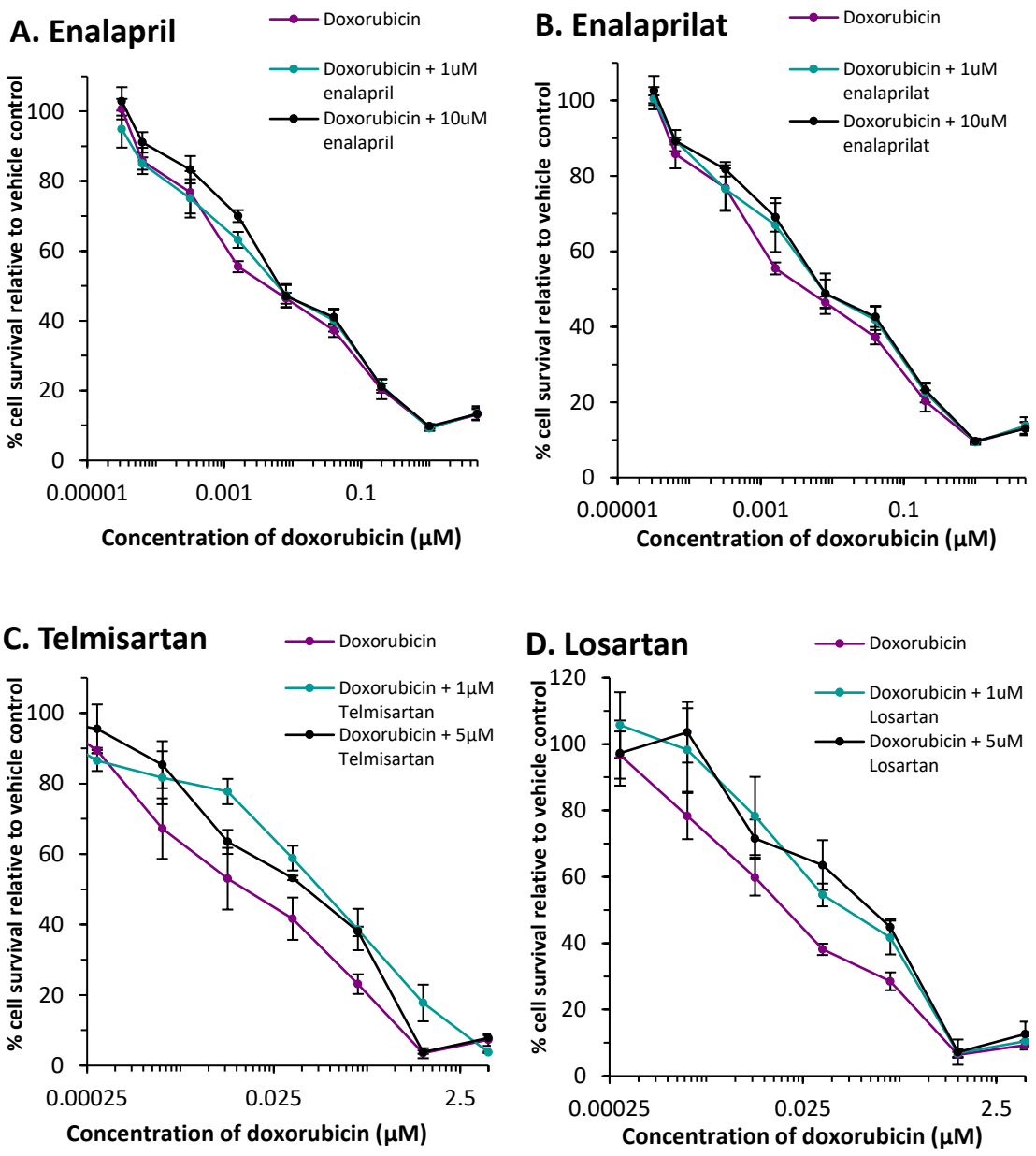

Figure 5.6 The effect of a combination of angiotensin targeting drugs and doxorubicin on viability of AC10 cardiomyocytes

Dose response curves showing the effect on cell viability following 96 hour exposure to 5µM – 32pM doxorubicin alone and in combination with **A.** Enalapril, **B.** Enalaprilat, **C.** Telmisartan and **D.** Losartan. Results are expressed as % cell survival relative to vehicle control, data is representative of n=3 ± SE.

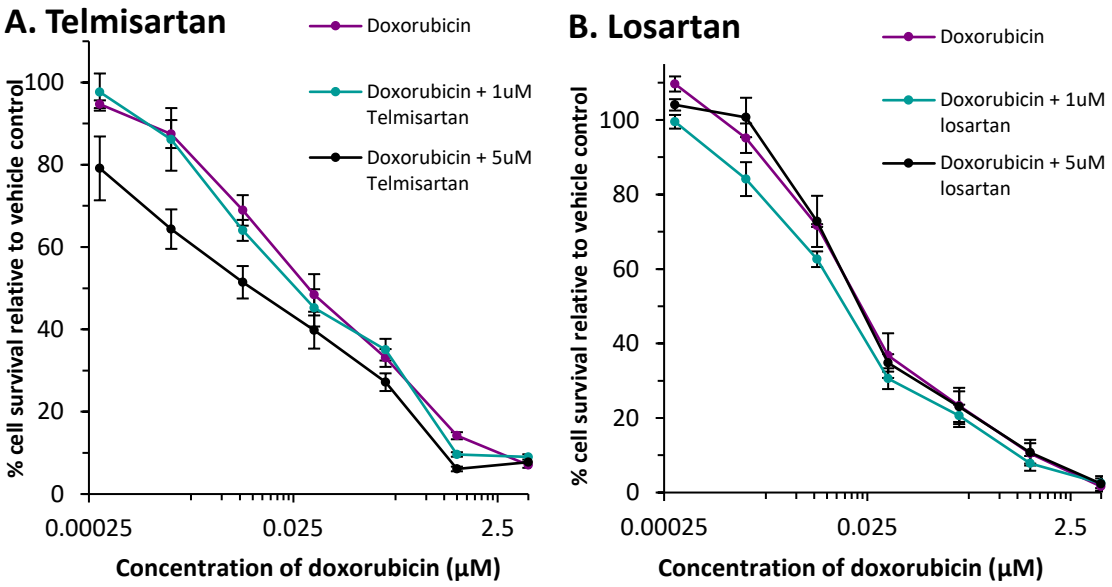

Figure 5.7 **Angiotensin receptor blockade does not decrease the therapeutic efficacy of doxorubicin in H460 lung cancer cells**

Dose response curves showing H460 cell viability following 96 hour exposure to 5µM – 0.32nM doxorubicin alone and in combination with **A.** Telmisartan and **B.** Losartan. Results are expressed as % cell survival relative to vehicle control, data is representative of n=3 ± SE.

	IC_{50} (nM)	
	AC10 Cardiomyocytes	**H460 Lung cancer cell line**
Doxorubicin	14.66 ± 3.31	21.33 ± 1.78
Doxorubicin + 1µM Losartan	65.67 ± 18.92	15.66 ± 1.78
Doxorubicin + 5µM Losartan	71.33 ± 27.44	19 ± 1.69
Doxorubicin	14.66 ± 3.31	40.66 ± 13.81
Doxorubicin + 1µM Telmisartan	96.67 ± 27.32	23 ± 4.96
Doxorubicin + 5µM Telmisartan	90 ± 30.03	10.66 ± 2.76

Table 5.1 **IC_{50} values of AC10 cardiomyocytes and H460 lung cancer cells treated with doxorubicin alone and in combination with 1µM/5µM telmisartan and losartan for 96 hours, data is representative of n=3 ± SE.**

5.3.7 Angiotensin receptor blockade reduces morphology changes induced by doxorubicin in AC10 cardiomyocytes

Following the viability studies that showed angiotensin blockade increased the survival of AC10-CMs treated with doxorubicin, but did not affect the therapeutic efficacy of doxorubicin in lung cancer cells**,** doxorubicin and the ARB telmisartan were combined and the effects on morphology and behaviour of AC10-CMs were monitored in real-time using the xCELLigence RTCA. Cells in exponential growth phase were exposed to telmisartan for a total of 96 hours, within which cells were exposed to doxorubicin for 24 hours. Figure 5.8A shows that when normalised to the point of doxorubicin addition, cell index increased higher than the level of control in cells in both treatment groups, however cells treated with doxorubicin and telmisartan showed reduced cell index compared to doxorubicin alone from 48 to 96 hours (Figure 5.8B). Paired with the dose response curves shown above in figure 5.6C where AC10-CMs treated in an identical manner had improved viability with concurrent angiotensin blockade (summarised in figure 5.8C), this suggests that angiotensin blockade concurrent to doxorubicin treatment improves viability of AC10-CMs and reduces hypertrophy. Telmisartan alone was also added to AC10-CMs for 72 hours and had no effect on the cell index when normalised to the point of first telmisartan addition, as the readings obtained were similar to that of control (inset - figure 5.8A).

5.8A

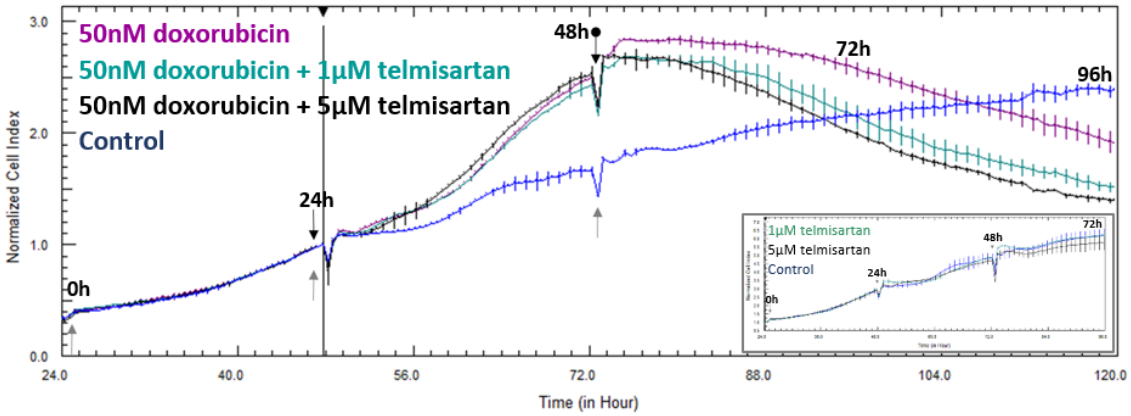

5.8B

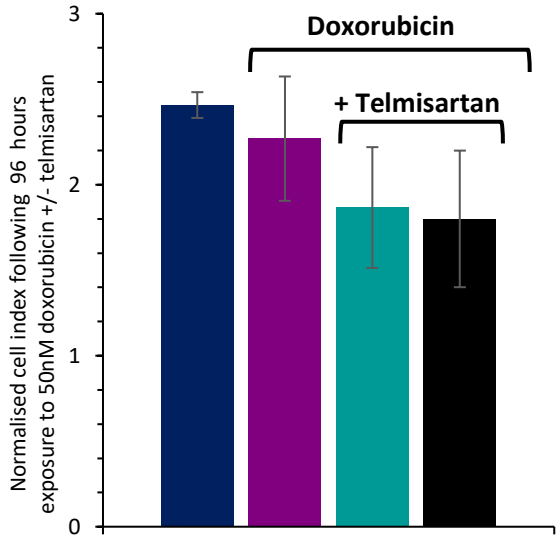

5.8C

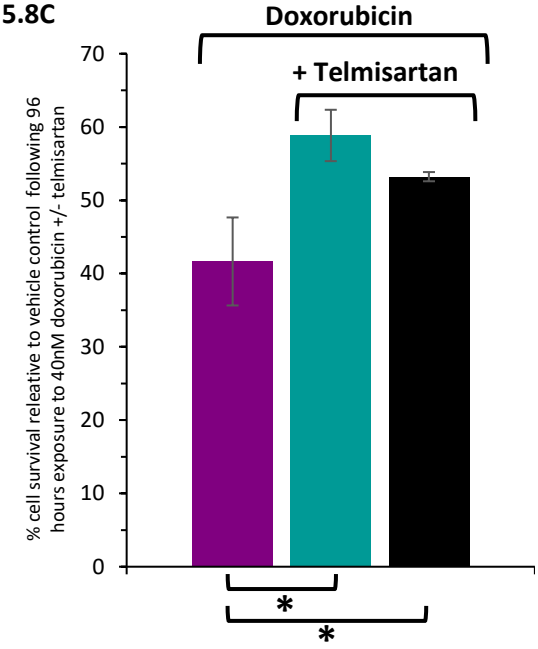

Figure 5.8 Angiotensin receptor blockade reduces morphology changes induced by doxorubicin in AC10 cardiomyocytes

A. xCELLigence trace showing time (hours) vs normalised cell index of AC10-CMs exposed to doxorubicin and telmisartan with points of telmisartan addition (grey arrows), doxorubicin addition (black arrow), doxorubicin removal (round headed arrow) and exposure time indicated, data points shown are average ± SD. **A (inset)** xCELLigence trace showing time (hours) vs normalised cell index of AC10-CMs exposed to telmisartan with points of addition (grey arrows) and exposure time indicated, data representative of n=3, data points shown are average ± SD. **B.** Normalised cell index following 96h exposure to 50nM doxorubicin +/- telmisartan, data is n=2 ± SE and **C**. % AC10-CM cell survival relative to vehicle control following 96h exposure to 40nM doxorubicin +/- telmisartan measured by MTT assay, data is n=3 ± SE. ∗ p< 0.05 (Doxorubicin treatment group compared to doxorubicin/telmisartan treatment groups) ■ control, ■ 50nM doxorubicin, ■ 50nM doxorubicin + 1µM telmisartan, ■ 50nM doxorubicin + 5µM telmisartan.

5.3.8 Angiotensin receptor blockade reduces doxorubicin-induced changes to morphology but does not affect contractility of hiPSC-derived cardiomyocytes

In chapter 4, doxorubicin was found to induce morphology and contractility changes to hiPSC-CMs when used alone. Using the xCELLigence cardio system the effect of a combination of doxorubicin plus ARB on the morphology and contractility of hiPSC-CMs was evaluated.

Stably beating Cor.4U cells were exposed to doxorubicin +/-telmisartan/losartan for 24 hours and the effects on cell behaviour were monitored in real-time. As shown in figure 5.9A, when normalised to the point of doxorubicin addition, cell index increased higher than the level of control in all three treatment groups, however the addition of telmisartan/losartan to 50nM doxorubicin resulted in less of an increase to cell index compared to 50nM doxorubicin alone. The greatest difference in cell index was approximately 6 hours after doxorubicin +/-losartan/telmisartan were added (figure 5.9B), indicating that the addition of the ARB telmisartan and losartan may have reduced the hypertrophy induced by doxorubicin. Telmisartan and losartan alone were also added to hiPSC-CMs and had no effect on the cell index when normalised to the point of drug addition, as the readings obtained were similar to that of control (inset - figure 5.9A).

Assessment of the effect of doxorubicin +/- telmisartan/ losartan on contractility of hiPSC-CMs was carried out after 6 hours and 24 hours, as these time-points represent the highest degree of hypertrophy observed and maximum exposure time. The representative traces of contractility shown for control and cells treated with doxorubicin +/- telmisartan/losartan in figure 5.10A show no visible changes in contractility following 6 hours exposure, however following 24 hours exposure, decreases in beat number and amplitude can be seen. Detailed analysis of beat rate and amplitude is shown in figures 5.10B and 5.10C respectively where there were no changes between doxorubicin +/- ARB treated cells.

5.9A

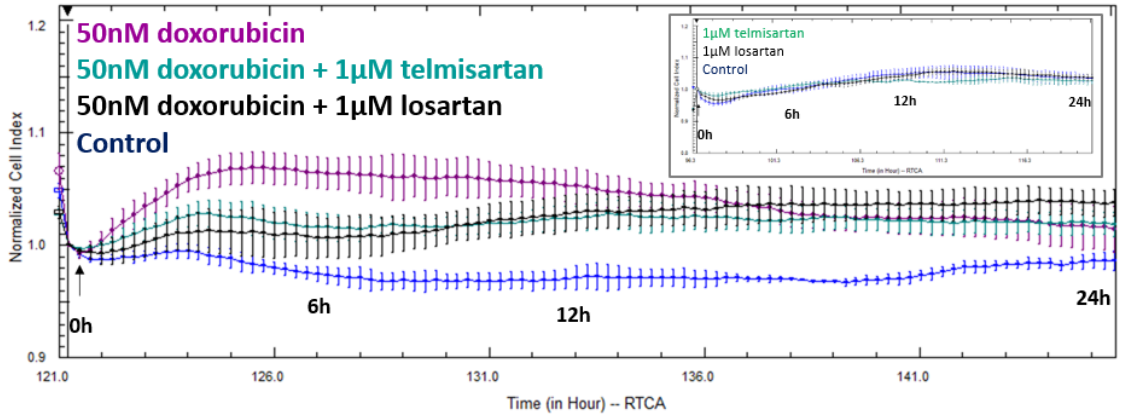

5.9B

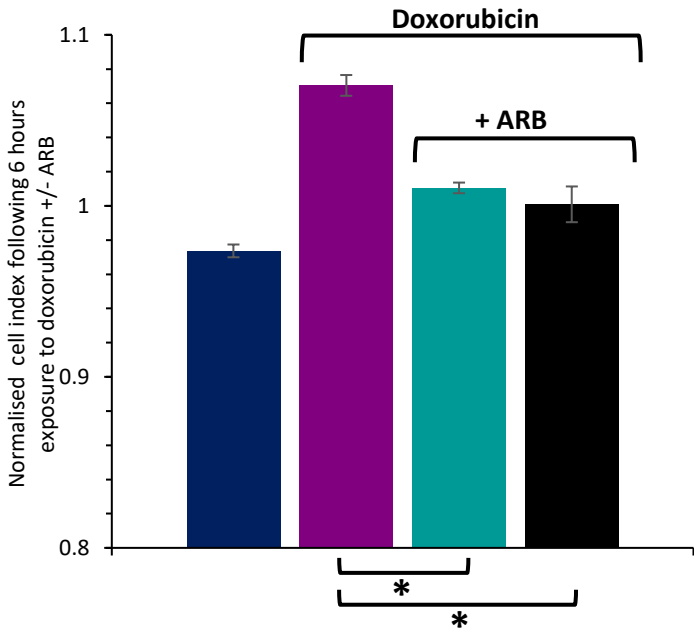

Figure 5.9 Angiotensin receptor blockade reduces doxorubicin-induced changes to morphology of hiPSC-derived cardiomyocytes

A. xCELLigence trace showing time (hours) vs normalised cell index of hiPSC-CMs exposed to doxorubicin +/- the ARBs telmisartan and losartan with point of addition (arrow) and exposure time indicated, data points shown are average ± SD. **A (inset)** xCELLigence trace showing time (hours) vs normalised cell index of hiPSC-CMs exposed to telmisartan and losartan with point of addition (arrow) and exposure time indicated, data points shown are average ± SD. **B.** Normalised cell index following 6 hours exposure to doxorubicin +/- the ARBs telmisartan and losartan**,** data points show average of 3 wells ± SE. ∗ p< 0.0001 (Doxorubicin treatment group compared to Doxorubicin/telmisartan treatment groups) ■ control, ■ 50nM doxorubicin, ■ 50nM doxorubicin + 1µM telmisartan, ■ 50nM doxorubicin + 1µM losartan.

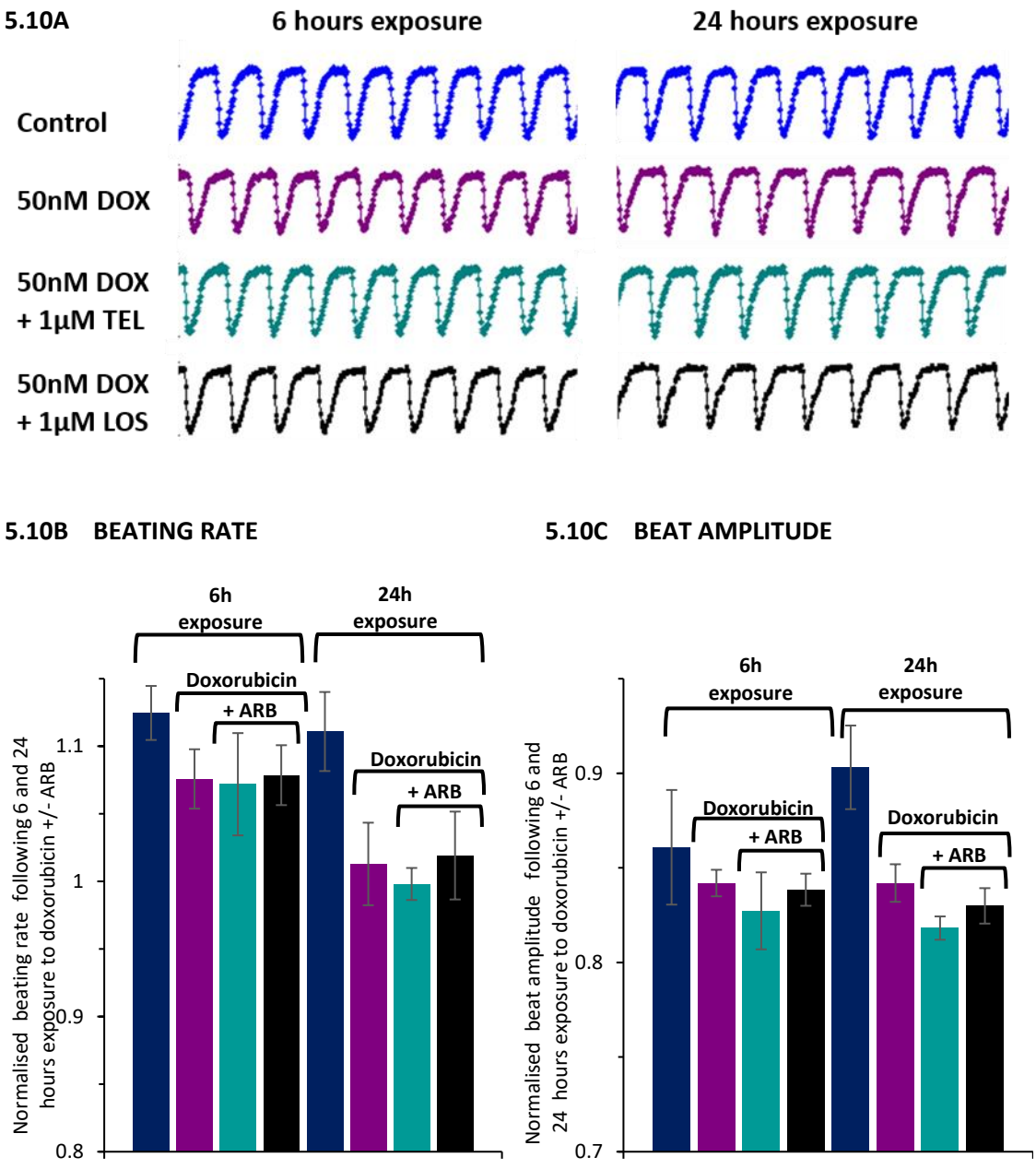

Figure 5.10 Angiotensin receptor blockade does not affect contractility of hiPSC-derived cardiomyocytes exposed to doxorubicin

A. Representative traces showing contractility of control cells and cells exposed to doxorubicin (DOX) +/- the ARB telmisartan (TEL) and losartan (LOS) for 6 and 24 hours. **B.** Normalised beating rate following 6 and 24 hours exposure to doxorubicin +/- the ARB telmisartan and losartan, data points show average of 3 wells ± SE and **C.** Normalised beat amplitude following 6 and 24 hours exposure to doxorubicin +/- the ARB telmisartan and losartan, data points show average of 3 wells ± SE. ■ control, ■ 50nM doxorubicin, ■ 50nM doxorubicin + 1µM telmisartan, ■ 50nM doxorubicin + 1µM losartan.

5.4 Discussion

The occurrence of cardiac liabilities following anthracycline treatment is well established clinically, particularly doxorubicin induced cardiotoxicity.[16] The mitigation of these toxicities using drugs that perturb angiotensin signalling has been investigated in both clinical studies and pre-clinically *in vivo* with encouraging results,[152] however the number of *in vitro* studies in this area remains limited. In addition, the direct effects upon and involvement of the cardiac system, as well as the molecular mechanism of cardioprotection have yet to be resolved. The aim of this stage of the project is to address these issues and determine if the previously discussed structural and functional cardiotoxicity induced by anthracyclines can be mitigated by the addition of ACEi and ARB using *in vitro* cardiomyocyte models.

5.4.1 Synergistic effects of angiotensin II and doxorubicin treatment

Accumulating evidence supports the role of the renin-angiotensin system as a modulator of cardiovascular remodelling; via interaction with the angiotensin type I receptor (ATR1), angiotensin II is a mediator of both cardiomyocyte growth and left ventricular hypertrophy.[75,231] The mitigation of anthracycline-induced cardiotoxicity (AIC) with therapeutics that limit angiotensin signalling suggests a role for the angiotensin signalling pathway in also mediating this toxicity; therefore initially the synergistic effects of angiotensin II and doxorubicin treatment were assessed in AC10 cardiomyocytes (AC10-CMs) and hiPSC-derived cardiomyocytes (hiPSC-CMs) following simultaneous treatment with doxorubicin and angiotensin II.

A relationship between angiotensin signalling and doxorubicin induced cardiomyopathy has previously been established by Toko *et al.* using ATR1 knockout mice (AT1KO).[265] In this elegant 12 week study, doxorubicin administered to wild type (WT) mice was found to impair cardiac function and cause histopathological abnormalities such as myofibrillar loss, increased numbers of apoptotic cells and cytoplasmic vacuolisation, however these changes were absent in the

AT1KO mice group and WT mice treated with an ATR1 antagonist. The protection afforded to the AT1KO mice and the mice treated with an ATR1 antagonist suggests that there is interplay between the angiotensin signalling pathway and doxorubicin-induced cardiomyopathy.[265]

As the aforementioned study by Toko *et al*. was conducted in mice, it is more challenging to ascertain the mechanism of cardioprotection in the mice with ablated angiotensin signalling. In addition to the effects of angiotensin signalling on remodelling activities in the heart, angiotensin II also has systemic effects in other organs such as the kidneys and blood vessels where it is involved in the absorbance of water and salt, and vasoconstriction respectively.[266] These activities have the overall effect of increasing blood pressure which could partially contribute to the improved cardiac function of the AT1KO mice treated with doxorubicin. In contrast, the current study focussed on isolated cardiomyocytes found that addition of a physiologically relevant dose of angiotensin II, previously found to induce hypertrophy of AC10-CMs, did not alter the toxicity profile of doxorubicin or augment the doxorubicin-induced hypertrophy of AC10-CMs when co-administered with doxorubicin. This may be due to the use of shorter exposure times that did not allow for the accumulation of further structural damage, or the use of a more simplistic *in vitro* model that does not fully represent the complexity of the cardiovascular system and human body.

Similar findings were observed in hiPSC-CMs exposed to a combination of angiotensin II and doxorubicin with respect to hypertrophy, however some changes were observed in the beat characteristics of the cells. Assessment of the effect of angiotensin II and doxorubicin on contractility of hiPSC-CMs was carried out after 6 hours and 24 hours, with 24 hours exposure resulting in a decrease in beat amplitude of the cells compared to cells treated with doxorubicin only. As a decrease in beat amplitude relates to negative inotropy (reduced force of muscle contraction), the reduction observed in beat amplitude observed following 24 hours exposure to doxorubicin and angiotensin II may be due to increased impairment to the contractile

machinery of the cells and myofibrillar loss. This would be in alignment with the findings from the study by Toko *et al.*, where AT1KO mice were protected from myofibrillar loss and cytoplasmic vacuolisation induced by doxorubicin treatment, as determined by electron microscopic analysis; thus supporting the notion that angiotensin signalling plays a role in AIC.[265] The results from the current study illustrate the advantages of hiPSC-CMs as an *in vitro* model that is capable of determining changes in contractility in a clinically relevant manner.

5.4.2 Synergistic effects of doxorubicin with concurrent angiotensin converting enzyme inhibitor and angiotensin receptor blocker treatment

Promising results from both clinical and *in vivo* studies utilising angiotensin receptor blockers (ARB) and angiotensin converting enzyme inhibitors (ACEi) point towards these medicines as a potential route for mitigation of AIC.[152] In the current study the ACEi enalapril and its active form enalaprilat did not augment the sensitivity of AC10-CMs to doxorubicin cytotoxicity. The lack of protection observed in AC10-CMs that were co-administered with enalapril and enalaprilat may be due to a combination of two factors: the use of an *in vitro* model and the mechanism of action of these compounds. In the human body, angiotensin converting enzyme (ACE) is required to convert angiotensin I to angiotensin II which has a variety of effects including vasoconstriction which increases blood pressure.

As an ACEi, enalaprilat, which is the active metabolite of enalapril, reduces production of angiotensin II, leading to decreased vasoconstriction and decreased blood pressure.[267] This process requires the starting peptide angiotensin I which is produced by cleavage of angiotensinogen by an enzyme called renin. Although these proteins are thought to primarily originate from the liver and kidneys respectively, more recent evidence points toward the existence of a local renin-angiotensin-system in the myocardium which produces all the

necessary elements to create angiotensin II except renin which is sequestered from the bloodstream.[231,268]

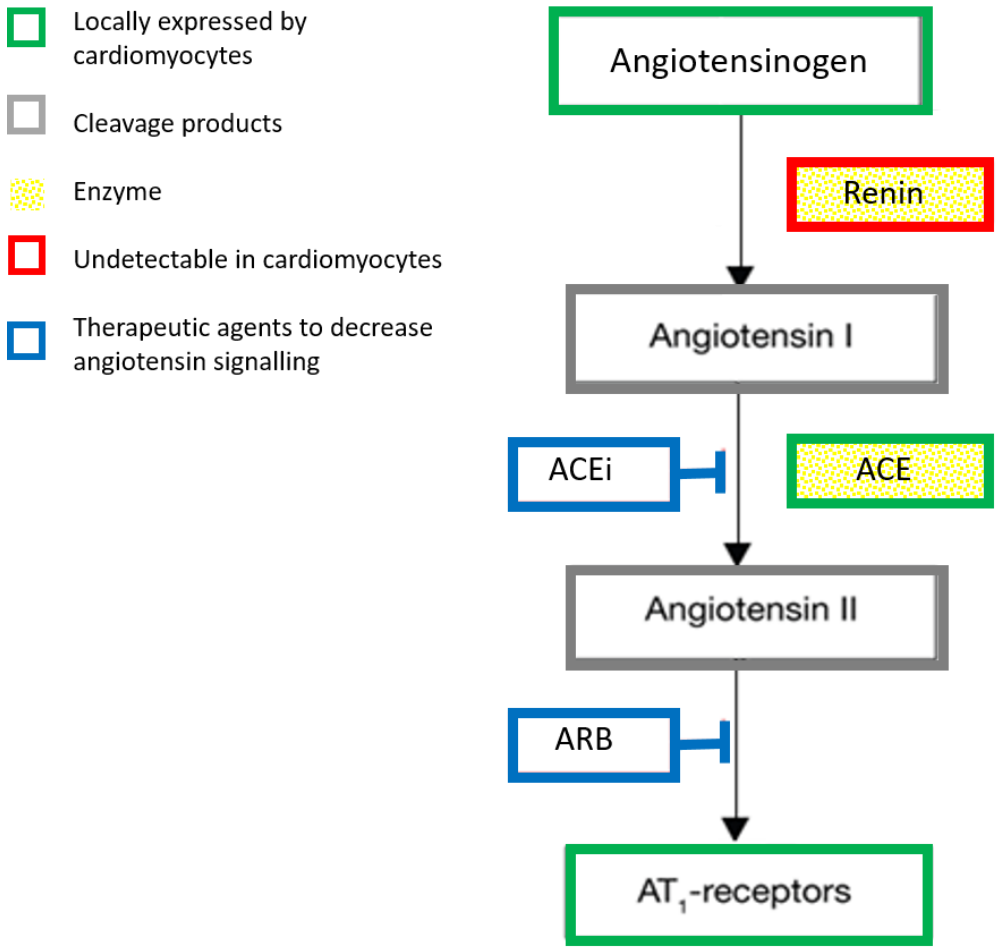

Figure 5.11 Angiotensin II synthesis in the myocardium

The pathway of angiotensin II production showing components expressed by the myocardium (green), pathway enzymes (yellow), cleavage products (grey) and therapeutic agents used to decrease angiotensin signalling (blue). The myocardium expresses all the necessary elements to produce angiotensin II except renin (red) which is sequestered from the bloodstream, therefore it is unlikely that *in vitro* cardiomyocyte cell models are able to produce angiotensin II.

Preliminary studies using reverse transcriptase polymerase chain reaction (RT-PCR) in the current study, detected gene expression of angiotensinogen and ACE in AC10-CMs, however expression of renin was not detected in the cells (See Appendix 5). With this is mind, it is unlikely that the AC10-CMs used in this study could produce angiotensin I, therefore the enalapril/enalaprilat added to this artificial system had no function as any ACE enzyme that was present would likely be inactive. The lack of direct interaction of enalapril/enalaprilat with cardiomyocytes is illustrated in toxicity studies where the compounds were added alone and the effects upon viability of AC10-CMs determined. At the highest concentration of 10μM the drugs exhibited negligible toxicity, with survival rates of approximately 94% for both compounds relative to vehicle control. In contrast, addition of the ARB telmisartan and losartan at 10μM yielded survival rates of 84% and 70% respectively which suggests direct interaction with the drugs' target, the ATR1. Indeed, preliminary studies using RT-PCR found positive expression of the ATR1 in AC10-CMs (See appendix 5) and the previously described results of angiotensin II induced hypertrophy (Section 3.3.4.1) suggests expression of the ATR1 in the AC10-CM cell line.

Unlike the ACEi enalapril and its active form enalaprilat, the ARB telmisartan and losartan were able to protect AC10-CMs from doxorubicin induced toxicity as evidenced by the increased IC_{50} values when cells were co-treated with telmisartan/losartan and doxorubicin compared to cells treated with doxorubicin alone. In relation to this, a recent study conducted by Gergely *et al.* used high-throughput screening to identify a novel compound with ability to protect H9c2 rat cardiomyocytes from doxorubicin induced damage.[269] Out of a library of 10,000 compounds only one was found to be convincingly cardioprotective – the compound is called EODB and possesses a benzimidazole moiety, which is also a feature of the ARB telmisartan. It is possible that the cardioprotection provided by EODB in this study was also related to ATR1 blockade, however further studies would be needed to elucidate the exact mechanism of cardioprotection. The authors of the study also investigated the effect that EODB had on cancer cell lines, as it is imperative that cardioprotectants do not compromise the anti-cancer activity of doxorubicin.

Encouragingly, it was found that EODB did not hamper the anti-cancer activities in cancer cell lines originating from the lung, bone and blood cells.[269] The same consideration was made in the current study, where no decreases to doxorubicin's anti-tumour efficacy was observed with telmisartan and losartan when added in tandem with doxorubicin to the H460 lung cancer cell line. In fact, 5μM telmisartan appeared to increase the sensitivity of H460 cells to doxorubicin as evidenced by the IC_{50} values which reduced from 40.66nM when cells were treated with doxorubicin alone, to 10.66nM when a combination of doxorubicin and 5μM telmisartan was added to the cells.

Having considered the ability of telmisartan and losartan to protect AC10-CMs from doxorubicin induced cell death without affecting therapeutic efficacy in H460 lung cancer cells, the impact of angiotensin blockade on cellular morphology of doxorubicin treated AC10-CMs and hiPSC-CMs was determined. Simultaneous to increased viability of AC10-CMs, blockade of the angiotensin receptor was also found to reduce the hypertrophic response induced by doxorubicin in both AC10-CMs and hiPSC-CMs.

A number of clinical studies have provided strong evidence that use of ARB alone can reduce left ventricular hypertrophy including the Losartan Intervention for Endpoint Reduction in Hypertension (LIFE) study[270] and the Swedish Irbesartan Left Ventricular Hypertrophy Investigation versus Atenolol (SILVHIA) study.[271] Both of these studies compared the use of ARB to the β-blocker atenolol and found that the ARB achieved a significantly greater reduction in left ventricular hypertrophy compared to atenolol, despite similar reductions in blood pressure. This suggests that blockade of the ATR1 may be a more efficient approach to curb the cardiac remodeling that occurs due to pressure overload and further supports the role of angiotensin II in development of pathogenic hypertrophy. In line with the symptoms of ordinary heart failure, the chronic and delayed forms of doxorubicin-induced cardiotoxicity are also associated with impairments to left ventricular function and changes to cardiomyocyte structure.[144] This links

with the findings from the current study which have shown using *in vitro* cardiomyocyte models that mitigation of the cardiomyocyte hypertrophy induced by doxorubicin is possible through blockade of the ATR1 by ARB.

Unlike the LIFE and SILVHIA clinical studies mentioned above, the current study was conducted *in vitro* and therefore is focussed on direct evaluation of cardiomyocyte behaviour independent of systemic effects. The reduction in cardiomyocyte hypertrophy observed in this study demonstrates that perturbation of angiotensin signalling in the context of doxorubicin-induced cardiotoxicity has direct protective effects on cardiomyocytes. This may relate to a reduction in the acute cardiotoxicity response which potentially primes cardiomyocytes for the more severe forms of cardiotoxicity that involve cardiac remodelling and ventricular hypertrophy.

A further implication of using *in vitro* cardiomyocyte models is that the cells used in this study were not exposed to circulating levels of angiotensin II that would ordinarily bind to the ATR1 and initiate signalling cascades. Evidence suggests that biomechanical stress (such as exposure to doxorubicin) to cardiomyocytes *in vitro* can induce changes to cardiomyocytes including the induction of ATR1 activation independent of agonist binding,[272] which may also be responsible for ATR1 activation in the current study. Considering this, in addition to exposure of a patient's myocardium to doxorubicin causing hypertrophy (biomechanical stress) and subsequent ATR1 activation independent of angiotensin II, patients also have their own circulating angiotensin II which regrettably may increase further due to the oxidative stress caused by exposure to doxorubicin. The doxorubicin-induced biomechanical stress and increased levels of angiotensin II could thereby likely further increase stimulation of ATR1 thus increasing the activity of this potentially cardiotoxic signalling cascade.

5.4.3 Conclusion

The findings from this chapter provide further evidence to the existing *in vivo* and clinical studies that support the use of drugs that interfere with angiotensin signalling as a means to mitigate AIC. As this study was conducted *in vitro* using AC10-CMs and hiPSC-CMs, this suggests that direct interaction of the ARB with the ATR1 on cardiomyocytes may be at least partially responsible for the protection afforded by ARB against AIC. As it is unlikely that the *in vitro* models used in this study produce angiotensin II, it is possible that an alternative mechanism of cardioprotection may exist that is independent of angiotensin signalling. Further work into clarifying the involvement of the ATR1 in the cardioprotective response observed is required and could be obtained using siRNA techniques. In addition to facilitating improved survival and reduced hypertrophy of cardiomyocytes treated with doxorubicin, telmisartan and losartan did not reduce the therapeutic efficacy of doxorubicin in H460 lung cancer cells, which is essential if ARB are to be used for cardiotoxicity mitigation in cancer treatment. The protection given to the cardiomyocytes used in this study is likely due to direct interaction of the ARB with the ATR1 on cardiomyocytes, however may occur via an off-target mechanism. This may relate to a reduction in the acute cardiotoxicity response which potentially primes cardiomyocytes for the more severe forms of cardiotoxicity that involve cardiac remodelling and ventricular hypertrophy. The interaction between angiotensin signalling and doxorubicin-induced cardiotoxicity will be investigated further in the following chapter.

Chapter 6: Molecular relationship between the angiotensin signalling pathway and anthracycline-induced cardiotoxicity

6.1 Introduction

In terms of heart failure, the reduction in the heart's ability to maintain sufficient cardiac output, compensatory mechanisms lead to cardiac remodelling and increases in cardiac beat rate. The purpose of this remodelling is to increase the stroke volume and cardiac capacity in order to return cardiac output to the required level. However, the alteration in cardiac structure decreases cardiac efficiency and increases myocardial strain, further deteriorating cardiac output, exasperating cardiac failure, and increasing the risk of arrhythmias and cardiac arrest.[82,273]

6.1.1 Angiotensin signalling pathways in the cardiac system

An important physiological mediator of cardiac output and cardiac stroke volume is the renin-angiotensin system. This system has an overall role in regulating blood pressure through altering blood volumes, via alteration of renal water retention, and perturbation of vascular resistance and cardiac tone.[231,266] Angiotensin II, the major effector of the RAS, is an octapeptide formed by sequential cleavage of angiotensinogen to angiotensin I by renin, followed by cleavage of angiotensin I to angiotensin II by angiotensin converting enzyme (ACE). The angiotensin receptor signalling pathway mediates the cellular response to angiotensin II through the angiotensin

receptors (ATR), of which there are two subtypes – ATR1 and ATR2 receptors.[274] The majority of the known physiological effects of angiotensin II are mediated by the ATR1 receptors.[75,76] Consequently, disruption of the RAS signalling pathway is a known pharmacological target, with drugs targeting this pathway used clinically for management of hypertension and heart failure (see section 1.4.5.2).[162,163]

Although the RAS system is predominantly systemic in activity and function, culminating in changes in blood volume and pressure, there is substantial evidence to also support a direct involvement of angiotensin signalling upon cardiac tissue.[231,268] The heart contains a variety of cell types including cardiomyocytes, fibroblasts, endothelial cells and pericytes (See section 1.4.3). These cell types play specific roles within the heart and rely on an array of signalling cascades to communicate and maintain optimal cardiac function. (See section 1.4.5). The heart is equipped with sophisticated mechanisms to respond to extracellular stimuli such as changes to cardiac demand, including G-protein coupled receptors such as the ATR.[69] The physiological importance of angiotensin II in the cardiovascular system is paramount, as it is responsible for regulating changes in vascular tone and blood flow to maintain cardiac output and function.

6.1.2 Perturbation of the angiotensin signalling pathway as a therapeutic strategy

Interruption of angiotensin signalling is a clinically utilised strategy for management of heart failure and hypertension, through either reducing the amount of circulating angiotensin II or preventing its binding to ATR.[162,163]

Inhibition of ACE is a frontline approach in this respect, preventing conversion of angiotensin I to II. The second strategy is through the use of angiotensin receptor blockers (ARB) which retard the binding of angiotensin II to ATR1, thereby disrupting angiotensin signalling. In contrast to ACE inhibition which has a general systemic effect and subsequent indirect effect upon cardiac

tissue, blockade of ATR1 is known to bind to receptors in the heart and directly curb angiotensin-induced changes such as cardiomyocyte hypertrophy and cardiac remodelling.[270,271] Interestingly, the ARB valsartan has been shown to simultaneously block signalling of ATR1 and β2 adrenergic receptors in mice, suggesting further complex receptor interactions and perhaps more use for angiotensin signalling modulators in heart failure.[78]

6.1.3 Inhibition of Angiotensin signalling for mitigation of anthracycline-induced cardiotoxicity

This project has previously demonstrated anthracyclines, such as doxorubicin, are associated with severe dose-limiting cardiotoxicity (see section 1.7.1.2).[16] As a result, many different strategies to reduce the occurrence of cardiotoxicity have been explored including iron chelators, liposomal formulations and co-administration of heart therapies such as those that augment angiotensin signalling.[28,152] The use of ARB and ACEi for reducing anthracycline-induced cardiotoxicity (AIC) has been investigated in clinical studies which have reported positive results, mainly in the area of preventing declines in left ventricular function associated with anthracycline treatment.[150,164–168] The findings of these studies are summarised in section 1.7.2.1 and table 1.2.

Although some of the cardioprotective properties of reducing angiotensin signalling can be attributed to a systemic reduction in blood pressure, it is likely that reduction of angiotensin signalling also affords some direct protection to cardiomyocytes. However, the mechanism by which anthracyclines, such as doxorubicin, induce structural and functional changes to cardiomyocytes has yet to be fully identified.

Collective evidence suggests that the cardiomyopathy initiated by doxorubicin is a progressive and multi-factorial process. At the subcellular level, exposure to doxorubicin causes cytoplasmic vacuoles, mitochondrial membrane disruption and disorder of myofibril arrangement.[116,144]

From a molecular perspective, mechanisms of doxorubicin-induced cardiomyopathy include impaired calcium handling, altered gene and protein expression of key pathways involved in cardiomyocyte survival and function, DNA breakage via inhibition of cellular topoisomerase IIβ (TopIIβ), intracellular collation of iron, inhibition of mitochondrial topoisomerase 1 (Top1mt) and consequent function, and the formation of oxygen free radicals that damage the mitochondria of the cells.[16,34,118,124,127] These mechanisms of doxorubicin-induced cardiotoxicity are discussed in detail in section 1.7.1.1.

Several studies have reported that angiotensin II promotes the generation of reactive oxygen species (ROS) from the mitochondria, a process involving activation of NADPH oxidase and mitochondrial ROS-induced ROS release (RIRR), and subsequent oxidative stress within cardiomyocytes.[275,276] In relation to anthracyclines, doxorubicin is also known to bind to the mitochondrial membrane protein cardiolipin, causing the accumulation of the drug within the cardiomyocyte, redox cycling and generation of substantial ROS.[91] Subsequently, the presence of iron (Fe^{2+}) fuels the process and production of further damaging reactive species, termed the iron and free radical hypothesis.[118]

Therefore, anthracycline-induced free radical production and angiotensin-mediated signalling is likely to result in exacerbation of oxidative stress, providing a possible rationale for the mitigation of cardiotoxicity by pharmaceutical agents that reduce angiotensin signalling. Such a hypothesis was addressed in a murine study by Taskin *et al*. who administered doxorubicin in the presence or absence of the ACEi captopril and/or the renin inhibitor aliskiren.[277] In this study doxorubicin decreased mitochondrial membrane potential and ATP levels in cardiomyocytes, a process shown to involve increased oxidative stress.[278] Whereas treatment with doxorubicin in the presence of ACE or renin inhibition resulted in much higher ATP levels and little change in the mitochondrial membrane potential, by a process postulated to involve decreased oxidative stress and inhibition of angiotensin II production.[277]

Another suggested mechanistic basis for the cardiotoxic effects of doxorubicin and involvement of angiotensin signalling is provided by the induction of mechanical stretch and subsequent physical stress by doxorubicin treatment. This hypothesis proposes that this drug-induced cardiomyocyte stretch further increases circulating levels of angiotensin II, a concept investigated by Okumura *et al*. who determined ACE activity in hamsters treated with doxorubicin.[279] Following two weeks treatment, activity of cardiac ACE increased in doxorubicin treated hamsters, suggesting cardiac ACE may play an important role in development of AIC, causing increased production of angiotensin II and exacerbated cardiac hypertrophy.[279] Increased levels of angiotensin II has the additional detrimental effect of down-regulating essential neuregulin signalling in cardiomyocytes.[175] As previously discussed in section 1.6.2.1 neuregulin signalling is involved in cardiac development and physiology, with studies in conditional gene knockout murine models demonstrating spontaneous dilated cardiomyopathy and increased susceptibility to stress such as pressure overload.[108] In terms of cardiotoxicity of oncology therapeutics, trastuzumab-induced cardiotoxicity reportedly involves inhibition of the neuregulin signalling pathway;[105] therefore it is possible that altered neuregulin signalling may play a role, alongside elevated angiotensin II levels and oxidative stress, in AIC.

With regards to angiotensin signalling and AIC, increased oxidative stress, decreases in survival signalling pathways and cardiac remodelling are areas of clear overlap. However, it is still unclear as to how the angiotensin signalling pathway and anthracycline-treatment interact to facilitate cardiotoxicity and the underpinning molecular mechanisms. Ultimately, greater understanding of the temporal and spatial involvement of the angiotensin-signalling pathway in this cardiotoxicity, at the level of the cardiomyocyte, will assist in the understanding of this toxicity and its detection and management.

6.1.4 Aims and objectives

This study has previously confirmed that ARB can mitigate anthracycline-induced structural changes in cardiomyocytes, utilising qualified *in vitro* models. The aim of this phase of the study is to interrogate the molecular mechanisms of the angiotensin-signalling pathway associated with anthracycline-induced cardiotoxicity, potentially indicating a molecular relationship between the angiotensin II signalling pathway and anthracycline-induced cardiotoxicity.

Specifically:

i) Studies will be conducted to evaluate the involvement and regulation of ATR1 in doxorubicin-induced cardiotoxicity using the previously qualified *in vitro* cardiomyocyte models.

ii) Molecular pathways perturbed by doxorubicin in cardiomyocytes at the genetic level will be examined and the relationship to the angiotensin-signalling pathway and cardiotoxicity will be addressed.

6.2 Materials and methods

Solution and gel compositions used for western blotting are outlined in Appendix 4.

6.2.1 Evaluation of protein expression by western blotting:

Cell lysate preparation of AC10 cardiomyocytes

AC10 cardiomyocytes (AC10-CMs) were seeded in 6-well plates at a density of 300,000 cells per well and cultured for 24 hours in complete culture medium. Cells were then incubated with doxorubicin (50-500nM) for a further 24 hours. Following culture media removal and cellular trypsinisation, the number of cells was adjusted to 500,000 cells per sample. After centrifugation for 5 minutes at 1000rpm, cell pellets were lysed by addition of 50µl of lysis buffer containing both protease and phosphatase inhibitors. The resultant cell lysates were centrifuged at 1000rpm and the supernatant (soluble fraction) transferred to a fresh tube, or the cell lysates were not centrifuged and the whole cell lysates (soluble and insoluble fraction) were stored at -20°C.

The amount of protein in the cell lysates was quantified using the Bradford assay.[280] A series of protein standards (0-1µg/µl) were made using bovine serum albumin (BSA) diluted in lysis buffer. 10µl of the test samples and standards were added to a 96 well plate in duplicate. To each well, 200µl of Bradford Reagent (BioRad, UK) diluted 1:5 in deionised water was added, the plate incubated at room temperature for 5 minutes to allow the reaction to occur, and the absorbance of the samples at measured at 595nm using a spectrophotometer plate reader (MultiSkan GO, Thermo Scientific, USA). The concentration of test samples was then calculated using the standard curve. Cell lysates were stored at -20°C until required.

6.2.1.1 Evaluation of protein expression by western blotting: Polyacrylamide gel electrophoresis and membrane transfer

Protein samples were diluted to a final concentration of 1µg/µl by mixing the calculated volume of cell lysate, water and 4x sample buffer (Containing 10% β-mercaptoethanol), heated at 95°C for 5 minutes to denature proteins, before transfer onto wet ice.

Protein samples (30µg) were separated through a 10% polyacrylamide SDS resolving gel and a 5% stacking gel using a BioRad mini-gel electrophoresis rig (BioRad, UK) filled with running buffer. For size determination, 5µl Precision Plus protein ladder (BioRad, UK) was also loaded into the gel. Proteins were separated at 200V for 1 hour or until the dye front reached the end of the gel.

Western blotting was conducted as per the methodology of Towbin *et al*.[281] Briefly, gels were removed from the tank and the proteins transferred from the polyacrylamide gel to a polyvinylidene difluoride (PVDF) membrane (Amersham Hybond, GE Healthcare Life Sciences, UK), as follows. Prior to use the PVDF membrane was activated by soaking in methanol for 15 seconds and then placed in transfer buffer. The western transfer cassette was assembled as shown in figure 6.1.

The resultant cassette was placed in a transfer tank (BioRad, UK) containing transfer buffer, immersed in wet ice and the proteins transferred at 300mA for 1 hour.

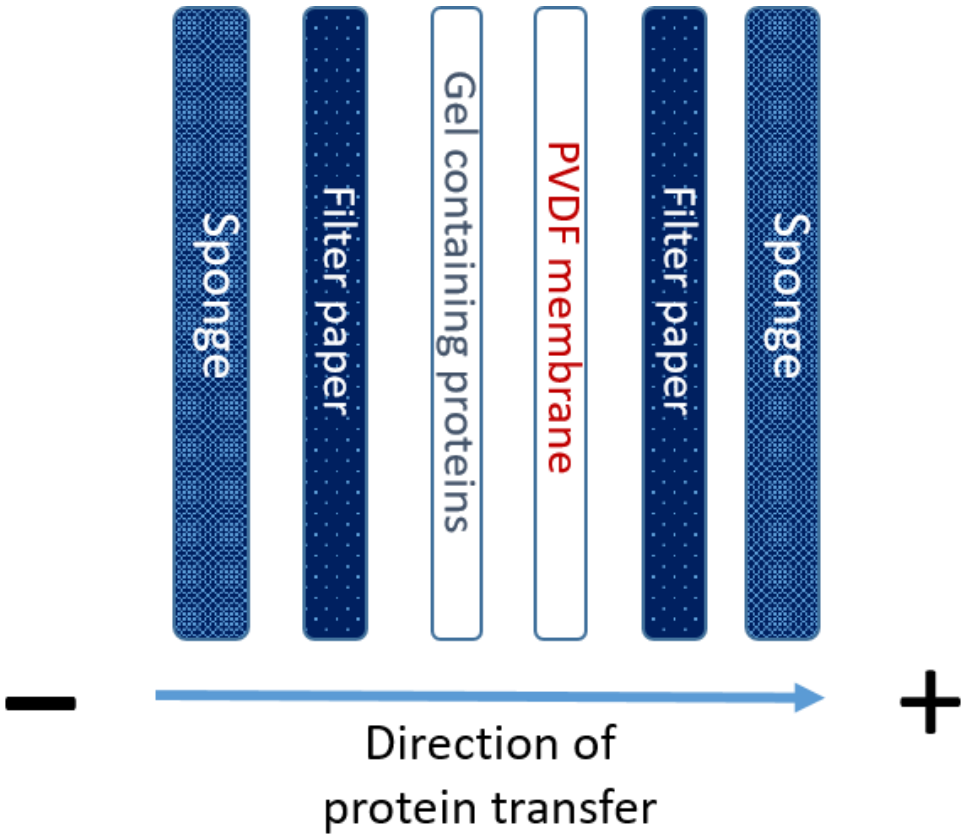

Figure 6.1 **Gel and PVDF membrane sandwich for protein transfer**

6.2.1.2 Evaluation of protein expression by western blotting: Antibody probing and protein detection

After completion of protein transfer, PVDF membranes were incubated in a solution of 5% non-fat dried milk in Tris-buffered saline with Tween-20 (TBS-T), for 1 hour at room temperature with agitation to block non-specific antibody binding. To probe for expression of specific proteins, 'blocked' membranes were then incubated overnight at 4°C with the respective primary antibody (table 6.1), diluted in 1% milk in TBS-T in a 50ml sample tube on a rotating mixer (Bibby Scientific, UK).

Primary antibody	Type	Company	Dilution	Secondary antibody	Molecular weight (kDa)
ATR1	Rabbit polyclonal	Millipore	1:250	Anti-rabbit (1:2000)	43
β-actin	Mouse monoclonal	Sigma	1:10000	Anti-mouse (1:2000)	42

Table 6.1 Characteristics of antibodies used in this study

After overnight antibody exposure, membranes were washed three times in TBS-T for 15 minutes on a shaker at room temperature to remove unbound antibody. The PVDF membranes were then incubated in the appropriate HRP-conjugated secondary antibody diluted in 1% milk in TBS-T (table 6.1) for 1 hour at room temperature. Membranes were than washed for 15 minutes on a rocker at room temperature to remove unbound secondary antibodies.

Antibody binding was detected by chemiluminescence, using a pre-mixed enhanced chemiluminescence solution (ECL) and left to react in the dark for 3 minutes. Excess ECL was removed by dabbing membranes onto tissue paper, before placing the membrane in a small plastic bag and marking the location of the protein ladder. Bands were detected using a ChemiDoc MP System (BioRad, UK). Exposed membranes were stored at 4°C for further analysis of protein expression.

Blots were stripped and re-probed for β-actin to ensure equal loading of all samples. Briefly, the membranes were incubated in acid stripping buffer for two 30 minute incubations and then the acid was neutralized by triplicate three minute washes in PBS. The membrane was blocked for 1 hour as previously described and then incubated in primary antibody diluted in 1% milk in TBS-T (table 6.1) for 1 hour and binding detected as previously described. Protein expression was analysed semi-quantitatively using densitometry on the ImageJ image processing package (National institute of Health, USA), with fold change in respective protein expression relative to vehicle control calculated.

Statistical tests were conducted on densitometry values using a one way analysis of variance (ANOVA) test. Statistical analysis was performed using GraphPad Prism (Version 7.04, GraphPad Software, Inc.).

6.2.2 Analysis of anthracycline-induced changes to gene expression relating to cardiotoxicity and angiotensin signalling

PCR arrays were used to analyse changes in expression of a panel of pathway specific genes to be profiled in cells following drug treatment. The PCR arrays used for these studies were the Human Cardiotoxicity array (PAHS-095Z) and the Human GPCR Signalling Pathway Finder (PAHS-071Z) (SABiosciences, Qiagen, Germany) using the previously described methodology.[282]

6.2.2.1 Production of cDNA from AC10 cardiomyocytes

AC10-CMs were seeded in 6-well plates at a density of 300,000 cells per well and grown for 24 hours prior to the addition of 50nM doxorubicin or 0.1% DMSO. After drug exposure for 24 hours, media was removed and the cells scraped in PBS and collected into a microcentrifuge

tube. Following centrifugation for 5 minutes at 1000rpm at 4°C (VWR, Micro Star 17R) cell pellets were stored at -20°C prior to RNA extraction.

RNA was extracted from AC10-CMs using the RNeasy mini kit, following the manufacturer's instructions (Qiagen, Germany).[283] Briefly, cell pellets were thawed, 350µl RLT buffer added, and the pellet homogenized using a QIAshredder spin column. RNA was precipitated from the lysate by addition of 350µl 70% ethanol. The RNA was isolated from the sample using an RNeasy spin column and then on column DNA digestion performed using an RNase-Free DNase set, by washing in RW1 buffer, digestion of DNA using RDD buffer and DNase I for 15 mins, and a final wash in RW1 and RPE buffers to remove unwanted biomolecules and salts. RNA was eluted by addition of RNase free water and centrifugation of the column. RNA was stored at -80 °C.

The quality and concentration of RNA in the samples was determined using the NanoDrop 2000c (Thermo Scientific, USA), analysing 1µl RNA sample relative to an RNase free water blank. The concentration of RNA in the samples was recorded, with a 260:280 absorbance ratio of greater than 1.8 confirming RNA quality.

cDNA was synthesised using the RT^2 First Strand Kit (Qiagen, Germany), according to the manufacturer's instructions.[284] Briefly, RNA was combined with genomic elimination (GE) and RNase-free water, to a total volume of 10µl, incubated at 42°C for 5 minutes, and then immediately placed on wet-ice ice. The reverse transcription reaction was developed by combination of the RNA sample (10µl) with Buffer BC3 (4µl), Control P2 (1µl), RNase-free water (3µl) and reverse transcriptase mix (2µl). The mixture was incubated at 42°C for 15 minutes and then rapidly incubated at 95°C for 5 minutes to halt the transcriptase reaction. The volume of reaction was then adjusted to a final amount of 111µl through addition of RNase-free water, and the cDNA stored at -20°C until required.

6.2.2.2 Pre-array verification of cDNA quality

Before undertaking real-time PCR (qRT-PCR), the quality of the cDNA was ascertained by checking the expression of the GAPDH house-keeping gene using semi-quantitative reverse-transcriptase PCR (RT-PCR). A PCR amplification mixture was created containing 10µl Taq MM (x2; New England Biolabs) 0.2µl GAPDH forward primer (5'-CCACCCATGGCAAATTCCATGGCA-3'), 0.2µl GAPDH reverse primer (5'-TCTAGACGGCAGGTCAGGTCCACC-3') (Invitrogen, UK), 2µl cDNA and 7.6µl RNase-free water. RT- PCR was then carried out using a thermocycler (Prime, Fischer Scientific, UK) on the samples using the following cycling conditions:

Step	**Temp (˚C)**	**Duration**	
Initial denaturation and activation of polymerase	94	5minutes	
Denature	94	30Seconds	30 cycles
Primer annealing	54	30seconds	
Extension	68	90seconds	
Final extension	68	5 minutes	

The PCR products were analysed by separation through a 1% (w/v) agarose gel, containing 0.01% ethidium bromide. Samples were combined with 10% loading dye (30% glycerol, 0.25% bromophenol blue) to allow sample visualisation and loaded into the gel alongside a DNA ladder (QuickLoad 100bp DNA ladder, New England Biolabs). Electrophoresis was performed in Tris-Acetate EDTA buffer (TAE; 40mM Tris, 20mM acetic acid and 1mM EDTA) at 100V for approximately 1 hour. The gel was viewed using a ChemiDoc MP System (BioRad, UK) and

ImageLab software (BioRad, UK). The expected PCR product size was 598bp, cDNA quality was deemed suitable if discrete bands of comparable intensity were observed.

6.2.2.3 Real-time PCR of Gene expression arrays

The qRT-PCR protocol and methodology was as per the manufacturers protocol.[284] A reaction mixture was produced by combination of 102µl test cDNA, 1048µl RNase-free water and 1150µl RT^2 SYBR Green ROX FAST 2x mastermix (Qiagen, Germany). To each well of the respective RT^2 Rotor-Disc 100 gene array, 20µl of the PCR mixture was added to each of the 100 wells. The plate was sealed, clipped into loading disc and locking ring, and inserted into the Rotor-Gene instrument (Qiagen, Germany). The associated RT^2 Rotor-Gene template was loaded into the Rotor-Gene Q software (V2.0) and the programme initiated. After the qRT-PCR run, the baseline was automatically defined and the threshold cycle value (CT) determined for each well. Changes in gene expression for control and doxorubicin treated cDNA samples were analysed using the SABiosciences data analysis web based software. Data was normalised using automatic selection from the housekeeping gene panel on the qRT-PCR Array. The CT values for these genes were then used for the ΔΔCT calculations. This is normalized gene expression expressed as fold change and is calculated by dividing CT values from the test sample by the control sample values. Fold change values greater than one indicate an up regulation and fold change values less than one indicate down regulation.

6.3 Results

6.3.1 Optimisation of western blotting for detection of the ATR1

Initially, the soluble supernatant fraction of cellular lysis was analysed for expression of the angiotensin type I receptor (ATR1). At all protein concentrations tested no band corresponding to ATR1 expression (43kDa) was detected in these samples (Figure 6.2A), however detection of β-actin expression (42kDa) confirmed the successful transfer of proteins to the membrane (Figure 6.2B).

Conversely, expression of ATR1 was detected in the whole cell lysates, containing both the soluble and insoluble proteins, at a level relative to the concentration of protein in the samples (Figure 6.3). This latter observation is indicative that the ATR1 is present in the insoluble fraction of the protein samples and whole cell lysates should be used for further experiments.

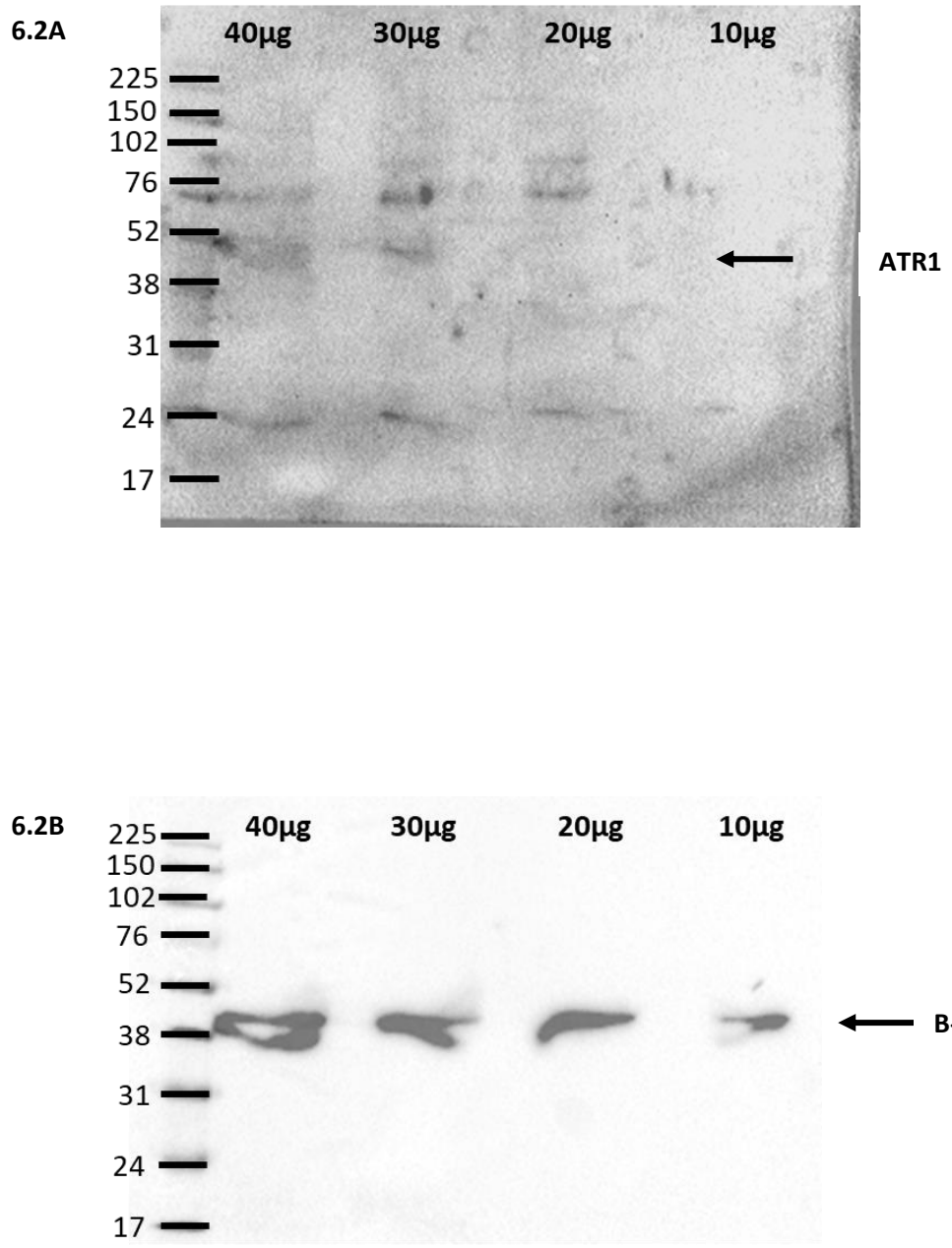

Figure 6.2 The ATR1 is absent from the soluble fraction of AC10 cardiomyocyte cell lysates

A. Western blot showing various concentrations of the soluble proteins from AC10-CM probed for the ATR1, expected band size 43kDa **B.** The same blot stripped and re-probed for β-actin, expected band size 42kDa. Protein concentration for each lane indicated on the top, arrows indicate location where bands would be expected, molecular markers for protein size are shown on the left.

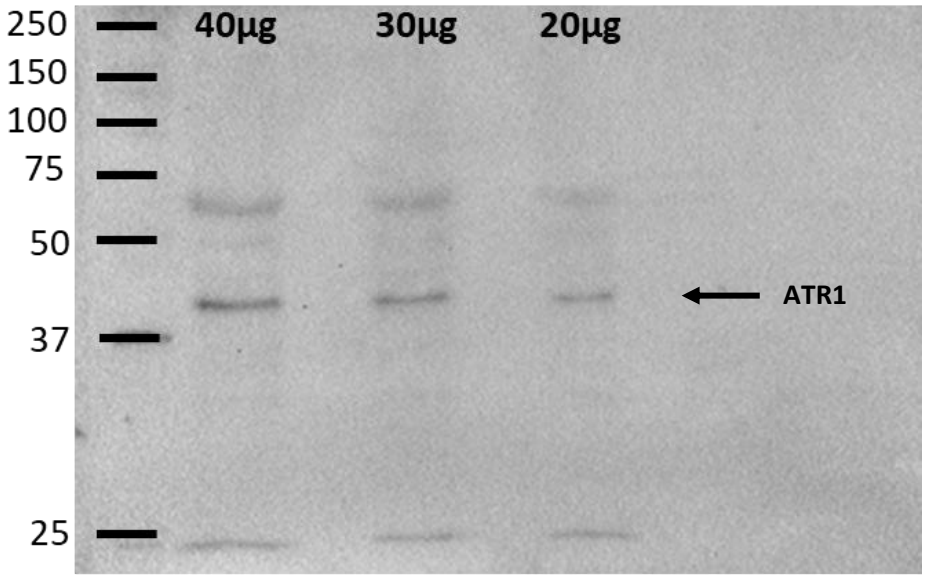

Figure 6.3 The ATR1 is present in the insoluble fraction of AC10 cardiomyocyte cell lysates

Western blot showing various protein concentrations of the whole cell lysate from AC10-CM probed for the ATR1, expected band size 43kDa, arrow indicates location where bands would be expected. Protein concentration for each lane indicated on the top, molecular markers for protein size are shown on the left

6.3.2 Doxorubicin increases the expression of the ATR1 in AC10 cardiomyocytes

The whole cell lysates of AC10-CMs treated with various concentrations of doxorubicin for 24 hours showed an increase in the expression of ATR1 expression relative to vehicle control (Figure 6.4A). Densitometric analyses of the ATR1/β-actin expression ratio shows that ATR1 expression is approximately 2-3 fold higher in AC10-CMs treated with doxorubicin, with the highest increase in expression in AC10-CMs treated with 250nM doxorubicin showing a 4.1 fold increase (Figure 6.5). Although treatment with 500nM doxorubicin did increase ATR1 expression relative to vehicle control, the levels were lower than that observed with 250nM doxorubicin. This observation is similar to that observed when evaluating cytotoxicity (section 4.3.1), suggesting a relationship to cellular viability.

6.4A

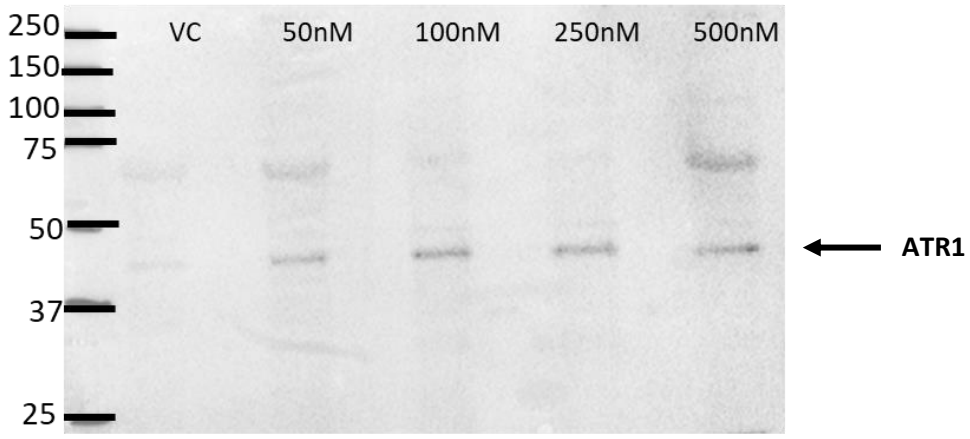

6.4B

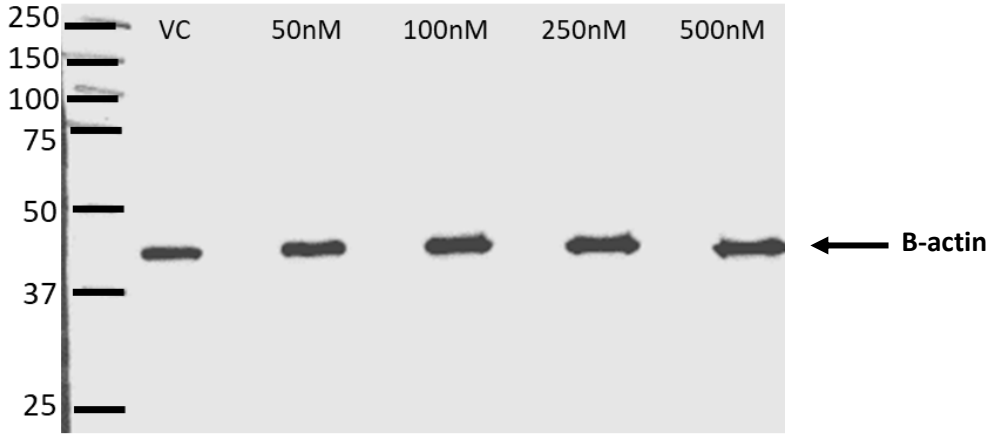

Figure 6.4 Doxorubicin increases the expression of the ATR1 in AC10 cardiomyocytes

A. Representative western blot showing whole cell lysates of AC10-CMs treated with various concentrations of doxorubicin for 24 hours probed for the ATR1, **B.** The same blot stripped and re-probed for β-actin. Concentration of doxorubicin applied to AC10-CMs in each lane indicated on the top (VC = vehicle control), molecular markers for protein size are shown on the left, arrows indicate location where bands would be expected. All images are representative of n=4.

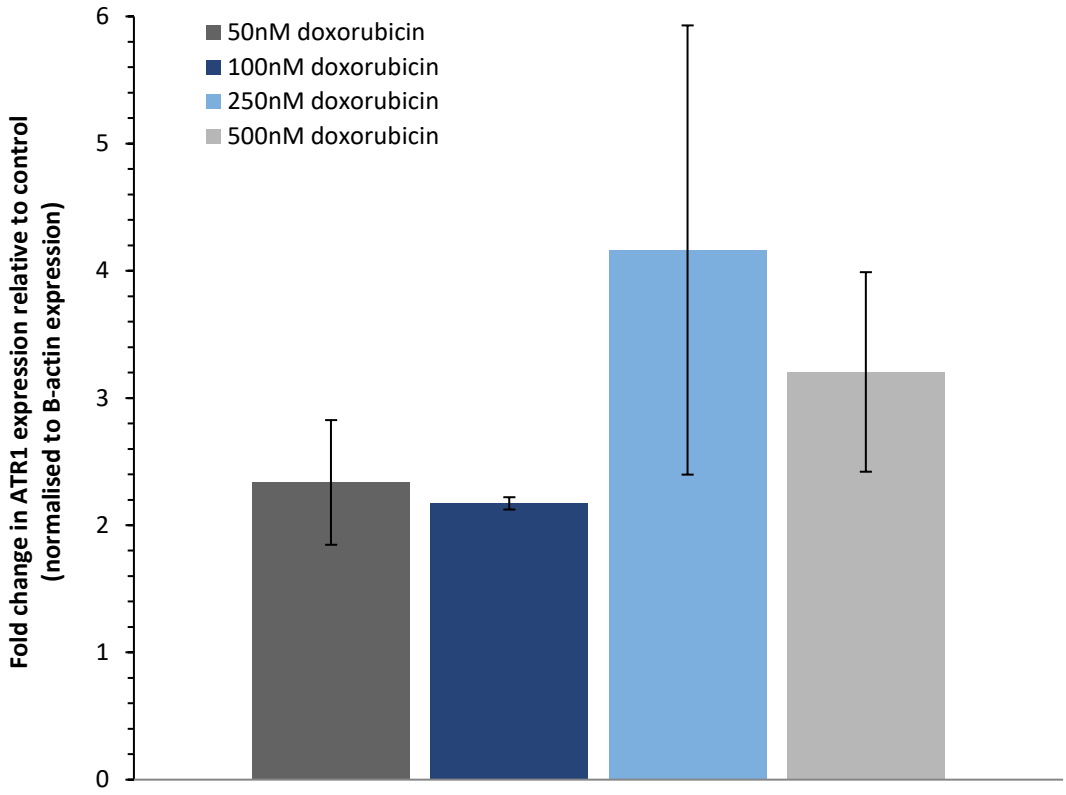

Figure 6.5 Doxorubicin treatment increases the expression of the ATR1 in AC10 cardiomyocytes – Densitometric analysis

Densitometric analysis of 4 individual repeats of the western blot shown in Figure 6.4, showing fold change in ATR1 expression relative to vehicle control (normalised to β-actin expression) (n=4). Errors are calculated as standard errors of the mean.

6.3.3 Pre-array verification of cDNA quality

Prior to conducting qRT-PCR gene arrays, the cDNA quality was ascertained by examining gene expression of a house-keeping gene in the control and treated samples using reverse transcriptase PCR (RT-PCR). Figure 6.6 shows that GAPDH was detected at visibly equal levels in cDNA samples generated from untreated and doxorubicin treated AC10-CMs and therefore is suitable for use in gene array experiments.

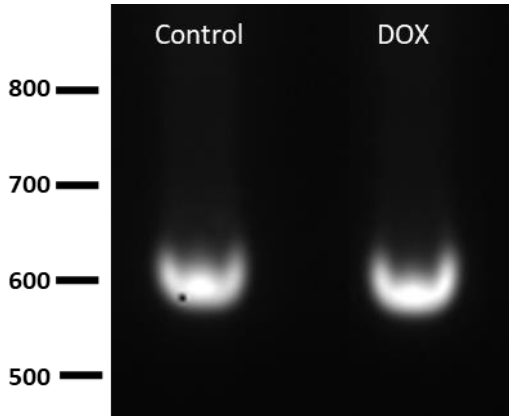

Figure 6.6 GAPDH was detected at equal levels in cDNA generated from untreated and doxorubicin treated AC10 cardiomyocytes

Reverse-transcriptase PCR showing expression of GAPDH in cDNA generated from untreated and doxorubicin treated AC10-CMs, expected band size 598bp. Molecular markers for determination of product size shown on the left.

6.3.4 Doxorubicin alters expression of genes associated with cardiotoxicity in AC10 cardiomyocytes

Changes in gene expression in 84 genes involved in drug induced or chemical cardiotoxicity were assessed following exposure of AC10-CMs to 50nM doxorubicin for 24 hours, of which 21 genes showed greater than 2-fold changes to gene expression (Figure 6.7). This is outlined in figure 6.8 and the full name and function of the proteins encoded by these genes is shown in table 6.2.

	01	02	03	04	05	06	07	08	09	10	11	12
A	ABHD2 -1.04	ABRA 1.72	ACTA1 -1.04	ADRA2A -12.13	AIFM1 1.07	AK3 -1.73	ASH1L -2.00	ATP5J 1.14	BCAT1 -1.65	BGN -1.91	BSN -1.16	BTG2 -1.47
B	CCL7 -1.28	CCR1 -13.45	CD14 -2.60	CFD -1.53	CH25H 2.77	CKM 1.25	COL15A1 -1.66	COL3A1 -1.95	CREM -1.54	CSNK2A2 1.13	DUSP8 -14.62	EGR1 -3.20
C	FCGR2B -2.11	FHL1 -1.69	FOSL1 -1.52	GJA1 -1.40	GPM6A 1.25	HAMP 3.71	HSPA2 1.33	HSPH1 -1.30	IFT20 -1.04	IGFBP5 1.01	IL6 1.88	ITPR2 -1.60
D	KLHL41 -1.20	KLHL40 4.53	KCNJ12 1.25	MCM6 -2.55	MT1F 2.57	NEXN -1.12	NFIB 1.25	PDK4 -1.45	PKN2 -1.51	PLA2G4A -1.73	PLAU -1.28	PLN -1.62
E	BPIFA1 1.25	POSTN 2.36	PPBP 1.25	PPP1R14C 1.25	PRKAB2 -1.16	PSMA2 3.10	PSMD7 1.62	PUM2 1.66	PVR -2.36	RBM3 1.01	REG3G 1.25	RND1 -1.27
F	RPS6KB1 1.60	S1PR2 -1.17	SERPINE1 1.03	SIK1 1.59	SLC4A3 -1.43	SOX4 -4.17	SPP1 2.41	TCF4 1.58	TGFB2 1.60	THRAP3 1.04	TIAM1 -4.89	TIMP1 1.14
G	TUBB6 -1.34	TXNIP 1.29	UBA5 1.99	UBXN2A 2.38	UCK2 1.13	UCP1 11.31	VCAN -1.16	VEGFA 1.89	VIM 2.04	WIPI1 1.66	ZNF148 1.67	ZNF23 1.93

Figure 6.7 Changes in gene expression profile of 84 genes involved in cardiotoxicity following doxorubicin exposure in AC10 cardiomyocytes

Out of 84 genes analysed, 21 showed more than a 2-fold change in gene expression. Increases in gene expression were recorded for 10 genes (green), and decreases in gene expression were recorded for 11 genes (blue) following exposure to 50nM doxorubicin for 24 hours

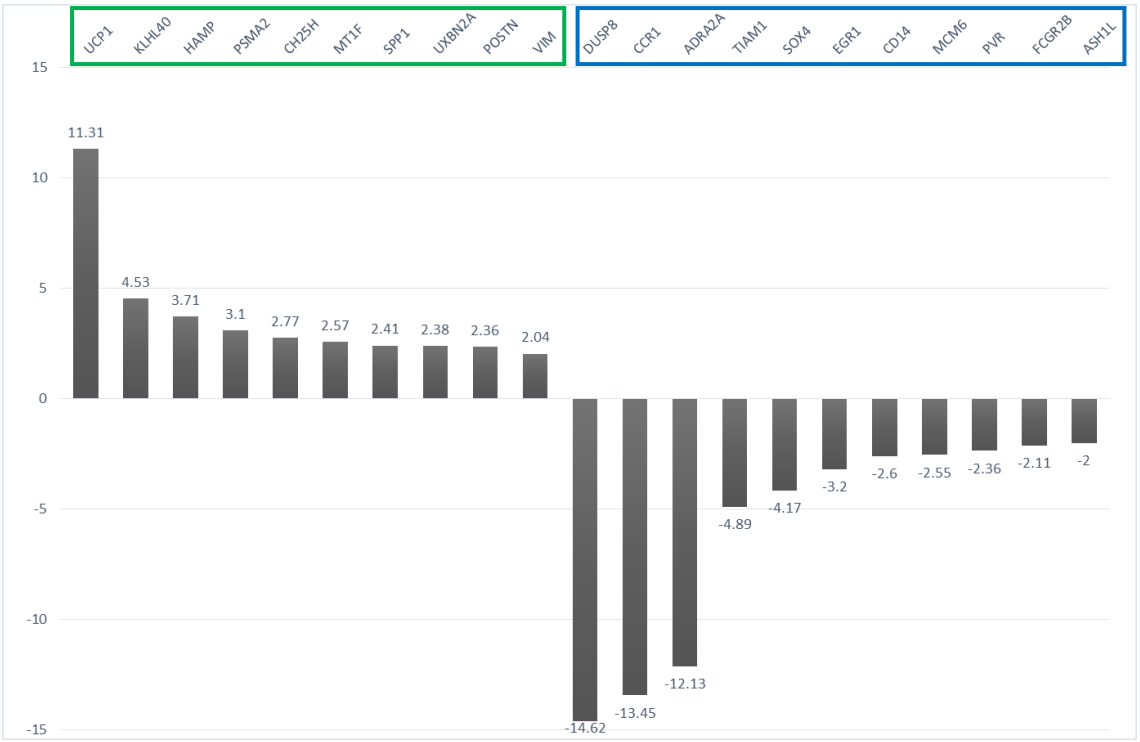

Figure 6.8 Doxorubicin alters expression of genes associated with cardiotoxicity in AC10 cardiomyocytes

Clustered bar graph showing genes with more than a 2-fold change in gene expression. Increases in gene expression were recorded for 10 genes (green), and decreases in gene expression were recorded for 11 genes (blue) following exposure to 50nM doxorubicin for 24 hours

Gene	Full name	Function
UCP1	Uncoupling protein 1 (mitochondrial, proton carrier)	Carries anions and protons between inner and outer mitochondrial membrane
KLHL40	Kelch repeat and BTB (POZ) domain containing 5	Involved in protein-protein interactions, including actin and cullin 3 ubiquitin ligases
HAMP	Hepcidin antimicrobial peptide	Iron regulation and metabolism
PSMA2	Proteasome (prosome, macropain) subunit, alpha type, 2	Mediates ubiquitin-independent protein degradation
CH25H	Cholesterol 25-hydroxylase	Lipid metabolism - Catalyses the formation of 25-hydroxycholesterol from cholesterol
MT1F	Metallothionein 1F	Metal binding protein, plays a role in oxidative stress
SPP1	Secreted phosphoprotein 1	Increased during myocardial dysfunction
UXBN2A	UBX domain protein 2A	Ubiquitin regulatory proteins within the ubiquitination pathway
POSTN	Periostin, osteoblast specific factor	ECM protein that supports cellular adhesion and migration
VIM	Vimentin	Mesenchymal intermediate filament
DUSP8	Dual specificity phosphatase 8	Dephosphorylates and therefore inactivates target kinases, such as MAPKs which are involved in proliferation
CCR1	Chemokine (C-C motif) receptor 1	GPCR involved in recruitment of immune cells to site of inflammation
ADRA2A	Adrenergic, alpha-2A-, receptor	GPCR involved in adrenergic signalling
TIAM1	T-cell lymphoma invasion and metastasis 1	Regulate RHO-like GTPases which are involved in actin dynamics
SOX4	SRY (sex determining region Y)-box 4	Transcription factor involved in embryonic development and determination of cell fate
EGR1	Early growth response 1	Transcription factor
CD14	CD14 molecule	Immune system related co-receptor
MCM6	Minichromosome maintenance complex component 6	Essential for DNA replication, part of DNA unwinding enzyme complex
PVR	Poliovirus receptor	Involved in establishment of intercellular adherens junctions
FCGR2B	Fc fragment of IgG, low affinity IIb, receptor (CD32)	Immune system related co-receptor
ASH1L	Ash1 (absent, small, or homeotic)-like (Drosophila)	Transcriptional activator, regulates gene expression

Table 6.2 Doxorubicin alters expression of genes associated with cardiotoxicity in AC10 cardiomyocytes

Full name and function of the genes with more than a 2-fold change in gene expression. Increases in gene expression were recorded for 10 genes (green), and decreases in gene expression were recorded for 11 genes (blue) following exposure to 50nM doxorubicin for 24 hours

6.3.5 Doxorubicin alters expression of genes associated with GPCR signalling in AC10 cardiomyocytes

Changes in gene expression in 84 genes involved in G-protein coupled receptor (GPCR) signalling were assessed following exposure to 50nM doxorubicin for 24 hours, of which 40 genes showed greater than 2-fold changes to gene expression (Figure 6.9). This is outlined in figure 6.10 and the full name and function of the proteins encoded by these genes is shown in table 6.3.

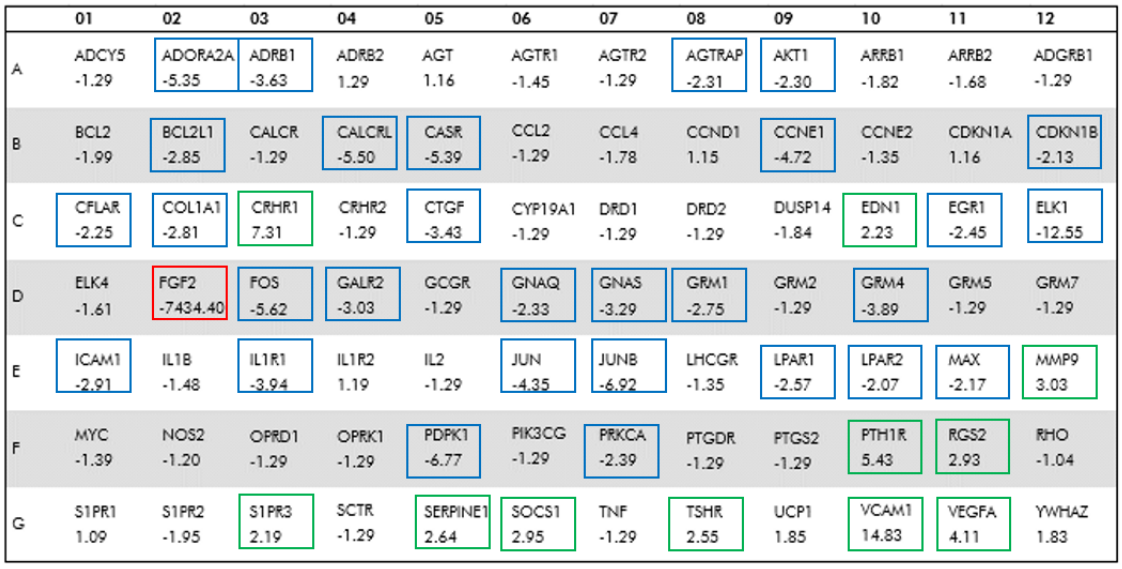

	01	02	03	04	05	06	07	08	09	10	11	12
A	ADCY5 -1.29	ADORA2A -5.35	ADRB1 -3.63	ADRB2 1.29	AGT 1.16	AGTR1 -1.45	AGTR2 -1.29	AGTRAP -2.31	AKT1 -2.30	ARRB1 -1.82	ARRB2 -1.68	ADGRB1 -1.29
B	BCL2 -1.99	BCL2L1 -2.85	CALCR -1.29	CALCRL -5.50	CASR -5.39	CCL2 -1.29	CCL4 -1.78	CCND1 1.15	CCNE1 -4.72	CCNE2 -1.35	CDKN1A 1.16	CDKN1B -2.13
C	CFLAR -2.25	COL1A1 -2.81	CRHR1 7.31	CRHR2 -1.29	CTGF -3.43	CYP19A1 -1.29	DRD1 -1.29	DRD2 -1.29	DUSP14 -1.84	EDN1 2.23	EGR1 -2.45	ELK1 -12.55
D	ELK4 -1.61	FGF2 -7434.40	FOS -5.62	GALR2 -3.03	GCGR -1.29	GNAQ -2.33	GNAS -3.29	GRM1 -2.75	GRM2 -1.29	GRM4 -3.89	GRM5 -1.29	GRM7 -1.29
E	ICAM1 -2.91	IL1B -1.48	IL1R1 -3.94	IL1R2 1.19	IL2 -1.29	JUN -4.35	JUNB -6.92	LHCGR -1.35	LPAR1 -2.57	LPAR2 -2.07	MAX -2.17	MMP9 3.03
F	MYC -1.39	NOS2 -1.20	OPRD1 -1.29	OPRK1 -1.29	PDPK1 -6.77	PIK3CG -1.29	PRKCA -2.39	PTGDR -1.29	PTGS2 -1.29	PTH1R 5.43	RGS2 2.93	RHO -1.04
G	S1PR1 1.09	S1PR2 -1.95	S1PR3 2.19	SCTR -1.29	SERPINE1 2.64	SOCS1 2.95	TNF -1.29	TSHR 2.55	UCP1 1.85	VCAM1 14.83	VEGFA 4.11	YWHAZ 1.83

Figure 6.9 Changes in gene expression profile of 84 genes involved in GPCR signalling following doxorubicin exposure in AC10 cardiomyocytes

Out of 84 genes analysed, 40 showed more than a 2-fold change in gene expression. Increases in gene expression were recorded for 11 genes (green), and decreases in gene expression were recorded for 29 genes (blue) following exposure to 50nM doxorubicin for 24 hours. The gene shown in red was omitted due to the unusually large fold change recorded.

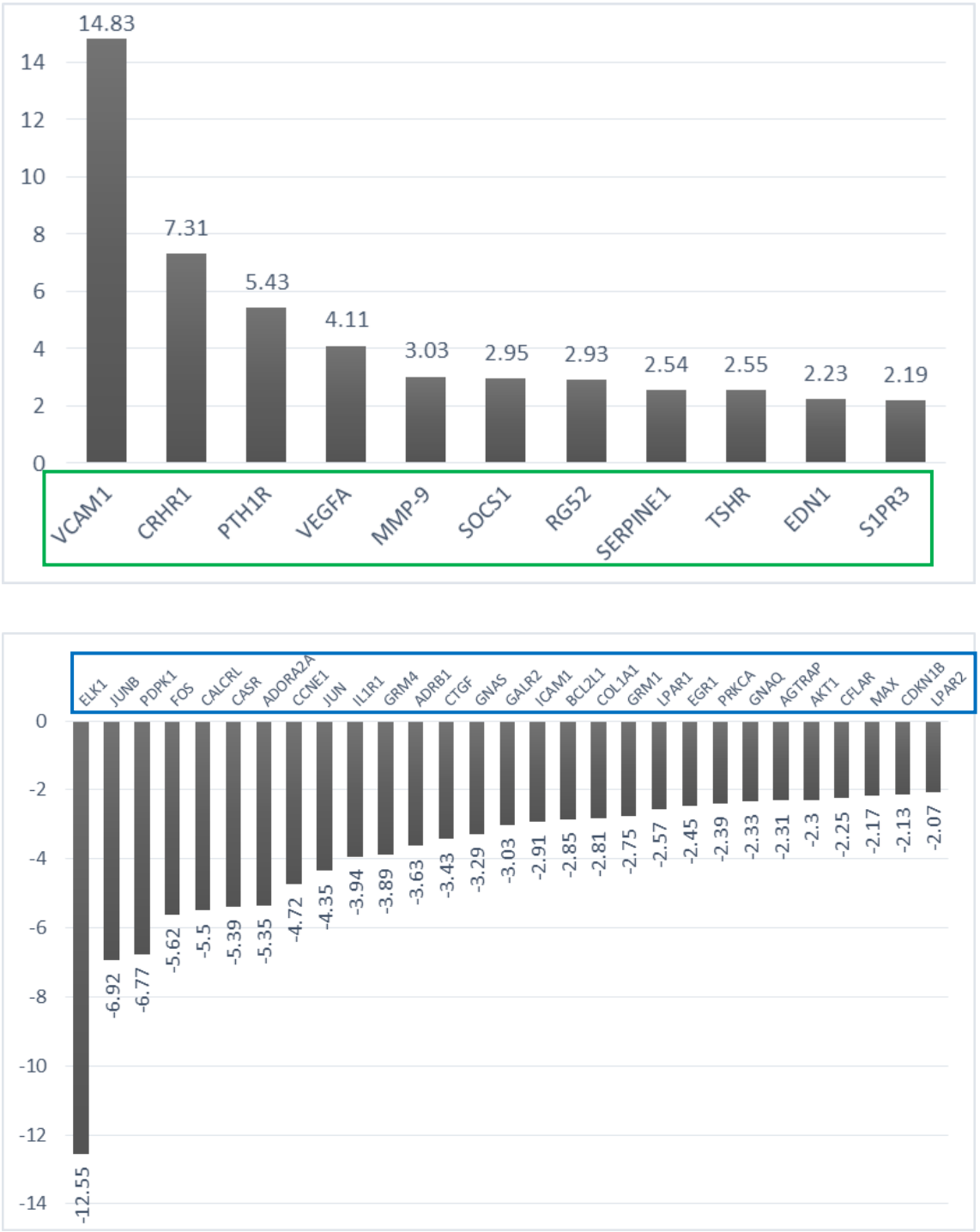

Figure 6.10 Doxorubicin alters expression of genes associated with GPCR signalling

Clustered bar graph showing genes with more than a 2-fold change in gene expression. Increases in gene expression were recorded for 11 genes (green), and decreases in gene expression were recorded for 29 genes (blue) following exposure to 50nM doxorubicin for 24 hours.

Gene	Full name	Function
VCAM1	Vascular cell adhesion molecule 1	Cell adhesion molecule that is also involved in signal transduction in epithelial cells
CRHR1	Corticotropin releasing hormone receptor 1	Important mediators in the stress response
PTH1R	Parathyroid hormone 1 receptor	GPCR involved in calcium ion homeostasis
VEGFA	Vascular endothelial growth factor A	Signalling protein that stimulates angiogenesis
MMP-9	Matrix metalloproteinase 9	Involved in the degradation of the extracellular matrix
SOCS1	Suppressor of cytokine signalling 1	Down-regulate cytokine signalling
RGS2	Regulator of G-protein signalling 2, 24kDa	Increases activity of the Gα subunit
SERPINE1	Serpin peptidase inhibitor, clade E (nexin, plasminogen activator inhibitor type 1), member 1	Inhibitor of tissue plasminogen activator (tPA)
TSHR	Thyroid stimulating hormone receptor	Stimulates production of thyroxine and triiodothironine
EDN1	Endothelin 1	Precursor of the vasoconstrictor endothelin
S1PR3	Sphingosine-1-phosphate receptor 3	GPCR involved in vascular endothelial cell function
ELK1	ELK1, member of ETS oncogene family	Transcription factor involved in MAPK signalling
JUNB	Jun B proto-oncogene	Component of the AP-1 transcription factor
PDPK1	3-phosphoinositide dependent protein kinase-1	Kinase involved in signal transduction
FOS	FBJ murine osteosarcoma viral oncogene homolog	Component of the AP-1 transcription factor
CALCRL	Calcitonin receptor-like	GPCR involved in calcium ion homeostasis
CASR	Calcium sensing receptor	GPCR involved in calcium ion homeostasis
ADORA2A	Adenosine A2a receptor	GPCR involved in vasodilation
CCNE1	Cyclin E1	Co-ordination of the cell cycle
JUN	Jun proto-oncogene	Transcription factor
IL1R1	Interleukin 1 receptor, type I	Cytokine receptor involved in inflammatory response

Table 6.3 Doxorubicin alters expression of genes associated with GPCR signalling in AC10 cardiomyocytes (1)

Full name and function of the genes with more than a 2-fold change in gene expression. Increases in gene expression were recorded for 11 genes (green), and decreases in gene expression were recorded for 29 genes (blue) following exposure to 50nM doxorubicin for 24 hours.

Gene	Full name	Function
GRM4	Glutamate receptor, metabotropic 4	Linked with inhibition of cyclic AMP signalling
ADRB1	Adrenergic, beta-1-, receptor	GPCR involved in adrenergic signalling
CTGF	Connective tissue growth factor	ECM protein involved in cell adhesion, proliferation and migration
GNAS	GNAS complex locus	Component of a G-protein alpha sub-unit
GALR2	Galanin receptor 2	Neuromodulatory GPCR
ICAM1	Intercellular adhesion molecule 1	Stabilises cell-cell interactions
BCL2L1	BCL2-like 1	Apoptosis regulation
COL1A1	Collagen, type I, alpha 1	Component of connective tissue
GRM1	Glutamate receptor, metabotropic 1	Linked with inhibition of cyclic AMP signalling
LPAR1	Lysophosphatidic acid receptor 1	GPCR involved in encouraging cell division
EGR1	Early growth response 1	Transcription factor
PRKCA	Protein kinase C, alpha	Protein kinase involved in diverse cellular signalling pathways
GNAQ	Guanine nucleotide binding protein (G protein), q polypeptide	Involved in activation of G-protein subunits
AGTRAP	Angiotensin II receptor-associated protein	Negatively regulates angiotensin II signalling
AKT1	V-akt murine thymoma viral oncogene homolog 1	Protein kinase involved in diverse cellular signalling pathways
CFLAR	CASP8 and FADD-like apoptosis regulator	Regulator of apoptosis
MAX	MYC associated factor X	Transcription factor
CDKN1B	Cyclin-dependent kinase inhibitor 1B (p27, Kip1)	Cell cycle inhibitor protein
LPAR2	Lysophosphatidic acid receptor 2	GPCR involved in Calcium mobilisation

Table 6.3 Doxorubicin alters expression of genes associated with GPCR signalling in AC10 cardiomyocytes (2)

Full name and function of the genes with more than a 2-fold change in gene expression. Increases in gene expression were recorded for 11 genes (green), and decreases in gene expression were recorded for 29 genes (blue) following exposure to 50nM doxorubicin for 24 hours.

6.4 Discussion

The purpose of this phase of the project was to build on evidence indicating that blockade of the angiotensin type 1 receptor (ATR1) reduces anthracycline-induced hypertrophy of *in vitro* cardiomyocyte models. By appreciating the molecular changes involved in these activities the objective is to better understand the interaction between angiotensin signalling and anthracycline-induced cardiotoxicity (AIC).

The reduction in structural changes is thereby postulated to be due to direct interaction of angiotensin receptor blockers (ARB) with the ATR1 on cardiomyocytes. This is supported by observations in earlier phases of this study including angiotensin II induced hypertrophy of AC10-CMs and reduction of doxorubicin induced hypertrophy by angiotensin receptor blockade. Embedded within the cell membrane, the ATR1 is a G-protein coupled receptor (GPCR) responsible for mediating cellular responses to angiotensin II.[76,231]

6.4.1 Analysis of ATR1 expression in AC10 cardiomyocytes

In order to address this hypothesis is was thus important to evaluate selective expression of ATR1. The structural similarities between receptors that constitute the GPCR receptor family is reported to complicate their individual analysis, so this study evaluated ATR1 expression using an antibody against the extracellular N-terminus of the receptor, an epitope associated with part of ATR1 responsible for binding angiotensin II. Several studies have shown many of the residues that form this section of the receptor to be unique to ATR1,[285] unlike other receptor areas (such as the intracellular loops and C-terminus), as these areas are more structurally similar to other GPCRs.[286]

The ATR1 receptor protein was undetectable in the soluble fraction of the cell lysate of AC10-CMs; however was easily detectable when the whole cell lysate (which contains both soluble

and insoluble proteins) was used, with bands of expected size detected in samples containing as little as 20µg of protein from the whole cell lysate of AC10-CMs. Analysis of the expression of the ATR1 following exposure of AC10-CMs to doxorubicin for 24 hours revealed that the expression of the ATR1 relative to the vehicle control was approximately 2-3 fold higher in AC10-CMs treated with doxorubicin, with the highest increase in expression in AC10-CMs treated with 250nM doxorubicin where a 4.1 fold increase was observed. Although treatment with 500nM doxorubicin did increase ATR1 expression relative to vehicle control, the levels were lower than that observed with 250nM doxorubicin. This observation is similar to that observed when evaluating cytotoxicity suggesting a relationship to cellular viability. The increase in expression of the ATR1 in cells treated with doxorubicin may also cause increased levels of angiotensin signalling which will be discussed further later.

A recent study conducted by Huang *et al*. also reported upregulation of the ATR1 following doxorubicin treatment in the rat myoblast H9c2 cell line.[287] The increase in ATR1 expression was also found to occur in both a time dependent and dose dependent manner, albeit it at levels significantly higher than clinical cardiac exposures. These findings are in accordance with the results of the current study, however using a rodent rather than human derived cell line. The rodent study also provided further direct evidence of an interaction between doxorubicin-induced cardiotoxicity and increased angiotensin signalling, as levels of the G-protein Gαq also increased after doxorubicin treatment, substantiating the involvement of angiotensin signalling in doxorubicin induced cardiotoxicity.[287]

6.4.2 Molecular interactions between angiotensin signalling and anthracycline-induced cardiotoxicity

In order to elucidate the mechanisms by which anthracyclines facilitate angiotensin involvement, as being either direct induction of ATR1 or a consequence of perturbation of a subcellular signalling pathway, it was important to examine doxorubicin effects upon cardiomyocyte pathways. Changes in gene expression of 84 genes involved in drug induced or chemical cardiotoxicity were assessed following exposure of AC10-CMs to subclinical levels of doxorubicin, of which 21 genes showed greater than 2-fold changes to gene expression. Additionally, of the 84 genes involved in GPCR signalling evaluated, doxorubicin-induced greater than 2-fold changes relative to control cells in 40 genes. For the purposes of this project a selection of genes were chosen from each array and appraised with respect to their potential impact on anthracycline-induced cardiotoxicity (AIC) and relationship to angiotensin signalling.

6.4.2.1 Gene changes relating to anthracycline-induced cardiotoxicity mechanisms

It is well reported that doxorubicin induces oxidative stress within cardiomyocytes.[16,34,91] One of the highest changes in gene expression was observed in UCP1, an uncoupling protein and mitochondrial transporter responsible for decreasing the proton gradient associated with oxidative phosphorylation.[288] Therefore, unsurprisingly, doxorubicin alters mitochondrial bioenergetics and alters proteins involved with physiological regulation of ROS.

Similarly, doxorubicin increases expression of the regulator of iron homeostasis Hepcidin antimicrobial peptide (HAMP), involved in inhibiting the iron transport protein ferroportin and transport of iron outside the cell.[289] Disruption of this gene is indicative of altered cardiomyocyte iron handling, culminating in formation of doxorubicin-iron complexes, formation of ROS through its association with the inner mitochondrial membrane (See section 1.7.1.1.1), further

adding to cardiomyocyte oxidative stress and the effects manifested through UCP1 dysregulation.

Doxorubicin changes in cardiomyocyte structure and subsequent cardiac hypertrophy are also reflected in genetic changes observed in treated AC10-CMs. The reduced expression of dual specificity phosphatase 8 (DUSP8) is associated with increased activity of MAPK signalling pathways, strongly associated with regulation of cardiac hypertrophy and remodelling in response to increased workload or pathological insults.[290] Similarly, increased gene expression of the proteasomal subunit PSMA2 and proteins involved in the ubiquitination pathway (UXBN2A) following doxorubicin treatment indicates an increase in cellular proteolytic activities, linked to restructuring of contractile and structural proteins in cardiomyocytes.[291] The observation that expression of the transcription factor SOX4 was downregulated also adds to the cardiac remodelling aspects of doxorubicin-induced toxicity, through its role in controlling cell fate and cardiac development, and thus cardiomyocyte differentiation and sensescence.[292]

Transcriptional repression is also an effect of anthracycline treatment, which can affect the expression of critical genes in cardiomyocytes.[293] For example, JUNB is reported to be essential in maintenance of sarcomeric Z-disc structure and therefore crucial in maintaining sarcomere architecture and function.[294] Indeed in the current study the transcription factors ELK1, JUNB, FOS and EGR1 showed reduced expression which may relate to reductions in the expression of genes that are essential for cardiomyocyte function.

6.4.2.2 Gene changes relating to anthracycline-induced cardiotoxicity and angiotensin signalling

The induction of matrix metalloproteinase-9 (MMP-9) gene expression by doxorubicin adds to the structural remodelling activities of doxorubicin. The MMPs are central mediators of cellular remodelling such as ventricular dilation in the clinic.[295] Indeed, increased MMP activity is

associated with chronic doxorubicin cardiotoxicity and a recent study has linked acute doxorubicin treatment to increases in MMP-2 activity.[296] Unfortunately, MMP-2 was not evaluated in the current study. Importantly for this study, angiotensin II treatment is also reported to increase expression of MMP-9 in a monocyte cell line,[297] and also in rats in the context of cardiac hypertrophy[298] thus the increase in MMP-9 gene expression in the current study supports synergism between AIC and angiotensin signalling.

Corticotropin-releasing hormone receptor 1 (CRHR1) is also upregulated by doxorubicin in cardiomyocytes, with an involvement in the response to stress. Although this protein is primarily located in the nervous system, it is expressed at lower levels in other tissues including the heart.[299] Many studies have related angiotensin II exposure increases expression of CRHR1 or its agonist corticotrophin releasing hormone (CRH), and found that antagonism of the ATR1 reduces the levels of the receptor and agonist.[300] In addition CRHR1 has been linked to local inflammatory responses,[301] which links ATR1 activation with the occurrence of doxorubicin-induced hypertrophy in the current study.

One of the greatest genes upregulated in AC10-CMs following doxorubicin exposure when analysing the GPCR signalling pathway is vascular cell adhesion molecule 1 (VCAM1). This gene codes for an adhesion molecule on endothelial cells, with a central role in atherosclerotic lesion formation.[302] Interestingly, Pueyo *et al*. have shown angiotensin II stimulates both gene and protein expression of VCAM-1 via signalling through the ATR1 and relates to induction of intracellular oxidative stress.[303] Consequently, this suggests a mechanism for activation of the ATR1 as a response to doxorubicin independent of angiotensin II activity. As stimulation of VCAM-1 is associated with induction of intracellular oxidative stress which is a cardiotoxicity mechanism of anthracyclines this also suggests a link between angiotensin signalling and AIC.

6.4.2.3 Gene changes relating to angiotensin signalling

Changes in gene expression of components required for angiotensin signalling were also observed following exposure to doxorubicin. For example the regulator of G-protein signalling 2 (RGS2) which is involved in increasing activity of the Gα subunit[304] showed increased expression. This is in agreement with the study by Huang *et al.* who reported that the levels of the G-protein Gαq increased after doxorubicin treatment, substantiating the involvement of angiotensin signalling in doxorubicin-induced cardiotoxicity.[287] Similarly in the current study, expression of Angiotensin II receptor-associated protein (AGTRAP) decreased; AGTRAP is believed to negatively regulate angiotensin signalling[305] therefore decreased expression suggests an increase in angiotensin signalling in response to doxorubicin treatment. However some genes that would be associated with increased angiotensin signalling decreased following doxorubicin treatment, such as GNAS and GNAQ which form components of G-protein alpha sub-units[306] and are involved in the activation of G-protein subunits[307] respectively.

Genes usually stimulated by angiotensin II were also found to increase following doxorubicin treatment which suggests a link between angiotensin signalling and AIC. For example endothelin-1 gene expression increased following doxorubicin exposure; endothelin-1 is a vasoconstrictor that was found to be stimulated by angiotensin II in rat smooth muscle cells.[308]

Similar to the study described above, angiotensin II has been found to stimulate expression of Parathyroid hormone receptor 1 (PTH1R) via the ATR1 in the kidney where it has damaging effects[309] and angiotensin II also stimulates VEGF gene expression in rat heart endothelial cells, inhibited by addition of the ATR1 antagonist losartan.[310] In this study, both PTHR1R and VEGFA were found to be upregulated following doxorubicin treatment, thereby providing further evidence for upregulation of angiotensin signalling as a consequence of doxorubicin therapy.

A large decrease in gene expression of the α2A-adrenergic receptor (ADRA2A) and β1 adrenergic receptor (ADRB1) was reported in the current study following doxorubicin treatment. This may

also relate to angiotensin signalling as previous work in neonatal rat cardiomyocytes concluded that angiotensin II down-regulated mRNA levels of the α1A-adrenergic receptor, which was ATR1 dependent.[311] This also suggests a mechanism for activation of the ATR1 as a response to doxorubicin independent of angiotensin II activity.

Although some of the changes in gene expression are more difficult to specifically relate to angiotensin signalling or doxorubicin cardiotoxicity, the results in this section provide preliminary evidence that treatment of AC10-CMs with doxorubicin causes changes in gene expression that relate both to the cardiotoxicity mechanisms of anthracyclines and increased levels of angiotensin II signalling. In addition, there appears to be some areas of overlap between genes involved in anthracycline cardiotoxicity and genes stimulated by angiotensin signalling, which cause similar cellular effects (Figure 6.11). This implicates angiotensin signalling as having a direct effect on cardiomyocytes and potentiating the pathogenesis of doxorubicin mediated cardiotoxicity. As these results are preliminary, further work is needed to verify the changes in gene expression discussed, the work described herein is indicative of dysregulated pathways however further analyses are required to ascertain significance.

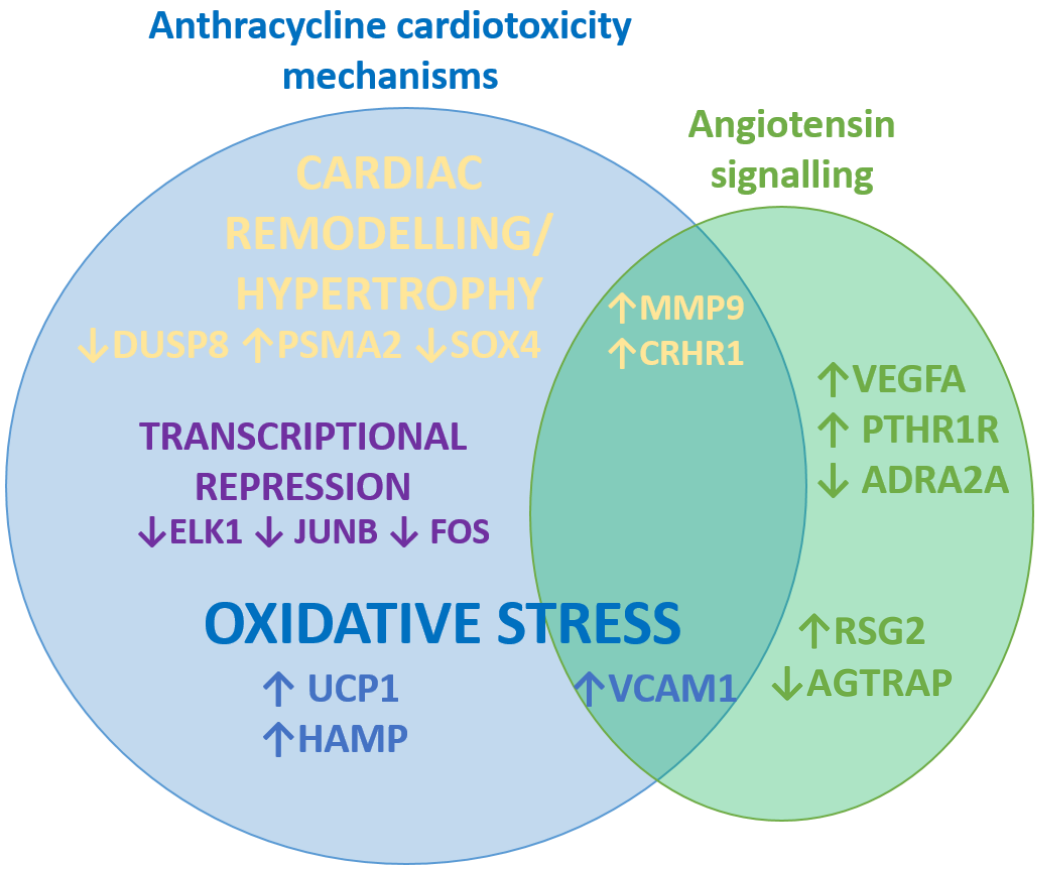

Figure 6.11 **Molecular changes in doxorubicin treated AC10 cardiomyocytes that potentially signify a relationship between anthracycline-induced cardiotoxicity and the angiotensin signalling pathway via the ATR1**

6.4.3 Conclusion

The purpose of this phase of the project was to build on evidence from the previous chapter indicating that blockade of the angiotensin type I receptor (ATR1) reduces doxorubicin induced hypertrophy and increases survival of *in vitro* cardiomyocyte models. Treatment of AC10-CMs with doxorubicin caused a 2-3 fold increase in the level of ATR1, activation of which may occur due to the biomechanical stress caused by doxorubicin-induced hypertrophy. In addition to increased expression of the ATR1, doxorubicin treatment also caused changes in gene expression relating to the drug's mechanisms of cardiotoxicity and indicative of induction of angiotensin signalling.

In addition, there appears to be some areas of overlap between genes with altered expression that are involved in both anthracycline cardiotoxicity mechanisms and genes stimulated by angiotensin signalling; which cause similar cellular effects including increased oxidative stress, cellular remodelling and hypertrophy. Although further work is needed to verify and add to the changes in gene expression discussed, the work described implicates angiotensin signalling as having a direct effect on cardiomyocytes and potentiating the pathogenesis of doxorubicin mediated cardiotoxicity. This suggests synergism between doxorubicin induced cardiotoxicity and angiotensin signalling and supports the use of these pharmaceuticals such as angiotensin receptor blockers for protection against doxorubicin-induced cardiotoxicity.

Chapter 7: Final discussion

The cardioprotective potential of therapies that act on the angiotensin signalling pathway has been demonstrated in recent clinical studies,[152] which strongly suggests that a relationship exists between anthracycline-induced cardiotoxicity (AIC) and angiotensin signalling (See table 1.2). Although a number of *in vivo* studies have added further support for the cardioprotective nature of these drugs,[257,258,260,263] there is a lack of *in vitro* studies, and the molecular mechanisms underpinning the cardioprotective mechanisms are currently unclear. The overall aim of this study was to investigate the structural and functional cardiotoxicities caused by anthracyclines using *in vitro* models paired with impedance-based technology, and to ascertain if toxicity mitigation was detectable in these models upon concomitant administration of drugs that perturb angiotensin signalling.

Initially the *in vitro* cardiomyocyte cell models (AC10 cardiomyocyte cell line (AC10-CMs) and hiPSC-derived cardiomyocytes (hiPSC-CMs)) were developed and qualified for use in the *in vitro* assessment of structural and functional drug-induced cardiotoxicity, using impedance-based methodologies.[205,210] Changes in cellular viability, morphology and functionality were assessed using impedance-based detection (xCELLigence technology) in response to the cardiac regulatory factor angiotensin II and the anti-cancer drug sunitinib. Overall, both cell models responded as clinically expected to both agents and both structural cardiotoxicity and functional changes to cell behaviour were observed.

As a well known mediator of cardiac hypertrophy angiotensin II was used to qualify the *in vitro* models for detection of structural cardiotoxicity.[228] Changes in morphology indicative of a hypertrophic response was detected in AC10-CMs and hiPSC-CMs following addition of physiologically relevant doses of angiotensin II, and analysis of contractility of hiPSC-CMs uncovered functional disturbances immediately after angiotensin II addition. The increases in

beat number and decreases in beat amplitude observed immediately after angiotensin II addition are in agreement with previous studies which reported positive chronotropy and negative inotropy in isolated rat cardiomyocyte cultures following exposure to angiotensin II for a few minutes.[230]

The anti-cancer drug sunitinib is associated with numerous cardiotoxicities including development of arrhythmias, hypertension and impairments to ventricular function.[98] As a well known functional cardiotoxicant and mediator of cardiac hypertrophy, it was used to qualify the *in vitro* models used in this study for detection of functional and structural cardiotoxicity. Induction of dose-dependent hypertrophy was observed following repeated addition of clinically relevant concentrations of sunitinib in AC10-CMs and hiPSC-CMs, with all three concentrations of sunitinib causing an immediate and sustained increase in cell index. Analysis of contractility in the hiPSC-CMs revealed that sunitinib also caused dose-dependent decreases in beat number and increased beat amplitude with 500nM sunitinib following 72 hour exposure. The changes observed in cell morphology and contractility are in agreement with other studies, for example Doherty *et al*. reported an enlarged hypertrophic like cell shape of hiPSC-CMs following exposure to 3µM sunitinib for 48 hours, and dose-dependent reductions in beat rate following 2 hours and 24 hours exposure to 625nM, 2.5µM and 10µM sunitinib.[232]

This study is the first to demonstrate both angiotensin II induced hypertrophy and sunitinib induced hypertrophy using impedance based systems and the *in vitro* AC10-CM and hiPSC-CM using human derived cell models. Previously, many *in vitro* studies involving angiotensin II have been conducted on primary cardiomyocytes from animals. Therefore the findings from the current study possess significant 3R's benefits as they demonstrate that the human derived *in vitro* models used are able to respond as expected to the hypertrophic mediator and therefore may replace or reduce the use of primary cardiomyocytes from animal sources for these purposes which require difficult culture techniques and animal sacrifice.[218]

In contrast to previous studies, where hypertrophy was detected at higher sunitinib concentrations, this study identified sunitinib hypertrophy at lower clinically relevant doses over prolonged periods that are more reflective of clinical exposures. This illustrates the utility of the xCELLigence systems to detect morphology changes to AC10-CMs and hiPSC-CMs in a manner that is translational to the clinical setting. The use of these *in vitro* models for detection of hypertrophy extends towards improved pre-clinical testing of pharmaceuticals as a means for early identification of structural cardiotoxicity. As mentioned in earlier chapters, the current method of pre-clinical testing for cardiac liabilities focusses narrowly on the ability of compounds to block the hERG potassium channel *in vitro*, followed by evaluation of the ability to prolong ventricular repolarisation and therefore prolong the QT-interval *in vivo.*[177] This screening strategy completely overlooks the development of structural changes, which are associated with a number of cancer therapeutics with the potential to cause cardiovascular liabilities.[29,34] Structural changes can have a huge impact on the pumping ability of the heart, therefore early identification of the problem is of crucial importance.

Further qualification for the use of the methods developed in chapter 3 for identification of structural cardiotoxicity is necessary and could be achieved by comparison of the effects of a known cardiotoxicant (such as sunitinib) and a drug that is not associated with clinical cardiotoxicity using the methods developed in chapter 3. A recent paper by Sharma *et al.* used hiPSC-CMs generated from 11 healthy individuals and 2 patients receiving cancer treatment, to screen tyrosine kinase inhibitors (TKI) for cardiotoxicities by measuring alterations in cardiomyocyte viability, contractility, electrophysiology, calcium handling, and signalling. Using this data, a cardiac safety index was generated to reflect the cardiotoxicities of the TKIs tested.[312] In agreement with clinical observations and the current study, sunitinib was assigned a relatively low cardiac safety index score, indicating that it has a high association with cardiotoxicity. Interestingly axitinib, a TKI with similar therapeutic targets to sunitinib, was not associated with

any cardiotoxicity occurrence, and therefore may be a suitable choice for future studies to further qualify these models for identification of structural cardiotoxicity.

Although cardiomyocytes are the cell type in the heart responsible for contraction and therefore gain a lot of attention in the area of pre-clinical screening for cardiotoxic effects, there are other cell types in the heart which may also be a target of drug-induced cardiotoxicity.[53] Pericytes were identified as a cellular target associated with sunitinib cardiotoxicity by Chintalgattu *et al*., where sunitinib treated mice developed coronary microvascular dysfunction and exhibited an impaired cardiac response to stress. These physiological changes were accompanied by a substantial depletion of coronary microvascular pericytes; whose function is dependent on platelet derived growth factor receptor (PDGFR) signalling. Sunitinib induced pericyte depletion and coronary microvascular dysfunction were recapitulated by a structurally distinct PDGFR inhibitor therefore confirming the role of PDGFR in pericyte survival and PDGFR inhibition in pericyte related sunitinib induced cardiotoxicity.[102] On a similar note, the co-culture of rat cardiomyocytes with fibroblasts was found to enhance cardiomyocyte hypertrophy in response to angiotensin II.[229] These examples illustrate both the importance of paracrine signalling in normal physiological functioning of the heart and the crucial role of support cells such as fibroblasts and pericytes which are also a target for drug-induced cardiotoxicity. The inclusion of other cell types in addition to cardiomyocytes in pre-clinical cardiotoxicity screening would allow for a more complete assessment of the cardiotoxic potential of drugs, and would be useful to include within screening paradigms.

The previously developed *in vitro* models and methods were used to determine if the structural and functional acute cardiotoxicity induced by the notoriously cardiotoxic anthracyclines can be recapitulated *in vitro*. Changes in cellular viability, morphology and functionality were assessed using impedance-based detection (xCELLigence technology) in response to the anthracyclines

doxorubicin, daunorubicin and epirubicin. Overall, all of the anthracyclines induced structural changes in both cell models and functional changes to cell behaviour were also observed.

The induction of hypertrophy that was observed in AC10-CMs and hiPSC-CMs following exposure to clinically relevant doses of doxorubicin demonstrates the detection of structural cardiotoxicity which may relate to the inflammatory acute cardiotoxicity response of doxorubicin. This manifests as transient arrhythmias and inflammation and may be involved in increasing susceptibility to the more severe chronic forms of cardiotoxicity.[141,144] The morphological changes to hiPSC-CMs were paired with altered contractility within 24 hours for all doses of doxorubicin used, and changes in contractility with the highest dose (250nM) applied were detected following just 6 hours exposure. Although the effects of doxorubicin on hiPSC-CMs has been assessed by many groups previously, the main focus was primarily on identifying changes to beat parameters using higher doses of doxorubicin.[249] This approach lacks clinical significance as the doses used are much higher than exposure levels in the body and are toxic to cells; therefore cell death occurs which makes acute toxicity responses such as hypertrophy difficult to ascertain. The results of the current work have shown that it is possible to detect both hypertrophy and contractile disturbances in human derived cell types using novel methodologies permissive of real-time and physiologically relevant analyses; with cellular changes occurring in response to clinically relevant concentrations of doxorubicin in as little as 6 hours. Thus providing additional data to support the use of these cells on an impedance-based platform in screening assays for detection of structural toxicity.

Very similar results were obtained when clinically relevant concentrations of doxorubicin, epirubicin and daunorubicin were compared using the same methodology. Little distinction was observed between the toxicity profiles attained for these anthracyclines where studies revealed similar IC_{50} values in AC10-CMs, similar levels of hypertrophy in AC10-CMs and hiPSC-CMs and similar aberrations to contractility following 24 hours exposure to anthracyclines. The lack of

distinction between the severity of toxicity induced by the anthracyclines does not align with the current clinical view that epirubicin is less cardiotoxic than doxorubicin.[237] However there are many additional factors, both pharmacokinetic and pharmacodynamic, that influence the development of clinical cardiotoxicity,[253] which are not accounted for using *in vitro* cardiomyocyte models. An interesting addition to the current study would be to utilise 3D cardiomyocyte spheroid models and imaging techniques to assess if anthracycline treatment causes enlargement (hypertrophy) of the spheroids.[198] Spheroid models more accurately recapitulate the *in vivo* cellular morphology and physiology than that of the more commonly used 2D cell models and are often developed to constitute different cell types (such as fibroblasts and endothelial cells).[197] Studies in cardiomyocytes, endothelial cells and fibroblasts isolated from neonatal rat hearts found that fibroblasts and endothelial cells were more sensitive to doxorubicin-induced cardiotoxicity than cardiomyocytes, thus illustrating that adverse effects following anthracycline exposure also in occur in other cell types of the heart.[255] Therefore the use of multicellular spheroid models would allow for the influence of these cell types on anthracycline-induced hypertrophy in a physiologically relevant manner.

Following detection of anthracycline-induced hypertrophy using *in vitro* cardiomyocyte models the possibility of using pharmaceuticals to reduce the hypertrophy and improve cell survival was explored. The mitigation of doxorubicin-induced cardiotoxicity using drugs that perturb angiotensin signalling has been investigated in both clinical studies[135,152,164,166,167] and pre-clinically *in vivo*[257,258,260,263] with encouraging results, however the number of *in vitro* studies in this area remains limited. In addition, the direct effects upon and involvement of the cardiac system, as well as the molecular mechanism of cardioprotection have yet to be resolved. To address these issues the formerly developed *in vitro* models and methods were used to determine if the previously elucidated structural and functional acute toxicity induced by doxorubicin in these models can be reduced by drugs that reduce angiotensin signalling. Changes in cellular viability, morphology and functionality were assessed using impedance-

based detection (xCELLigence technology) in response to the doxorubicin alone and in combination with drugs that augment angiotensin signalling. Angiotensin receptor blockers (ARB) increased cell viability of AC10-CMs and reduced the hypertrophic responses of both cell models treated with doxorubicin, whereas angiotensin converting enzyme inhibitors (ACEi) had no protective effects.

Due to the mechanism of action of ACEi it is unlikely that they would have been functionally active in the cell models used in this study (Discussed in section 5.4.2), therefore the protective effects that have been previously demonstrated in clinical and *in vivo* studies were not present in this *in vitro* study. This is because in more complex models (*in vivo*) all of the elements required for angiotensin synthesis would be present, therefore in these models ACEi would be able to decrease angiotensin signalling, whereas in the current study the ACEi had no cellular target.[231,268] The lack of direct interaction of ACEi with cardiomyocytes is illustrated in toxicity studies where the compounds alone exhibited negligible toxicity to AC10-CMs. In contrast, addition of the ARB telmisartan and losartan at 10μM yielded survival rates of 84% and 70% respectively which suggests direct interaction with the drugs' target, the angiotensin type I receptor (ATR1).[264] Indeed treatment with these ARB improved the viability of AC10-CMs treated with doxorubicin, whilst reducing hypertrophic responses in AC10-CMs and hiPSC-CMs, and importantly did not interfere with the efficacy of doxorubicin at killing cancer cells.

Because the current study was conducted *in vitro*, unlike previous studies it is focussed on direct evaluation of cardiomyocyte behaviour independent of systemic effects. The reduction in cardiomyocyte hypertrophy and improved viability observed in this study demonstrates that perturbation of angiotensin signalling in the context of doxorubicin-induced cardiotoxicity has direct protective effects on cardiomyocytes. This may relate to a reduction in the acute cardiotoxicity response which potentially primes cardiomyocytes for the more severe forms of cardiotoxicity that involve cardiac remodelling and ventricular hypertrophy.[113,144] Other work

has demonstrated that perturbation of angiotensin signalling is also useful for protecting endothelial cells from anthracycline-induced damage.[313] Due to the crucial role of cardiac endothelial cells in maintaining heart function, protection of these cells from AIC provides and additional benefit of reducing angiotensin signalling in patients treated with anthracyclines; in addition to systemic effects and the direct effect on cardiomyocytes demonstrated in the current study.

Further work to confirm that the reduction of doxorubicin-induced hypertrophy of cardiomyocytes by administration of ARB occurs via an ATR1 specific mechanism could encompass the use of siRNA to silence expression of the ATR1 in AC10-CMs, and then challenge the cells with doxorubicin and ARB in an identical manner. If the reduction in hypertrophy is absent and cell viability is not improved in cells with silenced ATR1 then this would illustrate that the protection afforded by ARB in doxorubicin-induced cardiotoxicity is ATR1 specific and further implicates angiotensin signalling in facilitation of the toxicity.

Another interesting addition to the current work would be to utilise patient specific hiPSC-CMs. A recent paper by Burridge *et al.* demonstrated that patient specific hiPSC–CMs can recapitulate individual patients' predilection to doxorubicin-induced cardiotoxicity at the cardiomyocyte level.[314] Cells derived from breast cancer patients who suffered clinical doxorubicin-induced cardiotoxicity were consistently more sensitive to doxorubicin toxicity, demonstrating decreased cell viability, increased sarcomeric disarray and impairments to contractility compared to hiPSC–CMs from patients who did not experience doxorubicin-induced cardiotoxicity. With reference to the current study, it would be useful to use cells such as those derived by Burridge *et al.* to investigate whether the cells from patients who suffered doxorubicin-induced cardiotoxicity are a) More prone to doxorubicin-induced hypertrophy and b) If ARB therapy is able to reduce hypertrophy in all or just some patient cells. This would help to uncover how relevant doxorubicin-induced hypertrophy of hiPSC–CMs is and therefore also

the importance of the acute toxicity response with respect to the risk of developing clinical chronic cardiotoxicity, and to what extent ARB treatment may be helpful. Patient specific hiPSC–CM models such as this would be a useful tool for continuation of work in this area in a translational manner to further clarify the role of angiotensin signalling in doxorubicin-induced cardiotoxicity.

The response of the AC10 *in vitro* cardiomyocyte model to anthracyclines +/- ARBs in this study was evaluated using mainly a combination of the MTT cellular viability assay and impedance-based technologies. As the toxicity mechanisms of anthracyclines involve perturbations to mitochondrial function (See section 1.7.1.1) and the MTT assay relies on mitochondrial conversion of tetrozolium to formazan as a measure of cell viability, the readings may not have been wholly accurate of viable cells as some cells may have still been viable but suffered reduced mitochondrial activity due to anthracycline treatment. Therefore, it may be useful to pair the MTT assay with other measures of cellular viability such as ATP assays, protease assays or trypan blue exclusion assays. Trypan blue exclusion assays allow identification of both viable and dead cells which would thereby complement and verify of the viability assessments from MTT assays. The response of hiPSC-CMs to anthracyclines +/- ARBs was evaluated using impedance-based technology only. As impedance readings are a measure of cellular contact with electrodes on the bottom of the wells, increases in impedance can represent either increased cell number or cell size, whereas decreases in impedance represent reductions in cell number or decreases in cell size. The occurrence of cellular hypertrophy of *in vitro* cardiomyocyte models upon anthracycline treatment and reduction with concomitant ARB treatment was a key finding from impedance-based technology in this study – Which in AC10-CMs was verified using a combination of the MTT assay and imaging. It would be worthwhile to perform similar studies with hiPSC-CMs to verify the occurrence of hypertrophy (i.e. check that the increased impedance is not due to increased cellular proliferation) as this would complement the hiPSC-CM data set presented in this study and confirm the findings. A further consideration for the use of

impedance-based technology for determination of cellular hypertrophy is that as well as increases in cellular dimensions on a 2D level (well plate surface) which is detectable by impedance changes, it is likely that cells would also increase on a 3D level (i.e. vertically). This would not be detectable by impedance-based technology therefore use of 3D spheroid models may be applicable for further work in this area.

Because the mitigation of doxorubicin-induced cardiotoxicity by drugs that perturb angiotensin signalling suggests a direct role of angiotensin II in facilitating this toxicity, the effects of co-administration of angiotensin II and doxorubicin with respect to changes in cellular viability, morphology and functionality were assessed in this study. Overall, the combination of angiotensin II and doxorubicin did not affect viability and morphology of AC10-CMs and hiPSC-CMs any more than cells treated with doxorubicin alone. This may be due to the use of short exposure times that did not allow for the accumulation of further structural damage, or the use of simplistic *in vitro* models that do not fully represent the complexity of the cardiovascular system and human body. Altered contractility, however, was observed following 24 hours exposure to doxorubicin and angiotensin II, where a decrease in beat amplitude of hiPSC-CMs was seen compared to cells treated with doxorubicin only. As a decrease in beat amplitude relates to negative inotropy (reduced force of muscle contraction), the reduced beat amplitude may be due to increased impairment to the contractile machinery of the cells and myofibrillar loss, however more work would be needed to clarify this.

Further work in elucidating the link between angiotensin signalling and doxorubicin-induced cardiotoxicity focussed on molecular changes that occur in AC10-CMs following doxorubicin treatment which may relate to angiotensin signalling, thereby indicating an interaction between angiotensin signalling and doxorubicin cardiotoxicity. Treatment of AC10-CMs with doxorubicin caused a 2-3 fold increase in the level of ATR1 expression and also induced changes in gene expression that relate both to the cardiotoxicity mechanisms of anthracyclines and increased

levels of angiotensin II signalling. In addition, there appears to be some areas of overlap between genes with altered expression that are involved in both anthracycline cardiotoxicity mechanisms and genes stimulated by angiotensin signalling; which cause similar cellular effects including increased oxidative stress, cellular remodelling and hypertrophy. Although further work is needed to verify and add to the changes in gene expression discussed, the work described implicates angiotensin signalling as having a direct effect on cardiomyocytes and potentiating the pathogenesis of doxorubicin mediated cardiotoxicity.

As the current study was conducted *in vitro*, the cardiomyocytes were not exposed to circulating levels of angiotensin II that would ordinarily bind to the ATR1 and initiate signalling cascades. Evidence suggests that biomechanical stress (such as exposure to doxorubicin causing hypertrophy) to cardiomyocytes *in vitro* can induce changes to cardiomyocytes including the induction of ATR1 activation independent of agonist binding,[272] which may also be responsible for ATR1 activation in the current study. Considering this, in addition to exposure of a patient's myocardium to doxorubicin causing hypertrophy (biomechanical stress) and subsequent ATR1 activation independent of angiotensin II, patients (unlike an *in vitro* system) will also be exposed to circulating angiotensin II which will further magnify and become additive to effects caused by anthracyclines, further exaggerating cardiac stress. However, the observations described in this study are focused specifically on the direct effects upon the cardiomyocyte and thereby elucidate the underpinning molecular mechanisms.

This has clinical implications as the level of angiotensin II that patients have is determined by the genotype of their angiotensin converting enzyme (ACE), which is responsible for the final step of angiotensin II production. There are three ACE genotypes: I/I, I/D and D/D, which are associated with low, medium and high levels of angiotensin II respectively.[315] Evidence suggests that the D/D genotype is a risk factor for heart disease,[316] and therefore this risk factor may extend to doxorubicin-induced cardiotoxicity. Therefore in addition to using patient derived

hiPSC-CMs for investigating if those who suffered doxorubicin-induced cardiotoxicity are more prone to doxorubicin-induced cardiomyocyte hypertrophy and evaluating if ARB therapy is able to reduce hypertrophy, it would also be useful to link this information to patient genotype and identify the impact of ACE genotype and angiotensin II levels to the risk of developing doxorubicin-induced cardiotoxicity.

7.1 Conclusion

The current study has qualified the AC10-CM and hiPSC-CM *in vitro* cardiomyocyte cell models for detection of structural and functional cardiotoxicity using impedance-based technologies and determined that anthracyclines induce hypertrophy of these cells which may relate to the acute cardiotoxicity response. The doxorubicin induced hypertrophy of *in vitro* cardiomyocyte models is associated with amplified expression of the ATR1 paired with increased expression of genes that would normally be stimulated by angiotensin II; therefore implicating angiotensin signalling as having a direct effect on cardiomyocytes and potentiating the pathogenesis of doxorubicin-induced cardiotoxicity. As it is possible that the observed cardioprotection occurs via an ATR1 independent mechanism, the aforementioned further work into clarifying the involvement of the ATR1 in the cardioprotective response is required and could be obtained using siRNA techniques. The mitigation of doxorubicin-induced hypertrophy by angiotensin blockade suggests that reduced angiotensin signalling protected cardiomyocytes from the additive toxicity caused by angiotensin signalling. This implicates synergism between doxorubicin induced cardiotoxicity and angiotensin signalling and further supports the use of these pharmaceuticals for protection against doxorubicin-induced cardiotoxicity. Furthermore, it is possible that the ACE genotype plays a role in susceptibility to doxorubicin-induced cardiotoxicity and may represent an additional risk factor that could be determined at the time of diagnosis to help guide appropriate cardioprotective strategies.

References

1. Hanahan, D. & Weinberg, R. A. Hallmarks of cancer: The next generation. *Cell* **144,** 646–674 (2011).

2. Hejmadi, M. *Introduction to cancer biology*. (Ventus publishing, 2010).

3. Cancer Research UK. Cancer statistics for the UK. (2018). at <http://www.cancerresearchuk.org/health-professional/cancer-statistics-for-the-uk>

4. Quaresma, M., Coleman, M. P. & Rachet, B. 40-year trends in an index of survival for all cancers combined and survival adjusted for age and sex for each cancer in England and Wales, 1971-2011: A population-based study. *Lancet* **385,** 1206–1218 (2015).

5. Smittenaar, C. R., Petersen, K. A., Stewart, K. & Moitt, N. Cancer incidence and mortality projections in the UK until 2035. *Br. J. Cancer* **115,** 1147–1155 (2016).

6. Miller, K. D. *et al.* Cancer treatment and survivorship statistics, 2016. *CA. Cancer J. Clin.* **66,** 271–289 (2016).

7. Maddams, J., Utley, M. & Møller, H. Projections of cancer prevalence in the United Kingdom, 2010-2040. *Br. J. Cancer* **107,** 1195–202 (2012).

8. Cancer Research UK. How chemotherapy works. (2018). at <http://www.cancerresearchuk.org/about-cancer/cancer-in-general/treatment/chemotherapy/how-chemotherapy-works>

9. Luqmani, Y. A. Mechanisms of drug resistance in cancer chemotherapy. *Med. Princ. Pract.* **14 Suppl 1,** 35–48 (2005).

10. Colvin, O. M. An overview of cyclophosphamide development and clinical applications. *Curr. Pharm. Des.* **5,** 555–60 (1999).

11. Medicines.org.uk. Cyclophosphamide summary of product characteristics. (2018). at <https://www.medicines.org.uk/emc/product/3525#PRODUCTINFO>

12. Sumandeep Dhesi, M. *et al.* Cyclophosphamide-Induced Cardiomyopathy: A Case Report, Review, and Recommendations for Management. *J. Investig. Med. High Impact Case Reports* 1–7 (2013). doi:10.1177/2324709613480346

13. Champoux, J. J. DNA topoisomerases: structure, function, and mechanism. *Annu. Rev. Biochem.* **70,** 369–413 (2001).

14. Nitiss, J. L. Targeting DNA topoisomerase II in cancer chemotherapy. *Nature Reviews Cancer* **9,** 338–350 (2009).

15. Medicines.org.uk. Doxorubicin summary of product characteristics. (2018). at <https://www.medicines.org.uk/emc/product/6112/smpc>

16. Volkova, M. & Russell, R. Anthracycline Cardiotoxicity: Prevalence, Pathogenesis and Treatment. *Curr. Cardiol. Rev.* **7,** 214–220 (2011).

17. Swain, S. M., Whaley, F. S. & Ewer, M. S. Congestive heart failure in patients treated with doxorubicin: A retrospective analysis of three trials. *Cancer* **97,** 2869–2879 (2003).

18. Collins, I. & Workman, P. New approaches to molecular cancer therapeutics. *Nature Chemical Biology* **2,** 689–700 (2006).

19. Downward, J. Targeting RAS signalling pathways in cancer therapy. *Nature Reviews Cancer* **3,** 11–22 (2003).

20. Arora, A. & Scholar, E. M. Role of tyrosine kinase inhibitors in cancer therapy. *J. Pharmacol. Exp. Ther.* **315,** 971–9 (2005).

21. Engelman, J. A. & Jänne, P. A. Mechanisms of acquired resistance to epidermal growth factor receptor tyrosine kinase inhibitors in non-small cell lung cancer. *Clin. Cancer Res.* **14,** 2895–9 (2008).

22. Sullivan, I. & Planchard, D. Next-Generation EGFR Tyrosine Kinase Inhibitors for Treating EGFR-Mutant Lung Cancer beyond First Line. *Front. Med.* **3,** (2017).

23. Medicines.org.uk. Gefitinib (Iressa) Summary of product characteristics. (2018). at <https://www.medicines.org.uk/emc/product/6602#PRODUCTINFO>

24. Jost, M., Kari, C. & Rodeck, U. The EGF receptor - An essential regulator of multiple epidermal functions. *European Journal of Dermatology* **10,** 505–510 (2000).

25. Lacouture, M. E. Mechanisms of cutaneous toxicities to EGFR inhibitors. in *Nature Reviews Cancer* **6,** 803–812 (2006).

26. Robinson, E. S., Khankin, E. V., Karumanchi, S. A. & Humphreys, B. D. Hypertension induced by vascular endothelial growth factor signaling pathway inhibition: Mechanisms and potential use as a biomarker. *Semin. Nephrol.* **30,** 591–601 (2010).

27. Small, H. Y., Montezano, A. C., Rios, F. J., Savoia, C. & Touyz, R. M. Hypertension due to antiangiogenic cancer therapy with vascular endothelial growth factor inhibitors: understanding and managing a new syndrome. *Can. J. Cardiol.* **30,** 534–43 (2014).

28. Hahn, V. S., Lenihan, D. J. & Ky, B. Cancer therapy-induced cardiotoxicity: Basic mechanisms and potential cardioprotective therapies. *J. Am. Heart Assoc.* **3,** (2014).

29. Ewer, M. S. & Ewer, S. M. Cardiotoxicity of anticancer treatments. *Nat Rev Cardiol* **12,** 547–558 (2015).

30. Mulrooney, D. A. *et al.* Cardiac outcomes in a cohort of adult survivors of childhood and adolescent cancer: retrospective analysis of the Childhood Cancer Survivor Study cohort. *Bmj* **339,** b4606 (2009).

31. Lipshultz, S. E. *et al.* Cardiotoxicity and Cardioprotection in Childhood Cancer. *Acta Haematol.* **132,** 391–399 (2014).

32. Carver, J. R. *et al.* American society of clinical oncology clinical evidence review on the ongoing care of adult cancer survivors: Cardiac and pulmonary late effects. *J. Clin. Oncol.* **25,** 3991–4008 (2007).

33. K.C. Oeffinger, A.C. Mertens, C. A. S. Chronic health conditions in adult survivors of childhood cancer. *N Engl J Med* **355,** 1572–1582 (2006).

34. Lenneman, C. G. & Sawyer, D. B. Cardio-Oncology An update on cardiotoxicity of cancer-related treatment. *Circ. Res.* **118,** 1008–1020 (2016).

35. Kesteloot, H., Sans, S. & Kromhout, D. Dynamics of cardiovascular and all-cause mortality in Western and Eastern Europe between 1970 and 2000. *Eur. Heart J.* **27,** 107–113 (2006).

36. Reicher-Reiss, H., Jonas, M., Goldbourt, U., Boyko, V. & Modan, B. Selectively increased risk of cancer in men with coronary heart disease. *Am. J. Cardiol.* **87,** 459–62, A6 (2001).

37. British heart foundation. Risk factors for cardiovascular disease. (2018). at <https://www.bhf.org.uk/heart-health/risk-factors>

38. Cancer Research UK. Risk factors for cancer. (2018). at <http://www.cancerresearchuk.org/about-cancer/causes-of-cancer>

39. Barros-Gomes, S. *et al.* Rationale for setting up a cardio-oncology unit: our experience at Mayo Clinic. *Cardio-Oncology* **2,** 5 (2016).

40. Lenihan, D. J. *et al.* Cardio-Oncology Training: A Proposal From the International Cardioncology Society and Canadian Cardiac Oncology Network for a New Multidisciplinary Specialty. *J. Card. Fail.* **22,** 465–471 (2016).

41. Cardinale, D. Cardio-oncology: A new medical issue. *Ecancermedicalscience* **2,** 1–13 (2008).

42. Jensen, B. C. & McLeod, H. L. Pharmacogenomics as a risk mitigation strategy for chemotherapeutic cardiotoxicity. *Pharmacogenomics* **14,** 205–13 (2013).

43. Rossant, J. & Howard, L. Signaling Pathways in Vascular Development. *Annu. Rev. Cell Dev. Biol.* **18,** 541–573 (2002).

44. Aaronson, P. & Ward, J. *The cardiovascular system at a glance*. (Wiley-Blackwell, 2007).

45. Zhou, P. & Pu, W. T. Recounting cardiac cellular composition. *Circulation Research* **118,** 368–370 (2016).

46. Woodcock, E. A. & Matkovich, S. J. Cardiomyocytes structure, function and associated pathologies. *Int. J. Biochem. Cell Biol.* **37,** 1746–1751 (2005).

47. Huxley, H. E. Fifty years of muscle and the sliding filament hypothesis. *European Journal of Biochemistry* **271,** 1403–1415 (2004).

48. Blausen.com staff. Medical gallery of Blausen Medical 2014. (2014). doi:10.15347/wjm/2014.010

49. Bers, D. M. Cardiac excitation contraction coupling. *Nature* **415,** 198–205 (2002).

50. Flucher, B. E. Structural analysis of muscle development: Transverse tubules, sarcoplasmic reticulum, and the triad. *Developmental Biology* **154,** 245–260 (1992).

51. Fabiato, A. & Fabiato, F. Contractions induced by a calcium-triggered release of calcium from the sarcoplasmic reticulum of single skinned cardiac cells. *J. Physiol.* **249,** 469–495 (1975).

52. Fabiato, A. Calcium-induced release of calcium from the cardiac sarcoplasmic reticulum. *Am. J. Physiol.* **245,** C1–C14 (1983).

53. Pinto, A. R. *et al.* Revisiting cardiac cellular composition. *Circ. Res.* **118,** 400–409 (2016).

54. Baudino, T. & Carver, W. Cardiac fibroblasts: friend or foe? *Am. J. …* 1015–1026 (2006). doi:10.1152/ajpheart.00023.2006.

55. Kamkin, A., Kiseleva, I., Lozinsky, I. & Scholz, H. Electrical interaction of mechanosensitive fibroblasts and myocytes in the heart. *Basic Res. Cardiol.* **100,** 337–345 (2005).

56. Rohde, D. *et al.* Cardiomyocytes, endothelial cells and cardiac fibroblasts: S100A1's triple action in cardiovascular pathophysiology. *Future Cardiol.* **11,** 309–321 (2015).

57. Brutsaert, D. L. Cardiac Endothelial-Myocardial Signaling: Its Role in Cardiac Growth, Contractile Performance, and Rhythmicity. *Physiol. Rev.* **83,** 59–115 (2003).

58. Aird, W. C. Endothelium in health and disease. in *Pharmacological Reports* **60,** 139–143 (2008).

59. Avolio, E. & Madeddu, P. Discovering cardiac pericyte biology: From physiopathological mechanisms to potential therapeutic applications in ischemic heart disease. *Vascul. Pharmacol.* **86,** 53–63 (2016).

60. Nees, S. *et al.* Isolation, bulk cultivation, and characterization of coronary microvascular pericytes: the second most frequent myocardial cell type in vitro. *AJP Hear. Circ. Physiol.* **302,** H69–H84 (2012).

61. Nees, S., Weiss, D. R. & Juchem, G. Focus on cardiac pericytes. *Pflugers Archiv European Journal of Physiology* **465,** 779–787 (2013).

62. Goodenough, D. A. & Paul, D. L. Gap junctions. *Cold Spring Harbor perspectives in biology* **1,** (2009).

63. Delmar, M. & Makita, N. Cardiac connexins, mutations and arrhythmias. *Current Opinion in Cardiology* **27,** 236–241 (2012).

64. Van Norstrand, D. W. *et al.* Connexin43 mutation causes heterogeneous gap junction loss and sudden infant death. *Circulation* **125,** 474–481 (2012).

65. Ziolo, M. T., Kohr, M. J. & Wang, H. Nitric oxide signaling and the regulation of myocardial function. *Journal of Molecular and Cellular Cardiology* **45,** 625–632 (2008).

66. Cotton, J. M., Kearney, M. T. & Shah, a M. Nitric oxide and myocardial function in heart failure: friend or foe? *Heart* **88,** 564–6 (2002).

67. Wheeler-Jones, C. P. D. Cell signalling in the cardiovascular system: an overview. *Heart* **91,** 1366–1374 (2005).

68. Dzimiri, N. Receptor crosstalk. Implications for cardiovascular function, disease and therapy. *European Journal of Biochemistry* **269,** 4713–4730 (2002).

69. Salazar, N. C., Chen, J. & Rockman, H. A. Cardiac GPCRs: GPCR signaling in healthy and failing hearts. *Biochimica et Biophysica Acta - Biomembranes* **1768,** 1006–1018 (2007).

70. Lincoln, T. M., Dey, N. & Sellak, H. cGMP-dependent protein kinase signaling mechanisms in smooth muscle: from the regulation of tone to gene expression. *J. Appl. Physiol.* **91,** 1421–1430 (2001).

71. Wallukat, G. The beta-adrenergic receptors. *Herz* **27,** 683–90 (2002).

72. Rockman, H. A., Koch, W. J. & Lefkowitz, R. J. Seven-transmembrane-spanning receptors and heart function. *Nature* **415,** 206–212 (2002).

73. Azevedo, P. S., Polegato, B. F., Minicucci, M. F., Paiva, S. a R. & Zornoff, L. a M. Cardiac Remodeling: Concepts, Clinical Impact, Pathophysiological Mechanisms and Pharmacologic Treatment. *Arq. Bras. Cardiol.* 62–69 (2015). doi:10.5935/abc.20160005

74. Chatterjee, S. *et al.* Benefits of β blockers in patients with heart failure and reduced ejection fraction: network meta-analysis. *BMJ* **346,** f55 (2013).

75. Higuchi, S. *et al.* Angiotensin II signal transduction through the AT_1 receptor: novel insights into mechanisms and pathophysiology. *Clin. Sci.* **112,** 417–428 (2007).

76. Mehta, P. K. & Griendling, K. K. Angiotensin II cell signaling: physiological and pathological effects in the cardiovascular system. *Am. J. Physiol. - Cell Physiol.* **292,** C82–C97 (2007).

77. Erhardt, L. R. A review of the current evidence for the use of angiotensin-receptor blockers in chronic heart failure. *Int. J. Clin. Pract.* **59,** 571–578 (2005).

78. Barki-Harrington, L., Luttrell, L. M. & Rockman, H. A. Dual inhibition of B-adrenergic and angiotensin II receptors by a single antagonist: A functional role for receptor-receptor interaction in vivo. *Circulation* **108,** 1611–1618 (2003).

79. Forrester, S. J. *et al.* Epidermal Growth Factor Receptor Transactivation: Mechanisms, Pathophysiology, and Potential Therapies in the Cardiovascular System. *Annu. Rev. Pharmacol. Toxicol.* **56,** annurev-pharmtox-070115-095427 (2016).

80. Matthew, K. *Cardiac Drug Safety: A bench to bedside approach*. (World Scientific Publishing, 2012).

81. British heart foundation. Cardiac arrest. (2018). at <https://www.bhf.org.uk/heart-health/conditions/cardiac-arrest>

82. Kemp, C. D. & Conte, J. V. The pathophysiology of heart failure. *Cardiovascular Pathology* **21,** 365–371 (2012).

83. Laverty, H. G. *et al.* How can we improve our understanding of cardiovascular safety liabilities to develop safer medicines? *British Journal of Pharmacology* **163,** 675–693 (2011).

84. Sibbald, B. Rofecoxib (Vioxx) voluntarily withdrawn from market. *CMAJ* **171,** 1027–1028 (2004).

85. Jüni, P. *et al.* Risk of cardiovascular events and rofecoxib: Cumulative meta-analysis. *Lancet* **364,** 2021–2029 (2004).

86. Mason, R. P., Walter, M. F., Day, C. A. & Jacob, R. F. A biological rationale for the cardiotoxic effects of rofecoxib: comparative analysis with other COX-2 selective agents and NSAids. *Subcell Biochem* **42,** 175–190 (2007).

87. Woosley, R. L., Chen, Y., Freiman, J. P. & Gillis, R. A. Mechanism of the Cardiotoxic Actions of Terfenadine. *JAMA J. Am. Med. Assoc.* **269,** 1532–1536 (1993).

88. Sereno, M. *et al.* Cardiac toxicity: Old and new issues in anti-cancer drugs. *Clin. Transl. Oncol.* **10,** 35–46 (2008).

89. Ewer, M. S. Type II Chemotherapy-Related Cardiac Dysfunction: Time to Recognize a New Entity. *J. Clin. Oncol.* **23,** 2900–2902 (2005).

90. Cancer Research UK. Side effects of chemotherapy. (2018). at <http://www.cancerresearchuk.org/about-cancer/cancer-in-general/treatment/chemotherapy/side-effects/about>

91. Angsutararux, P., Luanpitpong, S. & Issaragrisil, S. Chemotherapy-Induced Cardiotoxicity: Overview of the Roles of Oxidative Stress. *Oxid. Med. Cell. Longev.* **2015,** 1–13 (2015).

92. Moslehi, J. J. Cardiovascular Toxic Effects of Targeted Cancer Therapies. *N. Engl. J. Med.* **375,** 1457–1467 (2016).

93. Force, T., Krause, D. S. & Van Etten, R. a. Molecular mechanisms of cardiotoxicity of tyrosine kinase inhibition. *Nat. Rev. Cancer* **7,** 332–344 (2007).

94. Capdeville, R., Buchdunger, E., Zimmermann, J. & Matter, A. Glivec (STI571, imatinib), a rationally developed, targeted anticancer drug. *Nat. Rev. Drug Discov.* **1,** 493–502 (2002).

95. Kerkelä, R. *et al.* Cardiotoxicity of the cancer therapeutic agent imatinib mesylate. *Nat. Med.* **12,** 908–916 (2006).

96. Medicines.org.uk. Sunitinib summary of product characteristics. (2018). at <https://www.medicines.org.uk/emc/product/227>

97. Weis, S. M. & Cheresh, D. A. Tumor angiogenesis: Molecular pathways and therapeutic targets. *Nature Medicine* **17,** 1359–1370 (2011).

98. Chu, T. F. *et al.* Cardiotoxicity associated with tyrosine kinase inhibitor sunitinib. *Lancet* **370,** 2011–2019 (2007).

99. Qi, D. & Young, L. H. AMPK: Energy sensor and survival mechanism in the ischemic heart. *Trends in Endocrinology and Metabolism* **26,** 422–429 (2015).

100. Kerkela, R. *et al.* Sunitinib-induced cardiotoxicity is mediated by off-target inhibition of AMP-activated protein kinase. *Clin. Transl. Sci.* **2,** 15–25 (2009).

101. Ferrara, N. VEGF-A: A critical regulator of blood vessel growth. *European Cytokine Network* **20,** 158–163 (2009).

102. Chintalgattu, V. *et al.* Cardiomyocyte PDGFR-β signaling is an essential component of the mouse cardiac response to load-induced stress. *J. Clin. Invest.* **120,** 472–484 (2010).

103. Medicines.org.uk. Trastuzumab summary of product characteristics. (2018). at <https://www.medicines.org.uk/emc/product/3856>

104. Seshacharyulu, P. *et al.* Targeting the EGFR signaling pathway in cancer therapy. *Expert Opin. Ther. Targets* **16,** 15–31 (2012).

105. Keefe, D. L. Trastuzumab-associated cardiotoxicity. *Cancer* **95,** 1592–1600 (2002).

106. Lemmens, K., Doggen, K. & De Keulenaer, G. W. Role of Neuregulin-1/ErbB Signaling in Cardiovascular Physiology and Disease: Implications for Therapy of Heart Failure. *Circulation* **116,** 954–960 (2007).

107. Negro, a. Essential Roles of Her2/erbB2 in Cardiac Development and Function. *Recent Prog. Horm. Res.* **59,** 1–12 (2004).

108. Odiete, O., Hill, M. F. & Sawyer, D. B. Neuregulin in Cardiovascular Development and Disease. *Circ. Res.* **111,** 1376–1385 (2013).

109. Di Marco, A., Cassinelli, G. & Arcamone, F. The discovery of daunorubicin. *Cancer Treat. Rep.* **65 Suppl 4,** 3–8 (1981).

110. DiMarco, A., Gastani, M. & Scarpinato, B. Adriamycin: A new antibiotic with antitumor activity. *Cancer Chemother. Reports* **53,** 33–37 (1969).

111. Minotti, G. Anthracyclines: Molecular Advances and Pharmacologic Developments in Antitumor Activity and Cardiotoxicity. *Pharmacol. Rev.* **56,** 185–229 (2004).

112. Lefrak, E. a, Pitha, J., Rosenheim, S. & Gottlieb, J. a. A clinicopathologic analysis of adriamycin cardiotoxicity. *Cancer* **32,** 302–314 (1973).

113. von Hoff, D. D. *et al.* Risk factors for doxorubicin-induced congestive heart failure. *Ann. Intern. Med.* **91,** 710–717 (1979).

114. Groarke, J. D. & Nohria, A. Anthracycline Cardiotoxicity: A New Paradigm for an Old Classic. *Circulation* 1946–1950 (2015). doi:10.1161/CIRCULATIONAHA.115.016704

115. Capranico, G., Tinelli, S., Austin, C. A., Fisher, M. L. & Zunino, F. Different patterns of gene expression of topoisomerase II isoforms in differentiated tissues during murine development. *BBA - Gene Struct. Expr.* **1132,** 43–48 (1992).

116. Rahman, A., Schein, P. S. & More, N. Doxorubicin-Induced Chronic Cardiotoxicity and its Protection by Liposomal Administration. *Cancer Res.* **42,** 1817–1825 (1982).

117. Goffart, S., Von Kleist-Retzow, J. C. & Wiesner, R. J. Regulation of mitochondrial proliferation in the heart: Power-plant failure contributes to cardiac failure in hypertrophy. *Cardiovascular Research* **64,** 198–207 (2004).

118. Gammella, E., Maccarinelli, F., Buratti, P., Recalcati, S. & Cairo, G. The role of iron in anthracycline cardiotoxicity. *Front. Pharmacol.* **5,** 25 (2014).

119. Minotti, G., Salvatorelli, E., Menna, P., Ronchi, R. & Cairo, G. Doxorubicin irreversibly inactivates iron regulatory proteins 1 and 2 in cardiomyocytes: Evidence for distinct metabolic pathways and implications for iron-mediated cardiotoxicity of antitumor therapy. *Cancer Res.* **61,** 8422–8428 (2001).

120. Minotti, G. *et al.* The secondary alcohol metabolite of doxorubicin irreversibly inactivates aconitase/iron regulatory protein-1 in cytosolic fractions from human myocardium. *FASEB J.* **12,** 541–52 (1998).

121. Gustafson, D. L., Swanson, J. D. & Pritsos, C. A. Modulation of glutathione and glutathione dependent antioxidant enzymes in mouse heart following doxorubicin therapy. *Free Radic. Res.* **19,** 111–120 (1993).

122. Yen, H. C., Oberley, T. D., Vichitbandha, S., Ho, Y. S. & St Clair, D. K. The protective role of manganese superoxide dismutase against adriamycin-induced acute cardiac toxicity in transgenic mice. *J Clin Invest* **98,** 1253–1260 (1996).

123. Heestand, G. M., Schwaederle, M., Gatalica, Z., Arguello, D. & Kurzrock, R. Topoisomerase expression and amplification in solid tumours: Analysis of 24,262 patients. *Eur. J. Cancer* **83,** 80–87 (2017).

124. Zhang, S. *et al.* Identification of the molecular basis of doxorubicin-induced cardiotoxicity. *Nat. Med.* **18,** 1639–1645 (2012).

125. Douarre, C. *et al.* Mitochondrial topoisomerase I is critical for mitochondrial integrity and cellular energy metabolism. *PLoS One* **7,** (2012).

126. Lebrecht, D., Kokkori, A., Ketelsen, U. P., Setzer, B. & Walker, U. A. Tissue-specific mtDNA lesions and radical-associated mitochondrial dysfunction in human hearts exposed to doxorubicin. *J. Pathol.* **207,** 436–444 (2005).

127. Khiati, S. *et al.* Mitochondrial topoisomerase i (Top1mt) is a novel limiting factor of doxorubicin cardiotoxicity. *Clin. Cancer Res.* **20,** 4873–4881 (2014).

128. McCaffrey, T. A. *et al.* Genomic profiling reveals the potential role of TCL1A and MDR1 Deficiency in chemotherapy-induced cardiotoxicity. *Int. J. Biol. Sci.* **9,** 350–360 (2013).

129. Hanna, A. D., Lam, A., Tham, S., Dulhunty, A. F. & Beard, N. A. Adverse Effects of Doxorubicin and Its Metabolic Product on Cardiac RyR2 and SERCA2A. *Mol. Pharmacol.* **86,** 438–449 (2014).

130. Blanco, J. G. *et al.* Genetic polymorphisms in the carbonyl reductase 3 gene CBR3 and the NAD(P)H:quinone oxidoreductase 1 gene NQO1 in patients who developed anthracycline-related congestive heart failure after childhood cancer. *Cancer* **112,** 2789–2795 (2008).

131. Medicines.org.uk. Epirubicin summary of product characteristics. (2018). at <https://www.medicines.org.uk/emc/product/8808>

132. Medicines.org.uk. Daunorubicin summary of product characteristics. (2018). at <https://www.medicines.org.uk/emc/product/4004#UNDESIRABLE_EFFECTS>

133. Minotti, G. *et al.* Anthracycline metabolism and toxicity in human myocardium: Comparisons between doxorubicin, epirubicin, and a novel disaccharide analogue with a reduced level of formation and [4Fe-4S] reactivity of its secondary alcohol metabolite. *Chem. Res. Toxicol.* **13,** 1336–1341 (2000).

134. Ewer, M. S. & Yeh, E. in *Cancer and the heart* (BC Decker, 2006).

135. Cardinale, D. *et al.* Early detection of anthracycline cardiotoxicity and improvement with heart failure therapy. *Circulation* **131,** 1981–1988 (2015).

136. Lipshultz SE, Cochran TR, Franco VI, M. T. Treatment-related cardiotoxicity in survivors of childhood cancer. *Nat. Rev. Clin. Oncol.* (2013).

137. De Angelis, A. *et al.* Anthracycline cardiomyopathy is mediated by depletion of the cardiac stem cell pool and is rescued by restoration of progenitor cell function. *Circulation* **121,** 276–292 (2010).

138. Huang, C. *et al.* Juvenile exposure to anthracyclines impairs cardiac progenitor cell function and vascularization resulting in greater susceptibility to stress-induced myocardial injury in adult mice. *Circulation* **121,** 675–683 (2010).

139. Grenier, M. A. & Lipshultz, S. E. Epidemiology of anthracycline cardiotoxicity in children and adults. *Semin. Oncol.* **25,** 72–85 (1998).

140. Fidler, M. M. *et al.* Population-Based Long-Term Cardiac-Specific Mortality Among 34 , 489 Five-Year Survivors of Childhood Cancer in Great Britain. **44,**

141. Steinberg, J. S., Cohen, A. J., Wasserman, A. G., Cohen, P. & Ross, A. M. Acute arrhythmogenicity of doxorubicin administration. *Cancer* **60,** 1213–1218 (1987).

142. Bristow, M. R. *et al.* Early anthracycline cardiotoxicity. *The American Journal of Medicine* **65,** 823–832 (1978).

143. Swain, S. M., Whaley, F. S. & Ewer, M. S. Congestive heart failure in patients treated with doxorubicin: A retrospective analysis of three trials. *Cancer* **97,** 2869–2879 (2003).

144. Billingham, M. E., Mason, J. W., Bristow, M. R. & Daniels, J. R. Anthracycline cardiomyopathy monitored by morphologic changes. *Cancer Treat. Rep.* **62,** 865–72 (1978).

145. Minow, R. A. Adriamycin cardiomyopathy-risk factors. *Cancer* **39,** 1397–1402 (1977).

146. Altena, R., Perik, P. J., van Veldhuisen, D. J., de Vries, E. G. & Gietema, J. A. Cardiovascular toxicity caused by cancer treatment: strategies for early detection. *Lancet Oncol.* **10,** 391–399 (2009).

147. Seidman, A. *et al.* Cardiac dysfunction in the trastuzumab clinical trials experience. *J. Clin. Oncol.* **20,** 1215–1221 (2002).

148. Salvatorelli, E. *et al.* The concomitant management of cancer therapy and cardiac therapy. *Biochim. Biophys. Acta - Biomembr.* (2015). doi:10.1016/j.bbamem.2015.01.003

149. Stoodley, P. W. *et al.* Two-dimensional myocardial strain imaging detects changes in left ventricular systolic function immediately after anthracycline chemotherapy. *Eur. J. Echocardiogr.* **12,** 945–952 (2011).

150. Cardinale, D. *et al.* Prevention of high-dose chemotherapy-induced cardiotoxicity in high-risk patients by angiotensin-converting enzyme inhibition. *Circulation* **114,** 2474–2481 (2006).

151. Colombo, A., Sandri, M. T., Salvatici, M., Cipolla, C. M. & Cardinale, D. Cardiac complications of chemotherapy: Role of biomarkers. *Curr. Treat. Options Cardiovasc. Med.* **16,** (2014).

152. Kalam, K. & Marwick, T. H. Role of cardioprotective therapy for prevention of cardiotoxicity with chemotherapy: A systematic review and meta-analysis. *Eur. J. Cancer* **49,** 2900–2909 (2013).

153. Albini, A. *et al.* Cardiotoxicity of anticancer drugs: The need for cardio-oncology and cardio-oncological prevention. *J. Natl. Cancer Inst.* **102,** 14–25 (2010).

154. Cvetković, R. S. & Scott, L. J. Dexrazoxane: A review of its use for cardioprotection during anthracycline chemotherapy. *Drugs* **65,** 1005–1024 (2005).

155. van Dalen, E. C., Caron, H. N., Dickinson, H. O. & Kremer, L. C. Cardioprotective interventions for cancer patients receiving anthracyclines. *Cochrane database Syst. Rev.* CD003917 (2011). doi:10.1002/14651858.CD003917.pub4

156. Lipshultz, S. E. *et al.* Dexrazoxane for reducing anthracycline-related cardiotoxicity in children with cancer: An update of the evidence. *Prog. Pediatr. Cardiol.* **36,** 39–49 (2014).

157. Henninger, C. & Fritz, G. Statins in anthracycline-induced cardiotoxicity: Rac and Rho, and the heartbreakers. *Cell Death Dis.* **8,** e2564 (2017).

158. Clinicaltrials.gov. Preventing Anthracycline Cardiovascular Toxicity With Statins (PREVENT). (2018). at <https://clinicaltrials.gov/ct2/show/NCT01988571>

159. Medicines.org.uk. Carvedilol summary of product characteristics. (2018). at <https://www.medicines.org.uk/emc/product/3106#PRODUCTINFO>

160. Spallarossa, P. *et al.* Carvedilol prevents doxorubicin-induced free radical release and apoptosis in cardiomyocytes in vitro. *J. Mol. Cell. Cardiol.* **37,** 837–846 (2004).

161. Kalay, N. *et al.* Protective Effects of Carvedilol Against Anthracycline-Induced Cardiomyopathy. *J. Am. Coll. Cardiol.* **48,** 2258–2262 (2006).

162. Cohn, J. N. & Tognoni, G. (Val-HeFT Trial) A randomized trial of the angiotensin-receptor blocker valsartan in chronic heart failure. *N. Engl. J. Med.* **345,** 1667–1675 (2001).

163. Arnold, J. M. O. *et al.* Prevention of heart failure in patients in the Heart Outcomes Prevention Evaluation (HOPE) study. *Circulation* **107,** 1284–1290 (2003).

164. Bosch, X. *et al.* Enalapril and carvedilol for preventing chemotherapy-induced left ventricular systolic dysfunction in patients with malignant hemopathies: The OVERCOME trial (prevention of left ventricular dysfunction with enalapril and caRvedilol in patients submitted t. *J. Am. Coll. Cardiol.* **61,** 2355–2362 (2013).

165. Janbabai, G. *et al.* Effect of Enalapril on Preventing Anthracycline-Induced Cardiomyopathy. *Cardiovasc. Toxicol.* **17,** 130–139 (2017).

166. Nakamae, H. *et al.* Notable effects of angiotensin II receptor blocker, valsartan, on acute cardiotoxic changes after standard chemotherapy with cyclophosphamide, doxorubicin, vincristine, and prednisolone. *Cancer* **104,** 2492–2498 (2005).

167. Cadeddu, C. *et al.* Protective effects of the angiotensin II receptor blocker telmisartan on epirubicin-induced inflammation, oxidative stress, and early ventricular impairment. *Am. Heart J.* **160,** (2010).

168. Gulati, G. *et al.* Prevention of cardiac dysfunction during adjuvant breast cancer therapy (PRADA): A 2 ?? 2 factorial, randomized, placebo-controlled, double-blind clinical trial of candesartan and metoprolol. *Eur. Heart J.* **37,** 1671–1680 (2016).

169. Dessì, M. *et al.* Long-term, up to 18 months, protective effects of the angiotensin II receptor blocker telmisartan on Epirubin-induced inflammation and oxidative stress assessed by serial strain rate. *Springerplus* **2,** 198 (2013).

170. Meattini, I. *et al.* SAFE trial: an ongoing randomized clinical study to assess the role of cardiotoxicity prevention in breast cancer patients treated with anthracyclines with or without trastuzumab. *Med. Oncol.* **34,** 75 (2017).

171. Clinicaltrials.gov. PROACT: Can we Prevent Chemotherapy-related Heart Damage in Patients With Breast Cancer? (PROACT). (2018). at <https://clinicaltrials.gov/ct2/show/NCT03265574>

172. Lipshultz, S. E. Long-term enalapril therapy for left ventricular dysfunction in doxorubicin-treated survivors of childhood cancer. *J Clin oncol* (2002).

173. Cancer Research UK. R-CHOP chemotherapy regimen. (2018). at <http://www.cancerresearchuk.org/about-cancer/cancer-in-general/treatment/cancer-drugs/drugs/r-chop>

174. Ewer, M. S. Y. E. in *Cancer and the heart* (BC Decker, 2006).

175. Zeglinski, M., Ludke, A., Jassal, D. S. & Singal, P. K. Trastuzumab-induced cardiac dysfunction: A 'dual-hit'. *Exp. Clin. Cardiol.* **16,** 70–74 (2011).

176. de Korte, M. A. *et al.* 111Indium-trastuzumab visualises myocardial human epidermal growth factor receptor 2 expression shortly after anthracycline treatment but not during heart failure: A clue to uncover the mechanisms of trastuzumab-related cardiotoxicity. *Eur. J. Cancer* **43,** 2046–2051 (2007).

177. International conference on harmonisation of technical requirements for registration of pharmaceuticals for human use. *ICH-S7B Guidelines: The nonclinical evaluation of the potential for delayed ventricular repolarization (QT-prolongation) by human pharmaceuticals.* (2005). at <http://www.ich.org/fileadmin/Public_Web_Site/ICH_Products/Guidelines/Safety/S7B/Step4/S7B_Guideline.pdf>

178. Gintant, G. An evaluation of hERG current assay performance: Translating preclinical safety studies to clinical QT prolongation. *Pharmacol. Ther.* **129,** 109–119 (2011).

179. Ferri, N. *et al.* Drug attrition during pre-clinical and clinical development: Understanding and managing drug-induced cardiotoxicity. *Pharmacol. Ther.* **138,** 470–484 (2013).

180. Holzgrefeb, I. C. & H. Comprehensive in vitro Proarrhythmia Assay, a novel in vitro/in silico paradigm to detect ventricular proarrhythmic liability: a visionary 21st century initiative. *Expert Opin. Drug Saf.* **13,** (2014).

181. Gintant, G., Sager, P. T. & Stockbridge, N. Evolution of strategies to improve preclinical cardiac safety testing. *Nat. Rev. Drug Discov.* **15,** 1–15 (2016).

182. Force, T. & Kolaja, K. L. Cardiotoxicity of kinase inhibitors: the prediction and translation of preclinical models to clinical outcomes. *Nat. Rev. Drug Discov.* **10,** 111–126 (2011).

183. Kimes, B. W. & Brandt, B. L. Properties of a clonal muscle cell line from rat heart. *Exp. Cell Res.* **98,** 367–381 (1976).

184. Maayah, Z. H., Ansari, M. A., El Gendy, M. a., Al-Arifi, M. N. & Korashy, H. M. Development of cardiac hypertrophy by sunitinib in vivo and in vitro rat cardiomyocytes is influenced by the aryl hydrocarbon receptor signaling pathway. *Arch. Toxicol.* **88,** 725–738 (2014).

185. Sardão, V. a., Oliveira, P. J., Holy, J., Oliveira, C. R. & Wallace, K. B. Morphological alterations induced by doxorubicin on H9c2 myoblasts: Nuclear, mitochondrial, and cytoskeletal targets. *Cell Biol. Toxicol.* **25,** 227–243 (2009).

186. Watkins, S. J., Borthwick, G. M. & Arthur, H. M. The H9C2 cell line and primary neonatal cardiomyocyte cells show similar hypertrophic responses in vitro. *Vitr. Cell. Dev. Biol. - Anim.* **47,** 125–131 (2011).

187. Claycomb, W. C. *et al.* HL-1 cells: a cardiac muscle cell line that contracts and retains phenotypic characteristics of the adult cardiomyocyte. *Proc. Natl. Acad. Sci. U. S. A.* **95,** 2979–84 (1998).

188. Davidson, M. M. *et al.* Novel cell lines derived from adult human ventricular cardiomyocytes. *J. Mol. Cell. Cardiol.* **39,** 133–147 (2005).

189. Takahashi, K. & Yamanaka, S. Induction of Pluripotent Stem Cells from Mouse Embryonic and Adult Fibroblast Cultures by Defined Factors. *Cell* **126,** 663–676 (2006).

190. Laflamme, M. A. *et al.* Cardiomyocytes derived from human embryonic stem cells in pro-survival factors enhance function of infarcted rat hearts. *Nat. Biotechnol.* **25,** 1015–1024 (2007).

191. Braam, S. R. *et al.* Prediction of drug-induced cardiotoxicity using human embryonic stem cell-derived cardiomyocytes. *Stem Cell Res.* **4,** 107–116 (2010).

192. Robertson, C., Tran, D. & George, S. Concise Review: Maturation Phases of Human Pluripotent Stem Cell-Derived Cardiomyocytes. *Stem Cells* **31,** 1–17 (2013).

193. Lundy, S. D., Zhu, W.-Z., Regnier, M. & Laflamme, M. A. Structural and Functional Maturation of Cardiomyocytes Derived from Human Pluripotent Stem Cells. *Stem Cells Dev.* **22,** 1991–2002 (2013).

194. Li, R. K. *et al.* Human pediatric and adult ventricular cardiomyocytes in culture: Assessment of phenotypic changes with passaging. *Cardiovasc. Res.* **32,** 362–373 (1996).

195. Tang, S., Xie, M., Cao, N. & Ding, S. Patient-Specific Induced Pluripotent Stem Cells for Disease Modeling and Phenotypic Drug Discovery. *J. Med. Chem.* 150904083047005 (2015). doi:10.1021/acs.jmedchem.5b00789

196. Ravenscroft, S. The role of non-myocytes in drug-induced cardiovascular toxicity. (University of Liverpool, 2014).

197. Polonchuk, L. *et al.* Cardiac spheroids as promising in vitro models to study the human heart microenvironment. *Sci. Rep.* **7,** (2017).

198. Cyprotex. 3D cardiac hypertrophy model. (2018). at <http://www.cyprotex.com/toxicology/3d-microtissue-models/3d-cardiac-hypertrophy>

199. Ogden, D. & Stanfield, P. Patch clamp techniques for single channel and whole-cell recording. *Currents* **2,** 53–78 (1981).

200. Clements, M. & Thomas, N. High-throughput multi-parameter profiling of electrophysiological drug effects in human embryonic stem cell derived cardiomyocytes using multi-electrode arrays. *Toxicol. Sci.* **140,** 445–461 (2014).

201. Blinova, K. *et al.* Comprehensive Translational Assessment of Human Induced Pluripotent Stem Cell Derived Cardiomyocytes for Evaluating Drug-Induced Arrhythmias. *Toxicol. Sci.* (2016). doi:10.1093/toxsci/kfw200

202. Harmer, A. R. *et al.* Validation of an in vitro contractility assay using canine ventricular myocytes. *Toxicol. Appl. Pharmacol.* **260,** 162–172 (2012).

203. Pointon, A. *et al.* Assessment of cardiomyocyte contraction in human-induced pluripotent stem cell-derived cardiomyocytes. *Toxicol. Sci.* **144,** 227–237 (2015).

204. Hamamatsu. Hamamatsu system for measuring calcium currents. (2018). at <http://www.hamamatsu.com/us/en/FDSS_uCELL.html>

205. Xi, B. *et al.* Functional Cardiotoxicity Profiling and Screening Using the xCELLigence RTCA Cardio System. *J. Lab. Autom.* **16,** 415–421 (2011).

206. Peters, M. F., Lamore, S. D., Guo, L., Scott, C. W. & Kolaja, K. L. Human Stem Cell-Derived Cardiomyocytes in Cellular Impedance Assays: Bringing Cardiotoxicity Screening to the Front Line. *Cardiovasc. Toxicol.* (2014). doi:10.1007/s12012-014-9268-9

207. Guo, L. *et al.* Estimating the Risk of Drug-induced Proarrhythmia using Human Induced Pluripotent Stem Cell Derived Cardiomyocytes. *Toxicol. Sci.* **123,** 281–289 (2011).

208. Doherty, K. R. *et al.* Structural and functional screening in human induced-pluripotent stem cell-derived cardiomyocytes accurately identifies cardiotoxicity of multiple drug types. *Toxicol. Appl. Pharmacol.* **285,** 51–60 (2015).

209. Mosmann, T. Rapid colorimetric assay for cellular growth and survival: Application to proliferation and cytotoxicity assays. *J. Immunol. Methods* **65,** 55–63 (1983).

210. Ke, N., Wang, X., Xu, X. & Abassi, Y. A. The xCELLigence system for real-time and label-free monitoring of cell viability. *Methods Mol. Biol.* **740,** 33–43 (2011).

211. Lamore, S. D. & Scott, C. W. Cardiomyocyte Impedance Assays Assay Guidance Manual.

212. Axiogenesis/Ncardia. Cor.4U in xCELLigence RTCA Cardio assays. (2018). at <https://ncardia.com/files/documents/manuals/Protocol_Cor.4U_xCELLigence_RTCA_Cardio.pdf>

213. Siramshetty, V. B. *et al.* WITHDRAWN - A resource for withdrawn and discontinued drugs. *Nucleic Acids Res.* **44,** D1080–D1086 (2016).

214. Clancy, C. E., Kurokawa, J., Tateyama, M., Wehrens, X. H. T. & Kass, R. S. K+ channel structure-activity relationships and mechanisms of drug-induced QT prolongation. *Annu. Rev. Pharmacol. Toxicol.* **43,** 441–461 (2003).

215. Roden, D. M. Drug-Induced Prolongation of the QT Interval. 1013–1022 (2004).

216. Quasar. Action potential ventricular myocyte. (2010). at <https://commons.wikimedia.org/wiki/File:Action_potential_ventr_myocyte.gif>

217. Grilo, L. S., Carrupt, P. A. & Abriel, H. Stereoselective inhibition of the hERG1 potassium channel. *Front. Pharmacol.* **1,** 1–11 (2010).

218. National centre for the replacement, refinement and reduction of animals in research (NC3Rs). The 3Rs. (2018). at <https://www.nc3rs.org.uk/the-3rs>

219. O'Hara, T. & Rudy, Y. Quantitative comparison of cardiac ventricular myocyte electrophysiology and response to drugs in human and nonhuman species. *AJP Hear. Circ. Physiol.* **302,** H1023–H1030 (2012).

220. International conference on harmonisation of technical requirements for registration of pharmaceuticals for human use. *ICH-S9 Guidelines: Non clinical evaluation for anticancer pharmaceuticals*. (2009). at <http://www.ich.org/fileadmin/Public_Web_Site/ICH_Products/Guidelines/Safety/S9/Step4/S9_Step4_Guideline.pdf>

221. Curigliano, G. *et al.* Cardiotoxicity of Anticancer Treatments : Epidemiology , Detection, and Management. *A Cancer J. Cliinicians* **0,** 1–16 (2016).

222. Truong, J., Mailloux, R. J. & Chan, H. M. Impact of methylmercury exposure on mitochondrial energetics in AC16 and H9C2 cardiomyocytes. *Toxicol. Vitr.* **29,** 953–961 (2015).

223. Xiao, Y. *et al.* Cucurbitacin B Protects Against Pressure Overload Induced Cardiac Hypertrophy. *J. Cell. Biochem.* **118,** 3899–3910 (2017).

224. European medicines agency. *Sunitinib scientific discussion*. (2018). at <http://www.ema.europa.eu/docs/en_GB/document_library/EPAR_-_Scientific_Discussion/human/000687/WC500057733.pdf>

225. Shelburne, N. *et al.* Cancer Treatment-Related Cardiotoxicity: Current State of Knowledge and Future Research Priorities. *JNCI J. Natl. Cancer Inst.* **106,** dju232-dju232 (2014).

226. Abassi, Y. Functional maturation of human iPSC-derived cardiomyocytes and assessment of inotropic compounds. in *ACEA cardiosymposium* (2017).

227. Watkins, S. J., Borthwick, G. M., Oakenfull, R., Robson, A. & Arthur, H. M. Angiotensin II-induced cardiomyocyte hypertrophy in vitro is TAK1-dependent and Smad2/3-independent. *Hypertens. Res.* **35,** 393–398 (2012).

228. Liu, Y. *et al.* Angiotensin II stimulation in vitro induces hypertrophy of normal and postinfarcted ventricular myocytes. *Circ. Res.* **82,** 1145–1159 (1998).

229. Gray, M. O., Long, C. S., Kalinyak, J. E., Li, H. T. & Karliner, J. S. Angiotensin II stimulates cardiac myocyte hypertrophy via paracrine release of TGF-β1and endothelin-1 from fibroblasts. *Cardiovasc. Res.* **40,** 352–363 (1998).

230. Allen, I., Cohen, N. & Dhallan, R. Angiotensin II increases spontaneous contractile frequency and stimulates calcium current in cultured neonatal rat heart myocytes: insights into the underlying biochemical mechanisms. *Circ. …* **62,** 524–534 (1988).

231. De Mello, W. C. *Renin angiotensin system and the heart*. (John Wiley & Sons, 2004).

232. Doherty, K. R. *et al.* Multi-parameter in vitro toxicity testing of crizotinib, sunitinib, erlotinib, and nilotinib in human cardiomyocytes. *Toxicol. Appl. Pharmacol.* **272,** 245–255 (2013).

233. Yeh, E. T. H. & Vejpongsa, P. Subclinical Cardiotoxicity Associated With Cancer TherapyEarly Detection and Future Directions∗. *J. Am. Coll. Cardiol.* **65,** 2523–2525 (2015).

234. Herrmann Joerg, L. A. An update on cardio-oncology. *Trends Cardiovasc. Med.* **1,** 6–12 (2014).

235. Chatterjee, K., Zhang, J., Honbo, N. & Karliner, J. S. Doxorubicin cardiomyopathy. *Cardiology* **115,** 155–162 (2010).

236. Pecoraro, M. *et al.* Inflammatory mediators in a short-time mouse model of doxorubicin-induced cardiotoxicity. *Toxicol. Appl. Pharmacol.* **293,** 44–52 (2016).

237. Ewer, M. S. & Yeh, E. T. H. in (BC Decker, 2006).

238. Coombes, R. C. *et al.* Adjuvant Cyclophosphamide, Methotrexate, and Fluorouracil Versus Fluorouracil, Epirubicin, and Cyclophosphamide Chemotherapy in Premenopausal Women with Axillary Node-Positive Operable Breast Cancer: Results of a Randomized Trial. *J. Clin. Oncol.* **14,** 35–45 (1996).

239. Ryberg, M. *et al.* Epirubicin cardiotoxicity: An analysis of 469 patients with metastatic breast cancer. *J. Clin. Oncol.* **16,** 3502–3508 (1998).

240. Halazun, J. F., Wagner, H. ., Gaeta, J. F. & Sinks, L. F. Daunorubicin cardiac toxicity in children with acute lymphocytic leukemia. *Cancer* **33,** 545–554 (1974).

241. Feijen, E. A. M. *et al.* Equivalence ratio for daunorubicin to doxorubicin in relation to late heart failure in survivors of childhood cancer. *J. Clin. Oncol.* **33,** 3774–3780 (2015).

242. Speth, P. a, Linssen, P. C., Boezeman, J. B., Wessels, H. M. & Haanen, C. Leukemic cell and plasma daunomycin concentrations after bolus injection and 72 h infusion. *Cancer Chemother. Pharmacol.* **20,** 311–315 (1987).

243. Barpe, D. R., Rosa, D. D. & Froehlich, P. E. Pharmacokinetic evaluation of doxorubicin plasma levels in normal and overweight patients with breast cancer and simulation of dose adjustment by different indexes of body mass. *Eur. J. Pharm. Sci.* **41,** 458–463 (2010).

244. Eksborg, S. Anthracycline pharmacokinetics. Limited sampling model for plasma level monitoring with special reference to epirubicin (Farmorubicin). *Acta Oncol. (Madr).* **29,** 339–342 (1990).

245. Ahmadi, M. *et al.* Hypoxia modulates the activity of a series of clinically approved tyrosine kinase inhibitors. *Br. J. Pharmacol.* **171,** 224–236 (2014).

246. Chularojmontri, L., Gerdprasert, O. & Wattanapitayakul, S. K. Pummelo protects doxorubicin-induced cardiac cell death by reducing oxidative stress, modifying glutathione transferase expression, and preventing cellular senescence. *Evidence-based Complement. Altern. Med.* **2013,** (2013).

247. Unverferth, D. V *et al.* Human myocardial morphologic and functional changes in the first 24 hours after doxorubicin administration. *Cancer Treat. Rep.* **65,** 1093–1097 (1981).

248. Merten, K. E., Jiang, Y., Feng, W. & Kang, Y. J. Calcineurin Activation Is Not Necessary for Doxorubicin- Induced Hypertrophy in H9c2 Embryonic Rat Cardiac Cells : Involvement of the Phosphoinositide 3-Kinase-Akt Pathway. *Pharmacology* **319,** 934–940 (2006).

249. Koci, B. *et al.* An impedance-based approach using human iPSC-derived cardiomyocytes significantly improves in vitro prediction of in vivo cardiotox liabilities. *Toxicol. Appl. Pharmacol.* **329,** 121–127 (2017).

250. Wu, Z.-J. *et al.* Sodium Ferulate Prevents Daunorubicin - Induced Apoptosis in H9c2 Cells via Inhibition of the ERKs Pathway. *Cell. Physiol. Biochem.* **36,** 2121–2136 (2015).

251. Toldo, S. *et al.* Comparative Cardiac Toxicity of Anthracyclines In Vitro and In Vivo in the Mouse. *PLoS One* **8,** 4–11 (2013).

252. Chan, E. M., Thomas, M. J., Bandy, B. & Tibbits, G. F. Effects of doxorubicin, 4'-epirubicin, and antioxidant enzymes on the contractility of isolated cardiomyocytes. *Can.J.Physiol Pharmacol.* **74,** 904–910 (1996).

253. Ramanathan-Girish, S. & Boroujerdi, M. Contradistinction between doxorubicin and epirubicin: in-vitro interaction with blood components. *J. Pharm. Pharmacol.* **53,** 815–21 (2001).

254. Kania, K., Dragojew, S. & Wiak, Z. J. Ó. Ź. Morphological and Biochemical Changes in Human fibroblast lines induced by anthracyclines. *Biol. Lett.* **8,** 121–126 (2003).

255. Wenzel, D. G. & Cosma, G. N. A model system for measuring comparative toxicities of cardiotoxic drugs for cultured rat heart myocytes, endothelial cells and fibroblasts. II. Doxorubicin, 5-fluorouracil and cyclophosphamide. *Toxicology* **33,** 117–128 (1984).

256. Myers C, Bonow R, Palmeri S, Jenkins J, Corden B, Locker G, Doroshow J, E. S. A randomized controlled trial assessing the prevention of doxorubicin cardiomyopathy by N-acetylcysteine. *Semin. Oncol.* **10,** 53–55 (1983).

257. Soga, M. *et al.* Effects of angiotensin II receptor blocker (candesartan) in daunorubicin-induced cardiomyopathic rats. *Int. J. Cardiol.* **110,** 378–385 (2006).

258. Iqbal, M., Dubey, K., Anwer, T., Ashish, A. & Pillai, K. K. Protective effects of telmisartan against acute doxorubicin-induced cardiotoxicity in rats. *Pharmacol. Reports* **60,** 382–390 (2008).

259. Maejima, Y. *et al.* Telmisartan, a unique ARB, improves left ventricular remodeling of infarcted heart by activating PPAR gamma. *Lab. Investig.* **91,** 932–944 (2011).

260. Chang, S. A. *et al.* A novel angiotensin type I receptor antagonist, fimasartan, prevents doxorubicin-induced cardiotoxicity in rats. *J. Korean Med. Sci.* **30,** 559–568 (2015).

261. Abd El-Aziz, M. A., Othman, A. I., Amer, M. & El-Missiry, M. A. Potential protective role of angiotensin-converting enzyme inhibitors captopril and enalapril against adriamycin-induced acute cardiac and hepatic toxicity in rats. *J. Appl. Toxicol.* **21,** 469–473 (2001).

262. Hiona, A. *et al.* Pre-treatment with ACE Inhibitor Attenuates Doxorubicin Induced Cardiomyopathy via Preservation of Mitochondrial Function. *Natl. Institutes Heal.* **142,** 396–403 (2011).

263. Ibrahim, M. A. *et al.* Angiotensin-converting enzyme inhibition and angiotensin AT1-receptor antagonism equally improve doxorubicin-induced cardiotoxicity and nephrotoxicity. *Pharmacol. Res.* **60,** 373–381 (2009).

264. The Medicines and Healthcare Products Regulatory Agency (MHRA). *Scientific discussions for telmisartan, losartan and enalapril*. (2018).

265. Toko, H. *et al.* Angiotensin II Type 1a Receptor Mediates Doxorubicin-Induced Cardiomyopathy. *Hypertens. Res.* 597–603 (2002).

266. Sparks, M. A., Crowley, S. D., Gurley, S. B., Mirotsou, M. & Coffman, T. M. Classical renin-angiotensin system in kidney physiology. *Compr. Physiol.* **4,** 1201–1228 (2014).

267. Medicines.org.uk. Enalapril Summary of product characteristics. (2018). at <https://www.medicines.org.uk/emc/product/561#PHARMACOLOGICAL_PROPS>

268. Danser, a H. Cardiac angiotensin II: does it have a function? *Am J Physiol Hear. Circ Physiol* **299,** H1304-6 (2010).

269. Gergely, S. *et al.* High Throughput Screening Identifies a Novel Compound Protecting Cardiomyocytes from Doxorubicin-Induced Damage. *Oxid. Med. Cell. Longev.* **2015,** 1–12 (2015).

270. Okin, P. M. Regression of Electrocardiographic Left Ventricular Hypertrophy by Losartan Versus Atenolol: The Losartan Intervention For Endpoint Reduction in Hypertension (LIFE) Study. *Circulation* **108,** 684–690 (2003).

271. Malmqvist, K. *et al. Regression of left ventricular hypertrophy in human hypertension with irbesartan. Journal of hypertension* **19,** (2001).

272. Zou, Y. *et al.* Mechanical stress activates angiotensin II type 1 receptor without the involvement of angiotensin II. *Nat. Cell Biol.* **6,** 499–506 (2004).

273. Peterson, K. L. Pressure Overload Hypertrophy and Congestive Heart Failure. *J. Am. Coll. Cardiol.* **39,** 672–675 (2002).

274. Haywood, G. a. *et al.* AT1 and AT2 angiotensin receptor gene expression in human heart failure. *Circulation* **95,** 1201–1206 (1997).

275. Zorov, D. B., Filburn, C. R., Klotz, L. O., Zweier, J. L. & Sollott, S. J. Reactive oxygen species (ROS)-induced ROS release: A new phenomenon accompanying induction of the mitochondrial permeability transition in cardiac myocytes. *J Exp Med* **192,** 1001–1014 (2000).

276. Brady, N. R. *et al.* Coordinated behavior of mitochondria in both space and time: A reactive oxygen species-activated wave of mitochondrial depolarization. *Biophys. J.* **87,** 2022–2034 (2004).

277. Taskin, E., Kindap, E. K., Ozdogan, K., Aycan, M. B. Y. & Dursun, N. Acute adriamycin-induced cardiotoxicity is exacerbated by angiotension II. *Cytotechnology* **68,** 33–43 (2016).

278. Satoh, T., Enokido, Y., Aoshima, H., Uchiyama, Y. & Hatanaka, H. Changes in mitochondrial membrane potential during oxidative stress-induced apoptosis in PC12 cells. *J. Neurosci. Res.* **50,** 413–420 (1997).

279. Okumura, K., Jin, D., Takai, S. & Miyazaki, M. Beneficial effects of angiotensin-converting enzyme inhibition in adriamycin-induced cardiomyopathy in hamsters. *Jpn. J. Pharmacol.* **88,** 183–8 (2002).

280. Bradford, M. M. A rapid and sensitive method for the quantitation of microgram quantities of protein utilizing the principle of protein-dye binding. *Anal. Biochem.* **72,** 248–254 (1976).

281. Towbin, H., Staehelin, T. & Gordon, J. Electrophoretic transfer of proteins from polyacrylamide gels to nitrocellulose sheets: procedure and some applications. *Proc. Natl. Acad. Sci.* **76,** 4350–4354 (1979).

282. Arikawa, E., Quellhorst, G. & Han, Y. *RT2 Profiler PCR Arrays: Pathway-focused gene expression profiling with qRT-PCR*. (2015).

283. Qiagen. *RNeasy Mini Handbook*. (2012).

284. Qiagen. *RT2 Profiler PCR Array Handbook*. (2014).

285. Fillion, D. *et al.* Structure of the human angiotensin II type 1 (AT1) receptor bound to angiotensin II from multiple chemoselective photoprobe contacts reveals a unique peptide binding mode. *J. Biol. Chem.* **288,** 8187–8197 (2013).

286. Kobilka, B. K. G protein coupled receptor structure and activation. *Biochim. Biophys. Acta - Biomembr.* **1768,** 794–807 (2007).

287. Huang, C. Y. *et al.* Mitochondrial ROS-induced ERK1/2 activation and HSF2-mediated AT1R upregulation are required for doxorubicin-induced cardiotoxicity. *J. Cell. Physiol.* **233,** 463–475 (2018).

288. National centre for biotecnhology information (NCBI). Gene information - UCP1 uncoupling protein 1. (2018). at <https://www.ncbi.nlm.nih.gov/gene/7350>

289. National centre for biotecnhology information (NCBI). Gene information - HAMP hepcidin antimicrobial peptide. (2018). at <https://www.ncbi.nlm.nih.gov/gene?Db=gene&Cmd=DetailsSearch&Term=57817>

290. Ruijie, L., Van berlo, J. H. & York, A. J. DUSP8 Regulates Cardiac Ventricular Remodeling by Altering ERK1/2 Signaling. *Circ. Res.* **119,** 249–260 (2016).

291. Wang, X. & Ranek, M. J. Activation of the ubiquitin-proteasome system in doxorubicin cardiomyopathy. *Current Hypertension Reports* **11,** 389–395 (2009).

292. National centre for biotecnhology information (NCBI). Gene information - SOX4 SRY-box 4. (2018). at <https://www.ncbi.nlm.nih.gov/gene/6659>

293. Poizat, C., Sartorelli, V., Chung, G., Kloner, R. A. & Kedes, L. Proteasome-mediated degradation of the coactivator p300 impairs cardiac transcription. *Mol. Cell. Biol.* **20,** 8643–8654 (2000).

294. Meder, B. *et al.* JunB-CBFbeta signaling is essential to maintain sarcomeric Z-disc structure and when defective leads to heart failure. *J. Cell Sci.* **123,** 2613–20 (2010).

295. Kelly, D. *et al.* Plasma matrix metalloproteinase-9 and left ventricular remodelling after acute myocardial infarction in man: A prospective cohort study. *Eur. Heart J.* **28,** 711–718 (2007).

296. Polegato, B. F. *et al.* Acute doxorubicin-induced cardiotoxicity is associated with matrix metalloproteinase-2 alterations in rats. *Cell. Physiol. Biochem.* **35,** 1924–1933 (2015).

297. Yaghooti, H., Firoozrai, M., Fallah, S. & Khorramizadeh, M. R. Angiotensin II differentially induces matrix metalloproteinase-9 and tissue inhibitor of metalloproteinase-1 production and disturbs MMP/TIMP balance. *Avicenna J. Med. Biotechnol.* **2,** 79–85 (2010).

298. Wang, S. *et al.* Angiotensin II Facilitates Matrix Metalloproteinase-9-Mediated Myosin Light Chain Kinase Degradation in Pressure Overload-Induced Cardiac Hypertrophy. *Cell. Physiol. Biochem.* **44,** 2281–2295 (2018).

299. National centre for biotecnhology information (NCBI). CRHR1 corticotropin releasing hormone receptor 1. (2018). at <https://www.ncbi.nlm.nih.gov/gene/1394>

300. Armando, I., Volpi, S., Aguilera, G. & Saavedra, J. M. Angiotensin II AT1receptor blockade prevents the hypothalamic corticotropin-releasing factor response to isolation stress. *Brain Res.* **1142,** 92–99 (2007).

301. Mastorakos, G., Karoutsou, E. I. & Mizamtsidi, M. Corticotropin releasing hormone and the immune/inflammatory response. *Eur. J. Endocrinol.* **155,** S77–S84 (2006).

302. Ley, K. & Huo, Y. VCAM-1 is critical in atherosclerosis. *Journal of Clinical Investigation* **107,** 1209–1210 (2001).

303. Pueyo, M. E. *et al.* Angiotensin II stimulates endothelial vascular cell adhesion molecule-1 via nuclear factor-kappaB activation induced by intracellular oxidative stress. *Arterioscler. Thromb. Vasc. Biol.* **20,** 645–651 (2000).

304. National centre for biotecnhology information (NCBI). Gene information - RGS2 regulator of G protein signaling 2. (2018). at <https://www.ncbi.nlm.nih.gov/gene/5997>

305. National centre for biotecnhology information (NCBI). Gene information - AGTRAP angiotensin II receptor associated protein. (2018). at <https://www.ncbi.nlm.nih.gov/gene/57085>

306. National centre for biotecnhology information (NCBI). GNAS GNAS complex locus. (2018). at <https://www.ncbi.nlm.nih.gov/gene/2778>

307. National centre for biotecnhology information (NCBI). GNAQ G protein subunit alpha q. (2018). at <https://www.ncbi.nlm.nih.gov/gene/2776>

308. Hong, H. J. *et al.* Angiotensin II induces endothelin-1 gene expression via extracellular signal-regulated kinase pathway in rat aortic smooth muscle cells. *Cardiovasc Res* **61,** 159–168 (2004).

309. Lorenzo, O. *et al.* Angiotensin II increases parathyroid hormone-related protein (PTHrP) and the type 1 PTH/PTHrP receptor in the kidney. *J. Am. Soc. Nephrol.* **13,** 1595–1607 (2002).

310. Chua, C. C., Hamdy, R. C. & Chua, B. H. Upregulation of vascular endothelial growth factor by angiotensin II in rat heart endothelial cells. *Biochim. Biophys. Acta* **1401,** 187–94 (1998).

311. Li, H. T. *et al.* Cross talk between angiotensin AT1 and alpha 1-adrenergic receptors: angiotensin II downregulates alpha 1a-adrenergic receptor subtype mRNA and density in neonatal rat cardiac myocytes. *Circ Res* **81,** 396–403 (1997).

312. Sharma, A. *et al.* High-throughput screening of tyrosine kinase inhibitor cardiotoxicity with human induced pluripotent stem cells. *Sci. Transl. Med.* **9,** 2231–2247 (2017).

313. Morbidelli, L., Donnini, S. & Ziche, M. Targeting endothelial cell metabolism for cardio-protection from the toxicity of antitumor agents. *Cardio-Oncology* **2,** 3 (2016).

314. Burridge, P. W. *et al.* Human induced pluripotent stem cell – derived cardiomyocytes recapitulate the predilection of breast cancer patients to doxorubicin-induced cardiotoxicity. *Nat Med.* **22,** 547–556 (2016).

315. Danser, A. H. J. *et al.* Angiotensin-converting enzyme in the human heart: Effect of the deletion/insertion polymorphism. *Circulation* **92,** 1387–1388 (1995).

316. Cambien, F. *et al.* Deletion polymorphism in the gene for angiotensin-converting enzyme is a potent risk factor for myocardial infarction. *Nature* **359,** 641–644 (1992).

Appendix 1: Conference Abstracts

Characterisation of novel molecular mechanisms involved in anthracycline-induced cardiotoxicity

Rockley KL, Richardson G and Gill JH

Cardiotoxicity is a major complication of many anticancer therapies, impacting the quality of life and overall survival of patients, manifesting as both an acute toxicity and frequently a chronic toxicity occurring months/years after conclusion of therapy. Consequently, greater understanding of the molecular mechanisms responsible for these toxicities, or identification of therapeutic strategies to mitigate and overcome these toxicities are significantly important. Recently, clinical studies have demonstrated administration of angiotensin-converting enzyme inhibitors (ACEi) and/or β-blockers may reduce the cardiotoxicity of anthracyclines. However, despite showing promise, the molecular mechanisms responsible for toxicity mitigation are currently unknown. Furthermore, the majority of studies to date have either used inappropriate cell models or utilised end-point assays to evaluate this mechanism, both strategies that fail to account for the progressive nature of human toxicity development. In this study, using a human adult cardiomyocyte cell line and *in vitro* real-time impedance-based cell analyses (xCELLigence technology) we demonstrate the induction of cardiomyocyte hypertrophy by doxorubicin, and through its reduction by blockade of the angiotensin pathway, implicate synergism between doxorubicin-mediated toxicity and direct activity of angiotensin II upon cardiomyocytes. The methodologies in this study offer a robust clinically relevant model for assessing drug-induced cardiotoxicity, with the study identifying a novel mechanism for anthracycline-induced cardiotoxicity.

Presented at the British toxicology society (BTS) annual symposium held in Manchester in April 2016

Awarded a student bursary to attend the BTS annual symposium

Won annual best poster presentation prize

Characterisation of novel molecular mechanisms involved in anthracycline-induced cardiotoxicity

Rockley KL[1], Richardson G[2] and Gill JH[1]

[1]School of Medicine, Pharmacy and Health, Durham University, Stockton-on-Tees, UK
[2]Institute of Genetic Medicine, Newcastle University, International Centre for Life, Newcastle-upon-tyne, UK

Cardiotoxicity is a major complication of many anticancer therapies, often impacting the quality of life and overall survival of patients. Consequently, greater understanding of the molecular mechanisms responsible for these adverse effects and identification of therapeutic strategies to mitigate the underpinning toxicities are of the upmost importance. Recent clinical studies have demonstrated that medicines acting upon the angiotensin signalling pathway may reduce anthracycline-induced cardiotoxicity and improve clinical outcomes. However, despite showing promise, the molecular mechanisms and pathways responsible for angiotensin-mediated mitigation of anthracycline toxicity are currently unclear.

STUDY AIMS

- The aim of this study was to investigate the molecular mechanisms of anthracycline-induced cardiotoxicity and identify the role of angiotensin II.
- Using *in vitro* real-time impedance-based cell analyses (xCELLigence system) changes in cell survival, morphology and drug response were evaluated against a human adult ventricular cardiomyocyte cell line (AC10).
- The response of cardiomyocytes to angiotensin II, doxorubicin (anthracycline), and blockade of the angiotensin II receptor in the presence/absence of doxorubicin were then evaluated.

METHOD

Figure 1. Overview of xCELLigence Real Time Cell Analysis (RTCA) technology

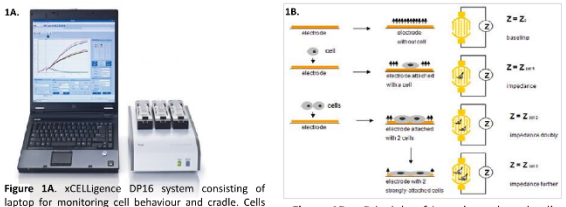

Figure 1A. xCELLigence DP16 system consisting of laptop for monitoring cell behaviour and cradle. Cells are seeded inside a 16 well E-plate which is kept inside the cradle

Figure 1B. Principle of impedance based cell detection

Figure 2. Characterisation of cardiac phenotype of AC10 cells

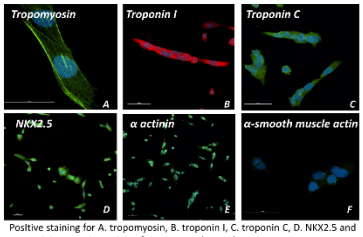

Positive staining for A. tropomyosin, B. troponin I, C. troponin C, D. NKX2.5 and E. α actinin. Negative staining for F. α-smooth muscle actin.

RESULTS

Figure 3. Angiotensin II induces hypertrophy of AC10 cardiomyocytes

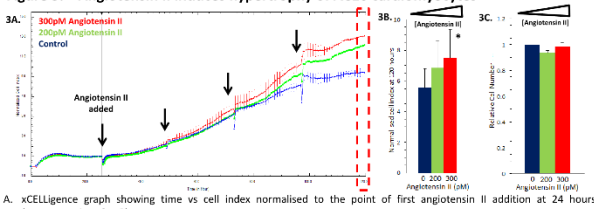

A. xCELLigence graph showing time vs cell index normalised to the point of first angiotensin II addition at 24 hours (representative of n=3)
B. Normalised cell index at 120 hours following daily addition of angiotensin II (n=3±SE) *p<0.05
C. Relative cell number at 120 hours following daily addition of angiotensin II measured by MTT assay (n=3±SE)

Increased cell index without increase in cell number indicates that angiotensin II induces cardiomyocyte hypertrophy.

Figure 4. Doxorubicin induces hypertrophy of AC10 cardiomyocytes

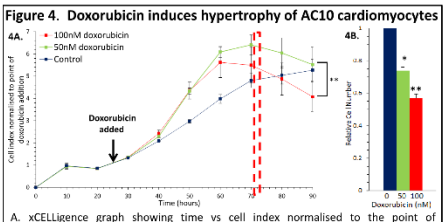

A. xCELLigence graph showing time vs cell index normalised to the point of doxorubicin addition at 24 hours (n=3±SE), **p<0.01
B. Relative cell number at 72 hours following doxorubicin treatment measured by MTT assay (n=3±SE) *p<0.05, **p<0.01

Increased cell index with a decrease in cell survival indicates that doxorubicin induces cardiomyocyte hypertrophy.

Figure 5. Blockade of the angiotensin receptor reduces toxicity of doxorubicin in cardiomyocytes, but does not affect efficacy of doxorubicin in cancer cells

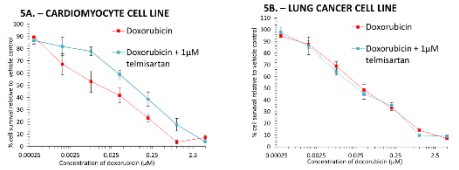

A. % cell survival of AC10 cells treated with doxorubicin +/- 1μM telmisartan (n=3±SE)
B. % cell survival of lung cancer cells treated with doxorubicin +/- 1μM telmisartan (n=3±SE)

5C.	IC50 (nM) AC10 Cardiomyocytes	IC50 (nM) Lung caner cell line
Doxorubicin	16 ± 12.02	37.33 ± 11.58
Doxorubicin + 1μM Telmisartan	96.67 ± 27.32 *	32.6 ± 9.34
Doxorubicin + 5μM Telmisartan	90 ± 30.03 *	14.5 ± 5.5

C. Telmisartan reduces cardiotoxicity of doxorubicin in AC10 cardiomyocytes at both low and high concentrations relative to doxorubicin alone (n=3±SE) *p<0.05

Figure 6. The angiotensin receptor blocker telmisartan reduces doxorubicin-induced cardiomyocyte hypertrophy

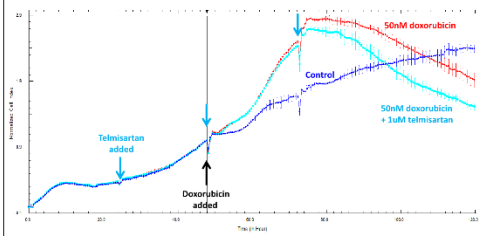

6. xCELLigence graph showing time vs cell index normalised to the point of doxorubicin addition at 48 hours. Telmisartan was added at 24, 48 and 72 hours.

CONCLUSION

- Angiotensin II and doxorubicin induce cardiomyocyte hypertrophy.
- Blockade of the angiotensin receptor by telmisartan mitigates the hypertrophic and cardiotoxic effects of doxorubicin, but does not affect anti-cancer efficacy.
- Reduction of doxorubicin induced cardiomyocyte hypertrophy by blockade of the angiotensin pathway strongly implies a relationship between doxorubicin-mediated toxicity and direct activity of angiotensin II upon cardiomyocytes.
- These data support blockade of angiotensin signalling as a therapeutic strategy for managing anthracycline-induced cardiotoxicity.

ACKNOWLEDGMENT: We would like to thank Durham University for providing funding to support this project.

Characterisation of novel molecular mechanisms involved in anthracycline-induced cardiotoxicity

Rockley KL, Richardson G and Gill JH

Recent advances in cancer treatment have improved cancer survivorship; however as a result the incidence of cancer therapy induced cardiotoxicity has increased. This major complication can present both as an acute toxicity or a chronic toxicity and can impose substantial detriment to both the quality of life and survival of patients. Consequently, greater understanding of the molecular mechanisms responsible for these toxicities, and identification of therapeutic strategies to mitigate and overcome these toxicities are significantly important. Recently, clinical studies have demonstrated that administration of drugs that act upon the angiotensin system may reduce the cardiotoxicity of anthracyclines. However, despite showing promise, the molecular mechanisms responsible for toxicity mitigation are currently unknown. This study has utilised a variety of human cardiomyocyte *in vitro* models and real-time impedance-based cell analyses (xCELLigence technology) to demonstrate induction of cardiomyocyte hypertrophy by doxorubicin, and through its reduction by blockade of the angiotensin pathway, implicates synergism between doxorubicin-mediated toxicity and angiotensin signalling in cardiomyocytes. Beat characteristics of iPSC derived cardiomyocytes have also been assessed using xCELLigence Cardio technology during exposure to doxorubicin alone and during angiotensin blockade in an attempt to elucidate the effects of cardiomyocyte hypertrophy on contractility of these cells. The methodologies used in this study offer a robust clinically relevant model for assessing drug-induced cardiotoxicity, with the study identifying a novel mechanism for anthracycline-induced cardiotoxicity.

Presented at the Safety Pharmacology Society (SPS) annual meeting and the ACEA cardio symposium both held in Vancouver in September 2016

Awarded a student travel bursary to attend the SPS annual meeting

Awarded 1st place in the SPS junior investigator poster competition

Characterisation of novel molecular mechanisms involved in anthracycline-induced cardiotoxicity

Rockley KL[1], Richardson G[2] and Gill JH[1]

[1]School of Medicine, Pharmacy and Health, Durham University, Stockton-on-Tees, UK; [2]Institute of Genetic Medicine, Newcastle University, International Centre for Life, Newcastle-upon-tyne, UK

Cardiotoxicity is a major complication of many anticancer therapies, often impacting the quality of life and overall survival of patients. Consequently, greater understanding of the molecular mechanisms responsible for these adverse effects and identification of therapeutic strategies to mitigate the underpinning toxicities are of the upmost importance. Recent clinical studies have demonstrated that medicines acting upon the angiotensin signalling pathway may reduce anthracycline-induced cardiotoxicity and improve clinical outcomes. However, despite showing promise, the molecular mechanisms and pathways responsible for angiotensin-mediated mitigation of anthracycline toxicity are currently unclear.

STUDY AIMS

- The aim of this study was to investigate the molecular mechanisms of anthracycline-induced cardiotoxicity and identify the role of angiotensin II.
- Using *in vitro* real-time impedance-based cell analyses (xCELLigence system) changes in cell survival, morphology and drug response were evaluated against a human adult ventricular cardiomyocyte cell line (AC10).
- iPSC-derived cardiomyocytes (axioGENESIS) were also evaluated for changes in contractility, morphology and drug response using the CARDIO xCELLigence system.
- The response of these cardiomyocytes to angiotensin II, doxorubicin (anthracycline), and blockade of the angiotensin II receptor in the presence/absence of doxorubicin were then evaluated.

RESULTS

Figure 1. Cardiac phenotype of AC10 cells

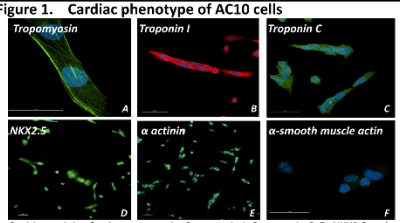

Positive staining for A. tropomyosin, B. troponin I, C. troponin C, D. NKX2.5 and E. α actinin. Negative staining for F. α-smooth muscle actin.

Figure 2. Angiotensin II induces hypertrophy of AC10 cardiomyocytes

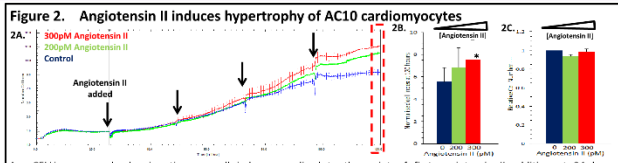

A. xCELLigence graph showing time vs cell index normalised to the point of first angiotensin II addition at 24 hours (representative of n=3)
B. Normalised cell index at 120 hours following daily addition of angiotensin II (n=3±SE) *p<0.05
C. Relative cell number at 120 hours following daily addition of angiotensin II measured by MTT assay (n=3±SE)

Increased cell index without increase in cell number indicates that angiotensin II induces cardiomyocyte hypertrophy.

Figure 3. Angiotensin II induces hypertrophy of iPSC-derived cardiomyocytes but does not affect contractility

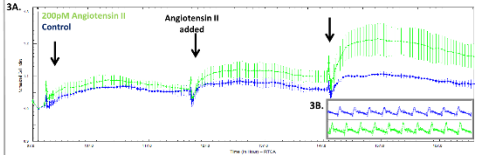

A. xCELLigence graph showing time vs cell index normalised to the point of first angiotensin II addition
B. Stable beating of control and angiotensin II treated iPSC-derived cardiomyocytes

Figure 4. Doxorubicin induces hypertrophy of AC10 cardiomyocytes

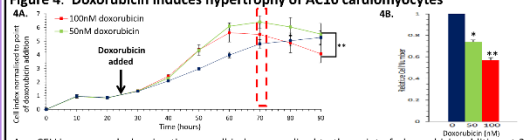

A. xCELLigence graph showing time vs cell index normalised to the point of doxorubicin addition at 24 hours (n=3±SE), **p<0.01
B. Relative cell number at 72 hours following doxorubicin treatment measured by MTT assay (n=3±SE) *p<0.05, **p<0.01

Increased cell index with a decrease in cell survival indicates that doxorubicin induces cardiomyocyte hypertrophy.

Figure 5. Doxorubicin induces hypertrophy of iPSC-derived cardiomyocytes and does not affect contractility

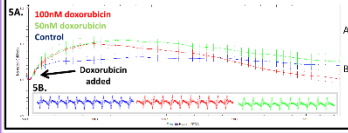

A. xCELLigence graph showing time vs cell index normalised to the point of doxorubicin addition
B. Stable beating of control and doxorubicin treated iPSC-derived cardiomyocytes

Figure 6. The angiotensin receptor blocker telmisartan reduces doxorubicin-induced AC10 cardiomyocyte hypertrophy

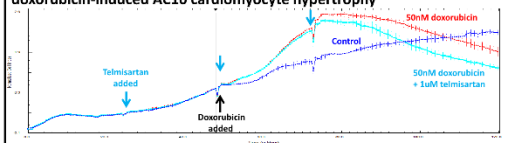

6. xCELLigence graph showing time vs cell index normalised to the point of doxorubicin addition at 48 hours. Telmisartan was added at 24, 48 and 72 hours

Figure 7. Telmisartan reduces doxorubicin-induced iPSC-derived cardiomyocyte hypertrophy and does not affect contractility

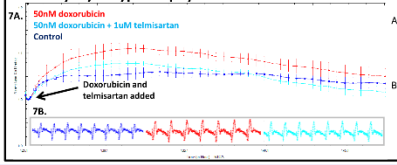

A. xCELLigence graph showing time vs cell index normalised to the point of doxorubicin addition.
B. Stable beating of control and doxorubicin treated iPSC-derived cardiomyocytes

Figure 8. Blockade of the angiotensin receptor reduces toxicity of doxorubicin n cardiomyocytes, but does not affect efficacy of doxorubicin in cancer cells

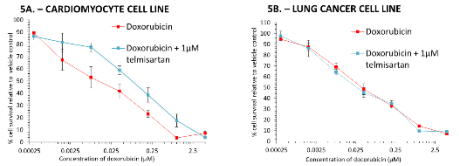

A. % cell survival of AC10 cells treated with doxorubicin +/- 1μM telmisartan (n=3±SE)

B. % cell survival of lung cancer cells treated with doxorubicin +/- 1μM telmisartan (n=3±SE)

8C.

	IC50 (nM)	
	AC10 Cardiomyocytes	Lung caner cell line
Doxorubicin	16 ± 12.02	37.33 ± 11.58
Doxorubicin + 1μM Telmisartan	96.67 ± 27.32 *	32.6 ± 9.34
Doxorubicin + 5μM Telmisartan	90 ± 30.03 *	14.5 ± 5.5

C. Telmisartan reduces cardiotoxicity of doxorubicin in AC10 cardiomyocytes at both low and high concentrations relative to doxorubicin alone (n=3±SE) *p<0.05

CONCLUSION

- Angiotensin II and doxorubicin induce cardiomyocyte hypertrophy in AC10 and iPSC-derived cardiomyocytes and do not affect contractility.
- Blockade of the angiotensin receptor by telmisartan mitigates the hypertrophic and cardiotoxic effects of doxorubicin, but does not affect anti-cancer efficacy.
- Reduction of doxorubicin induced cardiomyocyte hypertrophy by blockade of the angiotensin pathway strongly implies a relationship between doxorubicin-mediated toxicity and angiotensin II activity.
- These data support blockade of angiotensin signalling as a therapeutic strategy for managing anthracycline-induced cardiotoxicity.

ACKNOWLEDGMENT: We would like to thank Durham University for providing funding to support this project.

ACEA BIOSCIENCES, INC.

axioGENESIS

In vitro assessment of anthracycline-induced cardiotoxicity and mitigation through angiotensin blockade

Rockley KL, Pointon RA, Triffitt KL, Richardson G and Gill JH

Cardiotoxicity is a major complication of many anticancer therapies, particularly anthracyclines, impacting the quality of life and overall survival of patients. Consequently, greater understanding of the molecular mechanisms responsible for these toxicities, and identification of therapeutic strategies to mitigate and overcome these toxicities are significantly important. Recently, clinical studies have demonstrated that administration of drugs that act upon the angiotensin system may reduce the cardiotoxicity of anthracyclines. However, despite showing promise, the molecular mechanisms responsible for toxicity mitigation are currently unknown. Furthermore, the majority of studies to date have either used inappropriate cell models or utilised end-point assays to evaluate this mechanism, both strategies that fail to account for the progressive nature of human toxicity development. This study has utilised a variety of human cardiomyocyte *in vitro* models and real-time impedance-based cell analyses (xCELLigence technology) to demonstrate induction of cardiomyocyte hypertrophy by anthracyclines. Through its reduction by blockade of the angiotensin pathway, a relationship between anthracycline-mediated toxicity and angiotensin signalling in cardiomyocytes is demonstrated. The effect of angiotensin and the anthracyclines is also shown to be independent of cardiomyocyte contractility, as assessed be changes in cellular impedance (xCELLigence Cardio technology). The methodologies used offer a model for assessing drug-induced cardiotoxicity that is robust, clinically relevant and animal-free, with the study identifying a novel mechanism for anthracycline-induced cardiotoxicity.

Presented at the NC3Rs/Safety Pharmacology Society regional meeting: The use of human tissues for safety assessment held in Coventry in May 2017

In vitro assessment of anthracycline-induced cardiotoxicity and mitigation through angiotensin blockade

Rockley KL[1], Pointon RA[1], Triffitt KL[1], Richardson G[2] and Gill JH[1]

[1]School of Medicine, Pharmacy and Health, Durham University, Stockton-on-Tees, UK
[2]Institute of Genetic Medicine, Newcastle University, International Centre for Life, Newcastle-upon-Tyne, UK

Cardiotoxicity is a major complication of many anticancer therapies, often impacting the quality of life and overall survival of patients. Consequently, greater understanding of the molecular mechanisms responsible for these adverse effects and identification of therapeutic strategies to mitigate the underpinning toxicities are of the utmost importance. Recent clinical studies have demonstrated that medicines acting upon the angiotensin signalling pathway may reduce anthracycline-induced cardiotoxicity and improve clinical outcomes. However, despite showing promise, the molecular mechanisms and pathways responsible for angiotensin-mediated mitigation of anthracycline toxicity are currently unclear.

STUDY AIMS

- The aim of this study was to investigate the molecular mechanisms of anthracycline-induced cardiotoxicity and identify the role of angiotensin II.
- Using *in vitro* real-time impedance-based cell analyses (xCELLigence system) changes in cell survival, morphology and drug response were evaluated against a human adult ventricular cardiomyocyte cell line (AC10).
- iPSC-derived cardiomyocytes (Cor.4U - axiogenesis) were also evaluated for changes in contractility, morphology and drug response using the CARDIO xCELLigence system.
- The response of these cardiomyocytes to angiotensin II, anthracyclines (doxorubicin), and blockade of the angiotensin II receptor in the presence/absence of doxorubicin were then evaluated.

RESULTS

Figure 1. Characterisation of Cardiac phenotype of AC10 cardiomyocytes

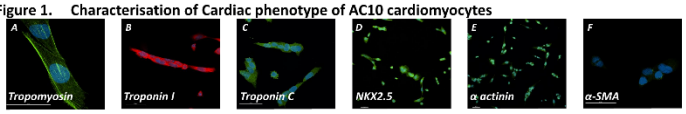

Positive staining for A. tropomyosin, B. troponin I, C. troponin C, D. NKX2.5 and E. α actinin. Negative staining for F. α-smooth muscle actin.

Figure 2. Angiotensin II induces hypertrophy of AC10 cardiomyocytes

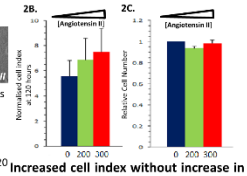

A. Angiotensin II treated cells
B. Normalised cell index at 120 hours following daily addition of angiotensin II (n=3±SE)
C. Relative cell number at 120 hours following daily addition of angiotensin II (n=3±SE)

Increased cell index without increase in cell number indicates that angiotensin II induces cardiomyocyte hypertrophy.

Figure 3. Angiotensin II induces hypertrophy of iPSC-derived cardiomyocytes but does not affect contractility

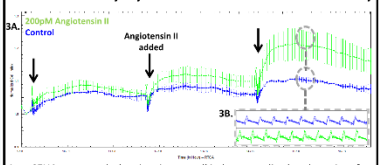

A. xCELLigence graph showing time vs cell index normalised to the point of first angiotensin II addition
B. Stable beating of control and angiotensin II treated iPSC-derived cardiomyocytes

Figure 4. Anthracyclines exhibit similar toxicity profiles on AC10 cardiomyocytes in both the exponential and plateau phases of growth

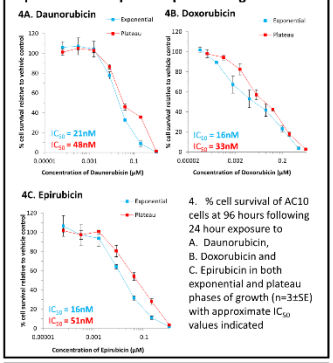

4. % cell survival of AC10 cells at 96 hours following 24 hour exposure to A. Daunorubicin, B. Doxorubicin and C. Epirubicin in both exponential and plateau phases of growth (n=3±SE) with approximate IC_{50} values indicated

Figure 5. Anthracyclines induce hypertrophy of AC10 cardiomyocytes in exponential and plateau growth phase

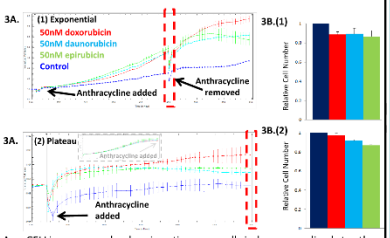

A. xCELLigence graph showing time vs cell index normalised to the point of anthracycline addition in (1) cells in exponential growth phase and (2) cells in plateau growth phase
B. Relative cell number at 24 hours following anthracycline treatment in (1) cells in exponential growth phase and (2) cells in plateau growth phase measured by MTT assay (n=3±SE)

Increased cell index with a decrease in cell survival indicates that anthracyclines induce cardiomyocyte hypertrophy.

Figure 6. Doxorubicin induces hypertrophy of iPSC-derived Cardiomyocytes and does not affect contractility

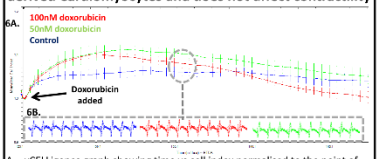

A. xCELLigence graph showing time vs cell index normalised to the point of doxorubicin addition
B. Stable beating of control and doxorubicin treated iPSC-derived cardiomyocytes

Figure 8. Angiotensin blockade reduces toxicity of doxorubicin in cardiomyocytes, but does not affect efficacy of doxorubicin in cancer cells

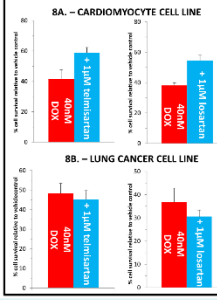

A. % cell survival of AC10 cells treated with 40nM doxorubicin +/- losartan and telmisartan (n=3±SE)

B. % cell survival of lung cancer cells treated with doxorubicin +/- losartan and telmisartan (n=3±SE)

Figure 7. Angiotensin blockade reduces doxorubicin-induced iPSC-derived cardiomyocyte hypertrophy and does not affect contractility

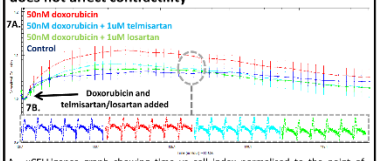

A. xCELLigence graph showing time vs cell index normalised to the point of doxorubicin addition
B. Stable beating of control and doxorubicin treated iPSC-derived cardiomyocytes

Figure 9. Angiotensin blockade reduces doxorubicin-induced AC10 cardiomyocyte hypertrophy

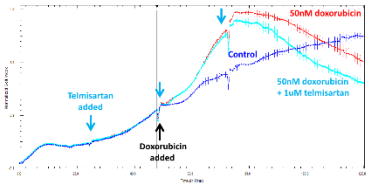

6. xCELLigence graph showing time vs cell index normalised to the point of doxorubicin addition at 48 hours. Telmisartan was added at 24, 48 and 72 hours

CONCLUSION

- Angiotensin II and anthracyclines induce cardiomyocyte hypertrophy in AC10 and iPSC-derived cardiomyocytes and do not affect contractility.
- Blockade of the angiotensin receptor by telmisartan and losartan mitigates the hypertrophic and cardiotoxic effects of doxorubicin, but does not affect anti-cancer efficacy.
- Reduction of doxorubicin induced cardiomyocyte hypertrophy by blockade of the angiotensin pathway strongly implies a relationship between doxorubicin-mediated toxicity and direct activity of angiotensin II upon cardiomyocytes.
- These data support blockade of angiotensin signalling as a therapeutic strategy for managing anthracycline-induced cardiotoxicity.

Miss Kimberly Rockley k.l.rockley@durham.ac.uk Final year PhD student

The use of xCELLigence systems to detect structural and functional cardiotoxicities of cancer therapies

Rockley KL, Brown S, Pointon RA and Gill JH

Recent advances in cancer treatment have improved cancer survivorship; however the cardiac safety of cancer therapeutics has lagged behind in comparison. Accurate predication of structural and functional cardiac liabilities pre-clinically is therefore of crucial importance. Both of these toxicities can be detected using iPSC-derived cardiomyocytes (iPSC-CMs) on the xCELLigence cardio system, and the similar xCELLigence real-time cell analyser (RTCA) system can detect morphology changes to cardiomyocyte cell lines such as AC10 cardiomyocytes (AC10-CMs). Both of these systems have the advantage that long-term experiments can be conducted, thus allowing recapitulation of the progressive nature of human toxicity development. This study has utilised these systems to demonstrate induction of cardiomyocyte hypertrophy by the tyrosine kinase inhibitor sunitinib and the notoriously cardiotoxic anthracyclines, with changes in contractility also detected with sunitinib addition. The sensitivity of these systems at detecting changes in cellular morphology is evidenced by concurrent anthracycline and angiotensin receptor blocker (ARB) treatment, where reductions in hypertrophy were observed. Recent clinical studies have demonstrated that administration of drugs that act upon the angiotensin system may reduce the cardiotoxicity of anthracyclines, thus the reduction of anthracycline-induced hypertrophy by ARBs shows the translational potential of these systems. The methodologies used offer a model for assessing drug-induced cardiotoxicity that is robust, clinically relevant and animal-free, with the study identifying both structural and functional cardiotoxicities and a novel mechanism for anthracycline-induced cardiotoxicity.

Presented at the ACEA cardio symposium held in Berlin in September 2017

The use of xCELLigence systems to detect structural and functional cardiotoxicities of cancer therapies

Rockley KL[1,2], Brown S[1], Pointon RA[1]and Gill JH[1,2] [1]School of Medicine, Pharmacy and Health, Durham University, Stockton-on-Tees, UK; [2]Northern Institute for cancer research, Newcastle University, Newcastle-upon-tyne, UK

Recent advances in cancer treatment have improved cancer survivorship; however the cardiac safety of cancer therapeutics has lagged behind in comparison. Cardiotoxicity is a major complication of many anticancer therapies such as sunitinib and anthracyclines, which frequently impacts the quality of life and overall survival of patients. Consequently, accurate predication of structural and functional cardiac liabilities pre-clinically, and identification of therapeutic strategies to mitigate the toxicities are of crucial importance. Recent clinical studies have demonstrated that medicines acting upon the angiotensin signalling pathway may reduce anthracycline-induced cardiotoxicity and improve clinical outcomes. However, despite showing promise, the molecular mechanisms and pathways responsible for angiotensin-mediated mitigation of anthracycline toxicity are currently unclear.

STUDY AIMS

- The aim of this study was to investigate the structural and functional cardiotoxicities induced by sunitinib and anthracyclines using *in vitro* real-time impedance-based cell analyses (xCELLigence systems)
- Changes in cell survival, morphology and drug response were evaluated against the AC10 human adult ventricular cardiomyocyte cell line (AC10-CMs) using clinically relevant doses
- Human iPSC-derived cardiomyocytes (Cor.4U - axiogenesis) were also evaluated for changes in contractility, morphology and drug response using the CARDIO xCELLigence system using clinically relevant doses
- The influence of angiotensin receptor blockade on doxorubicin (anthracycline) induced cardiotoxicity was evaluated in the cardiomyocytes in addition to its effect on expression of the AT_1 angiotensin receptor

RESULTS

1. Sunitinib induces hypertrophy of AC10 cardiomyocytes

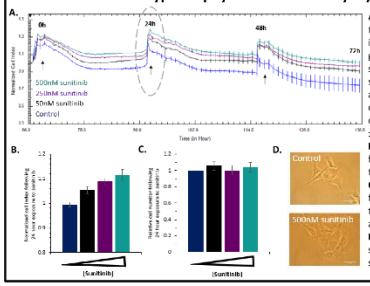

A. xCELLigence trace showing time (hours) vs normalised cell index of AC10-CMs in plateau growth phase exposed to sunitinib with points of sunitinib addition (arrows) and exposure time indicated, data representative of n=3, data points shown are average ± SD
B. Normalised cell index following 24 hours exposure to sunitinib, data is n=3 ± SE.
C. Relative cell number following 24 hours exposure to sunitinib measured by MTT assay, data is n=3 ± SE
D. Images of untreated and sunitinib treated AC10-CMs showing a morphology change

2. Sunitinib induces hypertrophy of iPSC-derived cardiomyocytes and induces contractility changes

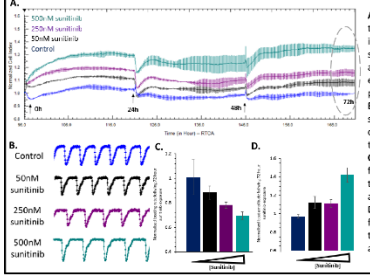

A. xCELLigence trace showing time (hours) vs normalised cell index of iPSC-CMs exposed to sunitinib with points of addition (arrows) and exposure time indicated, data points shown are average ± SD
B. Representative traces showing contractility of control cells and cells exposed to sunitinib for 72 hours
C. Normalised beating rate following 72 hours exposure to sunitinib, data points show average of 3 wells ± SE
D. Normalised beat amplitude following 72 hours exposure to sunitinib, data points show average of 3 wells ± SE.

3. Anthracyclines induce hypertrophy of AC10 cardiomyocytes

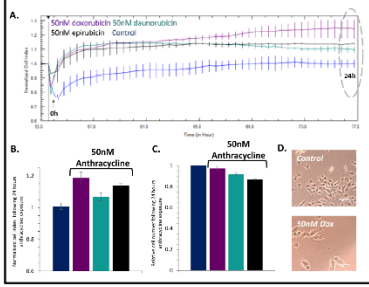

A. xCELLigence trace showing time (hours) vs normalised cell index of AC10-CMs in plateau growth phase exposed to anthracyclines with point of anthracycline addition (arrow) and exposure time indicated, data representative of n=3, data points shown are average ± SD
B. Normalised cell index following 24 hours exposure to anthracyclines, data is n=3 ± SE.
C. Relative cell number following 24 hours exposure to anthracyclines measured by MTT assay, data is n=3 ± SE
D. Images of untreated and doxorubicin treated AC10-CMs showing a morphology change

4. Anthracyclines induce hypertrophy of iPSC-derived cardiomyocytes and induce contractility changes, which are increased at higher doses

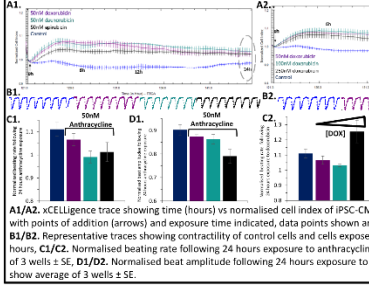

A1/A2. xCELLigence trace showing time (hours) vs normalised cell index of iPSC-CMs exposed to anthracyclines with points of addition (arrows) and exposure time indicated, data points shown are average ± SD
B1/B2. Representative traces showing contractility of control cells and cells exposed to anthracyclines for 24 hours, **C1/C2.** Normalised beating rate following 24 hours exposure to anthracyclines, data points show average of 3 wells ± SE, **D1/D2.** Normalised beat amplitude following 24 hours exposure to anthracyclines, data points show average of 3 wells ± SE.

5. Angiotensin receptor blockers reduce doxorubicin-induced iPSC-derived cardiomyocyte hypertrophy and do not affect contractility

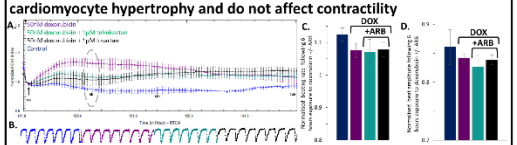

A. xCELLigence trace showing time (hours) vs normalised cell index of iPSC-CMs exposed to doxorubicin +/- ARBs with points of addition (arrow) and exposure time indicated, data points shown are average ± SD
B. Representative traces showing contractility of control cells and cells exposed to doxorubicin +/- ARB for 6 hours, **C.** Normalised beating rate following 6 hours exposure to doxorubicin +/- ARB, data points show average of 3 wells ± SE, **D.** Normalised beat amplitude following 6 hours exposure to doxorubicin +/- ARB, data points show average of 3 wells ± SE.

6. Blockade of the angiotensin receptor reduces toxicity of doxorubicin in AC10 cardiomyocytes, but does not affect doxorubicin efficacy in cancer cells

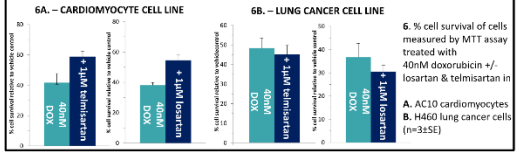

6. % cell survival of cells measured by MTT assay treated with 40nM doxorubicin +/- losartan & telmisartan in
A. AC10 cardiomyocytes
B. H460 lung cancer cells (n=3±SE)

7. Doxorubicin increases expression of the AT_1 angiotensin receptor in AC10 cardiomyocytes

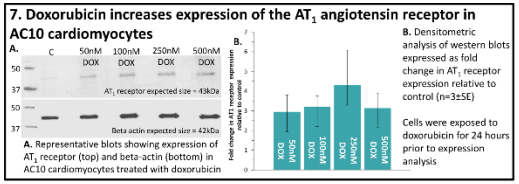

A. Representative blots showing expression of AT_1 receptor (top) and beta-actin (bottom) in AC10 cardiomyocytes treated with doxorubicin
B. Densitometric analysis of western blots expressed as fold change in AT_1 receptor expression relative to control (n=3±SE)

Cells were exposed to doxorubicin for 24 hours prior to expression analysis

CONCLUSION

- Sunitinib and the anthracyclines doxorubicin, daunorubicin and epirubicin induce cardiomyocyte hypertrophy in AC10 and iPSC-derived cardiomyocytes at clinically relevant doses
- Changes in contractility of iPSC-derived cardiomyocytes also occur with clinically relevant doses of sunitinib and doxorubicin
- Blockade of the angiotensin receptor by telmisartan and losartan mitigates the hypertrophic and cardiotoxic effects of doxorubicin, but does not affect anti-cancer efficacy
- In addition, increased expression of the AT_1 angiotensin receptor following doxorubicin treatment strongly implies a relationship between doxorubicin-mediated toxicity and angiotensin II activity
- These data support blockade of angiotensin signalling as a therapeutic strategy for managing anthracycline-induced cardiotoxicity.

k.l.rockley@durham.ac.uk *Miss Kimberly Rockley* *Final year PhD student*

The use of impedance-based systems to detect the structural and functional cardiotoxicity of cancer therapies

Accurate predication of cardiac liabilities pre-clinically is of crucial importance, with current methodologies proving inadequate, evidenced by drug withdrawals and the association of many cancer therapeutics with occurrence of cardiotoxicity. The adverse effects of cancer therapies on the heart can be broadly classified into structural and functional cardiotoxicities, both of which can be detected using iPSC-derived cardiomyocytes (iPSC-CMs) on the real-time impedance-based xCELLigence cardio system. Due to the rapid data acquisition and ability to record the transient minute movements of iPSC-CMs via changes in impedance, information on overall cell health, morphology and contractility can be monitored. Using a similar system, the xCELLigence real-time cell analyser (RTCA), changes in morphology can be detected on cardiomyocyte cell lines such as AC10 cardiomyocytes (AC10-CMs), showing the potential of this platform for detection of structural cardiotoxicities. Both of these impedance-based systems have the advantage that long-term experiments can be conducted, thus allowing recapitulation of the progressive nature of human toxicity development. This study has utilised these real-time impedance-based xCELLigence systems to demonstrate induction of cardiomyocyte hypertrophy by the tyrosine kinase inhibitor sunitinib and the notoriously cardiotoxic anthracyclines, with changes in contractility also detected with sunitinib addition. The sensitivity of these systems at detecting changes in cellular morphology is evidenced by concurrent anthracycline and angiotensin receptor blocker (ARB) treatment, where reductions in hypertrophy were observed. Recent clinical studies have demonstrated that administration of drugs that act upon the angiotensin system may reduce the cardiotoxicity of anthracyclines, thus the reduction of anthracycline-induced hypertrophy by ARBs shows the translational potential of these systems. The methodologies used offer a model for assessing drug-induced cardiotoxicity that is robust, clinically relevant and animal-free, with the study identifying both structural and functional cardiotoxicities and a novel mechanism for anthracycline-induced cardiotoxicity.

Oral presentation at the IVTS annual meeting held in London in November 2017

Appendix 2: Axol application note

Similar to the qualification of Cor.4U hiPSC-CMs (axiogenesis) described in Chapter 3 (Section 3.3.3), a study was conducted using Axol hiPSC-CMs which was published in Nature Methods Application Notes in November 2016.

axol

Application note

Non-invasive impedance monitoring of contractility in Axol Human iPSC-Derived Cardiomyocytes

The ability to monitor cardiomyocyte beat rate in real time is a powerful tool for drug discovery research, particularly when used in conjunction with human induced pluripotent stem cell (iPSC)-derived cells. This offers a physiologically relevant model in which to reliably assess cardiac liability, enabling lead compounds to be identified sooner, thereby reducing the rate of drug attrition and adverse reactions such as proarrythmias. To do this, human iPSC-derived cardiomyocytes (iPSC-CMs) (Axol Bioscience Ltd.) were cultured in a non-invasive impedance monitoring system (xCELLigence®) to assess cardiotoxicity and cell contractility in a 96-well plate format.

Materials and methods

Cardiomyocyte media preparation

Contents of the Axol Cardiomyocyte Maintenance Medium Kit (ax2530-500) were thawed overnight at 4°C. The supplement was then added to the Cardiomyocyte Maintenance Medium to make the complete medium. To make the plating medium, 10% fetal bovine serum (FBS) was added to an aliquot of complete Cardiomyocyte Maintenance Medium.

Plate preparation

50 µL of fibronectin coating solution (10 µg/mL in phosphate buffered saline (PBS) containing Ca^{2+} and Mg^{2+}) was added to each well of the E-Plate® Cardio 96 (ACEA Biosciences, Inc.), and incubated overnight at 4°C. The following day, excess fibronectin was aspirated, 180 µL of pre-warmed plating medium was added to each well and the plate was equilibrated in a 5% CO_2 incubator at 37°C. After 30 mins, the plate was transferred to the xCELLigence® RTCA Cardio in the incubator and background impedance measured as per the manufacturer's protocol.

Cell seeding

Four vials ($1x10^6$ cells/vial) of Axol Human iPSC-Derived Ventricular Cardiomyocytes (ax2505) were removed from liquid nitrogen storage and placed on dry ice before being thawed rapidly in a 37°C water bath. The vials were swirled constantly and once only a small ice clump was evident, the vials were transferred to a sterile laminar flow hood. The contents of all four vials were transferred to a sterile centrifuge tube containing 6 mL of pre-warmed plating medium. The cell suspension was centrifuged at 200 x *g* for 5 mins and the resulting cell pellet carefully resuspended in 10 mL of fresh plating medium. Cell viability was calculated via trypan blue exclusion using a hemocytometer. Plating medium was used to achieve a final concentration of between $2.4x10^6$ and $3.0x10^6$ viable cells in a total volume of 18 mL. All media was aspirated from the plate and 180 µL of cell suspension was added to each well resulting in a total of $2.4x10^4$ to $3.0x10^4$ cells per well. The plate was left in the laminar flow hood for 30 mins to allow the cells to settle and attach after which it was transferred to the xCELLigence® RTCA Cardio in the incubator. Impedance readings were automatically recorded every 30 mins.

Cardiomyocyte maintenance

Once a day, the instrument was paused and the plate transferred to the laminar flow hood in a transfer module at which point 90 µL of medium was removed and replaced with an equal volume of fresh, pre-warmed medium. This was repeated three times before returning the plate to the xCELLigence® RTCA Cardio in the incubator. The iPSC-CMs were cultured using plating medium until cell growth kinetics demonstrated a plateau, indicative of cell coverage of the well and proliferation cessation (approximately 72-96 hrs post-plating). Upon achieving a stable cell index, all plating media was carefully removed from the plate and replaced with complete Cardiomyocyte Maintenance Medium (i.e. serum-free).

Drug application

After approximately 24-72 hrs in serum-free complete medium, a stable synchronous beat rate should be observed. After an additional 72 hrs, a range of concentrations of the β-adrenergic receptor agonist (isoproterenol) or antagonist (carvedilol) were added to selected wells and the iPSC-CMs response evaluated.

1

Results

Initial impedance readings

Prior to plating, the background reading of all wells within the E-plate® Cardio 96 were found to be within the acceptable range and therefore suitable for the addition of cells and further study evaluation. Post-plating, impedance readings strongly indicated attachment of viable cells to the fibronectin.

Cell growth

During the post-seeding period in plating medium, an increase in impedance (as determined by cell index) was measured in all wells within the plate. This increase was indicative of cell growth and continued viability, with a plateau and cessation of growth reached by 93 hrs (**Figure 1**).

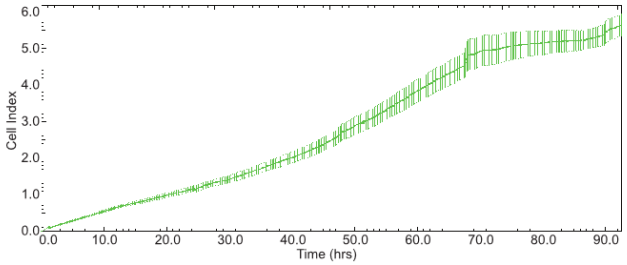

Figure 1: Increased cell index of iPSC-CMs over time. Each well contained 2.4x10^4 cells in plating medium. Exponential cell growth was demonstrated over the initial 93 hrs post-seeding. Cell index (impedance) values plateaued after 93 hrs indicating confluency and cessation of cell proliferation.

Cell contractility and synchronous beating

All wells were monitored for evidence of contractility and synchronicity throughout sub-sequent phases of the study. At 24 hrs post-plating, an indication of primitive cell contractility was observed (**Figure 2a**), with indicative contractility observed by 48 hrs (**Figure 2b**) and synchronous cell contractility at 120 hrs (**Figure 2c**).

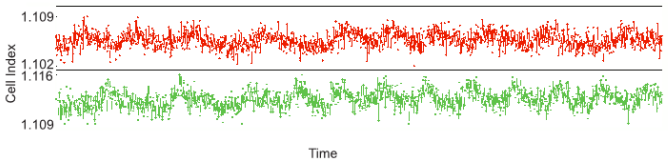

Figure 2a: Primitive asynchronous cell contraction at 24 hrs post-plating in plating medium.

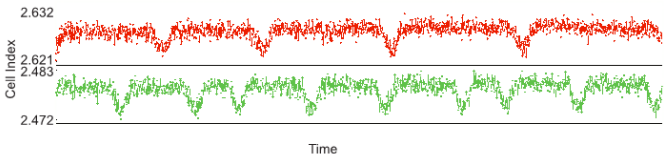

Figure 2b: Indicative evidence of cell contractility at 48 hrs post-plating in plating medium.

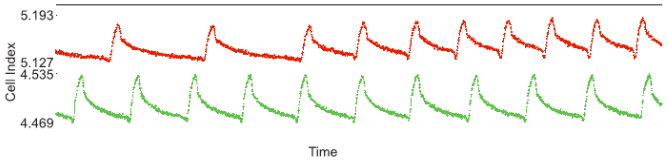

Figure 2c: Indicative evidence of synchronous cell contractility at 120 hrs post-plating (24 hrs in complete Cardiomyocyte Maintenance Medium).

Evaluation of drug effect on cardiomyocyte contractility

A range of isoproterenol and carvedilol concentrations were added to selected wells. The iPSC-CMs responded to the addition of isoproterenol and carvedilol as expected and in a dose-dependent manner (**Figure 3**). This strongly indicates the 'clinical' relevance of these cells and their utility for drug screening applications.

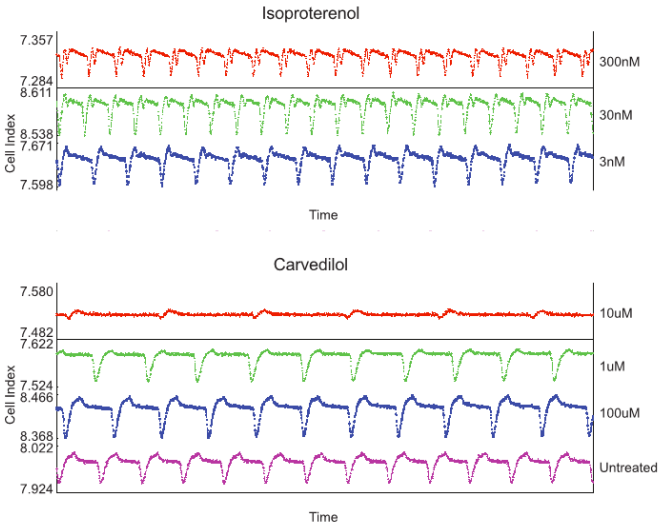

Figure 3: Effect of isoproterenol and carvedilol upon cardiomyocyte contractility.

Conclusions

Axol iPSC-CMs are suitable for use on the xCELLigence® RTCA Cardio instrument when cultured in the E-Plate® Cardio 96 pre-coated with fibronectin. Initial plating of the cells requires the use of a serum-rich plating medium. The iPSC-CMs demonstrate potential for excitation-contraction in the plating medium, but culture of the iPSC-CMs in complete Cardiomyocyte Maintenance Medium (without serum) is conducive for longer-term cell survival and viability. The latter is permissive of excitation-contraction coupled cell contractility, with a clearly defined clinically relevant contractile phenotype. The iPSC-CMs respond to cardiac drugs and therefore have potential for use in cardiotoxicity and cardiomyocyte-pharmacology studies.

Acknowledgements

We thank our collaborators Kimberly Rockley and Jason Gill, PhD at the School of Medicine, Pharmacy and Health, Durham University, UK for conducting this evaluation study.

Address
Axol Bioscience Limited | Suite 3 | The Science Village |
Chesterford Research Park | Little Chesterford | Cambridgeshire | CB10 1XL

International phone
+44-1223-751-051

US phone
+1-800-678-AXOL (2965)

Email
support@axolbio.com

Web
www.axolbio.com

Appendix 3: Publications

Contributions in the form of experimental and analytical assistance using the MTT assay were made to a project resulting in the following research papers:

Jasmine M. Cross, Tim R. Blower, Natalie Gallagher, Jason H. Gill, Kimberly L. Rockley and James W. Walton, *Anticancer Ru^{II} and Rh^{III} Piano-Stool Complexes that are Histone Deacetylase Inhibitors.* ChemPlusChem, 2016.

Jasmine M. Cross, Natalie Gallagher, Jason H. Gill, Mohit Jain, Archibald W. McNeillis, Kimberly L. Rockley, Fiona H. Tscherny, Natasha J. Wirszycz, Dmitry S. Yufit and James W. Walton, *Pyridylphosphinate metal complexes: synthesis, structural characterisation and biological activity.* Dalton Transactions, 2016

ChemPubSoc Europe
DOI: 10.1002/cplu.201600413
CHEMPLUSCHEM Communications

Anticancer Ru^{II} and Rh^{III} Piano-Stool Complexes that are Histone Deacetylase Inhibitors

Jasmine M. Cross,[a] Tim R. Blower,[b] Natalie Gallagher,[c] Jason H. Gill,[c] Kimberly L. Rockley,[c] and James W. Walton*[a]

The first examples of Ru^{II} and Rh^{III} piano-stool complex histone deacetylase (HDAC) inhibitors are presented. The novel complexes have antiproliferative activity against H460 non-small-cell lung carcinoma cells that is comparable to the clinically used HDAC inhibitor suberoylanilide hydroxamic acid (SAHA). Strong evidence for HDAC inhibition as a primary mechanism of action is provided. The complexes reported here represent an important step towards the design of highly active and selective HDAC inhibitors.

Historically the treatment of advanced or disseminated cancer has involved the systemic administration of cytotoxic compounds targeting nucleic acid replication or synthesis, many of which have been approved for clinical use since the 1960s.[1] Mechanistically these agents do not exclusively target cancer cells, and will also attack any rapidly proliferating cell type, commonly resulting in dose-limiting toxicity.[2] Over the past decade, increased understanding of the molecular basis of cancer has advanced cancer therapy into an era of "targeted molecular therapeutics".[3] This new class of targeted drugs exhibit a broad range of therapeutic mechanisms, including inhibition of extracellular growth receptors,[4] activation of cell death pathways,[5] retardation of cell motility,[6] kinase inhibition,[7] and toxin delivery,[8] to name a few. Subsequently, inhibition of enzymes associated with key regulatory pathways in cancer is an attractive alternative to targeting DNA.[9] In principle, "molecularly targeted" agents are highly selective agents against the growth and survival of tumour cells, whilst sparing normal cells.

The histone deacetylases (HDACs) are a class of enzymes recently shown to be suitable molecular targets for anticancer activity.[10] HDACs, working in tandem with histone acetylase transferases, control the extent of acetylation of ε-lysine residues in the tail of histone proteins[11] and several other cellular proteins, such as tubulin.[12] In terms of histones, deacetylation leads to a positively charged histone core, which interacts strongly with DNA, leading to a condensed chromatin structure. As a consequence, transcription of tumour-suppressor genes is repressed and cancer cell survival is promoted.[13] Consequently, HDAC inhibitors have received much attention as drug candidates, with suberoylanilide hydroxamic acid (SAHA, Figure 1) approved for clinical use against cutaneous T-cell lymphoma.[14] The hydroxamic acid group in SAHA binds to a Zn^{2+} ion located at the bottom of a hydrophobic cavity in the active site of HDAC enzymes.

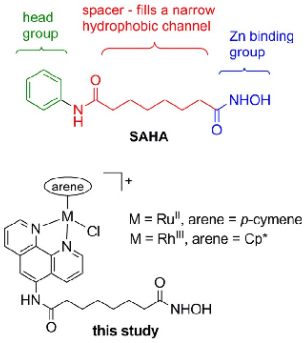

Figure 1. The HDAC inhibitor SAHA and the piano-stool complexes featured in this study. Cp* = pentamethylcyclopentadienyl.

It is known that the HDAC protein family is comprised of several sub-families demonstrating a wide range of roles across the cell, in addition to modulation of histone-regulated gene transcription.[15] Therefore there is significant interest in the development of HDAC inhibitors with the capability of selectively targeting a specific enzyme or sub-family,[16] with the objective of avoiding HDACs involved in normal physiological function and drug-induced toxicities.

[a] J. M. Cross, Dr. J. W. Walton
Department of Chemistry
Durham University
South Road, Durham DH1 3LE (United Kingdom)
E-mail: james.walton@durham.ac.uk
[b] Dr. T. R. Blower
School of Biological and Biomedical Sciences
Durham University
South Road, Durham DH1 3LE (United Kingdom)
[c] N. Gallagher, Dr. J. H. Gill, K. L. Rockley
School of Medicine, Pharmacy and Health
Durham University, Wolfson Research Institute
Queen's Campus, Stockton on Tees TS17 6BH (United Kingdom)
Supporting information and the ORCID identification number(s) for the author(s) of this article can be found under http://dx.doi.org/10.1002/cplu.201600413.

This article is part of the "Early Career Series". To view the complete series, visit: http://chempluschem.org/earlycareer.

In terms of selectivity, although the enzymatic cavity is relatively comparable between HDACs, there is clear variability in the protein structure towards the entrance of the cavity. The phenyl headgroup of enzyme-bound SAHA sits in this region and offers scope for modification toward the development of HDAC-selective agents or more potent drugs through greater chemical affinity. In recent years, HDAC inhibitors have been developed in which the phenyl headgroup is replaced or functionalised with a metal complex. Examples include ferrocene-,[17] platinum-,[18] rhenium-[19] and ferrocifen-based[20] inhibitors. In each case the pharmacological effects are retained and, in some cases, improved cytotoxicity relative to SAHA was observed. Luminescent octahedral polypyridyl–metal complexes have also been developed.[21] The advantages of metal complexes over purely organic compounds in enzyme inhibition include: 3D metal geometries, allowing simultaneous access to multiple areas of the active site; exchangeable ligands, for in situ activation and potential binding to amino acid residues in the active site; simple and modular syntheses, allowing rapid determination of structure–activity relationships.

To be a successful selective headgroup, the metal complex would ideally have scope and functionality amenable to modification for optimising the interactions with the cavity entrance. One such class of metal-based compounds demonstrating these characteristics is the piano-stool complexes, comprising a d^6 low-spin metal core capped by a η^6 or η^5 aromatic ligand. Functionality is varied at the three remaining coordination sites of the pseudo-octahedral complexes, which are occupied by mono-, bi- or tri-dentate ligands. A large number of metal complexes based on this motif have been investigated for their anticancer activity,[22] with modification of each component leading to dramatic changes in activity. However, Ru^{II} and Rh^{III} piano-stool complexes have not previously been investigated as HDAC inhibitors.

Herein, we present the first examples of Ru^{II} and Rh^{III} piano-stool complexes that show effective HDAC inhibition and antiproliferative activity against H460 non-small-cell lung carcinoma cells. Our initial biological studies indicate that these complexes inhibit class I and II HDAC enzymes, but show no covalent binding to DNA.

We chose to use a substituted phenanthroline moiety, as this ligand is known to form stable chelates with the platinum group metals.[22i,23] Following a literature procedure,[21a] 1,10-phenanthrolin-5-amine and methyl 8-chloro-8-oxooctanoate were reacted to give a methyl ester intermediate. Without further purification, this intermediate was converted to ligand **L1** by the addition of hydroxylamine (50% aqueous solution) and catalytic base (Scheme 1). Upon neutralisation, **L1** precipitated and was collected by filtration and dried under high vacuum. Complexation of **L1** with selected metal dimers ($[(arene)MCl_2]_2$) was achieved using a 2:1 ratio of **L1**/metal dimer in anhydrous methanol. After removing the excess solvent, the crude product was purified by recrystallisation by dropping a concentrated CH_2Cl_2 solution into stirred Et_2O in a dry-ice/acetone bath (Scheme 1). Formation and purity of the complexes was confirmed using ^1H NMR spectroscopy, mass spectrometry and elemental analysis (see the Supporting Information for details).

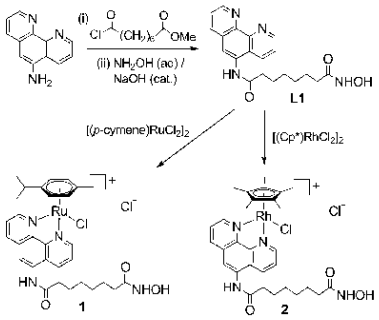

Scheme 1. Preparation of piano-stool complexes of Ru^{II} (**1**) and Rh^{III} (**2**).

^1H NMR spectroscopy in $[D_6]$DMSO confirmed the presence of the intact hydroxamic acid, with broad resonances at 10.30 and 8.63 ppm corresponding to the hydroxamic acid OH and NH protons of complex **1**, respectively (10.38 and 8.63 ppm for complex **2**). These resonances are near identical to those of **L1**, confirming that chelation to Ru occurs only through the phenanthroline N donors. In contrast, the resonances for protons H2 and H9, adjacent to the phenanthroline N atoms, shift by almost 1 ppm upon complexation.

To assess the aqueous stability of the complexes, a solution of complex **1** in D_2O was monitored by ^1H NMR spectroscopy over the course of 96 h. After 1 h, an equilibrium was established between the chlorido complex **1** and the aqua species, in which the chlorido ligand has exchanged with D_2O. The chlorido/D_2O ratio is approximately 9:1 and remains unchanged over the course of 96 h (see the Supporting Information for full details). These results show that the complex is stable in aqueous solution and likely to remain intact as the chlorido species in biological media.

With the new complexes in hand, we first examined their ability to inhibit the proliferation of the H460 non-small-cell lung carcinoma cell line in vitro. Cells were exposed for 96 h to each new complex, the ligand **L1** and the known HDAC inhibitor, SAHA, at concentrations ranging from 0.01 to 200 μM. Cell survival was then determined by the MTT assay[24] and the IC_{50} (concentration of compound required to inhibit cell proliferation by 50%) was calculated from the resulting dose–response curve (see the Supporting Information for full details). The results (Table 1) show that the new complexes are able to effectively inhibit cell growth. The Ru^{II} complex with the capping *p*-cymene ligand (complex **1**) has an IC_{50} value of approximately 20 μM, which is comparable to that found in cytotoxicity studies of many other Ru piano-stool complexes,[22] but is 15-fold higher than for SAHA. However, the much lower cytotoxic efficacy (IC_{50}: 4 μM) demonstrated by the Rh^{III} complex, capped with a Cp* ligand (complex **2**) is comparable with the most active Rh^{III} piano-stool complexes reported to date.[25] The lower IC_{50} value of complex **2** and the fact it is approaching that of the clinically approved anticancer agent, SAHA (IC_{50}:

Table 1. IC_{50} values measured using the MTT assay (96 h) against the non-small-cell lung carcinoma H460 cell line, and are reported as the mean value from at least three experiments.

Compound	Arene–metal	IC_{50} [μM]
1	*p*-cymene–Ru^{II}	21 ± 6
2	Cp*–Rh^{III}	4.1 ± 0.4
L1	–	1.5 ± 0.2
SAHA	–	1.4 ± 0.2

1.4 μM), gives us encouragement that piano-stool complexes have the potential to act as HDAC inhibitors. Within experimental error the ligand **L1** has the same activity as SAHA.

To investigate whether these complexes act by HDAC inhibition, as proposed, we carried out enzyme inhibition assays, using a commercially available assay kit.[26] Fluorescence measurements were used to determine the extent of HDAC activity, with no fluorescence indicating complete HDAC inhibition. The known inhibitor SAHA, **L1** and each new complex were incubated at 0.1 and 1 μM with a nuclear extract source of HDACs, prior to the addition of an acetylated substrate. As a positive control, the assay was also run in the absence of any inhibitor. Results are presented as a percentage of HDAC activity, relative to the positive control (Table 2). For all compounds tested at

Table 2. HDAC activity in presence of potential inhibitors at 0.1 and 1 μM concentration, measured using a commercially available assay kit. Values are reported as percentage activity relative to a positive control (no inhibitor).

Inhibitor conc^n [μM]	Control [%]	SAHA [%]	**1** [%]	**2** [%]	**L1** [%]
1	100	0.5	1.6	1.1	4.9
0.1	100	6.3	17.3	15.4	10.7

1 μM concentration, HDAC activity is low (< 5% activity), showing that these species are effective HDAC inhibitors. At 0.1 μM, HDAC activity is increased, but remains low, supportive of the inhibitory potency of these compounds. Although all tested compounds inhibit HDAC activity to the same order of magnitude, the extent of HDAC inhibition at the lower concentration follows the order SAHA > **L1** > **2** > **1**. This order mirrors the in vitro anticancer activity, which supports the hypothesis that HDAC inhibition is a putative mechanism of action of these species. Beyond this empirical observation, there are some interesting features within the results. Firstly, complex **2** showed a fourfold greater cytotoxic potency than complex **1**, but comparable HDAC inhibitory activity. This would suggest that the lower anticancer activity of the Ru^{II} complex is not entirely down to weaker HDAC inhibition. More likely, variation in processes such as cell uptake, localisation and egress of the compounds lead to the observed differences in cytotoxicity. A second observation from the data is that, despite being more active at 0.1 μM, at the higher concentration of 1 μM, the ligand **L1** leads to less enzyme inhibition than the complexes **1** and **2**. This might be due to aggregation of the planar aromatic **L1** at higher concentration,[27] leading to a reduction in compound available to bind to the enzyme, or might be due to lower solubility in the assay medium.

As a control, we measured the extent of HDAC inhibition by the known complex [(*p*-cymene)Ru(phen)Cl]Cl.[28] As expected, this complex shows no significant inhibition (100% HDAC activity at 1 μM complex), confirming that the hydroxamic acid moiety is essential for HDAC inhibition.

The HDAC assays clearly indicate that the new complexes are effective inhibitors of these enzymes. However, we wanted to determine whether this was the only mechanism of action that led to the observed cytotoxicity. Indeed, the majority of anticancer Ru^{II} piano-stool complexes are postulated to act through covalent binding to DNA. To test whether the complexes investigated herein interact with DNA, either through covalent modification or intercalation, DNA binding assays were performed. Firstly, to probe the ability of the complexes to covalently modify DNA, supercoiled pSG483 plasmid DNA was exposed to increasing concentrations of complex **2** and the resulting products were separated by agarose gel electrophoresis (Figure 2A). In comparison to a solvent only control (Figure 2A, lane 1), the migration of the supercoiled DNA is unaffected by complex **2**. As a comparison, the known DNA-binding complex cisplatin was examined under identical conditions (Figure 2B). As the concentration of cisplatin was increased, the compound formed covalent adducts with DNA that migrated more slowly, reaching a maximal shift at 2.5 μM. Above this concentration, the DNA signals became more disperse, likely indicating degradation of the DNA at higher concentrations of the compound. It is clear from this comparison that complex **2** does not covalently bind DNA.

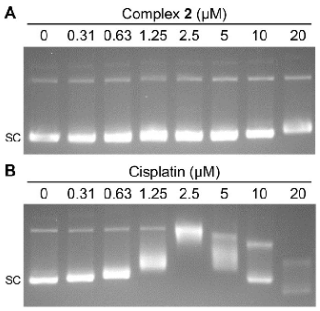

Figure 2. Covalent modification of DNA as determined by migration of substrate DNA during agarose gel electrophoresis. Supercoiled plasmid DNA was treated with increasing concentrations of complex **2** (A) and cisplatin (B). SC = supercoiled DNA.

Having confirmed that covalent binding to DNA is not favoured for complex **2**, we next explored the possibility of intercalation. Assays were run in which nicked pSG483 plasmid DNA was incubated with potential intercalators, then treated with DNA ligase (Figure 3). The ligase acts to re-seal the nicked DNA, trapping the current supercoiling state of the plasmid. In-

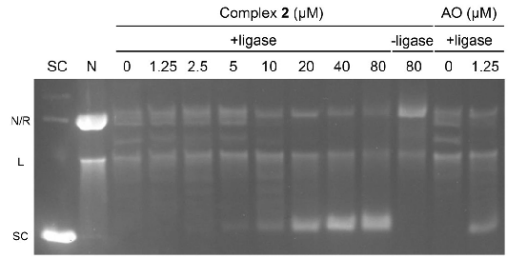

Figure 3. Intercalation of DNA demonstrated by the production of supercoiled DNA. Nicked plasmid DNA was treated with increasing concentrations of complex **2** and a positive control, acridine orange (AO). The supercoiled state was trapped by the addition of DNA ligase, where indicated. N/R = nicked/relaxed DNA, SC = supercoiled DNA, L = linear DNA.

tercalating compounds induce increased supercoiling within plasmid DNA, whereas non-intercalated nicked DNA treated with ligase will be sealed in a distribution of relaxed DNA topoisomers (Figure 3, lane 3). No intercalation was observed for concentrations of complex **2** below 20 μM, indicating that intercalation was not occurring at concentrations capable of causing HDAC inhibition or cytotoxicity. At higher doses, 20–80 μM of complex **2**, moderate intercalation could be observed. As a positive control, the known DNA intercalator acridine orange was tested at 1.25 μM, producing supercoiled DNA and demonstrating that in comparison, complex **2** does not intercalate DNA (Figure 3, lane 13).

From the assays carried out to determine one or more mechanism(s) of action, it is clear that HDAC inhibition is a potential therapeutic mechanism of anticancer activity in vitro. The results of our biological assays rule out covalent binding to DNA in a manner akin to cisplatin or many other Ru^{II} piano-stool complexes. Similarly, complex **2** does not intercalate with DNA at efficacious concentrations, as might be expected from a complex incorporating a planar aromatic ligand. Hence, we can be confident that a viable mechanism of anticancer activity of the new Ru^{II} and Rh^{III} complexes is through HDAC inhibition.

In conclusion, we have presented the first examples of Ru^{II} and Rh^{III} piano-stool complexes that inhibit HDAC enzymes, leading to growth inhibition of a lung carcinoma cell line. These complexes have comparable activity to the clinically approved inhibitor SAHA. The key advantage to using 3D piano-stool complexes for this application is the ease in which the structure of the metal complex can be varied. For example, the capping arene group or monodentate halide can be readily modulated to form 3D structures that might access new areas on the enzyme surface, leading to more efficient binding. This so-called "escape from flatland"[29] is much harder to envisage for the purely organic inhibitors, the synthesis of which would require longer and more challenging pathways. We are currently using computational modelling to aid in the design of more efficient piano-stool complex HDAC inhibitors.

Furthermore, whereas SAHA is a pan-HDAC inhibitor, the design of inhibitors that are selective towards a particular isoform is at the forefront of research in this area.[16] Piano-stool complexes, such as **2**, provide a platform from which selective HDAC inhibitors can be designed and synthesised with comparative ease. The use of selective inhibitors should provide more insight into the physiological roles of the HDAC isoforms and might reveal undiscovered functions of this important enzyme.

Acknowledgements

We thank Durham University and the Engineering and Physical Sciences Research Council (EPSRC) for funding.

Keywords: antitumour agents · bioorganometallic chemistry · histone deacetylase inhibitors · piano-stool complexes · ruthenium

[1] B. Rosenberg, L. van Camp, T. Krigas, *Nature* **1965**, *205*, 698–699.
[2] a) H. Matsushima, K. Yonemura, K. Ohishi, A. Hishida, *J. Lab. Clin. Med.* **1998**, *131*, 518–526; b) N. E. Madias, J. T. Harrington, *Am. J. Med.* **1978**, *65*, 307–314; c) M. Kartalou, J. M. Essigmann, *Mutat. Res.* **2001**, *478*, 23–43; d) K. J. Mellish, L. R. Kelland, K. R. Harrap, *Br. J. Cancer* **1993**, *68*, 240–250.
[3] a) I. Collins, P. Workman, *Nat. Chem. Biol.* **2006**, *2*, 689–700; b) D. R. Newell, *Eur. J. Cancer* **2005**, *41*, 676–682.
[4] P. M. Harari, *Endocr.-Relat. Cancer* **2004**, *11*, 689–708.
[5] a) D. R. McIlwain, T. Berger, T. W. Mak, *Cold Spring Harbor Perspect. Biol.* **2013**, *5*, a008656; b) N. Imaizumi, K. K. Lee, C. Zhang, U. A. Boelsterli, *Redox Rep. Redox Biol.* **2015**, *4*, 279–288.
[6] a) J. M. Coppola, M. S. Bhojani, B. D. Ross, A. Rehemtulla, *Neoplasia* **2008**, *10*, 363–370; b) A. Taiyab, C. M. Rao, *Biochim. Biophys. Acta Mol. Cell Res. Biochim. Biophys. Acta* **2011**, *1813*, 213–221.
[7] J. Zhang, P. L. Yang, N. S. Gray, *Nat. Rev. Cancer* **2009**, *9*, 28–39.
[8] X. Liao, A. E. Rabideau, B. L. Pentelute, *ChemBioChem* **2014**, *15*, 2458–2466.
[9] a) K. J. Kilpin, P. J. Dyson, *Chem. Sci.* **2013**, *4*, 1410–1419; b) A. Casini, J. Reedijk, *Chem. Sci.* **2012**, *3*, 3135–314; c) H.-J. Zhong, K.-H. Leung, L.-J. Liu, L. Lu, D. S.-H. Chan, C.-H. Leung, D.-L. Ma, *ChemPlusChem* **2014**, *79*, 508–511; d) S. M. Meier, C. Gerner, B. K. Keppler, M. A. Cinellu, A. Casini, *Inorg. Chem.* **2016**, *55*, 4248–4259; e) J. É. Debreczeni, A. N. Bullock, G. E. Atilla, D. S. Williams, H. Bregman, S. Knapp, E. Meggers, *Angew. Chem. Int. Ed.* **2006**, *45*, 1580–1585; *Angew. Chem.* **2006**, *118*, 1610–1615; f) A. J. Salmon, M. L. Williams, A. Hofmann, S.-A. Poulsen, *Chem. Commun.* **2012**, *48*, 2328–2330; g) C.-H. Leung, L.-J. Liu, K.-H. Leung, D.-L. Ma, *Coord. Chem. Rev.* **2016**, *319*, 25–34.
[10] a) K. Ververis, A. Hiong, T. C. Karagiannis, P. V. Licciardi, *Biologics* **2013**, *7*, 47–60; b) A. C. West, R. W. Johnstone, *J. Clin. Invest.* **2014**, *124*, 30–39.
[11] M. Haberland, R. L. Montgomery, E. N. Olson, *Nat. Rev. Genet.* **2009**, *10*, 32–42.
[12] M. A. Glozak, N. Sengupta, X. Zhang, E. Seto, *Gene* **2005**, *363*, 15–23.
[13] S. Ropero, M. Esteller, *Mol. Oncol.* **2007**, *1*, 19–25.
[14] a) P. A. Marks, R. Breslow, *Nat. Biotechnol.* **2007**, *25*, 84–90; b) P. A. Marks, *Oncogene* **2007**, *26*, 1351–1356.
[15] a) A. J. de Ruijter, A. H. van Gennip, H. N. Caron, S. Kemp, A. B. van Kuilenburg, *Biochem. J.* **2003**, *370*, 737–749; b) C. Simões-Pires, V. Zwick, A. Nurisso, E. Schenker, P.-A. Carrupt, M. Cuendet, *Mol. Neurodegener.* **2013**, *8*, 7–22; c) N. L. Regna, C. M. Reillya, *J. Clin. Cell. Immunol.* **2014**, *5*, 207.
[16] a) K. J. Falkenberg, R. W. Johnstone, *Nat. Rev. Drug Discovery* **2014**, *13*, 673–691; b) A. V. Bieliauskas, M. K. Pflum, *Chem. Soc. Rev.* **2008**, *37*, 1402–1413; c) K. V. Butler, J. Kalin, C. Brochier, G. Vistoli, B. Langley, A. P. Kozikowski, *J. Am. Chem. Soc.* **2010**, *132*, 10842–10846; d) J. H. Kalin, J. A. Bergman, *J. Med. Chem.* **2013**, *56*, 6297–6313.

[17] a) J. Spencer, J. Amin, M. Wang, G. Packham, S. S. Syed Alwi, G. J. Tizzard, S. J. Coles, R. M. Paranal, J. E. Bradner, T. D. Heightman, *ACS Med. Chem. Lett.* **2011**, *2*, 358 – 362; b) J. Spencer, J. Amin, R. Boddiboyena, G. Packham, B. E. Cavell, S. S. Syed Alwi, R. M. Paranal, T. D. Heightman, M. Wang, B. Marsden, P. Coxhead, M. Guille, G. J. Tizzard, S. J. Coles, J. E. Bradner, *Med. Chem. Commun.* **2012**, *3*, 61 – 64; c) A. Leonidova, C. Mari, C. Aebersold, G. Gasser, *Organometallics* **2016**, *35*, 851 – 854.

[18] a) D. Griffith, M. P. Morgan, C. J. Marmion, *Chem. Commun.* **2009**, 6735 – 6737; b) V. Brabec, D. M. Griffith, A. Kisova, H. Kostrhunova, L. Zerzankova, C. J. Marmion, J. Kasparkova, *Mol. Pharm.* **2012**, *9*, 1990 – 1999; c) J. Kasparkova, H. Kostrhunova, O. Novakova, R. Křikavová, J. Vančo, Z. Trávníček, V. Brabec, *Angew. Chem. Int. Ed.* **2015**, *54*, 14478 – 14482; *Angew. Chem.* **2015**, *127*, 14686 – 14690.

[19] D. Can, H. W. Peindy N'Dongo, B. Spingler, P. Schmutz, P. Raposinho, I. Santos, R. Alberto, *Chem. Biodiversity* **2012**, *9*, 1849 – 1866.

[20] J. de Jesús Cázares Marinero, M. Lapierre, V. Cavaillès, R. Saint-Fort, A. Vessières, S. Top, G. Jaouen, *Dalton Trans.* **2013**, *42*, 15489 – 15501.

[21] a) R.-R. Ye, Z.-F. Ke, C.-P. Tan, L. He, L.-N. Ji, Z.-W. Mao, *Chem. Eur. J.* **2013**, *19*, 10160 – 10169; b) R.-R. Ye, C.-P. Tan, L. He, M.-H. Chen, L.-N. Ji, Z.-W. Mao, *Chem. Commun.* **2014**, *50*, 10945 – 10948; c) R.-R. Ye, C.-P. Tan, Y.-N. Lin, L.-N. Ji, Z.-W. Mao, *Chem. Commun.* **2015**, *51*, 8353 – 8356.

[22] a) J. M. Cross, N. Gallagher, J. H. Gill, M. Jain, A. W. McNeillis, K. L. Rockley, F. H. Tscherny, N. J. Wirszycz, D. S. Yufit, J. W. Walton, *Dalton Trans.* **2016**, *45*, 12807 – 12813; b) C. Scolaro, A. Bergamo, L. Brescacin, R. Delfino, M. Cocchietto, G. Laurenczy, T. J. Geldbach, G. Sava, P. J. Dyson, *J. Med. Chem.* **2005**, *48*, 4161 – 4171; c) S. Murray, L. Menin, R. Scopelliti, P. J. Dyson, *Chem. Sci.* **2014**, *5*, 2536 – 2545; d) M. Pernot, T. Bastogne, N. P. E. Barry, B. Therrien, G. Koellensperger, S. Hann, V. Reshetov, M. Barberi-Heyob, *J. Photochem. Photobiol. B* **2012**, *117*, 80 – 89; e) A. A. Nazarov, S. M. Meier, O. Zava, Y. N. Nosova, E. R. Milaeva, C. G. Hartinger, P. J. Dyson, *Dalton Trans.* **2015**, *44*, 3614 – 3623; f) S. M. Meier, M. Hanif, Z. Adhireksan, V. Pichler, M. Novak, E. Jirkovsky, M. A. Jakupec, V. B. Arion, C. A. Davey, B. K. Keppler, C. G. Hartinger, *Chem. Sci.* **2013**, *4*, 1837 – 1846; g) A. F. A. Peacock, S. Parsons, P. J. Sadler, *J. Am. Chem. Soc.* **2007**, *129*, 3348 – 3357; h) K. D. Camm, A. El-Sokkary, A. L. Gott, P. G. Stockley, T. Belyaevab, P. C. McGowan, *Dalton Trans.* **2009**, 10914 – 10925; i) Z. Liu, A. Habtemariam, A. M. Pizarro, S. A. Fletcher, A. Kisova, O. Vrana, L. Salassa, P. C. A. Bruijnincx, G. J. Clarkson, V. Brabec, P. J. Sadler, *J. Med. Chem.* **2011**, *54*, 3011 – 3026.

[23] a) J. Canivet, L. Karmazin-Brelot, G. Süss-Fink, *J. Organomet. Chem.* **2005**, *690*, 3202 – 3211; b) M. A. Scharwitz, I. Ott, Y. Geldmacher, R. Gust, W. S. Sheldrick, *J. Organomet. Chem.* **2008**, *693*, 2299 – 2309.

[24] T. Mosmann, *J. Immunol. Methods* **1983**, *65*, 55 – 63.

[25] Y. Geldmacher, M. Oleszak, W. S. Sheldrick, *Inorg. Chim. Acta* **2012**, *393*, 84 – 102.

[26] The HDAC fluorometric assay kit was purchased from Enzo Life Sciences.

[27] For examples, see: J. R. Lakowicz, *Principles in Fluorescence Spectroscopy*, 2nd ed., Academic/Plenum Press, New York, **1999**.

[28] S. Betanzos-Lara, O. Novakova, R. J. Deeth, A. M. Pizarro, G. J. Clarkson, B. Liskova, V. Brabec, P. J. Sadler, A. Habtemariam, *J. Biol. Inorg. Chem.* **2012**, *17*, 1033 – 1051.

[29] F. Lovering, J. Bikker, C. Humblet, *J. Med. Chem.* **2009**, *52*, 6752 – 6756.

Manuscript received: August 11, 2016
Revised: September 20, 2016
Accepted Article published: September 21, 2016
Final Article published: October 12, 2016

Dalton Transactions

PAPER

View Article Online
View Journal | View Issue

Cite this: *Dalton Trans.*, 2016, **45**, 12807

Pyridylphosphinate metal complexes: synthesis, structural characterisation and biological activity†

Jasmine M. Cross,[a] Natalie Gallagher,[b] Jason H. Gill,[b] Mohit Jain,[b] Archibald W. McNeillis,[a] Kimberly L. Rockley,[b] Fiona H. Tscherny,[a] Natasha J. Wirszycz,[a] Dmitry S. Yufit[a] and James W. Walton*[a]

Received 1st April 2016,
Accepted 9th July 2016

DOI: 10.1039/c6dt01264g

www.rsc.org/dalton

For the first time, a series of 25 pseudo-octahedral pyridylphosphinate metal complexes (Ru, Os, Rh, Ir) has been synthesised and assessed in biological systems. Each metal complex incorporates a pyridylphosphinate ligand, a monodentate halide and a capping η^6-bound aromatic ligand. Solid- and solution-state analyses of two complexes reveal a structural preference for one of a possible two diastereomers. The metal chlorides hydrolyse rapidly in D_2O to form a 1 : 1 equilibrium ratio between the aqua and chloride adducts. The pK_a of the aqua adduct depends upon the pyridyl substituent and the metal but has little dependence upon the phosphinate R′ group. Toxicity was measured *in vitro* against non-small cell lung carcinoma H460 cells, with the most potent complexes reporting IC_{50} values around 50 μM. Binding studies with selected amino acids and nucleobases provide a rationale for the variation in toxicity observed within the series. Finally, an investigation into the ability of the chelating amino acid L-His to displace the phosphinate O–metal bond shows the potential for phosphinate complexes to act as prodrugs that can be activated in the intracellular environment.

Introduction

In the field of bioinorganic chemistry, platinum group metal complexes have found application in cellular imaging,[1] in enzyme inhibition[2] and as molecular probes of biological activity.[3] The therapeutic anticancer activity of these complexes is also often probed both *in vitro* and *in vivo*.[4] In the context of therapeutics, the advantages that metal complexes offer over purely organic species include: a variety of metal geometries and coordination numbers, allowing access to intricate 3-dimensional structures; numerous metal oxidation states, allowing redox-activated drugs; tuneable ligands to vary sterics and electronics about the metal centre; exchangeable ligands, for *in situ* activation and binding to biomolecules; simple and modular syntheses, allowing rapid determination of structure to activity relationships. Despite the wide-spread clinical use of the platinum-based drugs, cisplatin, oxaliplatin and carboplatin,[5] there remains issues associated with side-effects, including dose-limiting systemic toxicities[6] and acquisition of drug resistance, which reduce the efficacy and clinical utility of these drugs.[7]

One class of metal complexes that has shown great promise as alternatives to Pt drugs are the pseudo-octahedral piano stool complexes,[8] in which a low-spin d^6 metal ion is capped by an η^6-phenyl or η^5-cyclopentadienyl ligand, with the remaining 3 coordination sites occupied by tri- bi- or mono-dentate ligands.

Over the past decades, many examples of piano stool metal complexes have been reported that show excellent *in vitro*[9] and *in vivo*[10] activity against cancers (Fig. 1). Variation of each component of the piano stool arrangement alters the activity of the complex. For example, in the series $[(\eta^6\text{-arene})Ru(en)Cl]PF_6$ a

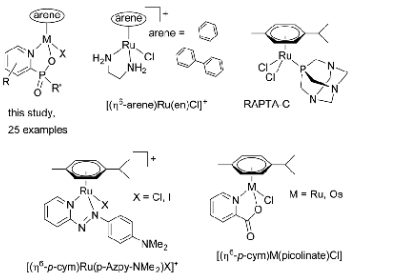

Fig. 1 Examples of metal complexes assessed for their anticancer activity.

[a]*Department of Chemistry, Durham University, South Road, Durham, DH1 3LE, UK. E-mail: james.walton@durham.ac.uk*
[b]*School of Medicine, Pharmacy and Health, Durham University, Wolfson Research Institute, Queen's Campus, Stockton on Tees, TS17 6BH, UK*

†Electronic supplementary information (ESI) available: Full experimental procedures and X-ray structural data. CCDC 1457275 and 1457276. For ESI and crystallographic data in CIF or other electronic format see DOI: 10.1039/c6dt01264g

3-fold increase in activity against human ovarian cancer cell line A2780 is observed when the arene is varied from benzene to biphenyl.[11] Similarly, modulation of the mono-dentate halide in the series $[(\eta^6\text{-}p\text{-cym})Ru(p\text{-Azpy-}NMe_2)X]PF_6$ from chloride to iodide results in a decrease in IC_{50}, the concentration of complex required to inhibit cell proliferation by 50%, from 13 μM to 0.69 μM in the A2780 cell line.[12] Finally, complexes with the same ligand can vary in activity, depending upon the central metal. In the $[(\eta^6\text{-}p\text{-cym})M(\text{picolinate})Cl]$ series, IC_{50} values (A2780 cell line) of 45 μM (ref. 13) and 4.5 μM (ref. 14) were reported for the Ru and Os complexes, respectively. Beyond Ru(II) and Os(II), there are also a host of Ir(III) and Rh(III) piano-stool complexes, whose activity often surpasses that of related Ru(II) complexes.[15] Although often not well understood, the mechanism of action of these complexes may involve DNA binding,[16] interactions with histone proteins,[17] redox modulation[18] or enzyme inhibition.[19]

The vast majority of reported piano stool complexes in the bioinorganic chemistry field incorporate polypyridyl, carboxylate or halide ligands. Only rarely are ligands explored that include elements other than C, N and O. However, there are a host of alternatives that may offer significant advantages over the more traditional ligand systems. In this study we present a novel ligand for platinum group metal complexes: the pyridylphosphinates. We report the synthesis, structural characterisation, aqueous properties and biological activities, including *in vitro* cytotoxicities, of a series of piano stool metal complexes incorporating the pyridylphosphinate ligand (Fig. 1). Lanthanide complexes incorporating this ligand have found application in cellular imaging.[20] However, the piano stool pyridylphosphinate complexes have never been studied. Advantages of the pyridylphosphinate ligand include: biocompatibility; the presence of a ^{31}P-NMR spectroscopic handle; control over lipophilicity at phosphorus; modular synthesis allowing rapid structure–activity relationship profile and, finally, the presence a stereogenic phosphorus, which presents an opportunity to develop enantiomerically pure metal-based complexes.[21]

Despite the host of piano stool complexes that have been reported, there is often a lack of information on biological behaviour, such as interactions between biologically relevant molecules (amino acids, proteins and nucleobases) and the metal complexes. This information is needed as the changes in structure of the complexes that take place in the cellular environment will have a profound effect upon the biological activity. Herein, we interrogate the behaviour of the novel pyridylphosphinate complexes in biological systems, by monitoring metal-halide hydrolysis, measuring pK_a values of the resultant aqua complexes and carrying out detailed binding studies with selected biomolecules.

Synthesis and structural characterisation

A series of complexes were synthesised in order to assess the factors that determine aqueous biological behaviour. Systematic variation in the metal–arene combination, the metal-bound halide, the phosphorus R′ group and the pyridyl R group led to a library of 25 new compounds (Scheme 1). Synthesis involves Pd-catalysed coupling of the phosphinate (HPO(OEt)R′) and bromo-pyridyl precursors.[22] Quantitative hydrolysis of the phosphinate ester was followed by neutralisation with NaOMe and complexation with the appropriate metal dimer $[(\text{arene})MX_2]_2$. Purification by recrystallisation from $CHCl_3/Et_2O$ gave the final complexes with 30–50% yields.†

The synthesis of complexes **7** and **8** (Scheme 2) proceeds *via* the 4-fluoropyridylphosphinate intermediate **L1**, which undergoes nucleophilic aromatic substitution to form the electron-rich 4-OCD_3- or electron-poor 4-Cl-pyridylphosphinate ligand, depending upon hydrolysis conditions.

Single crystals suitable for X-ray diffraction studies were grown of complexes **3** and **20** (Fig. 2A and 3). Complex **3** crystallises in the monoclinic crystal system and the $P2_1/c$ space group and displays the expected pseudo-tetrahedral geometry,

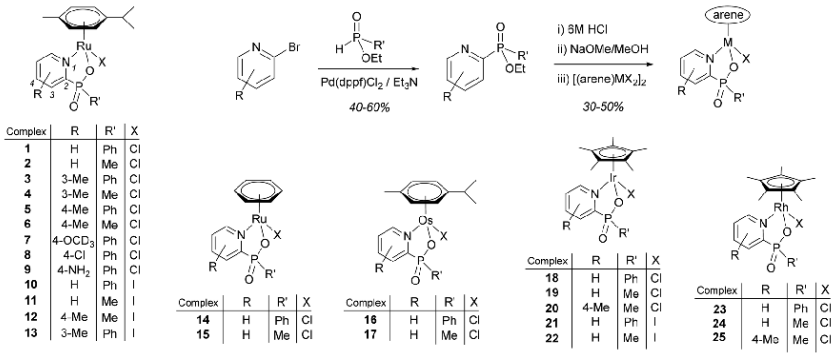

Complex	R	R′	X
1	H	Ph	Cl
2	H	Me	Cl
3	3-Me	Ph	Cl
4	3-Me	Me	Cl
5	4-Me	Ph	Cl
6	4-Me	Me	Cl
7	4-OCD_3	Ph	Cl
8	4-Cl	Ph	Cl
9	4-NH_2	Ph	Cl
10	H	Ph	I
11	H	Me	I
12	4-Me	Me	I
13	3-Me	Ph	I

Complex	R	R′	X
14	H	Ph	Cl
15	H	Me	Cl

Complex	R	R′	X
16	H	Ph	Cl
17	H	Me	Cl

Complex	R	R′	X
18	H	Ph	Cl
19	H	Me	Cl
20	4-Me	Me	Cl
21	H	Ph	I
22	H	Me	I

Complex	R	R′	X
23	H	Ph	Cl
24	H	Me	Cl
25	4-Me	Me	Cl

Scheme 1 General synthetic pathway and list of new complexes.

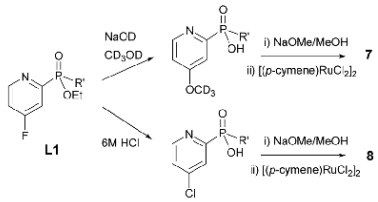

Scheme 2

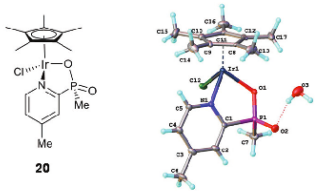

Fig. 3 X-ray crystal structures of Ir complex **20**.

with the η^6-*p*-cymene occupying one vertex. Ru–Cl (2.4155(6) Å), Ru–O (2.0809(14) Å) and Ru–N (2.1109(17) Å) bond lengths are almost identical to those reported for the analogous picolinate complex [(η^6-*p*-cym)Ru(picolinate)Cl],[13] however, the N–Ru–O bite angle is slightly larger in complex **3**, at 80.50(6)° (bite angle in picolinate complex is 77.95(7)°), reflecting the larger size of the phosphinate group. Intriguingly, of the four possible stereoisomers (*R* or *S* at Ru and P, denoted $Ru_{R/S}$ and $P_{R/S}$, respectively), only one enantiomeric pair is observed in the solid state structure – Ru_SP_R and Ru_RP_S. ^{1}H-NMR indicates that a single diastereomer is also present in solution, evidenced by one set of diastereotopic *p*-cymene protons in the region 5–6 ppm (Fig. 2B). The origin of this stereoselectivity, which has also been observed in lanthanide pyridylphosphinate complexes,[23] can be rationalised in terms of the steric interactions between the *p*-cymene ligand and the *P*-phenyl group, which are minimised in the observed diastereomer. Weak intramolecular hydrogen bonds between the P=O and *p*-cymene methyl-H (2.587 Å) and the *P*-phenyl and pyridyl methyl-H (3.065 Å) may also influence the observed stereochemistry. In solution, slight broadening of the pyridyl Me peak reflects its proximity to the *P*-phenyl aromatic system, but the presence of a sharp singlet peak for the *p*-cymene Me group suggests free rotation of the *p*-cymene ligand, as is expected for η^6-arene–metal bonds.[24]

The solid state structure of the Cp*–Ir complex **20** (Fig. 3) shows several differences from complex **3**, including a *Cc* space group, longer bond lengths between the central metal and coordinated ligands and a wider N–metal–O bite angle of 82.00(11)°. Despite the presence of the less sterically challenging *P*-methyl phosphinate ligand, once again only a single diastereoisomer is observed – Ir_SP_R and Ir_RP_S. No intramolecular H-bond interactions can be observed in the crystal structure, which presents further questions over the origin of this stereoselectivity. It may be that stereoselectivity originates from the initial attack of the phosphinate ligand on the metal dimer, during the formation of the complex.

Aqueous behaviour of the complexes

To gain an understanding of the intracellular behaviour of metal complexes with biological application, it is essential to have an appreciation of the aqueous behaviour of new compounds. Upon dissolving complex **1** in a $D_2O:CD_3OD$ (9 : 1) mix, equilibrium is established between the chloride (complex **1**) and aqua (complex **1a**) species (Fig. 4). ^{1}H-NMR of the *p*-cymene protons indicates that an approximate 1 : 1 (chloride : aqua) equilibrium is reached within 5 min and does

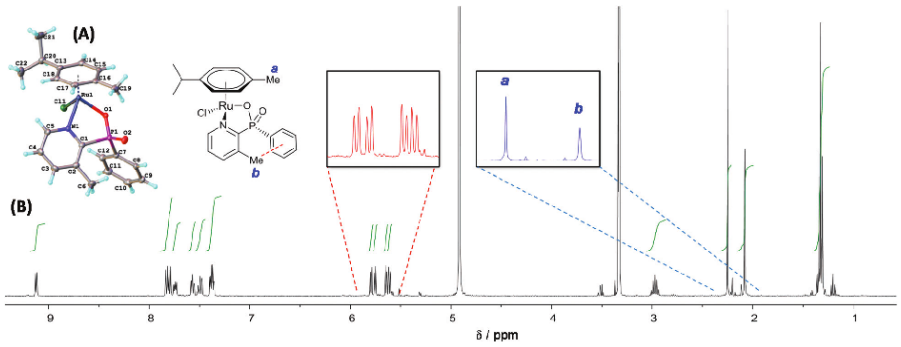

Fig. 2 (A) X-ray crystal structure of complex **3** and (B) ^{1}H-NMR spectrum (CD_3OD, 298 K, 400 MHz,), with expansions of the single set of diastereotopic *p*-cymene protons and of the two methyl groups.

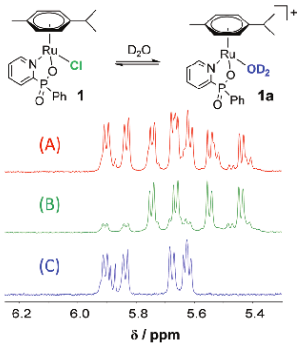

Fig. 4 ^{1}H-NMR spectra (D_2O : CD_3OD 9 : 1, 298 K, 400 MHz) of (A) complex **1** and **1a** at approximately 1 : 1 equilibrium ratio, (B) chloride complex **1**, following addition of 100 mM NaCl and (C) aqua complex **1a**, following addition of $AgNO_3$ and filtration of AgCl.

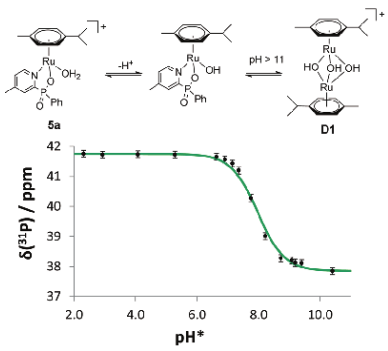

Fig. 5 Measurement of the pK_a^* of aqua complex **5a** by monitoring the ^{31}P-NMR spectrum (D_2O : CD_3OD 9 : 1, 298 K, 162 MHz) as a function of pH*. For Ru complexes, at approx. pH* >11 formation of the hydroxy-bridged dimer **D1** is observed.

not shift over the course of 24 h (Fig. 4A). To confirm that the observed species are the chloride and aqua adducts, the complex was dissolved in 100 mM NaCl (Fig. 4B) and in aqueous $AgNO_3$, followed by filtration of AgCl (Fig. 4C), leading to the selective formation of the chloride and aqua adducts, respectively, each showing a characteristic set of diastereotopic protons. The analogous Ru–iodide complex also undergoes rapid hydrolysis with around 60% of the complex remaining as the intact iodide species.

At the extracellular chloride concentration (approx. 100 mM), the pyridylphosphinate complexes remains intact as the chloride adduct, but at lower intracellular chloride concentration (approx. 20 mM in cytoplasm)[25] significant amounts of the aqua adduct are present. With this in mind, we sought to measure the pK_a of the bound water molecule and to establish how the pK_a varies with the choice of central metal and co-ordinated ligands. pK_a^* (pK_a measured in D_2O) values were measured by monitoring the ^{31}P- and ^{1}H-NMR spectra of selected aqua complexes in D_2O : CD_3OD (9 : 1) as a function of pH* (pH values in D_2O solution, Fig. 5), according to established procedures[25] (see ESI† for full details). pK_a^* values were converted to pK_a values using the equation $pK_a = 0.929pK_a^* + 0.42$.[26] By comparing pK_a values of selected aqua complexes (Table 1), it is apparent that a more electron donating pyridyl ligand leads to a higher pK_a. This is shown by the increase in values in the order **5a** < **3a** < **7a** for complexes with 4-Me, 3-Me and OCD_3 pyridyl substituents, respectively. This order reflects the higher pH required to deprotonate H_2O bound to a more electron-rich metal centre. The phosphorus-bound R′ group has little effect on pK_a, as can be seen by comparing values for **3a** and **4a**. Finally, as expected, the pK_a value for the Ir complex **20a** is lower than that of the equivalent Rh complex **25a**, reflecting the increased metal–oxygen bond strength of the heavier congener.[27] For each of the studied Ru complexes, the hydroxyl-bridged dimer **D1** (Fig. 5) forms at strongly basic pH (typically >pH 11), with concomitant loss of the pyridylphosphinate ligand.† The formation of this dimeric species from Ru piano stool complexes at elevated pH has been observed previously and the dimer is known to be non-cytotoxic.[28] NMR experiments indicate that dimer formation is partially reversible upon lowering the pH, but that complete regeneration of the starting complex does not take place.

Table 1 pK_a values for selected aqua complexes (D_2O : CD_3OD 9 : 1, 298 K). pK_a^* values were measured by monitoring changes in ^{31}P-NMR and ^{1}H-NMR spectra and converted to pK_a using the equation $pK_a = 0.929pK_a^* + 0.42$[26]

Complex	R	R′	{M(arene)}	pK_a
3a	3-Me	Ph	{Ru(*p*-cymene)}	9.34 ± 0.04
4a	3-Me	Me	{Ru(*p*-cymene)}	9.18 ± 0.19
5a	4-Me	Ph	{Ru(*p*-cymene)}	7.76 ± 0.13
7a	4-OCD_3	Ph	{Ru(*p*-cymene)}	10.08 ± 0.05
20a	4-Me	Me	{Ir(Cp*)}	9.31 ± 0.07
25a	4-Me	Me	{Rh(Cp*)}	10.95 ± 0.04

Cytotoxicity studies

The toxicity of each complex was assessed against non-small cell lung carcinoma H460 cells. Each complex was incubated with H460 cells for 96 h at concentrations ranging from 0.1 to 200 μM (aqueous media containing 0.1% DMSO) and IC_{50} values were measured using the MTT assay (see ESI† for details). The solubility of complexes at these concentrations was assessed to ensure the compounds are fully dissolved (see ESI† for details). Selected results are shown in Table 2 and represent the mean value for data from at least three experiments. All Ru complexes incorporating chloride ligands are non-toxic up to 200 μM. The most cytotoxic species are the iridium–Cp* complexes **21** and **22**, each with IC_{50} values of 50 ± 5 μM, respectively. The presence of the iodide ligand appears to play

Table 2 IC_{50} values for selected complexes measured using the MTT assay (96 h) against the non-small cell lung carcinoma H460 cell line. Entries are the mean value for data from at least three experiments. Complexes not included were found to have IC_{50} > 200 μM

Complex	R	R′	M	Arene	X	IC_{50}/μM
1	H	Ph	Ru	cym	Cl	>200
10	H	Ph	Ru	cym	I	65 ± 12
11	H	Me	Ru	cym	I	>200
18	H	Ph	Ir	Cp*	Cl	>200
19	H	Me	Ir	Cp*	Cl	>200
20	4-Me	Me	Ir	Cp*	Cl	140 ± 40
21	H	Ph	Ir	Cp*	I	52 ± 2
22	H	Me	Ir	Cp*	I	53 ± 4
25	4-Me	Me	Rh	Cp*	Cl	135 ± 17
Cisplatin	—	—	—	—	—	0.80 ± 0.01

an important role in the observed toxicity, as the analogous chloride complexes, **18** and **19**, gave IC_{50} values >200 μM. Comparing complexes **21** (*P*-phenyl) and **22** (*P*-methyl), it would appear that the phosphorus-R group has little influence upon the toxicity. However, this is not the case when comparing the Ru-*p*-cymene complexes **10** and **11**, for which the *P*-phenyl analogue has significantly greater cytotoxicity than the *P*-methyl complex. A comparison with cisplatin (IC_{50} = 0.80 ± 0.01 under the experimental conditions), shows that in general this class of complexes have low cytotoxicity. While ineffective as cytotoxic agents, this feature may bode well for uses in applications such as enzyme inhibitors.

A general feature within this series is that the complexes incorporating monodentate iodide ligands have higher toxicities than the corresponding chloride complexes. The extent of hydrolysis of the iodide complexes is less than that of the chloride complexes, leading to the conclusion that a mechanism of action involving hydrolysis and DNA binding, as is often proposed for piano stool metal complexes, may not be the main mechanism of action operating for this series of complexes. Whatever the mechanism, the observation of higher toxicity for iodide complexes is consistent with previously published reports[12,29] for both Ru- and Os-based anticancer complexes. Studies are ongoing to elucidate a potential mechanism of action for these species.

Binding studies

In general, the Ru complexes herein have IC_{50} values greater than 200 μM. In an attempt to understand this low cytotoxicity, binding studies were carried out with several biomolecules. Addition of $AgNO_3$ to complex **1** dissolved in D_2O, followed by filtration of the resulting AgCl precipitate, gave the aqua adduct, **1a**. Mass spectrometry and NMR spectroscopy (^1H and ^{31}P) were used to identify the presence and extent of biomolecule binding after addition of one and two equivalents of biomolecule to **1a**, at 1 h and 16 h time-points (Fig. 6 and Table 3). The biomolecules selected for investigation were L-alanine (L-Ala), L-threonine (L-Thr), L-histidine (L-His), imidazole and 9-ethylguanine (9-EtG). No evidence for binding between **1a** and 1 equivalent of amino acids L-Ala and L-Thr was observed after 1 h. In contrast, addition of 1 equivalent of 9-EtG led to a peak in the mass spectrum corresponding to the 9-EtG adduct of **1a**, following loss of H_2O. ^1H-NMR analysis indicated the formation of a bond between Ru and N7 on

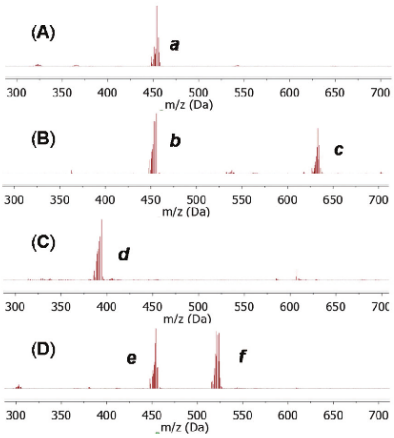

Fig. 6 Mass spectra for complex **1a** in the presence of (A) L-alanine, (B) 9-ethylguanine, (C) L-histidine and (D) imidazole. Peaks labelled ***a*–*f*** correlate to peaks in Table 3.

Table 3 Proposed species that give rise to mass peaks in Fig. 6, upon addition of selected biomolecules. Tabulated *m*/*z* values ***a*–*f*** correspond to mass peaks in Fig. 6

Biomolecule	*m*/*z*	Species
L-Ala	***a***: 454.3	$[\mathbf{1a} - H_2O]^+$ 
L-Thr	454.6	$[\mathbf{1a} - H_2O]^+$
9-EtG	***b***: 453.8	$[\mathbf{1a} - H_2O]^+$
	c: 632.9	**1b** 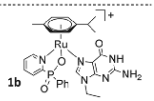
L-His	***d***: 390.6	**1c** 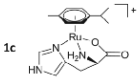
Imidazole	***e***: 454.0	$[\mathbf{1a} - H_2O]^+$
	f: 522.4	**1d** 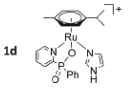

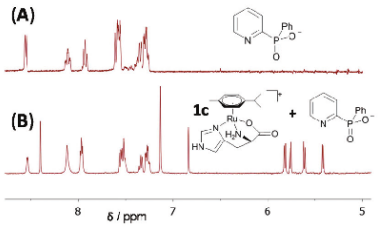

Fig. 7 ^{1}H-NMR spectra (D_2O : CD_3OD 9 : 1, 298 K, 400 MHz) of (A) uncomplexed pyridylphosphinate ligand and (B) products of addition of 2 equivalents of L-His to complex **1a**, showing the decomplexation of the pyridylphosphinate ligand and the formation of L-His complex, **1c**.

9-EtG, with around 50% bound complex in solution. This mode of binding is consistent with previous reports that have proposed a mechanism of action for the anticancer behaviour of Ru complexes to involve DNA binding, leading to apoptosis.[16]

Upon addition of 1 equivalent of L-His, an adduct was observed, consistent with replacement of H_2O for L-His, binding though an imidazole N. When the sample was subjected to a second equivalent of L-His and left to equilibrate over 16 h, a species formed in which the pyridylphosphinate ligand is displaced and the L-His binds κ^3 (Fig. 7). The observed Ru–(L-His) complex, **1c**, is known to be non-cytotoxic[30] and its formation presents a potential explanation of the low cytotoxicity of Ru chloride complexes described in this report. It follows that the higher cytotoxicity of the iodide-complexes, **10**, **21** and **22**, is due to the metal–iodide bond being less labile towards aquation and therefore less likely to undergo decomplexation by chelating biomolecules. It should be noted that the only tested biomolecule able to displace the pyridylphosphinate ligand was L-His. Addition of 2 equivalents of imidazole (16 h) leads to 1 : 1 adduct formation, with loss of H_2O, but no ligand displacement. The cytotoxicity of the displaced ligand of complex **1** (shown in Fig. 7A) was assessed using the MTT assay and found to by non-cytotoxic up to 200 μM. In future studies it may be possible to tune the lability of pyridylphosphinate ligands, so that the complexes remain intact in the high chloride concentration of the extracellular medium but are able to release some useful payload within the cell where the chloride concentration is lower.

Conclusions

A series of 25 new piano-stool pyridylphosphinate complexes has been synthesised, characterised and assessed in biologically-relevant systems. The properties of the complexes depend upon their various components – metal ion, arene, pyridyl substituent and *P*-alkyl group – which can be varied with relative ease. Aqueous solubility and stability is good. Ru–Cl complexes are non-toxic up to 200 μM, which bodes well for their use as a scaffold for metal-based enzyme inhibitors. Ir–I complexes are more toxic to cells, so may have the potential to act as anticancer agents, although toxicity remains low compared to cisplatin. It was discovered that decomplexation of the ligand from complex **1** occurs in the presence of excess L-His, following hydrolysis of the Ru–Cl bond. This has the potential to be exploited in the form of complexes that deliver and release useful payloads to the cell. The rate of aquation and the pK_a of the resulting aqua species can be tuned by varying the pyridyl substituent and the judicious choice of metal–halide combination. Studies are ongoing to investigate the cell uptake, localisation and any potential antimetastatic behaviour of these exciting new complexes and to exploit the lability of the phenylphosphinate Ru bond to design responsive biologically active complexes.

Acknowledgements

We thank Durham University and the EPSRC for funding.

Notes and references

1 (*a*) S. W. Botchway, M. Charnley, J. W. Haycock, A. W. Parker, D. L. Rochester, J. A. Weinstein and J. A. G. Williams, *Proc. Natl. Acad. Sci. U. S. A.*, 2008, **105**, 16071; (*b*) D. Lloyd, M. P. Coogan and S. J. A. Pope, *Rev. Fluoresc.*, 2012, **2010**, 15.
2 (*a*) M. Dorr and E. Meggers, *Curr. Opin. Chem. Biol.*, 2014, **19**, 76; (*b*) D. Hu, Y. Liu, Y.-T. Lai, K.-C. Tong, Y.-M. Fung, C.-N. Lok and C.-M. Che, *Angew. Chem., Int. Ed.*, 2016, **55**, 1387.
3 (*a*) F. E. Poynton, J. P. Hall, P. M. Keane, C. Schwarz, I. V. Sazanovich, M. Towrie, T. Gunnlaugsson, C. J. Cardin, D. J. Cardin, S. J. Quinn, C. Long and J. M. Kelly, *Chem. Sci.*, 2016, **7**, 3075; (*b*) K. K. W. Lo, T. K. M. Lee, J. S. Y. Lau, W. L. Poon and S. H. Cheng, *Inorg. Chem.*, 2008, **47**, 200; (*c*) K. K.-W. Lo, *Acc. Chem. Res.*, 2015, **48**, 2985.
4 For recent reviews of metal-based anticancer agents see. (*a*) G. Gasser, I. Ott and N. Metzler-Nolte, *J. Med. Chem.*, 2011, **54**, 3; (*b*) I. Ott and R. Gust, *Arch. Pharm.*, 2007, **340**, 117; (*c*) S. Medici, M. Peana, V. M. Nurchi, J. I. Lachowicz, G. Crisponi and M. A. Zoroddu, *Coord. Chem. Rev.*, 2015, 329; (*d*) N. Muhammad and Z. Guo, *Curr. Opin. Chem. Biol.*, 2014, **19**, 144.
5 (*a*) B. Rosenberg, L. van Camp and T. Krigas, *Nature*, 1965, **205**, 698; (*b*) Y. Kidani, K. Inagaki, M. Iigo, A. Hoshi and K. Kuretani, *J. Med. Chem.*, 1978, **21**, 1315; (*c*) K. R. Harrap, *Cancer Treat. Rev.*, 1985, **12**, 21.
6 (*a*) H. Matsushima, K. Yonemura, K. Ohishi and A. Hishida, *J. Lab. Clin. Med.*, 1998, **131**, 518; (*b*) N. E. Madias and J. T. Harrington, *Am. J. Med.*, 1978, **65**, 307.
7 (*a*) M. Kartalou and J. M. Essigmann, *Mutat. Res.*, 2001, **478**, 23; (*b*) K. J. Mellish, L. R. Kelland and K. R. Harrap, *Br. J. Cancer*, 1993, **68**, 240.

8 A. A. Nazarov, C. G. Hartinger and P. J. Dyson, *J. Organomet. Chem.*, 2014, **751**, 251.
9 (*a*) R. E. Morris, R. E. Aird, P. Del Socorro-Murdoch, H. Chen, J. Cummings, N. D. Hughes, S. Parsons, A. Parkin, G. Boyd, D. I. Jodrell and P. J. Sadler, *J. Med. Chem.*, 2001, **44**, 3616; (*b*) M. Pernot, T. Bastogne, N. P. E. Barry, B. Therrien, G. Koellensperger, S. Hann, V. Reshetov and M. Barberi-Heyob, *J. Photochem. Photobiol., B*, 2012, **117**, 80; (*c*) A. A. Nazarov, S. M. Meier, O. Zava, Y. N. Nosova, E. R. Milaeva, C. G. Hartinger and P. J. Dyson, *Dalton Trans.*, 2015, **44**, 3614; (*d*) S. M. Meier, M. Hanif, Z. Adhireksan, V. Pichler, M. Novak, E. Jirkovsky, M. A. Jakupec, V. B. Arion, C. A. Davey, B. K. Keppler and C. G. Hartinger, *Chem. Sci.*, 2013, **4**, 1837; (*e*) B. S. Murray, L. Menin, R. Scopelliti and P. J. Dyson, *Chem. Sci.*, 2014, **5**, 2536.
10 (*a*) C. Scolaro, A. Bergamo, L. Brescacin, R. Delfino, M. Cocchietto, G. Laurenczy, T. J. Geldbach, G. Sava and P. J. Dyson, *J. Med. Chem.*, 2005, **48**, 4161; (*b*) A. Weiss, R. H. Berndsen, M. Dubois, C. Müller, R. Schibli, A. W. Griffioen, P. J. Dyson and P. Nowak-Sliwinska, *Chem. Sci.*, 2014, **5**, 4742; (*c*) X. Meng, M. L. Leyva, M. Jenny, I. Gross, S. Benosman, B. Fricker, S. Harlepp, P. Hébraud, A. Boos, P. Wlosik, P. Bischoff, C. Sirlin, M. Pfeffer, J. P. Loeffler and C. Gaiddon, *Cancer Res.*, 2009, **69**, 5458.
11 (*a*) O. Novakova, H. Chen, O. Vrana, A. Rodger, P. J. Sadler and V. Brabec, *Biochemistry*, 2003, **42**, 11544; (*b*) R. E. Morris, R. E. Aird, P. Del Socorro-Murdoch, H. Chen, J. Cummings, N. D. Hughes, S. Parsons, A. Parkin, G. Boyd, D. I. Jodrell and P. J. Sadler, *J. Med. Chem.*, 2001, **44**, 3616.
12 S. H. Van Rijt, I. Romero-Canelón, Y. Fu, S. D. Shnyder and P. J. Sadler, *Metallomics*, 2014, **6**, 1014.
13 K. D. Camm, A. El-Sokkary, A. L. Gott, P. G. Stockley, T. Belyaevab and P. C. McGowan, *Dalton Trans.*, 2009, **48**, 10914.
14 A. F. A. Peacock, S. Parsons and P. J. Sadler, *J. Am. Chem. Soc.*, 2007, **129**, 3348.
15 (*a*) Z. Liu, A. Habtemariam, A. M. Pizarro, S. A. Fletcher, A. Kisova, O. Vrana, L. Salassa, P. C. A. Bruijnincx, G. J. Clarkson, V. Brabec and P. J. Sadler, *J. Med. Chem.*, 2011, **54**, 3011; (*b*) Z. Liu, I. Romero-Canelón, B. Qamar, J. M. Hearn, A. Habtemariam, N. P. E. Berry, A. M. Pizarro, G. J. Clarkson and P. J. Sadler, *Angew. Chem., Int. Ed.*, 2014, **53**, 3941; (*c*) Z. Liu and P. J. Sadler, *Acc. Chem. Res.*, 2014, **47**, 1174; (*d*) M. Grasa, B. Therrien, G. Süss-Fink, A. Casini, F. Edafe and P. J. Dyson, *J. Organomet. Chem.*, 2010, **695**, 1119; (*e*) L. C. Sudding, R. Payne, P. Govender, F. Edafe, C. M. Clavel, P. J. Dyson, B. Therrien and G. S. Smith, *J. Organomet. Chem.*, 2014, **774**, 79.
16 H. Chen, J. A. Parkinson, S. Parsons, R. A. Coxall, R. O. Gould and P. J. Sadler, *J. Am. Chem. Soc.*, 2002, **124**, 3064.
17 Z. Adhireksan, G. E. Davey, P. Campomanes, M. Groessl, C. M. Clavel, H. Yu, A. A. Nazarov, C. Hui Fang Yeo, W. Han Ang, P. Dröge, U. Rothlisberger, P. J. Dyson and C. A. Davey, *Nat. Commun.*, 2014, **5**, 3462.
18 (*a*) I. Romero-Canelón and P. J. Sadler, *Inorg. Chem.*, 2013, **52**, 12276; (*b*) K. Suntharalingam, Y. Song and S. J. Lippard, *Chem. Commun.*, 2014, **50**, 2465.
19 (*a*) A. de Almeida, B. L. Oliveira, J. D. G. Correia, G. Soveral and A. Casini, *Coord. Chem. Rev.*, 2013, **257**, 2689; (*b*) L. Feng, Y. Geisselbrecht, S. Blanck, A. Wilbuer, G. E. Atilla-Gokcumen, P. Filippakopoulos, K. Kräling, M. A. Celik, K. Harms, J. Maksimoska, R. Marmorstein, G. Frenking, S. Knapp, L.-O. Essen and E. Meggers, *J. Am. Chem. Soc.*, 2011, **133**, 5976; (*c*) E. Meggers, G. E. Atilla-Gokcumen, K. Gründler, C. Frias and A. Prokop, *Dalton Trans.*, 2009, 10882.
20 (*a*) S. J. Butler, M. Delbianco, L. Lamarque, B. K. McMahon, E. R. Neil, R. Pal, D. Parker, J. W. Walton and J. M. Zwier, *Dalton Trans.*, 2015, **44**, 4791; (*b*) M. Soulié, F. Latzko, E. Bourrier, V. Placide, S. J. Butler, R. Pal, J. W. Walton, P. L. Baldeck, B. Le Guennic, C. Andraud, J. M. Zwier, L. Lamarque, D. Parker and O. Maury, *Chem. – Eur. J.*, 2014, **20**, 8636; (*c*) A. J. Palmer, S. H. Ford, S. J. Butler, T. J. Hawkins, P. J. Hussey, R. Pal, J. W. Walton and D. Parker, *RSC Adv.*, 2014, **4**, 9356.
21 Examples of enantiomerically pure anticancer metal complexes include. (*a*) G. E. Atilla-Gokcumen, L. Di Costanzo and E. Meggers, *J. Biol. Inorg. Chem.*, 2011, **16**, 45; (*b*) E. Menéndez-Pedregal, Á. Manteca, J. Sánchez, J. Díez, M. P. Gamasa and E. Lastra, *Eur. J. Inorg. Chem.*, 2015, 1424.
22 (*a*) J. W. Walton, L. Di Bari, D. Parker, G. Pescitelli, H. Puschmann and D. S. Yufit, *Chem. Commun.*, 2011, **47**, 12289; (*b*) J. W. Walton, R. Carr, N. H. Evans, A. M. Funk, A. M. Kenwright, D. Parker, D. S. Yufit, M. Botta, S. De Pinto and K.-L. Wong, *Inorg. Chem.*, 2012, **51**, 8042.
23 (*a*) J. W. Walton, A. Bourdolle, S. J. Butler, M. Soulie, M. Delbianco, B. K. McMahon, R. Pal, H. Puschmann, J. M. Zwier, L. Lamarque, O. Maury, C. Andraud and D. Parker, *Chem. Commun.*, 2013, **49**, 1600; (*b*) S. J. Butler, R. Pal, B. K. McMahon, D. Parker and J. W. Walton, *Chem. – Eur. J.*, 2013, **19**, 9511.
24 C. Gossens, I. Tavernelli and U. Rothlisberger, *J. Phys. Chem. A*, 2009, **113**, 11888.
25 S. H. Van Rijt, A. F. A. Peacock, R. D. L. Johnstone, S. Parsons and P. J. Sadler, *Inorg. Chem.*, 2009, **48**, 1753.
26 A. Krezel and W. J. Bal, *Inorg. Biochem.*, 2004, **98**, 161.
27 P. Moore, in *Inorganic Reaction Mechanisms*, ed. A. McAuley, CRC Press, Boca Raton, 1988, vol. 4, p. 129.
28 (*a*) M. Melchart, A. Habtemariam, S. Parsons, S. A. Moggach and P. J. Sadler, *Inorg. Chim. Acta*, 2006, **359**, 3020; (*b*) W. Kandioller, C. Hartinger, A. A. Nazarov, M. L. Kuznetsov, R. John, C. Bartel, M. A. Jakupec, V. B. Arion and B. K. Keppler, *Organometallics*, 2009, **28**, 4249.
29 I. Romero-Canelón, L. Salassa and P. J. Sadler, *J. Med. Chem.*, 2013, **56**, 1291.
30 T. G. Scrase, M. J. O'Neill, A. J. Peel, P. W. Senior, P. D. Matthews, H. Shi, S. R. Boss and P. D. Barker, *Inorg. Chem.*, 2015, **54**, 3118.

Appendix 4: Solutions and gels

Solution and gel compositions for Western blotting

Composition of MRC lysis buffer

Stock lysis buffer was stored at -20˚C until required

Chemical	Concentration
Tris HCl pH 7.5	50mM
EGTA	1mM
EDTA	1mM
Sodium orthovanadate	1mM
β-glycerol phosphate	10mM
Sodium fluoride	50mM
Sodium pyrophosphate	5mM
Sucrose	0.27M
Triton x100	1% (v/v)
β-mercaptoethanol	0.1%
Mini protease inhibitor tablet (Roche, Germany)	1 tablet per 50ml of lysis buffer

Composition of 4x Sample buffer

SDS-sample buffer was stored at room temperature and 10% (v/v) β-mercaptoethanol was added prior to use.

Chemical	Concentration
Tris HCl pH 6.8	240mM
SDS	8% (w/v)
Glycerol	40% (v/v)
Bromophenol blue	0.04% (w/v)

Composition of 10% resolving gel

Chemical	Concentration
Bis/acrylamide	10% (v/v)
Tris HCl pH 8.8	375mM
SDS	0.1%
Ammonium persulfate	0.1%
TEMED	0.4µl/ml
Water	To volume

Composition of 5% stacking gel

Chemical	Concentration
Bis/acrylamide	5% (v/v)
Tris HCl pH 6.8	125mM
SDS	0.1%
Ammonium persulfate	0.1%
TEMED	1µl/ml
Water	To volume

Composition of running buffer

Chemical	Concentration
Trizma Base	250mM
Glycine	190mM
SDS	0.1% (w/v)
Water	To volume

Composition of transfer buffer

Chemical	Concentration
Trizma Base	20mM
Glycine	150mM
Methanol	20% (v/v)
Water	To volume

Composition of Tris-buffered saline with Tween-20 (TBS-T)

Chemical	Concentration
Trizma Base	20mM
NaCl	150mM
Tween-20	0.1% (v/v)

Composition of Enhanced chemiluminescence solution (ECL)

Prior to use solution 1 and solution 2 were mixed in equal volume

	Chemical	Concentration
Solution 1	Luminol	2.5mM
	p-Coumaric acid	0.4mM
	Tris HCl pH 8.5	100mM
	Water	To volume
Solution 2	H_2O_2	30% (v/v)
	Tris HCl pH 8.5	100mM
	Water	To volume

Composition of Acid Stripping Buffer

pH to 2.2 with concentrated HCl

Chemical	Concentration
Glycine	3% (w/v)
SDS	0.2% (w/v)
Tween-20	2% (v/v)
Water	To volume

Appendix 5: Preliminary RT-PCR studies

As discussed in Chapter 5 (Section 5.4.2) preliminary studies using reverse transcriptase polymerase chain reaction (RT-PCR) detected gene expression of angiotensinogen, angiotensin converting enzyme (ACE) and the angiotensin type I receptor (ATR1) in AC10 cardiomyocytes (AC10-CMs), however expression of renin was not detected in the cells.

The method used for RT-PCR can be found in Chapter 6 (Section 6.2.2.1 *Production of cDNA from AC10 cardiomyocytes* and Section 6.2.2.2 *Pre-array verification of cDNA quality*), except the cells were not exposed to doxorubicin. The same cycling conditions were used as outlined for analysis of GAPDH gene expression in section 6.2.2.2, however different annealing temperatures were optimised for each primer set.

The primers used, annealing temperature, expected product size and example gel are shown below:

Primer target	Primer sequence	Annealing temp (°C)	Product size	AC10-CM expression
Angiotensinogen	**F** TCCACCTCGTCATCCACA **R** GGCTCCCAGATAGAGAGA	53	329	YES
ACE	**F** CCGATCTGGCAGAACTTC **R** GTGTTCCAGATCGTCCTC	52	314, 408	YES
ATR1	**F** GATGATTGTCCCAAAGCTGG **R** TAGGTAATTGCCAAAGGGCC	54	255	YES
Renin	**F** AAATGAAGGGGGTGTCTGTGG **R** AAGCCAATGCGGTTGTTACGC	60*	397	NO

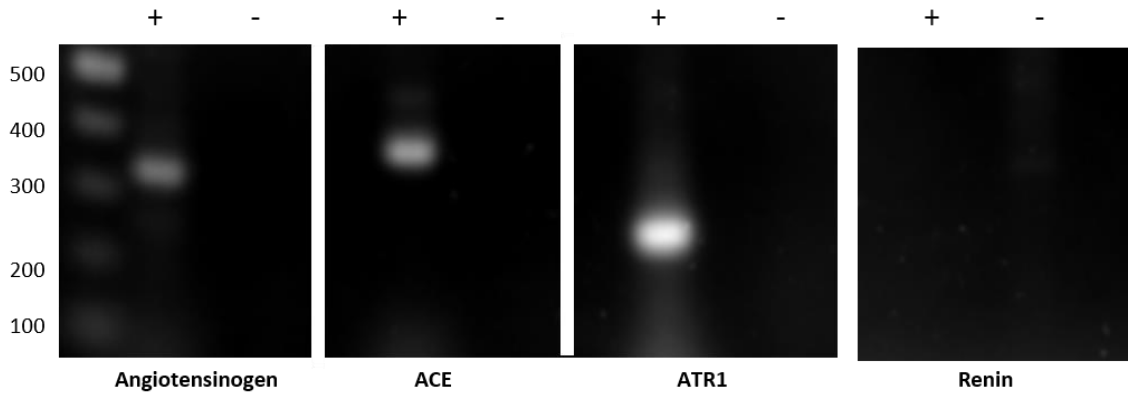

*Annealing temperature from paper by Wagner *et al.* (1996), positive expression was not detected for renin in this study.